

Université de Montréal

Complexes de cuivre(II) portant des ligands sulfonés ou carboxylates et leur application en catalyse

par Valérie Hardouin Duparc

Département de Chimie Faculté des Arts et des Sciences

Thèse présentée à la Faculté des études supérieures et postdoctorales en vue de l'obtention
du grade de Ph. D. en chimie

Juillet 2018

© Valérie Hardouin Duparc, 2018

Résumé

Ce manuscrit présente les résultats de travaux de recherche réalisés sur des complexes de cuivre(II). Des complexes cuivrés avec des ligands dikétiminosulfonate, pyridyliminosulfonate et pyridyliminocarboxylate ont été synthétisés et caractérisés par diverses méthodes.

Les complexes ont été investigués pour la polymérisation de lactide. Les complexes portant un ligand dikétiminosulfonate se sont avérés inactifs. Les complexes avec les deux autres ligands n'ont montré aucune réactivité à température ambiante et une faible activité catalytique à haute température dans le monomère fondu. Les caractéristiques structurales des polymères formés sont peu intéressantes avec une basse hétérotacticité observée et de très faibles poids moléculaire, dû à des réactions secondaires de transestérification.

Tous les catalyseurs ont été actifs en couplage de Chan-Evans-Lam. Les complexes avec des ligands carboxylates ont été moins actif en général et ceux avec les ligands dikétiminates ont été moins actifs envers les substrats encombrés. En terme général, ces catalyseurs sont très efficaces envers les substrats N-nucléophiles, mais ne le sont pas envers les phénols et les thiols. Les acides boroniques électroniquement pauvres nécessitent un oxydant auxiliaire ou une réaction de type photoredox. Aucune réactivité n'a été observée avec les acides alkylboroniques. Des études cinétiques ont été réalisées, en particulier pour les complexes portant des ligands pyridyliminosulfonates. Globalement, nos observations ont mené à proposer un mécanisme similaire à celui proposé dans la littérature avec quelques modifications. Notamment la formation de complexes désactivés entre le nucléophile et le catalyseur et le nucléophile et l'acide boronique. La transmétallation est proposée d'être l'étape limitante.

Mots clés : Couplage Chan-Evans-Lam, polymérisation lactide, complexes de cuivre, ligands sulfonés, ligand carboxylate, catalyse, études mécanistiques.

Abstract

This manuscript presents research on copper (II) complexes. Copper complexes with diketiminatosulfonate, pyridyliminosulfonate and pyridyliminocarboxylate ligands were synthesized and characterized by various methods.

The complexes were investigated for the polymerization of lactide. Complexes bearing a diketiminatosulfonate ligand were inactive. Complexes with the other two ligands showed no reactivity at room temperature and low catalytic activity at high temperature in molten monomer. Structural features of the formed polymers were unspectacular with low amounts of heterotacticity and very low molecular weight due to transesterification side reactions.

All catalysts were active in Chan-Evans-Lam coupling. Complexes with carboxylate ligands were generally less active, and those with diketiminates ligands were less active towards sterically bulky substrates. Overall, these catalysts are very efficient towards N-nucleophilic substrates, but not towards phenols and thiols. Electronically deficient boronic acids require an auxiliary oxidant or a photoredox reaction. No reactivity was observed with alkylboronic acids. Kinetic studies have been performed, particularly for complexes bearing pyridyliminosulfonate ligands. Our observations led to propose a mechanism, slightly modified from the one proposed in the literature. In particular, the formation of deactivated complexes between the nucleophile and the catalyst and the nucleophile and the boronic acid were observed. Transmetallation is proposed to be the rate-limiting step.

Key words: Chan-Evans-Lam coupling, lactide polymerization, copper complexes, sulfonated ligands, carboxylate ligand, catalysis, mechanistic studies.

Sommaire

Résumé	i
Abstract	ii
Sommaire.....	iii
Liste des tableaux	vi
Liste des schémas	viii
Liste des « Chart »	x
Liste des figures.....	xi
Liste des abréviations	xix
Remerciements	xxiv
1. INTRODUCTION	1
1.1. Généralités sur le cuivre	1
1.2. Polymérisation de lactide	7
1.3. Couplage de Chan-Evans-Lam.....	27
1.4. Objectif de recherche	55
2. SULFONATO-DIKETIMINE COPPER(II) COMPLEXES : SYNTHESIS AND APPLICATION AS CATALYSTS IN CHAN-EVANS-LAM COUPLINGS	65
2.1. Introduction.....	66
2.2. Results and discussion.....	67
2.2.1. Synthesis	67
2.2.2. Complex Stability in the Presence of Water	70
2.2.3. Attempted rac-Lactide Polymerization.....	72
2.2.4. Chan-Evans-Lam coupling	74
2.2.5. Substrate Scope	77
2.2.6. Mechanistic Investigations.....	79
2.3. Conclusions.....	86

2.4. Experimental section	87
2.5. Supporting information.....	90
2.6. References.....	96
3. SULFONATO-IMINO COPPER(II) COMPLEXES : FAST AND GENERAL CHAN-EVANS-LAM COUPLING OF AMINES AND ANILINES.....	99
3.1. Introduction.....	100
3.2. Results and discussion.....	101
3.2.1. Catalytic performance	102
3.2.2. Reactivity studies	104
3.3. Conclusions.....	108
3.4. Supporting information.....	109
3.5. References.....	123
4. CHAN-EVANS-LAM COUPLINGS WITH IMINO-ARYLSULFONATE COPPER COMPLEXES: SCOPE AND MECHANISM.....	127
4.1. Introduction.....	128
4.2. Results and Discussion	130
4.2.1. Catalyst synthesis and structures	130
4.2.2. Chan-Evans-Lam couplings: general reaction conditions	132
4.2.3. Substrate reactivity	137
4.2.4. Mechanism of CEL couplings with 1 and 3	145
4.3. Conclusions.....	163
4.4. Experimental section	164
4.6. References.....	169
4.7. Supporting information.....	178

5. ANION INFLUENCES ON THE STRUCTURES OF PYRIDYL-IMINOSULFONATE COPPER(II) COMPLEXES AND THEIR REACTIVITY IN <i>RAC</i> -LACTIDE POLYMERIZATION AND CHAN-EVANS-LAM COUPLINGS	189
5.1. Introduction.....	190
5.2. Results and discussion.....	192
5.2.1. Ligand and complex syntheses and structures	192
5.2.2. <i>rac</i> -Lactide Polymerisation	204
5.2.3. Chan-Evans-Lam couplings	210
5.3. Conclusions.....	217
5.4. Experimental section	218
5.6. References.....	225
5.7. Supporting Information.....	231
6. REPLACING SULFONATE BY CARBOXYLATE: APPLICATION OF PYRIDYLIMINOCARBOXYLATO COPPER(II) COMPLEXES IN <i>RAC</i> -LACTIDE POLYMERIZATION AND CHAN-EVANS-LAM COUPLING.....	238
6.2. Introduction.....	239
6.2. Results and Discussion	241
6.2.1. Ligand syntheses.....	241
6.2.2. UV/vis-spectra.....	246
6.2.3. <i>rac</i> -Lactide polymerization	247
6.2.4. Chan-Evans-Lam couplings	251
6.2. Conclusions.....	254
6.3. Experimental section.....	255
6.4. References	264
6.5. Supporting information.....	270
7. CONCLUSION ET PERSPECTIVES.....	277
7.1. Conclusions.....	277

7.2. Perspectives.....	280
-------------------------------	------------

Liste des tableaux

Tableau 1-1 : Tacticité du rac-lactide.	19
Tableau 1-2 : Tacticité du méso-lactide.....	19
Table 2-1 : Bond Lengths (Å) in Crystal Structures of 4–6.....	69
Table 2-2 : Initial Screening of Activity in Chan–Evans–Lam.....	75
Table 2-3 : Isolated yields in coupling of amines and anilines with Cu(OAc)₂ or 5 as catalyst.	76
Table 2-4 : Coupling of Aniline with Phenylborate Using 5 as a catalyst.^a	79
Table 2-5 : Conversions in Competition Experiments.^a	84
Table 4-1 : Geometrical data of complexes 1-4.....	131
Table 4-2 : Coupling of aniline and phenylboronic acid using 1 as a catalyst. ^a	133
Table 4-3 : Coupling of para-substituted anilines and phenylboronic acid with 3. ^a	140
Table 4-4 : Oxidation of <i>tert</i>-butyl aniline catalyzed by 3. ^a	142
Table 4-5 : Apparent First-Order Rate Constants for the N-Arylation of Aniline with 3. ^a....	147
Table 4-6 : CEL couplings of aniline with electron-deficient phenylboronic acids catalyzed by 3.	
^a	157
Table 4-7 : Coupling of aniline or RR'NH and <i>para</i>-fluorophenylboronic acid with 3 under photoredox conditions.....	158
Table 4-8 : CEL couplings of aniline with electron-deficient phenylboronic acids catalyzed by 3/Cu(OAc)₂. ^a	161
Table 4-9 : Experimental details of X-ray diffraction studies.	168
Table 5-1 : Ligand-copper bond distances for taurine-based complexes.	196
Table 5-2 : Ligand-copper bond distances for orthanilic acid-based complexes.	199
Table 5-3 : <i>rac</i>-Lactide polymerisation with copper pyridyliminosulfonate complexes.	206

Table 5-4 : Activity of iminosulfonates copper catalysts in the CEL coupling of aniline with phenylboronic acid.....	214
Table 5-5 : CEL couplings of phenylboronic acid with various amines catalysed by 17	215
Table 6-1 : Selected geometric data of X-ray structures of 1-5	243
Table 6-2 : Geometrical details of the X-ray structures of 6 , (L2H)CuCl ₂ , (L2)Cu(OAc)·Cu(OAc) ₂ and 7	245
Table 6-3 : Activities of 2-7 in <i>rac</i> -lactide polymerization under different conditions.	248
Table 6-4 : Chan-Evans-Lam coupling with phenylboronic acid.....	252
Table 6-5 : Details of X-ray Diffraction Studies.....	262

Liste des schémas

Scheme 2-1	66
Scheme 2-2	68
Scheme 2-3	75
Scheme 2-4	85
Scheme 3-1	101
Scheme 4-1	128
Scheme 4-2	130
Scheme 4-3	139
Scheme 4-4	143
Scheme 4-5	143
Scheme 4-6	144
Scheme 4-7	145
Scheme 4-8	148
Scheme 4-9	149
Scheme 4-10	155
Scheme 5-1	191
Scheme 5-2	194
Scheme 5-3	198
Scheme 5-4	203
Scheme 5-5	209
Scheme 5-6	212
Scheme 5-7	216
Scheme 6-1	240
Scheme 6-2	241
Scheme 6-3	242

Scheme 6-4	244
Scheme 6-5	246
Scheme 6-6	250
Scheme 6-7	251
Scheme 6-8	253
Schéma 7-1	281
Schéma 7-3	281
Schéma 7-4	282
Schéma 7-5	282
Schéma 7-6	283
Schéma 7-7	284

Liste des « Chart »

Chart 2-1 : Relative Reactivity of Different Amines and Anilines.	78
Chart 3-1 : Isolated yields for arylations with 2.....	103
Chart 3-2 : Conversion to product (determined by GC-MS vs. internal calibrated standard) for the coupling of nitrogen nucleophiles with phenyl boronic acid.	105
Chart 4-1	138

Liste des figures

Figure 1.1 : Anciennes utilisations du cuivre par l'homme (reproduit avec permission).....	1
Figure 1.2 : Degré d'oxydation du cuivre les plus courants (Reproduit avec permission).....	2
Figure 1.3 : États d'oxydation du cuivre et leurs potentiels réducteurs dans l'eau.....	3
Figure 1.4 : Polymérisation radicalaire par transfert d'atome (ATRP).	3
Figure 1.5 : Réaction de Glaser-Hay.	4
Figure 1.6 : Utilisation du cuivre en catalyse organique.	5
Figure 1.7 : Réaction de Gilman.....	6
Figure 1.8 : Réaction de Huisgen.	6
Figure 1.9 : Réaction de Sharpless-Meldal.	6
Figure 1.10 : Production des biopolymères en 2015/2016 (barres solides) et production annoncée pour 2020 (barres ombrées) en vert les bioplastiques biodégradables et en bleu les bioplastiques durables (reproduit avec permission).	8
Figure 1.11 : Voie naturelle pour la synthèse de l'acide lactique (reproduit avec permission).	10
Figure 1.12 : Voie de synthèse du polylactide.....	11
Figure 1.13 : Mécanisme anionique de la synthèse de PLA.	12
Figure 1.14 : Mécanisme nucléophilique de la synthèse de PLA.	12
Figure 1.15 : Mécanisme cationique de la synthèse de PLA.	12
Figure 1.16 : Mécanisme par activation du monomère de la synthèse de PLA.	13
Figure 1.17 : Mécanisme coordination-insertion de la synthèse de PLA.	14
Figure 1.18 : Réactions secondaires de transestérification.....	15
Figure 1.19 : Isomères du lactide.....	16
Figure 1.20 : Stéréocontrôle des PLA.	16
Figure 1.21 : Diade méso/racémique.	17
Figure 1.22 : Séquence différenciée par RMN.....	18

Figure 1.23 : Catalyseur bis(éthylhexanoate) d'étain.....	19
Figure 1.24 : Premier catalyseur de cuivre pour la polymérisation de lactide.....	20
Figure 1.25 : Premiers complexes homoleptiques avec ligand phénoxy-kétimine pour la polymérisation de lactide.	21
Figure 1.26 : Complexes de Bhunora pour la polymérisation de lactide.	21
Figure 1.27 : Premiers complexes cuivrés avec ligand type salen pour la polymérisation de lactide.....	22
Figure 1.28 : Catalyse de la polymérisation de lactide par l'acétate de cuivre	23
Figure 1.29 : Cuivre(II) diketiminate hétéroleptique pour la polymérisation de lactide.	24
Figure 1.30 : Cuivre(II) diketiminate homoleptique pour la polymérisation de lactide.....	24
Figure 1.31 : Cuivre(II) benzotriazole phenoxide (Gauche) et bis(3,5-diméthylpyrazole) (droite).	25
Figure 1.32 : Premier complexe chiral de cuivre(II) pour la polymérisation de lactide.	25
Figure 1.33 : Complexes dinucléaires diiminopyrrolides produisants des polymères isotactiques.....	26
Figure 1.34 : Couplage d'Ullmann et d'Ullmann-Goldberg.	27
Figure 1.35 : Couplage de Buchwald et Hartwig.	28
Figure 1.36 : Couplage de Buchwald au cuivre.....	28
Figure 1.37 : Couplage de Chan-Evans-Lam.	29
Figure 1.38 : Méthoxylation de l'ester tolylboronique.	30
Figure 1.39 : Mécanisme du couplage de Chan-Evans-Lam.	31
Figure 1.40 : Réaction secondaire de proto-déboration.	31
Figure 1.41 : Réaction secondaire de formation du phénol.....	31
Figure 1.42 : Réaction secondaire de formation du diphenyle.	32
Figure 1.43 : Réaction secondaire de formation du composé diazo.	32
Figure 1.44 : Réaction secondaire de formation d'imine.	33
Figure 1.45 : Compétition entre la O- et N-arylation de l'acide p-tolylboronique.....	34
Figure 1.46 : Réactivité groupement amidé.....	34

Figure 1.47 : Courbe de Hammett pour le substrat boronique appliqu� au couplage de Chan-Evans-Lam. ⁷²	35
Figure 1.48 : Premier couplage catalytique de la r�action de Chan-Evans-Lam.....	36
Figure 1.49 : R�action de Chan-Evans-Lam avec un catalyseur de cuivre sur support solide.	37
Figure 1.50 : Catalyse du couplage de Chan-Evans-Lam avec un catalyseur recycl� de type CuFAP.	38
Figure 1.51 : Catalyseur de Lin support� pour le couplage de CEL.	38
Figure 1.52 : Couplage de CEL avec un Cu ₂ -CD.	39
Figure 1.53 : Complexe de cuivre propos� par l�quipe de Chen pour la catalyse du couplage de CEL.....	39
Figure 1.54 : Complexe de cuivre propos� par l�quipe de Gogoi pour la catalyse du couplage de CEL.....	40
Figure 1.55 : Complexe de cuivre propos� par l�quipe de Chitosan pour la catalyse du couplage de CEL.....	41
Figure 1.56 : Complexe de cuivre propos� par l�quipe de Phukan pour la catalyse du couplage de CEL.....	41
Figure 1.57 : R�activit� des d�riv�s bor�s.	42
Figure 1.58 : Sels de trifluoroborate d'aryle et d'alc�nyle comme agent de couplage.	43
Figure 1.59 : Triolborate aryle de potassium comme agent de couplage.....	43
Figure 1.60 : Borylation et catalyse de CEL one-pot.....	44
Figure 1.61 : N-arylation versus O-arylation.....	44
Figure 1.62 : Protocole de Watson.	45
Figure 1.63 : Lam protocole pour les acides alc�nyles boroniques.....	45
Figure 1.64 : Les complexes trivinylboroxine/pyridine dans le couplage CEL.....	45
Figure 1.65 : Vinyls boronates en r�action.....	46
Figure 1.66 : L'acide cyclohexyle-boronique comme substrat dans le couplage de CEL.	46
Figure 1.67 : Tsuritani protocole pour le couplage avec l'acide cyclopropyle boronique.	47
Figure 1.68 : Zhu protocole pour le couplage avec l'acide cyclopropyle boronique.	47
Figure 1.69 : Monom�thylation de l'aniline.	47

Figure 1.70 : Cruces protocole pour le couplage avec l'acide cyclopropyle boronique.....	48
Figure 1.71 : Alkylboranes en réaction co-catalysée par du cuivre et un oxydant.	48
Figure 1.72 : Chan réaction avec les amines.	49
Figure 1.73 : Lam réaction avec les hétérocycles.	49
Figure 1.74 : Collman réaction avec les hétérocycles.	50
Figure 1.75 : Couplage avec les phénols.....	51
Figure 1.76 : Borylation/couplage avec phénol.....	51
Figure 1.77 : Réaction de Chan avec les thiols.	52
Figure 1.78 : Couplage de CEL avec les sulfinates.	52
Figure 1.79 : Couplage de CEL avec les thio-sulfonates.	53
Figure 1.80 : Couplage de CEL avec les disulfides.	53
Figure 1.81 : Protocole de couplage de thiol en milieux aqueux.	53
Figure 1.82 : Protocole de couplage des thiols avec un complexe de CuDMAP.	54
Figure 1.83 : Protocole de couplage des thiols avec un complexe portant un ligand de type salen.	54
Figure 1.84 : Complexes organométalliques cuivrés ciblés.....	56
Figure 1.85 : Coordination/décoordination du groupement sulfonate du ligand du métal pour la polymérisation de lactide.....	56
Figure 1.86 : Précoordination facilitant la transmétallation.	57
Figure 2.1 : X-ray structure of 3 . Hydrogen atoms were omitted for clarity. Thermal ellipsoids are drawn at 50% probability. Selected geometrical data: Bond distances [Å]: Cu1–Cl1: 2.2408(8), Cu1– Cl2: 2.2488(8), Cu1–N1: 1.998(2), Cu1–N2: 2.002(2), Li1–Cl2: 2.371(5), Li1–O2: 1.906(5), Li1–O3i : 1.909(5), Li1–N3: 2.030(5), S1–O1: 1.437(2), S1–O2: 1.460(2). Bond angles [°]: Cl1–Cu–Cl2: 95.48(3), N1–Cu1–N2: 92.32(9), X–Li1–Y: 96.2(2)–120.2(3).	68
Figure 2.2 : Crystal structure of 4 . Hydrogen atoms omitted for clarity.	70
Figure 2.3 : X-ray structure of 5 (left) and 6 (right). Hydrogen atoms and co-crystallized dichloromethane in 6 are omitted for clarity. Thermal ellipsoids are drawn at 50% probability.	70

Figure 2.4 : Top left: UV/vis spectra of **4** in methanol in the presence of 20 equiv of water. Top right: Change of the intensity of absorption at 700 nm over time in the presence or absence of an excess of water. Bottom left: Crystal structure of **4·2 H₂O**. Bottom right: Crystal structure of **7**. Hydrogen atoms (other than those of water), cocrystallized THF (**7**), and the second, similar molecule in the asymmetric unit (**7**) omitted for clarity. Ellipsoids drawn at 50% probability.

..... 72

Figure 2.5 : Decomposition products identified by X-ray diffraction. Bottom left: Crystal structure of **8**, bottom right: crystal structure of **9**. Hydrogen atoms, disordered THF (**8**), co-crystallized bis(pyridylmethoxide)copper, and CH₂Cl₂ (**9**) omitted for clarity (see Figure 2.S1 for full structure). Thermal ellipsoids drawn at 50% probability. 74

Figure 2.6 : Time-concentration profile for the coupling of aniline with phenylboronic acid. Conditions: 1 M aniline in CH₂Cl₂, 2.5 mol % **5**, 1.5 M PhB(OH)₂ (squares, circles) or 3.0 M PhB(OH)₂ (triangles). The inset shows the linearized plot according to first-order kinetics.... 83

Figure 3.1 : X-ray structure of **2**. Thermal ellipsoids are drawn at 50% probability. Hydrogen atoms and co-crystallized dichloromethane were omitted for clarity. Selected bond distances (Å) and angles (°): Cu-N1 = 2.0261(13), Cu-N2 = 1.967(1), Cu-O1 = 1.929(1), Cu-O4 = 2.015(1), Cu-O2= 2.379(1), Cu-O4 = 2.488(1), N1-Cu-N2 = 81.89(5), N2-Cu-O4 = 93.58(5), O1-Cu-O4 = 91.38(5), N1-Cu-O1 = 94.25(5), X-Cu-O2 = 82.18(4)- 94.18(5). 102

Figure 4.1 : Crystal structures of **2** (left) and **4** (right). Thermal ellipsoids were drawn at the 50% probability level. Hydrogen atoms, cocrystallized water (**2**) and the anion (**4**) were omitted for clarity..... 131

Figure 4.2 : Conversion-time profiles for the arylation of aniline with PhB(OH)₂ in methanol ([PhNH₂] = 1.0 M, [PhB(OH)₂] = 1.5 M, [Cu] = 25 mM, RT, air). Black triangles: **3**, average of 4 experiments, k_{app} = 0.50(1) h⁻¹. Red circles: **1**, average of 4 experiments, k_{app} = 0.40(2) h⁻¹. For the deviations at high conversion, see discussion of reaction kinetics. 135

Figure 4.3 : Semi-logarithmic conversion-time profiles for the arylation of aniline with PhB(OH)₂ catalyzed by **1** under various pre-activation conditions ([PhNH₂] = 1.0 M, [PhB(OH)₂] = 1.5 M, [Cu] = 25 mM, RT, air). The two datapoints per time indicate conversions calculated from appearance of diphenylamine and disappearance of aniline, respectively. 136

Figure 4.4 : Left: UV/vis titration of **3** (58 μM) in MeOH with aniline. The inset shows the isosbestic point obtained until 25 mM aniline. Middle: Absorption at different wavelengths vs aniline concentration. The lines indicate the results of the simultaneous non-linear regression presuming reaction with 2 aniline in the second equilibrium. Right: Concentration of **3** and its aniline adducts at different aniline concentrations, calculated from $K_1 = 50 \text{ M}^{-1}$ and $K_2 = 10 \text{ M}^{-2}$ 141

Figure 4.5 : Conversion vs time profile for the *N*-arylation of aniline. Four independent reactions under identical conditions are shown (MeOH, RT, 1.0 M aniline, 1.5 equiv PhB(OH)₂, 2.5 mol% **3**). Filled symbols: conversion determined from remaining aniline. Hollow symbols: conversion determined from diphenyl amine product. The solid, black line is calculated from the pseudo-first-order rate constant $k_{\text{app}} = 0.50(1) \text{ h}^{-1}$, determined from all datapoints in the range of 30-140 min. The blue, dashed line is the best-fit conversion trace with a pseudo-first-order rate constant $k_{\text{app}} = 0.82 \text{ h}^{-1}$ and an equilibrium constant of $K_1 = 1 \text{ M}^{-1}$ for the coordination of aniline to **3**. The inset shows the linearized $\ln(c^0/c)$ plot. 146

Figure 4.6 : Conversion vs time profile for the *N*-arylation of aniline under different reactant concentrations (MeOH, RT, 1.0 M aniline). Squares, 1.5 M PhB(OH)₂, 2.5 mol% **3**, average of 4 experiments; red circles, 3.0 M PhB(OH)₂, 2.5 mol% **3**, 2 experiments; brown, hollow circles: 1.0 M PhB(OH)₂, 2.5 mol% **3**; diamonds, 1.5 M PhB(OH)₂, 5.0 mol% **3**; triangles, 1.5 M PhB(OH)₂, 1.0 mol% **3**, 2 experiments. The inset shows the linearized $\ln(c^0/c)$ plot. 147

Figure 4.7 : UV/vis spectra of **3** in methanol upon addition of phenylboronic acid. The slight apparent increase in ε is due to uncorrected trailing absorption of the phenylboronic acid added. 150

Figure 4.8 : Displacement of chemical shifts in the NMR spectra of aniline upon addition of phenylboronic acid (left) or of phenylboronic acid upon addition of aniline (right). The solid line represents the theoretical displacement assuming an equilibrium constant of $K_{AB} \approx 1 \text{ M}^{-1}$. 152

Figure 4.9 : Conversion vs time profiles for the *N*-arylation of aniline under different reactant concentrations (MeOH, RT, 1.0 M aniline). Solid lines are the simulated conversions based on $v = k\text{PhB(OH)}_2\text{PhNH}_2[\text{LCuX}]^{0.5}$ under consideration of aniline coordination to

phenylboronic acid. K_{AB} and k refined to best-fit values of $k = 0.4 \text{ M}^{-1.5}\text{min}^{-1}$ and $K_{AB} = 5 \text{ M}^{-1}$ (see supp. information).....	153
Figure 4.10 : Conversion vs time profile for the <i>N</i> -arylation of aniline with 3 /Cu(OAc) ₂ or Cu(OAc) ₂ only. solid squares: 3 /Cu(OAc) ₂ , FC ₆ H ₄ B(OH) ₂ ; hollow squares: Cu(OAc) ₂ , FC ₆ H ₄ B(OH) ₂ , two independent reactions with different induction periods shown; solid diamonds: 3 /Cu(OAc) ₂ , PhB(OH) ₂ ; hollow diamonds: Cu(OAc) ₂ , PhB(OH) ₂ . (MeOH, RT, 1.0 M aniline, 1.5 equiv ArB(OH) ₂). Solid lines are the simulated conversions calculated from the rate constants and induction periods determined by linear regression (Table 4-8, Fig. 4.S10)....	162
Figure 5.1 : X-ray structures of 2 (left), 3 (middle), and 4 (right). Hydrogen atoms, second molecule in the asymmetric unit (2) and anion disorder (2) omitted for clarity. Thermal ellipsoids are drawn at the 50% probability level. The insets show the 1D-coordination polymers formed by 2 and 4	194
Figure 5.2 : X-ray structures of 6 (left), 7 (middle), and 8 (middle) and 8b (right). Hydrogen atoms and anion disorder in 8 omitted for clarity. Thermal ellipsoids are drawn at the 50% probability level. The inset shows the 1D-coordination polymers formed by 8	200
Figure 5.3 : UV/vis spectra of 1-4 (left) and 5-8 (right).	202
Figure 5.4 : Crystal structure of 15 . Hydrogen atoms other than H ₂ were omitted for clarity. Thermal ellipsoids are drawn at the 50% probability level.	204
Figure 5.5 : X-ray structure of 17 . Hydrogen atoms were omitted for clarity. Thermal ellipsoids are drawn at the 50% probability level.....	209
Figure 5.6 : Selected kinetic traces for CEL couplings of aniline with phenylboronic acid catalysed by 1 and 5-8 . Conditions: 1.0 M aniline, 1.5 M PhB(OH) ₂ , 2.5 mol% [cat.], MeOH, RT. Two datapoints per time point indicate conversions determined independently from the concentration of remaining aniline and from the concentration of formed product. Solid lines are theoretical curves obtained in linear regression analysis of the semi-logarithmic plot in the pseudo-first order region of the profile (see Supp. Information for details).....	213
Figure 6.1 : X-ray structures of 1 (left), 3 (middle left), 4 (middle right) and 5 (right). Thermal ellipsoids are drawn at the 50% probability level. Hydrogen atoms and co-crystallized water (1 ,	

3, 4) and the nitrate anion (3) omitted for clarity. The inset shows the 1D coordination polymer (5) _n	242
Figure 6.2 : Crystal structures of 6 and 7 . Thermal ellipsoids are shown at 50% probability. Hydrogen atoms omitted for clarity.	245
Figure 6.3 : UV/vis spectra of 1 - 7 in DMSO.	247
Figure 6.4 : Concentration-time profiles for CEL couplings of cyclohexylamine with phenylboronic acid, catalyzed by 1-6 . Conditions: 1.0 M cyclohexylamine, 1.5 M PhB(OH) ₂ , 2.5 mol% catalyst, MeOH, RT, air. Conversion was calculated from absolute concentrations of product and starting material, obtained by calibrated GC-MS analyses vs. internal standard. The solid lines are theoretical conversions using the pseudo-first-order rate constants determined by linear regression of the semilogarithmic plot.....	253

Liste des abréviations

« m » diade meso

« r » diade racémique

Ac acétyle

APTS Acide paratoluènesulfonique

Ar aryle

ATP adénosine-triphosphate

Bn benzyle

bpy bipyridine

Cat catalyseur

CD cyclodextrine

CEL Chan-Evans-Lam

CV cyclovoltampérométrie cyclique

d doublet

DCE dichloroéthane

dd doublet de doublet

dipp 2,6-diisopropylphényle

DMAP 4-Diméthylaminopyridine

DMF diméthylformamide

DMSO diméthylsulfoxyde

EPR résonance paramagnétique électronique

équiv. (equiv) équivalent

Et éthyle

FQRNT Fonds de recherche du Québec - Nature et technologies

GC chromatographie phase gazeuse

Gof qualité de l'ajustement

GPC chromatographie par perméation de gel

HDMS Bis(triméthylsilyl)amine

*i*Pr isopropyle

L ligand

LA lactide

LMCT transfert de charge métal ligand

m multiplet

MALDI Désorption-ionisation laser assistée par matrice

Me méthyle

M_w/M_n polymolécularité d'un polymère

MS spectroscopie de masse

nacnac β -diketiminate, diiminate

NAD nicotinamide adénine dinucléotide

NMP N-Méthyl-2-pyrrolidone

NSERC Natural Sciences and Engineering Research Council

o position ortho

Oct octyl

OTf triflate

p position para

PC photocatalyseur

PDI index de polydispersité

Ph phényle

PLA polylactide, acide polylactique

P_m probabilité de générer un diade « m » par insertion ppm partie par million

ppm partie par million

P_r probabilité de générer un diade « r » par insertion

Py pyridine

q quadruplet

rac- mélange racémique

ref. référence

Rint *merging error* mesure précision

RMN/NMR résonance magnétique nucléaire / nuclear magnetic resonance

ROP polymérisation par ouverture de cycle

RT *room temperature* (temperature ambiante)

R1 facteur de confiance sur les données observées

R σ ratio signal sur bruit

s singulet

SET transfert à un électron

t triplet

T température

tBu tert-butyle

TEMPO (2,2,6,6-tétraméthylpipéridin-1-yl)oxy

THF tétrahydrofurane

T_m température fusion

TMEDA Tétraméthyléthylènediamine

TOF « Turn-Over Frequency » fréquence de passage de cycle

TON « Turn-Over Number » nombre de passage de cycle

T_p température pièce

UV-vis ultraviolet visible

wR2 facteur de confiance sur toutes les données

1D une dimension

3D trois dimensions

*À la mémoire de mon
père, mon amour pour toi ne
s'éteindra jamais.*

Remerciements

En premier lieu, je souhaite exprimer ma profonde reconnaissance au Pr Frank Schaper pour m'avoir accueilli au sein de son groupe de recherche et permis de réaliser cette thèse de doctorat. Son encadrement, son enseignement et ses conseils avisés m'ont permis de travailler sur mes projets efficacement et de rapporter plusieurs publications dans cette thèse. Grâce à notre travail, j'ai acquis de nombreuses connaissances et compétences supplémentaires durant mes recherches par rapport à ma formation initiale qui me seront utile pour la suite de mon parcours professionnel. La liberté qu'il m'a offerte dans la gestion de mes travaux de recherche, et la possibilité de superviser des stagiaires durant ma thèse furent très appréciées pour la réussite de ce doctorat. De plus, je lui adresse toute ma gratitude pour m'avoir permis de participer et présenter mes résultats de recherche à différentes conférences à travers le Canada.

Mes remerciements s'adressent également aux professeurs qui ont accepté de faire partie du jury de ma thèse et d'évaluer ce manuscrit. Merci du temps que vous accordez à lecture de mon mémoire et des discussions passées sur ma recherche.

Je tiens également à remercier tous mes collègues du groupe, membres présents et passés, avec qui j'ai eu la chance de partager le laboratoire dans la bonne humeur. Par Gol, Leila, Sueli et Fatima ont notamment contribué à rendre ces années stimulantes et enrichissantes.

Je veux également adresser mes remerciements aux membres des groupes des professeurs Zargarian, Hanan, Reber et Skene avec qui j'ai eu plaisir à interagir tout au long de ma thèse que ce soit sur des sujets professionnels ou personnels. Leur présence auprès de moi fut source d'inspiration, d'échange et de découverte. Parmi eux, je souhaite remercier, spécifiquement, Loïc Mangin et Jean-Phillipe Cloutier pour le temps qu'ils ont consacré à l'entretien et au bon fonctionnement de la GC-MS utilisé pour mes analyses.

Concernant les employés de l'Université de Montréal, je voudrais remercier Thierry Maris du service de cristallographie pour m'avoir formé afin d'utiliser de manière autonome l'appareil de diffraction des rayons-X. Merci à lui de m'avoir transmis son savoir et d'avoir toujours été prêt à donner de son temps pour la résolution de structure cristalline difficile. Dans le service d'analyse élémentaire, je souhaite saluer le travail, principalement, d'Elena Nadezhina, mais également de Mihaela Cibian. Chaque analyse fut l'objet un travail appliquée et rapide qui contribua au bon avancement des projets. Je désire remercier, de plus, Sylvain Essiembre et Pierre Tremblay pour leur formation et constante disponibilité pour l'utilisation de l'appareil de GPC.

Un grand merci à tous les stagiaires qui ont travaillé sous ma supervision durant ma thèse, en particulier Clémentine Dimeck, Neha Choudarhy, Alexandre Thouvenin et Guillaume Bano. Leur investissement dans mes projets de recherche, de par leur motivation et leur productivité en laboratoire, m'ont permis de progresser dans les divers projets de recherche sur lesquels j'ai travaillé. Leur présence au sein du groupe contribua également à travailler dans un milieu possédant constamment une bonne ambiance.

Enfin, je voudrais remercier de tout mon cœur ma mère et mes frères et soeurs pour leur patience et leur support moral dans toutes les épreuves de la vie auxquelles nous avons été confrontés durant mon doctorat. Je suis fière de la force de ma famille qui m'a permis d'aller au bout de ma thèse malgré les difficultés personnelles.

1. Introduction

1.1. Généralités sur le cuivre

Le cuivre, qui est de la même famille que l'argent et l'or, est un élément du bloc *d* faisant partie des métaux de transition.¹ Le cuivre est l'un des plus vieux métaux connus de l'homme et est naturellement présent dans la croûte terrestre, à raison d'environ 550 millions de tonnes. Ce fut le premier métal travaillé par l'homme et de nos jours il est majoritairement utilisé sous forme de métal. Des objets en cuivre furent découverts en Iran datant de plus de 5 000 ans avant J.-C, de même que des mines de cuivre qui étaient exploitées au Moyen-Orient, dans les Balkans et sur l'île de Chypre (l'ère du cuivre est situé entre 3 000 et 2 000 avant J.-C, Figure 1.1).²



Ustensiles de cuisine

Tuyauterie

Monnaie

Figure 1.1 : Anciennes utilisations du cuivre par l'homme (reproduit avec permission).³

Le cuivre est toujours un métal utilisé, du fait qu'il reste relativement peu cher, bien que l'augmentation de sa consommation, au cours de ces dernières années, ait provoqué une hausse constante de son prix, jusqu'à une certaine stabilisation ces dernières années. Ces propriétés mécaniques (ductile et malléable), thermiques (bon conducteur de chaleur) et électroniques (bon conducteur d'électricité) sont bien connues, ce qui le rend utile dans

l'électronique et la télécommunication. Des alliages peuvent également être produits, en le combinant à d'autres métaux pour améliorer ses propriétés physiques. Dans les systèmes biologiques, le cuivre à faible dose est essentiel au développement de toute forme de vie et intervient dans un grand nombre de processus tels que le transfert d'électrons, la gestion des métaux, le transport de l'oxygène (hémocynine) et, parfois, il est impliqué dans des activités catalytiques.⁴

Le cuivre se trouve principalement dans les états d'oxydation 0 sous forme métallique ou élémentaire, +I et +II (Figure 1.2). Le cuivre(I) possède une configuration électronique d^{10} donnant généralement des composés incolores, sensibles à l'air et à l'humidité, qui peuvent être disproportionnés pour donner des espèces de cuivre(II) et de cuivre(0). D'autre part, les composés de cuivre(II), les plus répandus, ont une configuration électronique d^9 , se caractérisent par une couleur bleue ou verte et montrent plus de stabilité dans l'air que les composés de cuivre(I).⁵



Cu(0)

ta

Cu(I)

CuCl

[Ar] $3d^{10}$

Cu(II)

$\text{CuSO}_4 \cdot 5 \text{ H}_2\text{O}$

[Ar] $3d^9$

Figure 1.2 : Degré d'oxydation du cuivre les plus courants (Reproduit avec permission⁶).

Finalement, les composés du cuivre(III) sont très réactifs, particulièrement vers l'élimination réductrice et donc peu de complexes organocuivrés avec le centre métallique à l'état d'oxydation +III ont été isolés.⁸ Les quelques complexes publiés dans la littérature sont

constitués de ligand rigide, chelatant et/ou perfluoré.⁷ Cependant ils sont souvent postulés comme intermédiaires dans les cycles catalytiques.

L'utilisation du cuivre et la connaissance des mécanismes de réactions sont peu développées par rapport à d'autres métaux comme le palladium. En général, les réactions catalysées par le cuivre(I) passent par un processus similaire au palladium comprenant une addition oxydante, un échange de ligand et une élimination réductrice, avec un cycle catalytique où le cuivre passe par les états d'oxydation Cu(I)/Cu(III) (Figure 1.3). Mais la stabilité du cuivre à l'état d'oxydation +II permet des réactions qui impliquent un transfert d'un électron, d'où des mécanismes pouvant contenir les trois états d'oxydation Cu(I), Cu(II) et/ou Cu(III).

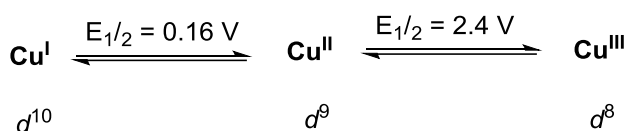


Figure 1.3 : États d'oxydation du cuivre et leurs potentiels réducteurs dans l'eau.

La chimie du cuivre est très riche à cause de ces multiples états d'oxydation possibles, ce qui fait qu'il peut réagir par différents processus à un ou deux électrons. Le cuivre(III), isoélectrique avec Pd(II), induit une élimination réductrice de manière rapide et spontanée pour former le produit. Le Cu(I) est formellement isoélectronique au Ni(0) et en raison de sa charge positive et de sa taille plus petite, le Cu(I) est un acide de Lewis plus dur que Ni(0) et a donc une plus grande affinité pour les ligands contenant les éléments O et N.

L'accessibilité des états d'oxydation (I) et (II) est utilisé par exemple, dans la polymérisation radicalaire par transfert d'atome (ATRP) où le cuivre gère la réactivité des radicaux libres (Figure 1.4).⁸

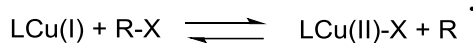


Figure 1.4 : Polymérisation radicalaire par transfert d'atome (ATRP).

Découverte en 1995 par Sawamoto et Matyjaszewski, cette polymérisation radicalaire vivante permet de former des polymères avec un poids moléculaire contrôlé, grâce à l'utilisation d'un

catalyseur constitué d'un métal de transition. Ce catalyseur engendre un équilibre entre une forme active (propageante) et une forme inactive du polymère (dormante).

Le cuivre est un métal peu cher, très répandu et non toxique, ce qui fait de lui un métal très intéressant à utiliser dans le domaine de la métallurgie et l'insdustrie chimique par exemple. Ainsi, ses propriétés chimiques sont largement étudiées, depuis de nombreuses années, dans des processus catalytiques, pour diverses applications de synthèse. L'origine de la chimie du cuivre remonte à 1869, date où Carl Glaser a découvert la synthèse des 1,3-diynes, par réaction d'homocouplage des alcynes terminaux avec l'addition d'ammoniaque, de chlorure de cuivre(I) et d'oxygène (Figure 1.5).⁹

Bien plus tard, en 1962, Allan Hay a également développé l'homocouplage des alcynes terminaux en utilisant une quantité catalytique de cuivre et de TMEDA (Figure 1.5).¹⁰ Le système cuivre-TMEDA utilisé est soluble dans une gamme plus large de solvants, de sorte que la réaction de couplage bien connu de Glaser-Hay est de nos jours utilisée dans divers domaines de recherche, pour la préparation d'oligomères et de polymères linéaires acétyléniques et la polymérisation de diacétylènes.¹¹

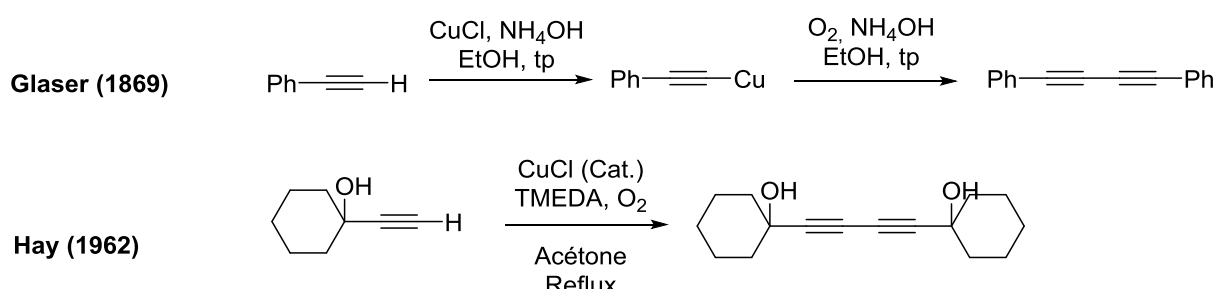


Figure 1.5 : Réaction de Glaser-Hay.

Les fondements de la catalyse moderne du cuivre ont été établis à partir des travaux de recherche menée par Ullmann et Goldberg dans les années 1900 (Figure 1.6).¹²

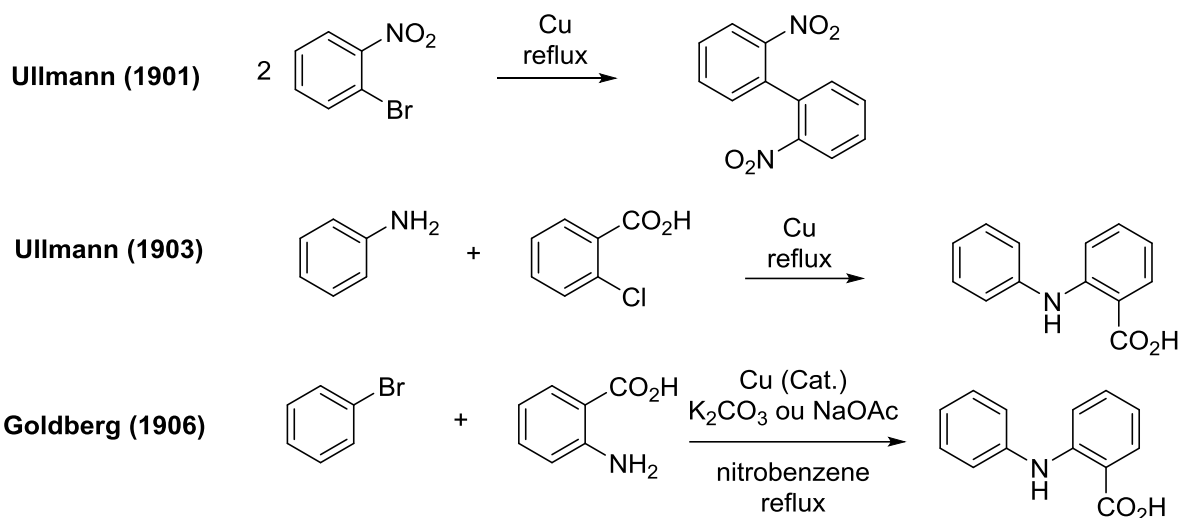


Figure 1.6 : Utilisation du cuivre en catalyse organique.

Le couplage d'Ullmann, rapporté pour la première fois en 1901 est un homocouplage de deux molécules d'halogénures d'aryle utilisant une quantité stœchiométrique de cuivre métallique (Figure 1.6).^{13a} Ullmann a ensuite rapporté une réaction de couplage croisé de l'acide orthochlorobenzoïque et de l'aniline, avec l'ajout de cuivre et à haute température, en 1905.^{13b} Après les travaux d'Ullmann, Goldberg a ensuite découvert que la réaction de couplage pouvait être réalisée en employant uniquement des quantités catalytiques de cuivre.^{13c} En effet, le couplage du bromobenzène et de l'acide anthranilique, en présence de carbonate de potassium, et de quantités catalytiques de cuivre, à haute température, donne le produit souhaité. Cette découverte fut une grande avancée puisque ces réactions peuvent être utilisées dans diverses applications industrielles : la synthèse de polymères et la synthèse organique de blocs de construction pour aboutir à différentes molécules plus grandes.¹³

Les premiers complexes organométalliques de cuivre furent synthétisés par Gilman en 1952. Dans cette première publication, le premier organocuprate lithié est rapporté (Figure 1.7).¹⁴ Depuis, les organocuprates lithiés (homocuprate) de type (R_2CuLi) sont aussi appelés réactifs de Gilman avec R étant un radical organique.

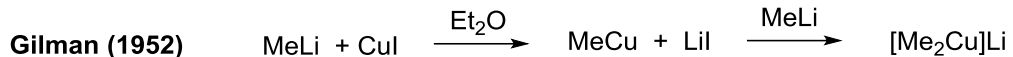


Figure 1.7 : Réaction de Gilman.

Sharpless, en 2001, introduit le terme de "Click Chemistry" pour décrire les réactions spécifiques, simples et à hauts rendement, fonctionnant sur une large gamme de substrats et créant seulement des sous-produits pouvant être enlevés sans chromatographie.¹⁵ Par exemple, la réaction de cycloaddition 1,3-dipolaire azide-alkyne, initialement rapporté par Huisgen, forme sélectivement à haute température des triazoles via un mécanisme concerté (Figure 1.8).¹⁶ Cependant, elle mène généralement à deux régioisomères lorsqu'un alcyne asymétrique est utilisé, ainsi dans ces conditions cette réaction n'entre pas dans les réactions dites de "Click Chemistry".

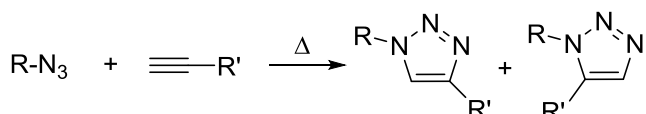


Figure 1.8 : Réaction de Huisgen.

La variante développée par Meldal et Sharpless en milieu aqueux et à température ambiante est catalysée par le cuivre (Figure 1.9).¹⁷ Cette réaction permet la synthèse du régioisomère 1,4-disubstitué spécifiquement et suit les règles déterminant une réaction de type « Click chemistry ».

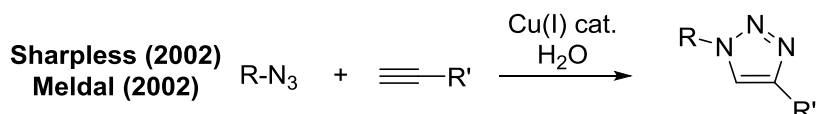


Figure 1.9 : Réaction de Sharpless-Meldal.

Malgré ces recherches prometteuses sur le cuivre comme catalyseur, le développement des méthodes de couplage croisé s'est concentré sur l'utilisation de catalyseurs de métaux précieux, comme le palladium. Cependant, un système de catalyse au

cuivre porte des avantages et les progrès dans la chimie moderne du cuivre le prouvent. Par exemple, certaines tolérances de groupes fonctionnels, problématiques dans les réactions catalysées par le palladium, ont forcé les chimistes à étudier d'autres métaux de transition comme catalyseurs et le cuivre est une alternative intéressante. Les groupes de Ma, Buchwald et Taillefer ont largement contribué à la révolution de la catalyse du cuivre et leurs travaux seront détaillés dans le chapitre 1.3.¹⁸ Maintenant, les réactions modernes catalysées par le cuivre peuvent se dérouler dans des conditions plutôt douces avec des rendements plus élevés, et elles ont été considérées comme un outil efficace de la synthèse organique.

Toutes ces observations nous ont poussés à choisir ce métal dans des projets visant à développer de nouveaux complexes sulfonatés pour des applications en catalyse de polymérisation de lactide et de couplage de Chan-Evans-Lam.

1.2. Polymérisation de lactide

Les polymères d'origine biotechnologique sont issus d'une combinaison de procédés biologiques et de la synthèse classique. Le polylactide (PLA) fait partie de ce type de polymère puisque des bactéries transforment l'amidon en acide lactique, qui sera à son tour transformé en PLA, à l'aide de procédés de synthèse classique. Plusieurs facteurs incitent à l'utilisation de plastiques biosourcés comme le PLA, faisant de lui un polymère au centre de nombreux projets de recherche.

1.2.1. Intérêt dans les polymères biodégradables et renouvelables

La forte dépendance de notre société envers les ressources pétrolières est devenue aujourd'hui un problème. La hausse de la consommation de ces ressources entraîne une baisse rapide des réserves terrestres et à long terme un manque potentiel. L'exploitation de réserve pétrolière ne peut être infinie, ce qui entraînera une augmentation des coûts. Du point de vue écologique, l'extraction et l'utilisation du pétrole sont très néfastes à l'environnement. En effet, de grandes quantités de gaz sont libérées et non valorisées contribuant à l'effet de serre

durant l'extraction, le transport, le traitement et l'utilisation de cette ressource naturelle fossile.

De nos jours, les considérations environnementales prennent une place importante. Dans le milieu industriel et de la recherche académique, de nouvelles orientations sont prises pour trouver des solutions à cette dépendance et à la dégradation de notre milieu de vie. Ainsi, beaucoup de recherches dans le domaine des polymères s'orientent maintenant sur des matériaux issus de ressources renouvelables et compostables, ce qui fait du PLA un très bon candidat pour remplacer les plastiques produits à partir du pétrole.¹⁹

Malgré l'enjeu, le marché des bioplastiques représente seulement 1% sur la totalité du marché, cependant leurs productions futures devraient fortement augmenter notamment pour le PLA (Figure 1.10).²⁰ Il existe deux principaux types de bioplastiques : les bioplastiques durables et les bioplastiques biodégradables.

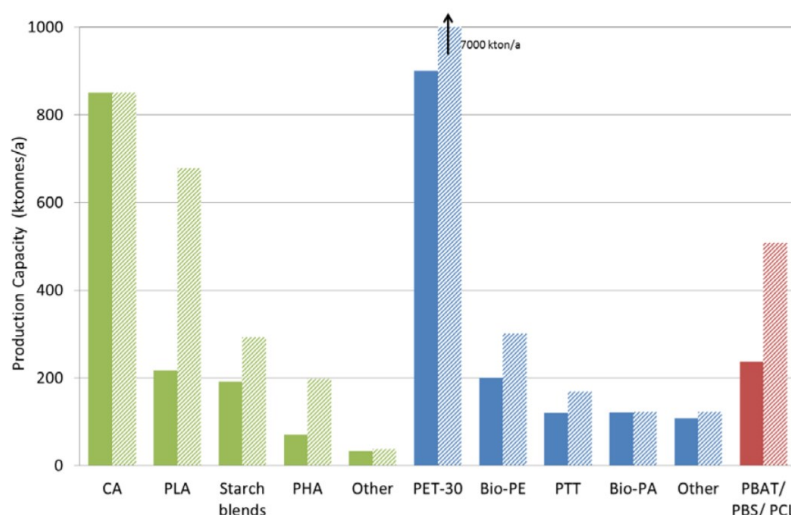


Figure 1.10 : Production des biopolymères en 2015/2016 (barres solides) et production annoncée pour 2020 (barres ombrées) en vert les bioplastiques biodégradables et en bleu les bioplastiques durables (reproduit avec permission).²¹

Les trois bioplastiques les plus répandus sont le biopolyéthylène (bio-PE), le biopolyéthylène téréphthalate (bio-PET) et le polylactide (PLA). Contrairement au PLA, deux d'entre eux ne sont

pas compostables, bien qu'ils soient de nos jours les plus utilisés (bio-PE et bio-PET).²² Le PLA est un polymère thermoplastique semi-cristallin dont les propriétés dépendent du type de lactide utilisé pour la polymérisation. Grâce à ses propriétés physique et chimique, le PLA possède un potentiel d'utilisation très vaste. Différents domaines d'application existent aujourd'hui, la plus ancienne fut dans le domaine pharmaceutique via le développement de produits biomédicaux comme des ustensiles de chirurgie. De nos jours, le PLA est principalement utilisé pour produire des produits domestiques (sacs, emballages, bouteilles, films...). L'application la plus récente s'inscrit dans l'ingénierie où ce type de matériau est utilisé dans l'impression 3D.²¹

1.2.2. Histoire du polylactide

Au 16^{ème} siècle, des écrits parlent déjà de polycondensation d'acide lactique formant des matériaux solides. Cependant, le PLA n'est pas réellement reconnu avant les travaux de Carothers et *al.* qui en 1932 présenta des travaux sur des réactions de polycondensation d'acide lactique en PLA.²² Il fallut 40 ans de plus (dans les années 1970) pour que les avantages et les applications possibles de ce polymère soient reconnus, du fait des coûts de production élevés.²³

Mais il fut, tout de même, le premier polymère biosourcé fabriqué de manière industrielle avec une production qui commença dans les années 1990.^{24a} Depuis ce jour, la production est de plus en plus importante chaque année jusqu'à atteindre de nos jours environ 150 000 tonnes.²⁰

1.2.3. Synthèse naturelle du précurseur de PLA

L'acide polylactique est un polymère créé à partir du monomère d'acide lactique qui est lui-même issu d'un processus de fermentation de l'amidon contenu dans des biomasses renouvelables (Figure 1.11).²⁴ À partir de produits naturels communs comme le maïs et le sucre de canne, l'acide lactide est formé à la fin d'un processus de transformation de plusieurs étapes. L'amidon contenu dans ces produits, qui peut être aisément isolé par un procédé par voie humide, est chauffé en présence d'acide ou d'enzyme pour être hydrolysé en dextrose (D-glucose).^{24a}

Cette première étape de fermentation est suivie d'une glycolyse. La glycolyse convertit le glucose en deux molécules de pyruvate. Lors du métabolisme des plantes, des animaux et de nombreux microorganismes, l'ATP est utilisée comme source d'énergie et NAD⁺ intervient pour oxyder le pyruvate.^{24a} Le pyruvate peut ensuite être métabolisé par un grand nombre de processus dépendant de l'organisme et de l'environnement. Pour former l'acide lactique, un simple processus de réduction a lieu avec NADH comme agent réducteur ce qui termine le processus de fermentation.^{24a}

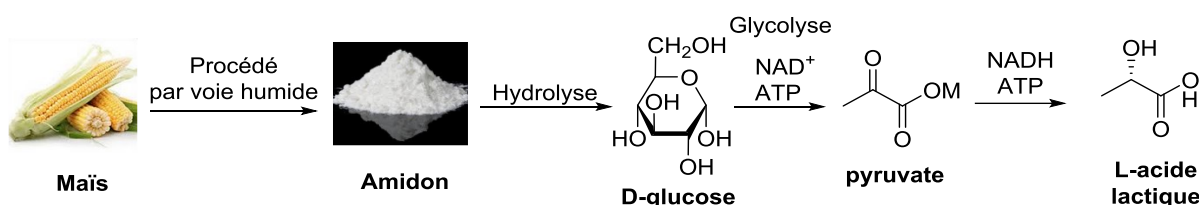


Figure 1.11 : Voie naturelle pour la synthèse de l'acide lactique (reproduit avec permission)²⁵.

1.2.4. Préparation du PLA

Après l'obtention de l'acide lactique par fermentation, deux réactions principales sont utilisées afin de polymériser le monomère : la polycondensation et la polymérisation par ouverture de cycle (Figure 1.12). D'abord, l'acide lactique est polymérisé par polycondensation en polymère de faible masse moléculaire.²⁶ Cette réaction de condensation nécessite un acide fort et une haute température pour former le polymère, en produisant de l'eau comme sous-produit.^{24a} De ce fait, lors de la polycondensation, le polymère double le poids moléculaire donnant lieu à un rapport M_w/M_n large. De plus, pour former des polymères avec de haut poids moléculaires, à chaque étape de la polymérisation, il faut enlever l'eau. Ces observations impliquent que le contrôle de cette réaction est difficile, le rendant ainsi inadéquat pour la plupart des applications industrielles.

Ainsi, afin d'obtenir un polymère de grande masse moléculaire, ce polymère est alors dépolymérisé en lactide. Cette dépolymérisation est une réaction non spécifique qui passe généralement par des réactions d'isomérisations partielles, qui amènent à des contaminations du stéréo-isomère du lactide.²⁷ Ensuite, par la présence de catalyseurs, ces substances

intermédiaires sont polymérisées de nouveau, mais cette fois par ouverture de cycle afin d'élaborer le polylactide (PLA) ayant une masse moléculaire importante et qui peut être utilisé comme matière plastique.²⁸ Il est nécessaire de bien contrôler le type de catalyseur utilisé et les conditions de polymérisation pour minimiser le risque d'isomériser encore plus le carbone chiral.

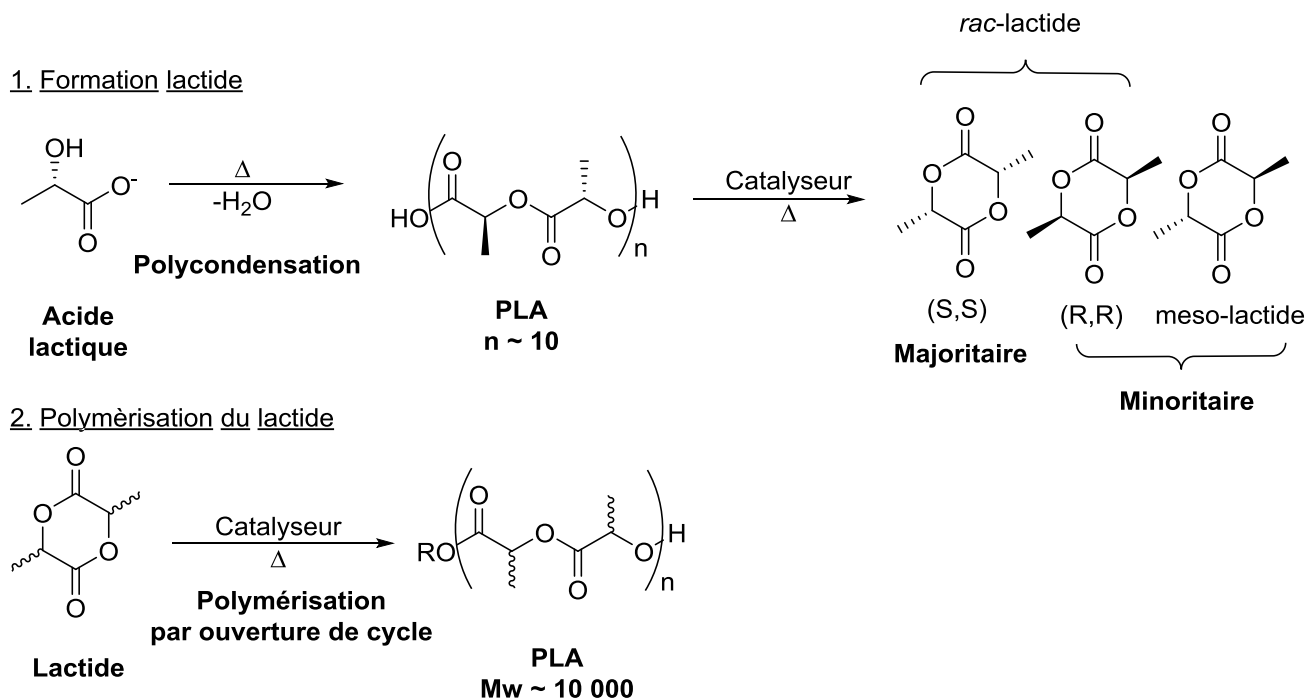


Figure 1.12 : Voie de synthèse du polylactide.

1.2.5. Différents mécanismes de polymérisation du lactide en PLA

L'étape à laquelle nous nous intéressons dans le groupe est la dernière, celle qui conduit à des polymères de haut poids moléculaire. Dépendamment de la nature de l'initiateur de la polymérisation par ouverture de cycle (ROP), plusieurs mécanismes peuvent avoir lieu. La ROP peut suivre cinq types de mécanismes dont deux sont spécifiques aux polymérisations faisant intervenir des complexes de coordination (coordination/embedding et activation du monomère).

Mécanisme anionique

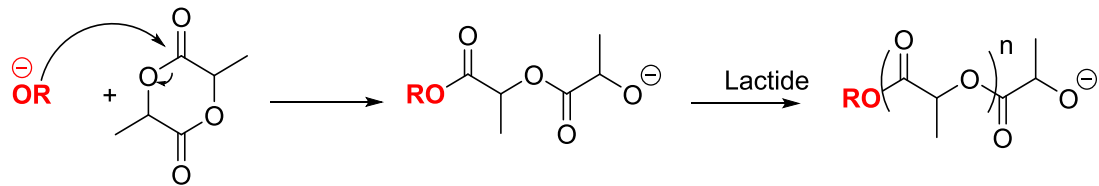


Figure 1.13 : Mécanisme anionique de la synthèse de PLA.

Les systèmes très basiques comme les alcoxydes de métaux alcalins initient la ROP anionique (Figure 1.13). Cette polymérisation est simple, mais est peu contrôlable, car elle entraîne de nombreuses réactions secondaires, comme la racémisation ou la transestérification.²⁹

Mécanisme nucléophile/ « organo-ROP »

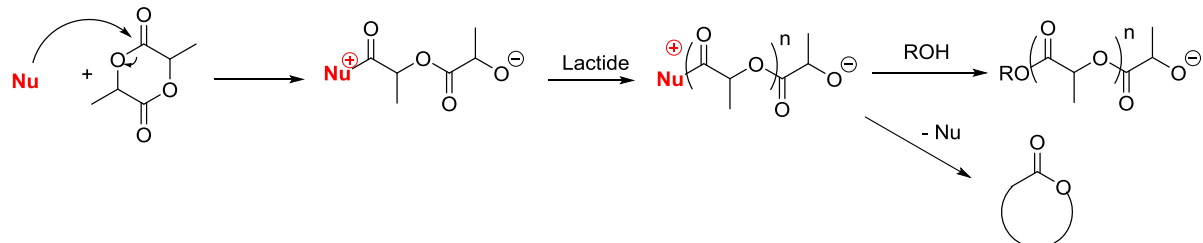


Figure 1.14 : Mécanisme nucléophile de la synthèse de PLA.

Au lieu des anions, les nucléophiles neutres comme la DMAP, peuvent aussi initier l'ouverture du cycle du lactide.³⁰ La propagation de la bétaine formée est similaire au mécanisme anionique, mais le nucléophile neutre ne reste pas dans le polymère, il est soit éliminé en work-up, soit libéré en formant un polymère cyclique (Figure 1.14).

Mécanisme cationique

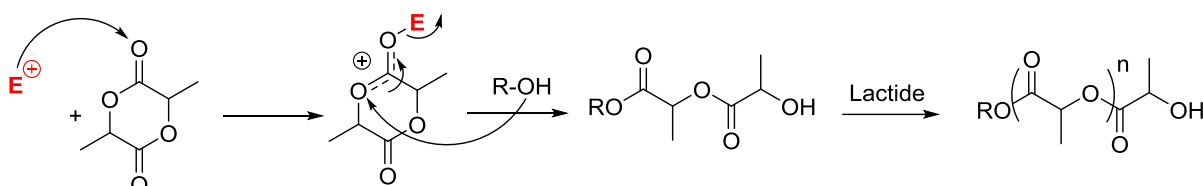


Figure 1.15 : Mécanisme cationique de la synthèse de PLA.

Pour ce mécanisme, le carbonyle du lactide est activé par un cation comme le proton (Figure 1.15).³¹ L'avantage du choix de ce type de mécanisme est la facilité de mise en œuvre, en revanche l'inconvénient est le peu de contrôle de la réaction

Mécanisme activation du monomère³²

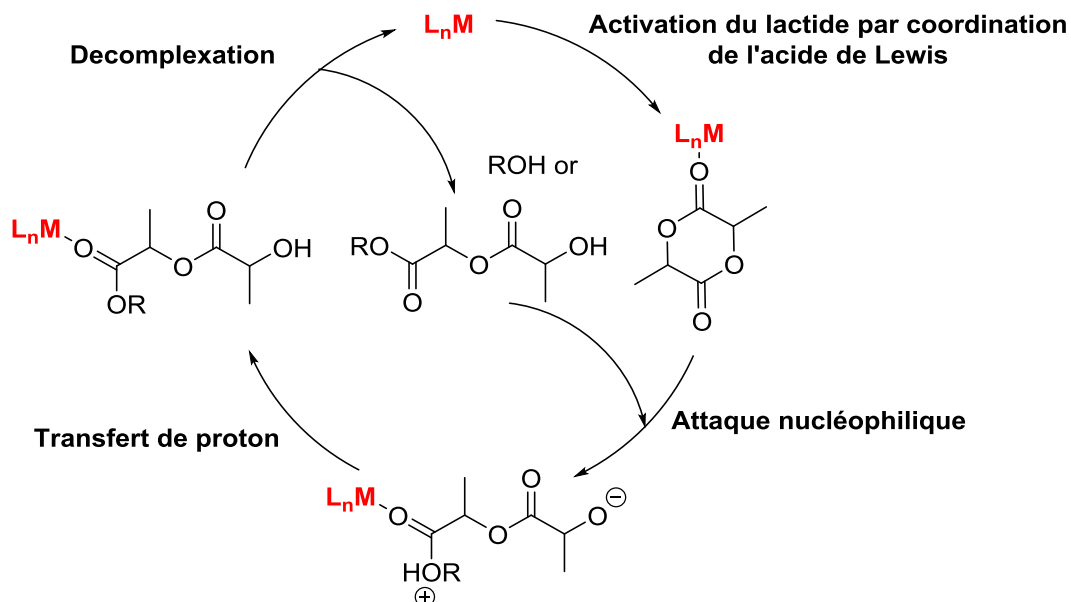


Figure 1.16 : Mécanisme par activation du monomère de la synthèse de PLA.

Des acides de Lewis se coordonnent au lactide puis un alcool s'additionne à l'intermédiaire formé pour donner un complexe zwitterionique et un échange de proton amène à l'alcool polymérique (Figure 1.16). Les complexes de coordination initiant la réaction de polymérisation par ce mécanisme sont typiquement très stables, cependant la réaction est moins facile à contrôler.

Mécanisme coordination-insertion³³

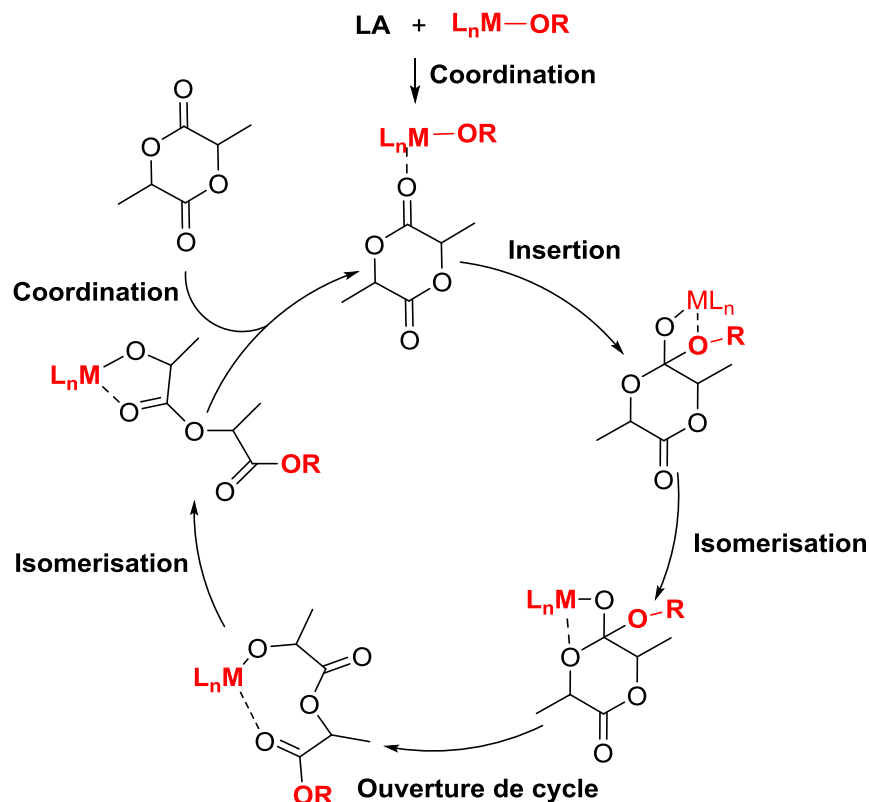


Figure 1.17 : Mécanisme coordination-insertion de la synthèse de PLA.

Le plus souvent les complexes de coordination portant un alcoxyde sont actifs via ce mécanisme (Sn, Zn, Mg, Al, Zr) (Figure 1.17). Le contrôle de la polymérisation est plus élevé, cependant les complexes de type M-OR sont souvent sensibles à l'air et à l'eau.

Au cours de ce processus, plusieurs réactions secondaires peuvent avoir lieu, en particulier des réactions de transestérification (Figure 1.18). Il en existe deux types :

- Intermoléculaire où a lieu une redistribution de chaîne menant à 2 chaînes ayant des poids moléculaires différents
- Intramoléculaire où l'on obtient des polymères cycliques.

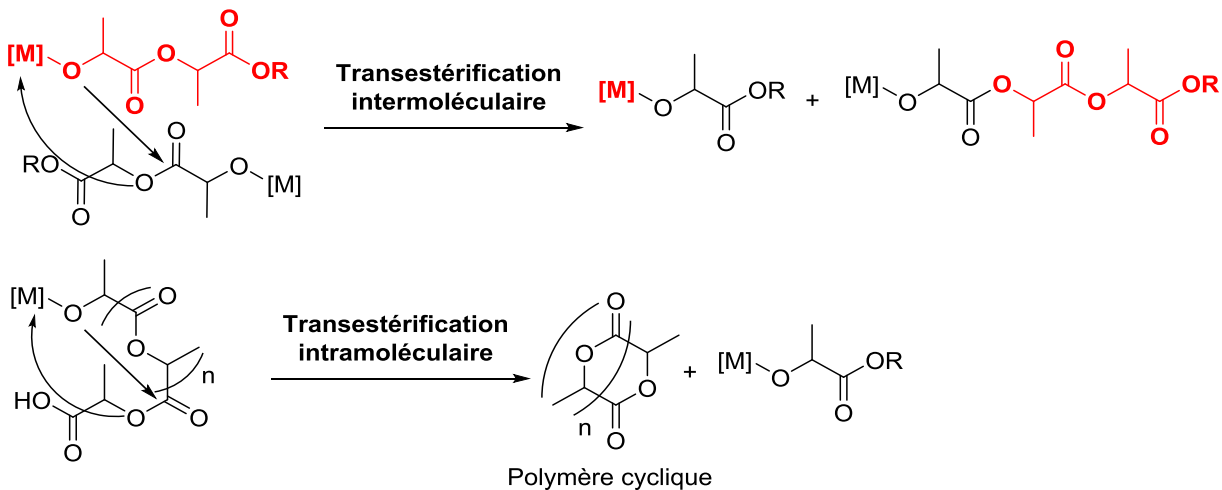


Figure 1.18 : Réactions secondaires de transestérification.

Dans les deux cas, on perd le contrôle sur le poids moléculaire et les réactions de transestérification sont donc à surveiller.

1.2.6. Chiralité et stéréocontrôle

La nature chirale de l'acide lactique induit plusieurs formes distinctes de PLA. Or les propriétés mécaniques et physiques du polymère sont fortement dépendantes de son poids moléculaire, de son PDI et de sa stéréochimie, d'où la nécessité de contrôler la réaction de polymérisation. En effet, la tacticité affecte notamment la température de fusion :

PLA hétérotactique : $T_m = 130 \text{ }^\circ\text{C}$

PLA syndiotactique : $T_m = 153 \text{ }^\circ\text{C}$

PLA isotactique : $T_m = 180 \text{ }^\circ\text{C}$

Le lactide possède deux centres stéréogènes, il existe de ce fait trois isomères de cette molécule : *D*-, *L*- et *DL*-lactide (composé *méso*) (Figure 1.19).

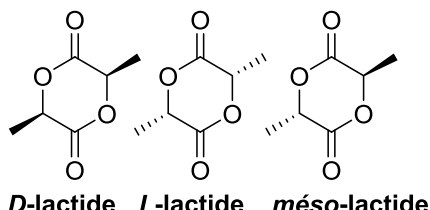


Figure 1.19 : Isomères du lactide

Les isomères du lactide sont commercialement disponibles sous forme pure ou sous forme racémique. Du fait de la présence de ces centres stéréogènes, le stéréocontrôle de la réaction de ROP peut conduire à une variété de PLA :

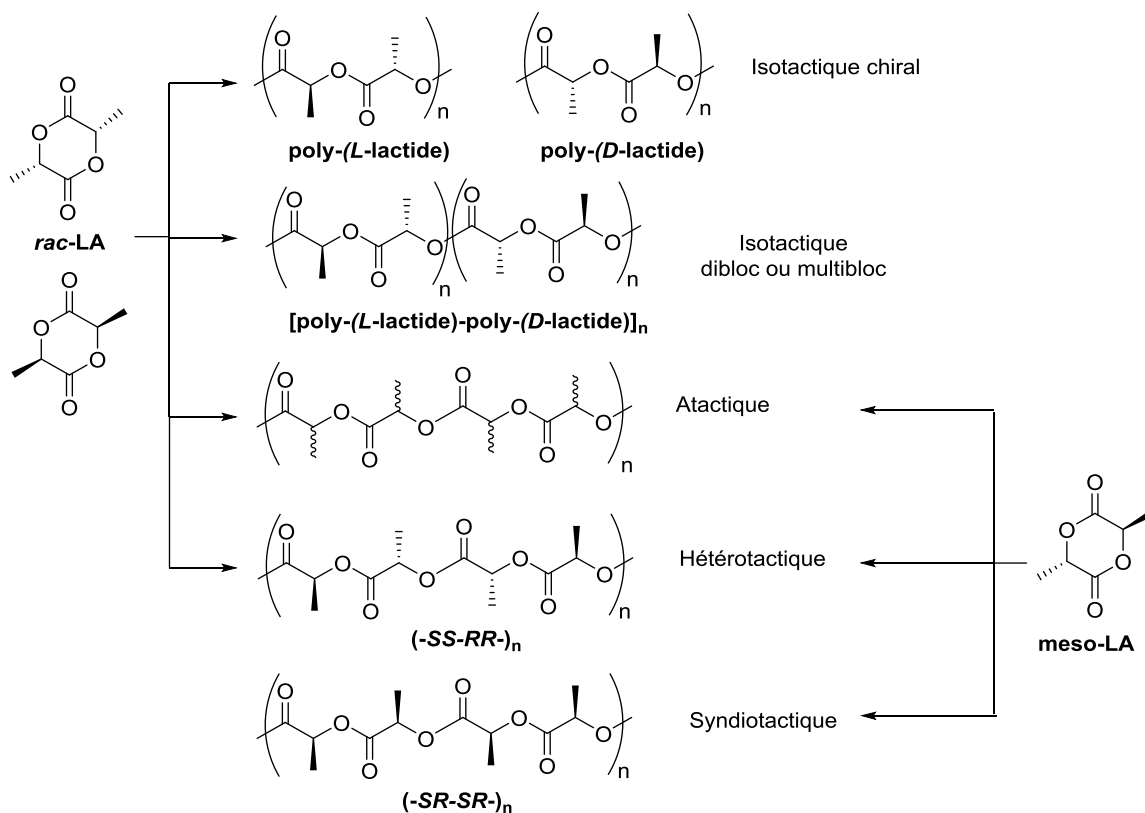


Figure 1.20 : Stéréocontrôle des PLA.

Une réaction de ROP sur un lactide énantiopur donne un PLA isotactique qui se caractérise par le fait que tous les centres stéréogènes du polymère possèdent la même configuration (RRRRRR ou SSSSSS). La ROP de *rac*-lactide conduit à différents polymères de tacticité variée suivant le stéréocontrôle qui a lieu durant la réaction. Lorsqu'il y a insertion

contrôlée des énantiomères identiques, on obtient des PLA isotactique dibloc ou multibloc. Le polymère hétérotactique se développe grâce à l'insertion alternative de monomère D- et L- et enfin les polymères atactiques sont obtenus lorsqu'il n'y a aucun contrôle de la polymérisation et donc des insertions aléatoires des monomères. À partir de *méso*-lactide, trois types de chaînes polymériques sont accessibles. Des polymères atactiques et hétérotactiques présentent les mêmes caractéristiques que lorsqu'ils sont obtenus à partir de monomère *rac*-lactide. Dans les polymères syndiotactiques, il y a une alternance stricte des centres stéréogènes (SRSRSRSRS).

La stéréochimie se contrôle via deux mécanismes de contrôle :

- Le contrôle par terminaison de chaîne : la stéréochimie est dictée par le dernier monomère inséré.
- Le contrôle par le site catalytique : le catalyseur contrôle la stéréochimie du prochain monomère à insérer grâce à l'environnement du site actif imposé par les ligands.

De plus, des réactions secondaires comme la transestérification, l'épimérisation et la terminaison de chaînes influencent la structure des polymères.

La tacticité des polymères peut être identifiée par RMN ^1H et ^{13}C homonucléaires découplés. À partir des spectres RMN et grâce aux diades, on est en mesure de caractériser les PLA. Une diade représente deux carbones chiraux consécutifs, s'ils sont de même chiralité, on appellera cette diade *méso* ou « m » et dans le cas contraire, la diade est racémique ou « r » (Figure 1.21).³⁴

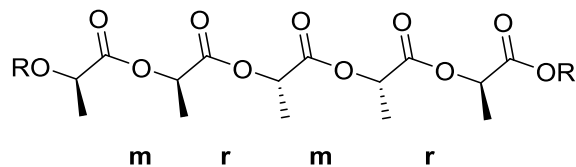


Figure 1.21 : Diade *méso/racémique*.

La nomenclature *méso/rac* a pour origine des α -oléfines où deux orientations identiques du substrat amènent à une symétrie miroir. À cause de l'incohérence d'appeler une séquence RR

méso et RS rac, quelques auteurs préfèrent utiliser la notation i et s pour diade isotactique et diade syndiotactique.

Pour caractériser la tacticité des PLA par RMN, on découpe les protons du méthyle par irradiation afin que le groupement méthine apparaisse sous la forme d'un singulet à la place d'un quadruplet. Ce proton est dans un environnement chimique particulier en fonction de la tacticité du polymère, ainsi une série de pics apparaîtra en dépendance de la capacité du spectromètre à différencier l'environnement en diades, triades, tétrades ou plus. En absence de réactions secondaires, la ROP de lactide donne une séquence de tétrades dont les intensités dépendent de la structure du polymère (Figure 1.22).

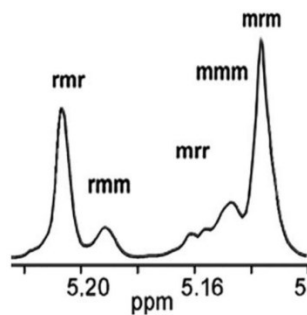


Figure 1.22 : Séquence différenciée par RMN.³⁵

Le degré de stéréorégularité peut donc être quantifié par cette deuxième analyse. Étant donné que le monomère est un dimère cyclique, la nature de chaque seconde diade est déjà déterminée par le monomère (m pour *rac*-lactide, r pour *méso*-lactide). La stéréorégularité dépend donc de diades formées par insertion. La probabilité de former une diade r est P_r tandis que la probabilité de former une diade m est P_m . Ces valeurs sont calculées à partir du spectre RMN proton découplé, en fonction des probabilités d'apparition des tétrades selon les statistiques de Bernoulli (Tableau 1-1 et Tableau 1-2). Suivant le type de lactide utilisé, les résultats attendus pour des polymères parfaits sont les suivants :

- Pour *rac*-lactide

Tableau 1-1 : Tacticité du *rac*-lactide.

Type de polymère	P_r	P_m
Atactique	0,5	0,5
Hétérotactique	1	0
Isotactique	0	1

- Pour *méso*-lactide

Tableau 1-2 : Tacticité du *méso*-lactide.

Type de polymère	P_r	P_m
Atactique	0,5	0,5
Hétérotactique	0	1
Syndiotactique	1	0

1.2.7. Initiateur organométallique cuivré pour les réactions de ROP de lactide

Depuis que Kleine, en 1959,³⁶ investit l'utilisation d'initiateurs métalliques pour la polymérisation de lactide, de nombreuses recherches avec ce type de catalyseur sont réalisées. Dans l'industrie de nos jours, l'un d'eux est le plus utilisé pour fabriquer le PLA : le bis(éthylhexanoate) d'étain ($\text{Sn}(\text{Oct})_2$) avec divers réactifs protiques comme co-initiateur (Figure 1.23).

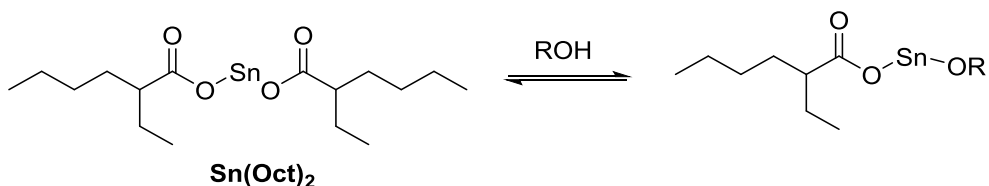


Figure 1.23 : Catalyseur bis(éthylhexanoate) d'étain.

Les études mécanistiques et cinétiques de cette réaction de ROP furent réalisées par les groupes de Penczek et Kowalski.³⁷ L'utilisation de ce catalyseur est de nos jours remise en question puisque son activité catalytique est faible (140 °C, 24 h) pour une conversion

incomplète du lactide (85%). Le problème majeur est qu'il y a peu de contrôle stéréosélectif au niveau de l'insertion des monomères.

Beaucoup d'autres métaux portant des alcoxydes initient efficacement la polymérisation. Typiquement, on observe un contrôle moins important s'ils portent plusieurs alcoxydes. Les métaux avec un seul site initiant la réaction avec un bon contrôle du poids polymérique, de la distribution et étant stéréosélectif, sont en développement encore de nos jours. La recherche s'oriente vers des complexes avec un centre métallique acide de Lewis portant un ligand coordonné et un groupement initiant de type alcoxyde. Les métaux les plus couramment utilisés pour cette catalyse et largement étudiés sont l'aluminium et le zinc. Mais un intérêt grandissant pour le cuivre dans tous les domaines de la catalyse (photochimique, couplage...), nous a incité à choisir ce métal et à étudier son potentiel dans la polymérisation. Les sels de cuivre(II) sont peu chers, peu toxiques, stables à l'air, de même que la plupart des complexes avec ce métal à ce degré d'oxydation.

Très peu de travaux ont été publiés sur la polymérisation de lactide catalysée par des complexes de cuivre(II). La première publication utilisant le cuivre(II) dans des complexes organométalliques pour réaliser la polymérisation de PLA date de 2002.³⁸ L'acide aspartique salicylidène, un ligand de type base de Schiff (Figure 1.24), fut utilisé pour former le complexe qui est capable d'initier la ROP (LA/Cat = 200), à haute température (130 °C), sans solvant afin d'aboutir à plus de 90% de conversion (12 h) et de former des polymères avec une distribution du poids moléculaire médiocre (PDI = 1,5).

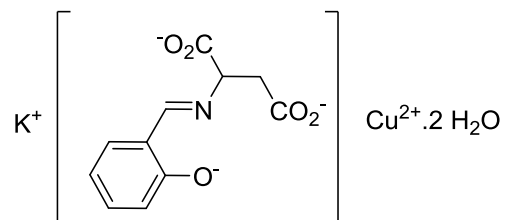
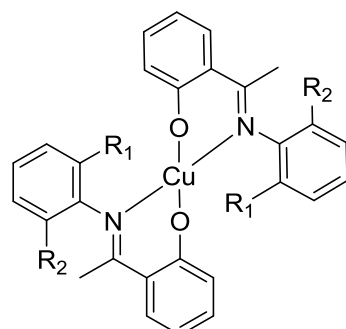


Figure 1.24 : Premier catalyseur de cuivre pour la polymérisation de lactide.

En 2007, un second groupe reporta des complexes de cuivre(II) actifs envers la polymérisation de lactide avec des complexes homoleptiques portant des ligands bidentates de type phénoxy-kétimine (Figure 1.25).³⁹ Dans ce cas, une température élevée est requise (160 °C) pour produire des polymères avec un poids moléculaire modéré ($M_n = 12000$) et une polydispersité faible ($PDI = 1,1$). Cette polymérisation sans solvant requiert 4 h pour atteindre 86% de conversion avec un ratio LA/Cu de 50.



R_1 et R_2 = H, Me ou Et

Figure 1.25 : Premiers complexes homoleptiques avec ligand phénoxy-kétimine pour la polymérisation de lactide.

Par la suite, d'autres groupes ont étudié le même type de complexe, dont le groupe de Bhunora (Figure 1.26).⁴⁰ Ces complexes permettent à 70 °C, après 35 h de réaction, dans le toluène, de produire des polymères avec une polydispersité de 1,3 et une conversion de 80%.

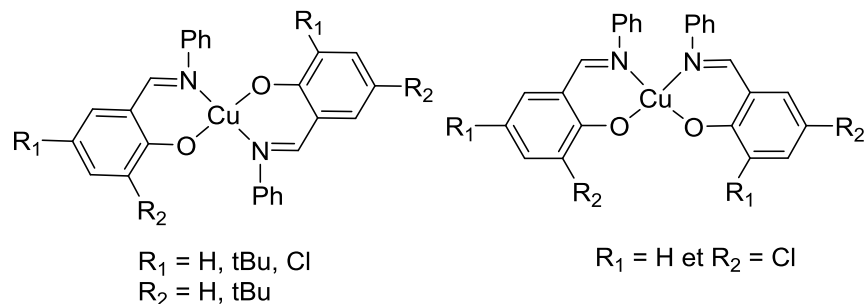


Figure 1.26 : Complexes de Bhunora pour la polymérisation de lactide.

À partir de ligand très proche structurellement, mais avec des variations au niveau électronique, Mandal et son groupe réalisèrent également des études de polymérisation de lactide.⁴¹ Ces nouveaux complexes polymérisent le lactide à 140 °C, sans solvant, en 5 h, avec plus de 90% de conversion. Avec un ratio LA/Cat. de 200, des polymères avec un poids moléculaire modéré et une large distribution du poids polymérique sont obtenus. L'ensemble des complexes de type base de Schiff présentent une géométrie plan carré. Leur activité catalytique pour la polymérisation de lactide est plutôt faible puisque de très hautes températures sont nécessaires, et de ce fait le contrôle de la polymérisation s'avère difficile et la taille des polymères est limitée.

Les ligands de type salen associé à un cuivre(II) sont également actifs pour la polymérisation de lactide d'après les travaux de Chen (Figure 1.27).⁴² À 130 °C, sans solvant, après 24 h, des polymères avec une bonne polydispersité (1,1) et un poids moléculaire élevé (ratio LA/Cat. = 1000) peuvent être obtenus.

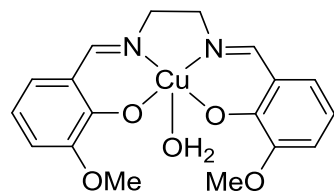


Figure 1.27 : Premiers complexes cuivrés avec ligand type salen pour la polymérisation de lactide.

L'équipe de Routaray s'intéressa également à ce type de complexe quelques années plus tard.⁴³

En 2011, l'acétate de cuivre fut également utilisé seul ou en combinaison avec l'isopropanol pour former des PLA (Figure 1.28).⁴⁴ Cette réaction réalisée à 145 °C, sans solvant, en 28 h, s'avère très contrôlable aboutissant à des polymères avec une très bonne polydispersité (1,0). De plus, de longues chaînes polymériques peuvent être réalisées en maintenant le contrôle (ratio LA/Cat. = 1000).

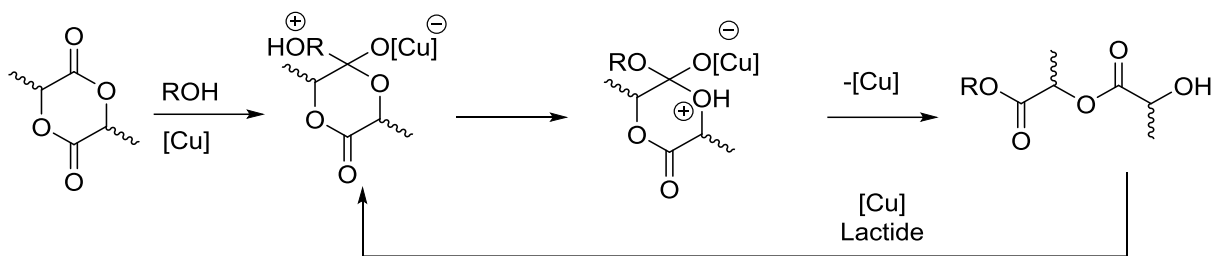


Figure 1.28 : Catalyse de la polymérisation de lactide par l'acétate de cuivre

Les catalyseurs de cuivre(II) actuellement présentés ont tendance à suivre le mécanisme par activation des monomères et montrent une faible activité catalytique pour la polymérisation de lactide (haute température et long temps réactionnel). De plus, la plupart ne permettent pas d'obtenir un bon contrôle de la polymérisation et/ou de longues chaînes polymériques. Et enfin pour aucun d'eux, la possibilité de contrôle de la tacticité ne fut observée. Jusqu'alors, il y avait donc beaucoup de potentiel au niveau de la recherche des applications de complexes de cuivre(II) pour cette réaction.

Notre groupe de recherche s'est inséré dans cette ouverture pour trouver des catalyseurs de cuivre(II) très actif et induisant un stéréocontrôle de la réaction. Les premiers travaux sur des cuivres(II) diketiminate isopropanolate ont abouti à des complexes, ayant une très haute activité catalytique (conversion complète en 3 min à température ambiante) (Figure 1.29).⁴⁵ Aucune réaction secondaire ou dégradation du catalyseur ne fut observée donnant lieu à une très bonne polydispersité (1,1). La forte activité serait reliée au ligand diketiminate qui est assez flexible pour permettre à un monomère de se coordiner, mais également suffisamment encombrant pour déstabiliser l'intermédiaire formé et donc favoriser l'insertion. Le complexe très stable présente une très bonne activité catalytique avec un très bon contrôle du poids polymérique. Cependant aucun contrôle de la stéréochimie n'est possible, ce qui limite fortement son intérêt.

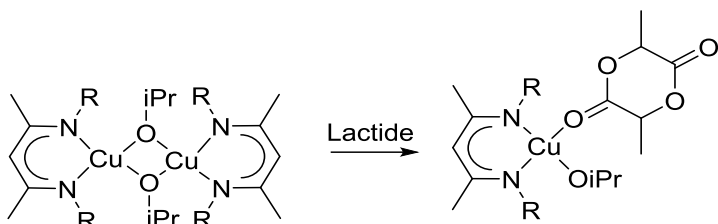


Figure 1.29 : Cuivre(II) diketiminate hétéroleptique pour la polymérisation de lactide.

Des complexes homoleptiques furent également synthétisés : en présence d'un alcool libre, cette forme est en équilibre avec une petite quantité de complexes hétéroleptiques, suffisante pour initier la polymérisation de lactide en moins de 60 min à température ambiante (Figure 1.30).⁴⁶

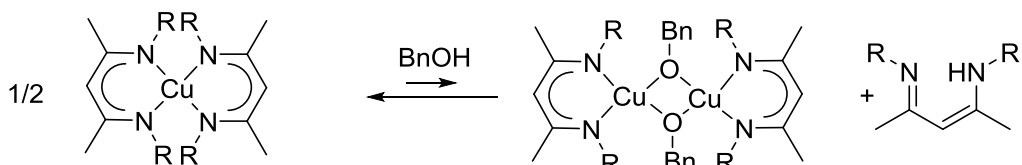


Figure 1.30 : Cuivre(II) diketiminate homoleptique pour la polymérisation de lactide.

Dès lors, plusieurs groupes ont publié des complexes de cuivre(II) actifs à température ambiante, comme en 2013 avec des ligands de type benzotriazole phénoxide (Figure 1.31).⁴⁷ La présence d'un alcool est nécessaire pour initier la ROP à température ambiante et donner des polymères avec un poids polymérique prédict, du fait d'une très bonne polydispersité (1,2). Cependant, avec ces complexes, 6 h de réaction sont nécessaires pour permettre de dépasser les 90% de conversion avec un ratio LA/Cat./ROH de 400/1/2.

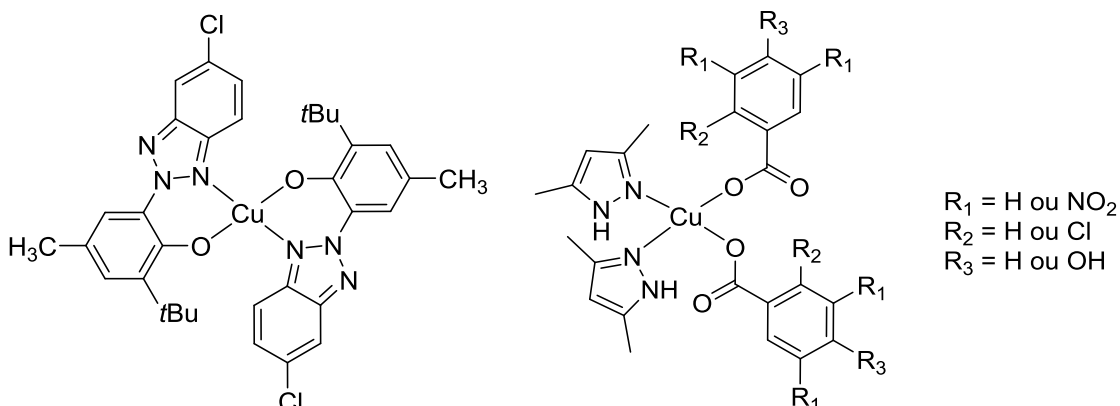


Figure 1.31 : Cuivre(II) benzotriazole phenoxide (Gauche) et bis(3,5-diméthylpyrazole) (droite).

Des complexes de cuivre(II) bis(3,5-diméthylpyrazole) polymérisent également le lactide à haute température sans solvant, produisant des polymères de poids polymérique et une polydispersité modérée (1,4, Figure 1.31).⁴⁸ Ce système catalytique est le premier qui, malgré la très haute température, présente un certain stéréocontrôle puisque le PLA est hétérotactique. Cependant 144 h sont requis pour terminer la réaction.

En 2015, le premier complexe chiral de cuivre(II) utilisé pour la polymérisation de lactide fut publié (Figure 1.32).⁴⁹ Basé sur des ligands de type naphtalène cyclohexane diamine, l'espèce active est générée *in situ* avec l'addition d'un alcoxyde libre donnant lieu à une polymérisation très rapide (30 secondes à température ambiante dans le dichlorométhane). De plus, ce système catalytique forme des PLA stéréo-enrichis puisque hétérotactique ($P_r = 0,90$).

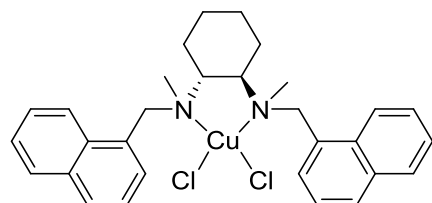


Figure 1.32 : Premier complexe chiral de cuivre(II) pour la polymérisation de lactide.

Divers dérivés du complexe précédent furent étudiés peu après, avec des résultats similaires pour leur activité catalytique (60 secondes, PDI = 1,3, tp, CH_2Cl_2 , LA/Cat. = 100).⁵⁰

En 2015, notre groupe reporta un nouveau catalyseur de cuivre(II) présentant une avancée importante dans ce domaine. En effet, les complexes dinucléaires diiminopyrrolide portant un alcoxyde catalysent la polymérisation à température ambiante, produisant des polymères isotactiques (8 h, LA/Cat. = 200, $P_m = 0,72$) (Figure 1.33).⁵¹ Cela constitue le premier système catalytique faisant intervenir un complexe de cuivre(II) menant à la préparation de PLA avec le stéréocontrôle souhaité. De plus, un très bon contrôle du poids polymérique est observé avec une polydispersité autour de 1,0-1,2.

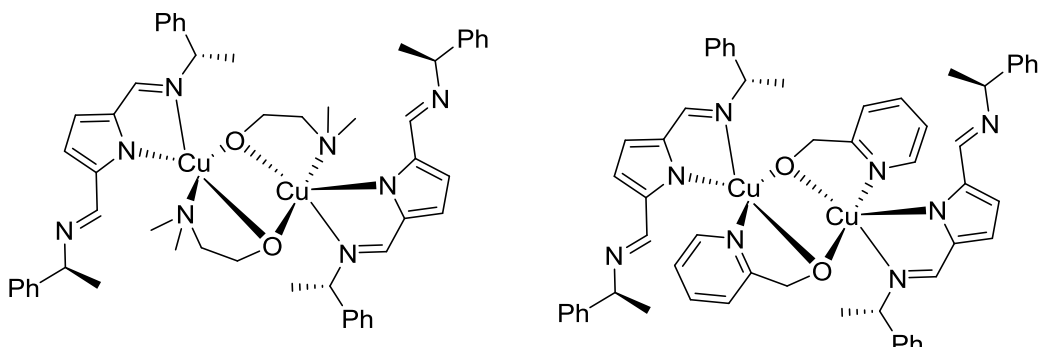


Figure 1.33 : Complexes dinucléaires diiminopyrrolides produisants des polymères isotactiques.

La dernière publication en date réalise la catalyse avec des complexes mononucléaires de type pyridineamine en générant *in situ* le dérivé Cu(II) alcoxyde.⁵² Leur activité est haute (7 min, tp, CH_2Cl_2) et donne des PLA hétéroenrichis avec une polydispersité de 1,4.

Les complexes de coordination de cuivre(II) qui catalysent la polymérisation de lactide sont donc toujours limités à quelques exemples. La plupart d'entre eux sont peu actifs, car ils nécessitent de longs temps réactionnels et de très hautes températures suivant un mécanisme de monomère activé. De plus, les polymérisations ne sont pas stéréosélectives et ne permettent pas généralement la synthèse de PLA à haut poids moléculaire. La géométrie de l'ensemble des complexes de cuivre(II) utilisés pour cette catalyse est plan carré, laissant ainsi des accès libres au centre métallique acide de Lewis au lactide. Les complexes existants se montrent très actifs en quelques minutes portent un alcoxyde et produisent souvent des polymères hétérotactiques. Dans la littérature, à l'heure actuelle, une seule publication décrit

des complexes de cuivre(II) formant des polymères isotactiques, cependant, ces complexes sont peu stables à l'air et à l'eau, et nécessitent 8 h de réaction pour atteindre plus de 90% de conversion. Dans ce contexte, nous envisageons de développer de nouveaux complexes de coordination possédant un cuivre comme centre métallique, qui sont stables à l'air, mais capable d'une polymérisation rapide et stéréospécifique, afin de former des PLA à haut poids moléculaire et isotactique idéalement.

1.3. Couplage de Chan-Evans-Lam

1.3.1. Généralités

La découverte, il y a une vingtaine d'années, de la réaction de couplage de Chan-Evans-Lam (CEL) promue par du cuivre avec des acides boroniques a fait avancer la chimie du couplage carbone-hétéroatome.⁵³ Cette méthodologie est maintenant un outil synthétique attractif notamment grâce aux conditions douces qu'elle requiert et son faible coût. De nombreux et significatifs progrès ont été réalisés pour augmenter l'étendue réactionnelle et la compréhension du mécanisme.

Avant l'apparition de ce couplage, deux méthodes principales existaient :

- Le couplage d'Ullmann et d'Ullmann-Goldberg (Figure 1.34) promu par le cuivre et découvert au début du vingtième siècle utilise une quantité stoechiométrique de cuivre pour générer des amines ou éthers aryliques à partir d'un dérivé halogéné. En plus d'une quantité importante de cuivre, une température très élevée est requise.^{13b, 54}

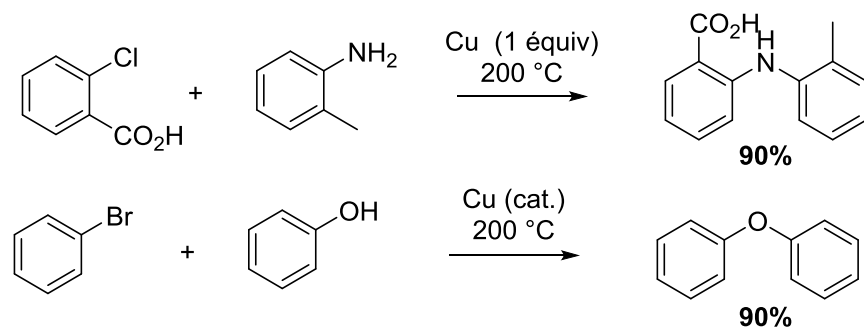


Figure 1.34 : Couplage d'Ullmann et d'Ullmann-Goldberg.

- Le couplage de Buchwald et Hartwig (Figure 1.35) est catalysé par une quantité catalytique de palladium à partir des mêmes types de réactifs que le couplage d'Ullmann-Goldberg.⁵⁵

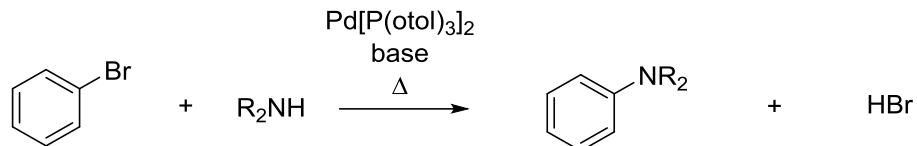


Figure 1.35 : Couplage de Buchwald et Hartwig.

Dans ce système, une base forte et un chauffage élevé permettent de former les produits souhaités. Cependant, le palladium est un métal cher, peu stable qui requiert donc différentes précautions lors de son utilisation. Buchwald travailla aussi en parallèle sur un couplage croisé catalysé au cuivre, comparable au couplage de Ullmann-Goldberg, entre un aryl halogéné et un substrat nucléophile (amine, alcool...) (Figure 1.36).

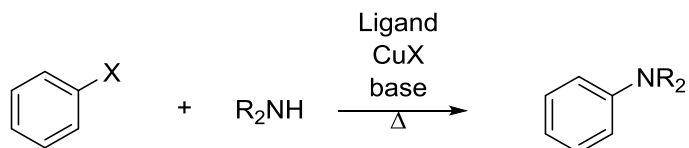


Figure 1.36 : Couplage de Buchwald au cuivre.

La première publication de ce couplage concerne les imidazoles et date de 1999,⁵⁶ par la suite, le groupe de Buchwald développa différents protocoles adaptés à différents types de nucléophiles : les amides,⁵⁷ les indoles,⁵⁸ les amines primaires⁵⁹ et les anilines.⁶⁰ Les modifications aux protocoles furent principalement orientées sur les ligands du cuivre ajoutés au milieu réactionnel. Concernant les amines secondaires non cycliques, leur réactivité dans ce type de couplage est faible probablement dû à des problèmes d'encombrement stérique.⁶¹ Par conséquent, ces méthodes requièrent des conditions très dures pour former un lien C-N ou C-O. Le couplage de Chan-Lam présente beaucoup d'avantages à l'origine de sa popularité. Cette réaction forme des liens carbone-hétéroatome dans des conditions douces (température

ambiante, base faible si nécessaire, atmosphère ambiante) en utilisant le cuivre comme catalyseur.

Dans les publications originales, le cuivre en quantité stoechiométrique initie la formation de liaison C-N, C-O et C-S entre un substrat nucléophile de type OH, NH ou SH et un acide aryle ou alcényle boronique pour former le produit arylé ou alcénylé correspondant (Figure 1.37).⁵³ Cette réaction se nomme maintenant couplage de Chan-Lam ou Chan-Evans-Lam en référence aux trois premières publications sur cette réaction.⁵³

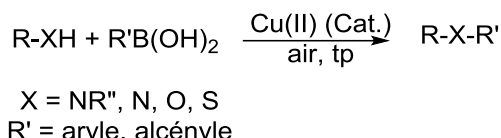


Figure 1.37 : Couplage de Chan-Evans-Lam.

De nos jours, énormément d'extensions ont été développées, avec différents groupements X (Se, Te, Br...), R (hétérocycle, composé aromatique ou aliphatique) et différents types d'organoborane (boroxine, acide alcényle-boronique, alkyle-boronique, alcynyle-boronique ou ester boronique $\text{B}(\text{OR})_2$).⁵³

1.3.2. Études mécanistiques

Dès les premières publications, les chercheurs se sont demandé s'il s'agissait d'une réaction radicalaire ou d'un cycle Cu(I)/Cu(III) similaire au couplage avec le palladium et connu de l'addition des cuprates aux doubles liaisons. Le couplage ne semble pas avoir lieu via un mécanisme avec des radicaux libres, puisque l'addition d'un inhibiteur de radicaux tel que la 1,1-diphénylène n'affecte pas le rendement de la réaction.^{53a} De plus dans cette réaction l'oxygène semble nécessaire, ce qui n'est pas le cas dans la réaction utilisant un cycle Cu(I)/Cu(III) pour fonctionner.

Ensuite il faudra attendre plusieurs années pour qu'une étude plus complète soit réalisée. L'équipe de Stahl reporta la première étude mécanistique approfondie du couplage catalysé au cuivre de Chan-Lam en 2009 via la méthoxylation de l'ester tolylboronique (Figure 1.38).⁶²

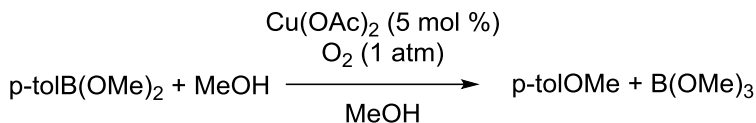


Figure 1.38 : Méthoxylation de l'ester tolylboronique.

Des données cinétiques ont révélé une réaction présentant une dépendance d'ordre $\frac{1}{2}$ en Cu(OAc)₂, un seuil de saturation en ester boronique et une dépendance d'ordre 0 en oxygène. Ces résultats indiquent que la réoxydation du cuivre(I) par l'oxygène est rapide et que le dérivé boré et le cuivre(II) sont impliqués dans l'étape limitante. Il a donc été proposé que l'étape limitante soit la transmétallation du groupement aryle sur le cuivre. De plus des analyses spectroscopiques RPE ont montré que le cuivre principalement observé dans le milieu réactionnel est à l'état d'oxydation 2. L'analyse des stœchiométries de la réaction a démontré que la formation du lien C-O n'est pas issue d'une élimination réductrice à partir du cuivre(II), mais d'une espèce aryle-cuivre(III) intermédiaire. Celle-ci s'est formée via l'oxydation de l'intermédiaire aryle-cuivre(II) par un autre équivalent de cuivre(II). Ce fait avait également été étudié un peu avant avec un couplage C-N en présence de différents amides nucléophiles.⁶³

Avec l'ensemble des résultats ci-dessus, Stahl postula un mécanisme comprenant quatre étapes principales (Figure 1.39) : la transmétallation qui est l'étape limitante, suivie d'une disproportionation de deux cuivres(II) en Cu(I) et (III), l'étape d'élimination réductrice qui formera le produit et enfin la réoxydation du Cu(I) en Cu(II) qui reformera le catalyseur.

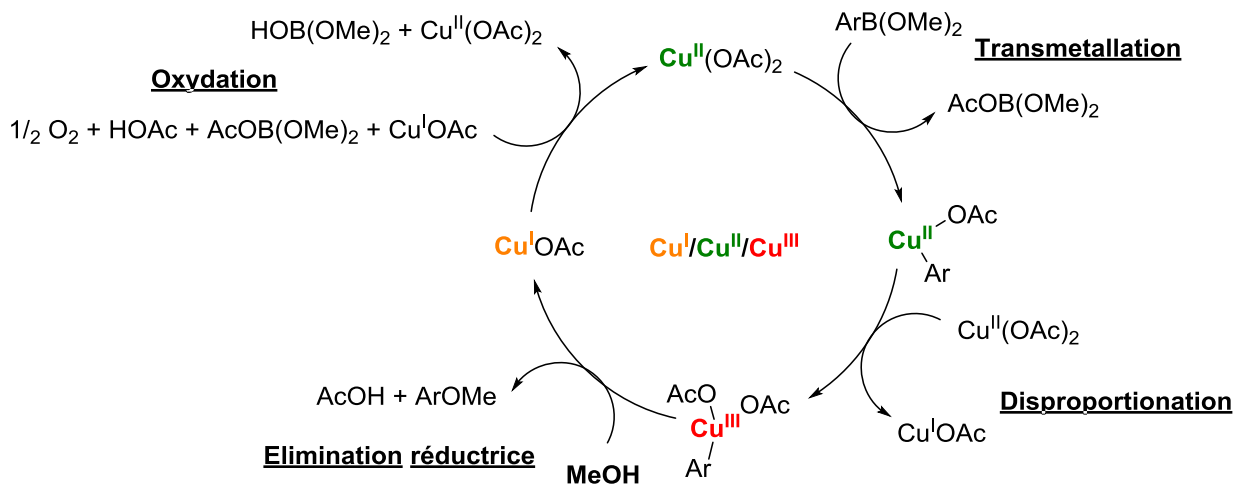


Figure 1.39 : Mécanisme du couplage de Chan-Evans-Lam.

1.3.3. Réactions secondaires

La réaction emploie typiquement un excès d'acide boronique parce que ce substrat induit plusieurs réactions secondaires.⁶⁴

- Proto-déboration (Figure 1.40)

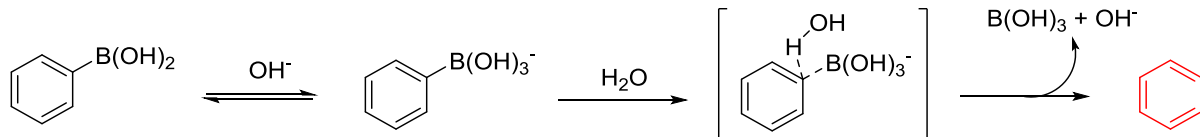


Figure 1.40 : Réaction secondaire de proto-déboration.

En milieu aqueux et basique, des réactions de proto-déboration ont lieu via la formation d'un intermédiaire borate puis de la protonation d'aryle par l'eau. Par conséquent, la quantité d'eau dans les réactions sera à surveiller.

- Conversion en phénol, réaction secondaire qui peut être éliminée parfois en présence de tamis moléculaire (Figure 1.41).

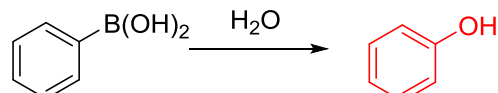


Figure 1.41 : Réaction secondaire de formation du phénol.

- Formation de diphenyle par dissociation homolytique du lien cuivre(II)-aryl après l'étape de transmétallation (Figure 1.42)

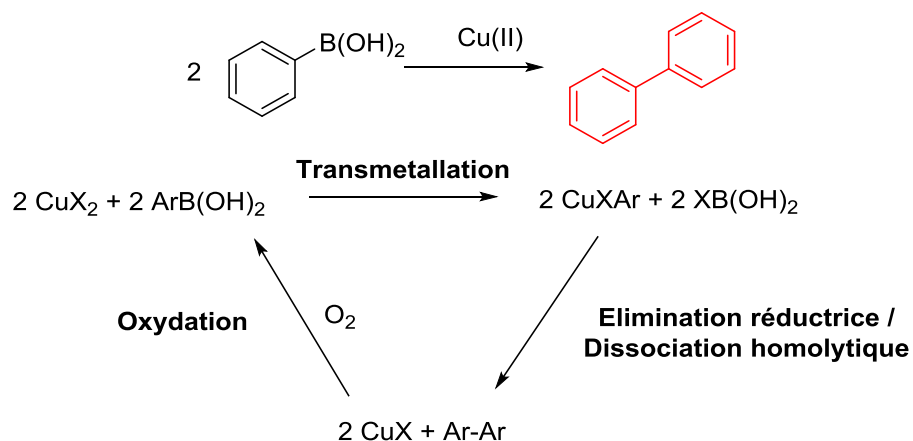


Figure 1.42 : Réaction secondaire de formation du diphenyle.

Une autre réaction secondaire, concernant cette fois le substrat nucléophile, est la formation d'un produit diazo avec des substrats de type aniline (Figure 1.43), qui fut cependant observé pour la première fois dans nos recherches (voir partie 3).

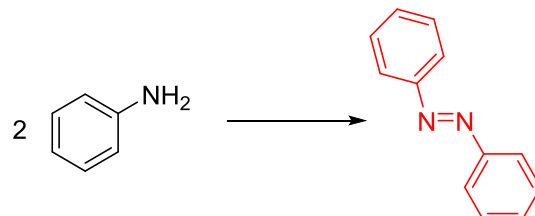


Figure 1.43 : Réaction secondaire de formation du composé diazo.

Des travaux publiés réalisent ce couplage entre deux anilines depuis les années 1950 en utilisant une quantité catalytique de cuivre(I) et en présence d'une base coordinante comme la pyridine.⁶⁵ Il a été prouvé que les substrats para-substitués réagissent bien, mais lorsque la position ortho est occupée, il y a inhibition de la formation du composé azo. De plus, la réactivité augmente avec le caractère riche en électrons des anilines. De faibles rendements sont obtenus pour les anilines portant un groupement électroattracteur et/ou une substitution en méta, tandis que les amines aliphatiques primaires ou les anilines secondaires ne

permettent pas l'oxydation.⁶⁶ Un mécanisme, pour la formation des composés azo à partir d'aniline, fut proposé passant par l'oxydation à un électron du substrat par le cuivre pour former une aniline radicalaire. Celle-ci réagit ensuite avec un autre équivalent radicalaire pour former l'hydrazobenzène et pour finir, grâce au cuivre, cet intermédiaire est transformé par oxydation en l'azobenzène correspondant.⁶⁷ L'oxygène, d'après les études mécanistiques, n'est pas seulement nécessaire pour oxyder l'espèce cuivré et terminer le cycle catalytique du cuivre, mais il joue un rôle important pour générer la radicale aniline initiale, possiblement par formation du peroxydicuivre(II) qui serait le catalyseur actif.⁶⁸

Par conséquent, du fait que durant le couplage est produit une espèce de cuivre(I) et que l'atmosphère de la réaction contient de l'oxygène, cette réaction secondaire pourra avoir lieu. Il faudra donc s'assurer que nous ne formons pas ce type de produit secondaire en particulier pour les anilines électroniquement riches.

Une dernière réaction à surveiller sera la possible formation d'un produit iminé observé pour des substrats aminés aliphatiques (Figure 1.44), observé uniquement jusqu'à présent dans nos travaux (voir partie 3).

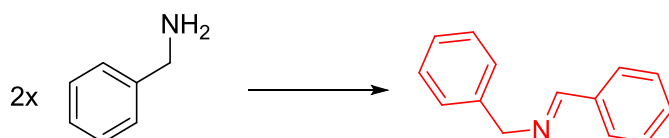


Figure 1.44 : Réaction secondaire de formation d'imine.

Dans la littérature, ce couplage fut d'abord obtenu à la suite d'une réaction indésirable lors de l'oxydation d'amine en imine ou nitrile⁶⁹ avant d'être étudié comme une réaction d'oxydation d'amine en imine secondaire à part entière.⁷⁰ Plusieurs mécanismes furent proposés, mais jusqu'à présent aucun ne fait l'unanimité, cependant ce qui est sûr c'est que ce couplage a lieu à partir de cuivre(I).

Le couplage CEL a lieu dans des conditions douces, cependant beaucoup de produits secondaires peuvent être formés qui donnent lieu à des rendements qui peuvent s'avérer très bas. Durant notre recherche nous ferons donc attention à ces potentielles réactions

secondaires, très peu analysées dans la littérature, qui peuvent avoir lieu principalement en présence d'eau et si la réoxydation du cuivre(I) en cuivre(II) est lente.

1.3.4. Sélectivité et réactivité des substrats

L'équipe de Lam étudia la compétition entre la O- et N-arylation de l'acide p-tolylboronique (Figure 1.45).^{50b} Les résultats montrèrent que la N-arylation est neuf fois plus rapide que la O-arylation, ce qui est en accord avec la force des nucléophiles.

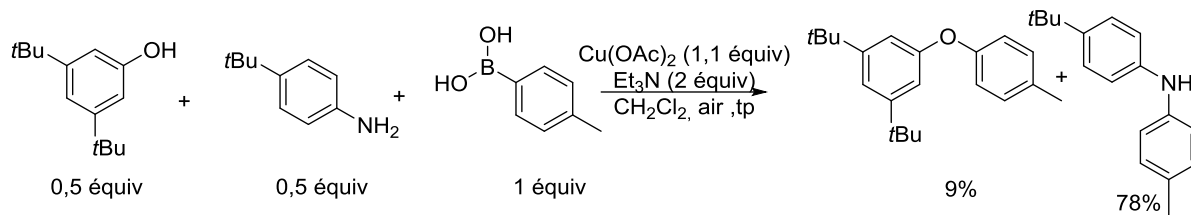


Figure 1.45 : Compétition entre la O- et N-arylation de l'acide p-tolylboronique.

En général, la N-arylation est plus rapide que la O-arylation, cependant il est possible de privilégier la O-arylation car la réaction est très sensible aux effets stériques. Donc si l'amine est encombrée, l'autre chemo-sélectivité peut être observée.⁷¹ L'équipe de Stahl a classé la réactivité de différents groupements amides envers cette réaction de couplage (Figure 1.46). D'après leur étude, les composés avec un groupement NH plus acide réagissent plus rapidement que ceux moins acides.⁶²

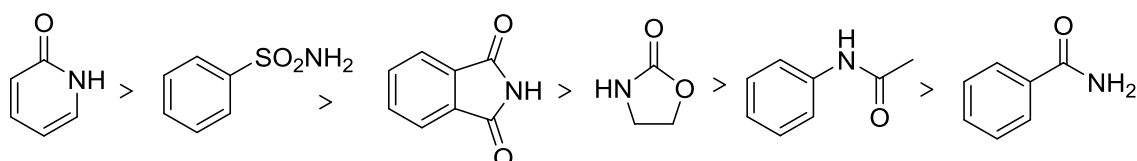


Figure 1.46 : Réactivité groupement amidé.

La modification du groupement organique sur l'ester boronique a un impact significatif sur la vitesse de la réaction. Stahl a également réalisé une courbe de Hammett pour mettre en évidence scientifique cette observation générale (Figure 1.47).⁷² Ainsi, les esters boroniques électroniquement riches possèdent un meilleur turnover.

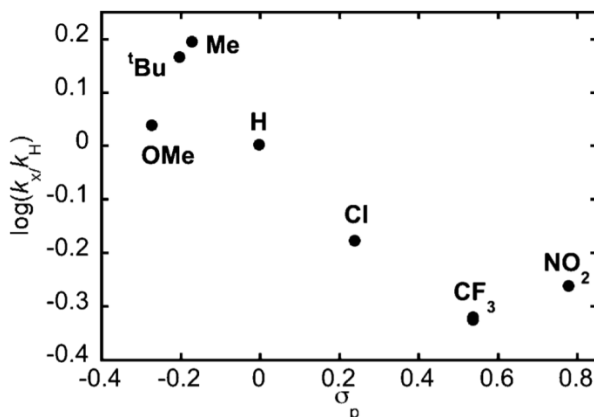
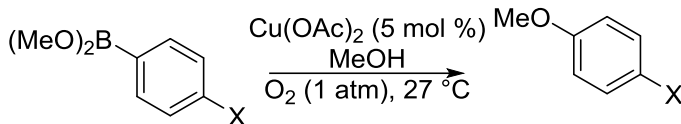


Figure 1.47 : Courbe de Hammett pour le substrat boronique appliquée au couplage de Chan-Evans-Lam.⁷²

D'après les quelques études mécanistiques de ce couplage, plus le nucléophile est fort plus la réaction est rapide, de même plus l'acide ou l'ester aryle-boronique est riche en électron plus la réaction est efficace. La vitesse du couplage est donc dépendante de la nucléophilie du substrat nucléophile et de la concentration électronique sur l'acide boronique. Malgré ces observations, surprenamment, les esters alkyle-boroniques réagissent moins vite que les esters aryle-boroniques. Parmi les modifications aux couplages standards, le substrat borylé fut étudié plus tardivement à partir de 2003. Dans un premier temps, les esters boroniques et boroxines étaient ciblés, puis les acides alkyle-boroniques.

1.3.5. Complexe cuivré catalysant le couplage

En 2001, l'équipe de Collman fut la première à proposer une version catalytique du couplage de Chan-Lam (Figure 1.48).⁷³ Le système catalytique mis au point, requiert 10 mol % de catalyseur (ce qui est relativement élevé) pour coupler l'imidazole avec l'acide phényle boronique, en 12 h, à température ambiante, dans le dichlorométhane anhydre et sous oxygène. L'étude fut principalement orientée sur la comparaison de l'activité avec différents ligands et anions sur le cuivre(II). Des ligands bichélatants tel que les bipyridines, biimidazoles

et composés diaminés furent ciblés et il s'avère que le TMEDA est le ligand dont le complexe de cuivre issu est le plus actif pour catalyser la réaction. Tandis que le chlore et le triflate sont les contre-anions du cuivre qui induisent la meilleure activité catalytique.

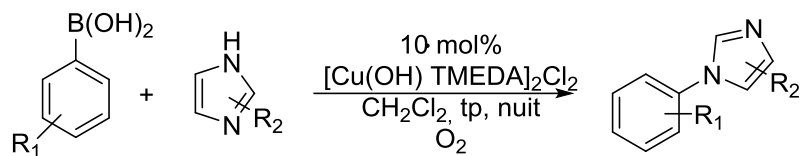


Figure 1.48 : Premier couplage catalytique de la réaction de Chan-Evans-Lam.

Ainsi, le $[\text{Cu}(\text{OH})\text{TMEDA}]_2\text{Cl}_2$ fut utilisé afin de réaliser le couplage de Chan-Lam. Avantageusement, les conditions de Collmann ne nécessitent pas de base et la réaction peut avoir lieu à température ambiante, avec une quantité catalytique de cuivre. Cependant, le protocole développé requiert une atmosphère d'oxygène pour que le couplage soit effectif et l'étude était limitée au substrat de type imidazole.

Quelques années plus tard, Berker et son groupe ont étudié l'activité catalytique des complexes de cuivre(II) portant des ligands bichelatants dans les réactions de couplage de Chan-Evans-Lam.⁷⁴ Le système catalytique fut optimisé afin de réaliser la réaction avec seulement 5 mol % de catalyseur et à l'air ambiant dans un mélange NMP/H₂O, tout en préservant le fait de ne pas utiliser de base et de faire la réaction à température ambiante. Comme Collman, l'étude s'est concentrée sur le choix du ligand pour le cuivre et de nouveau le TMEDA est le meilleur choix.

De plus, d'après leur observation basée sur les résultats des tests catalytiques, il suggère que la première étape de la réaction est la coordination de l'imidazole. L'eau finalement ne semble pas être désavantageuse dans ce couplage comme le suggérait le choix d'un solvant anhydre par Collman. Berker, grâce à ces travaux, a dans un sens amélioré le système catalytique proposé par Collman en diminuant la quantité de catalyseur et utilisant l'air ambiant au lieu d'un atmosphère d'oxygène. Cependant, l'eau et la NMP ne sont pas des solvants aisés à enlever à la fin de la réaction et l'étude est une nouvelle fois limitée aux imidazoles.

Par la suite, différents groupes ont choisi d'étudier les possibilités de déposer le catalyseur de cuivre sur un support solide afin de le recycler.

Tout d'abord, Chiang étudia l'utilisation d'une résine modifiée de type Wang pour déposer le complexe de cuivre(II) dont la structure est la suivante⁷⁵ :

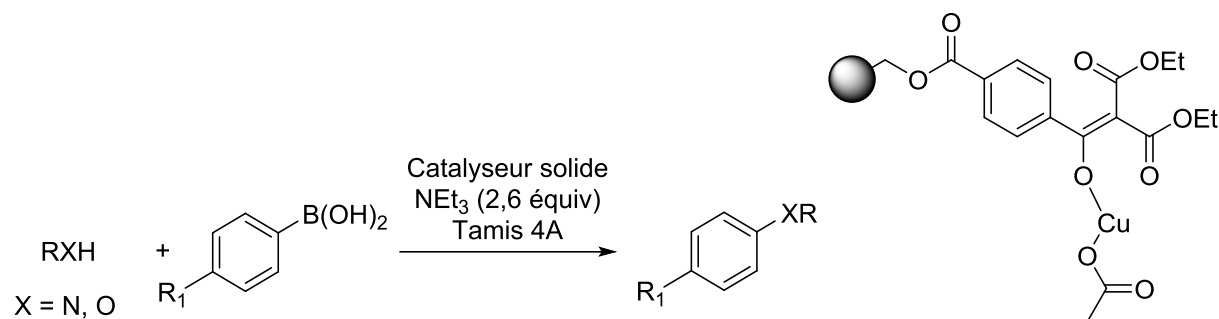


Figure 1.49 : Réaction de Chan-Evans-Lam avec un catalyseur de cuivre sur support solide.

Le protocole développé dans le dichlorométhane à température ambiante inclut une quantité substœchiométrique de base (Et_3N) et du tamis moléculaire. Après une journée de réaction, des substrats de type aniline, phénol, amide... peuvent être couplés avec un acide boronique aromatique. L'avantage principal de ces travaux est la possibilité de recycler le catalyseur, mais plusieurs additifs sont ajoutés au système catalytique et doivent donc être à chaque cycle ajoutés à nouveau. De plus, le couplage est relativement long pour des substrats plutôt aisés tels que l'aniline.

En 2006, Choudary avec la même idée de recyclage utilisa le CuFAP (cuivre fluoroapatite) pour réaliser ce type de couplage (Figure 1.50).⁷⁶ À température ambiante, dans le méthanol à l'air libre, en 5 h, le couplage est terminé pour divers substrats (anilines, amines aliphatiques, benzimidazoles, imidazoles).

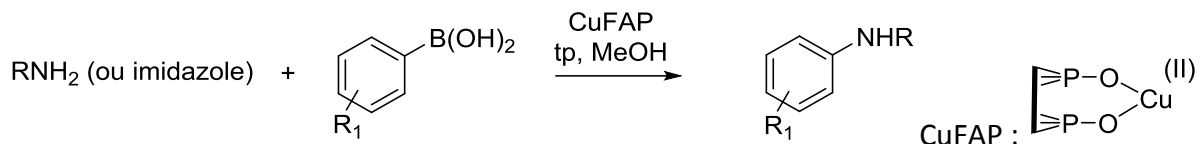


Figure 1.50 : Catalyse du couplage de Chan-Evans-Lam avec un catalyseur recyclé de type CuFAP.

Enfin, la dernière publication portant sur un catalyseur de cuivre supporté sur une résine fut publiée en 2016 par Lin (Figure 1.51).⁷⁷ La structure du complexe avec le sulfonate comme contre ion sur le cuivre avec un ligand bichélatant est la suivante :

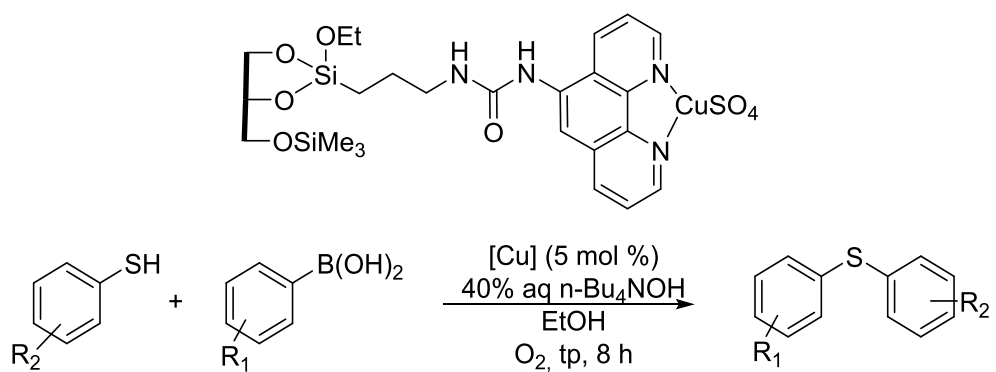


Figure 1.51 : Catalyseur de Lin supporté pour le couplage de CEL.

Les travaux furent uniquement orientés sur les thiols, et non les substrats standards du couplage qui sont les anilines et les phénols. Le protocole utilise 5 mol % du catalyseur de cuivre dans l'éthanol, à température ambiante, sous atmosphère d'oxygène. L'ajout d'une base est nécessaire pour obtenir de bons rendements, la base organique n-Bu₄NOH s'est avérée beaucoup plus efficace que les bases de types carboxylates. Le couplage des thiols est considéré comme difficile, car il mène généralement à la formation de bisulphide qui n'est plus un substrat pour induire facilement le couplage de Chan-Lam. Ainsi, ces conditions, bien que plus dures que pour un couplage sur des anilines, sont plutôt simples et efficaces pour des substrats thiolés.

En 2011, le groupe de Kaboutin a choisi un ligand de type cyclodextrine (Figure 1.52).⁷⁸ Dans l'eau, à température ambiante, à l'air, en quelques heures, cette équipe est en mesure de coupler des amines aromatiques et aliphatiques.

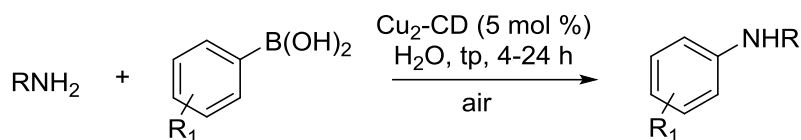


Figure 1.52 : Couplage de CEL avec un $\text{Cu}_2\text{-CD}$.

Chen et son équipe, en 2010, ont mis au point un nouveau complexe de cuivre(II) pour catalyser la réaction de Chan-Lam (Figure 1.53).⁷⁹ Le composé est un tétramère portant deux groupements hydroxy pontant et quatre anions non-coordinants. Seulement deux ligands hexadentates pour quatre cuivres complètent les sphères de coordination avec une géométrie pyramidale à base carré légèrement distordue.

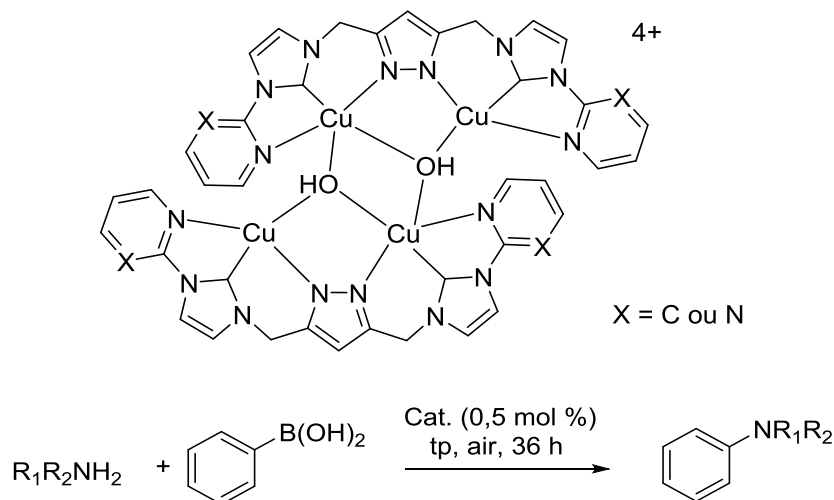


Figure 1.53 : Complex de cuivre proposé par l'équipe de Chen pour la catalyse du couplage de CEL.

Le mode opératoire est très simple en ne requérant aucun additif (O_2 , base) et ayant lieu à température ambiante. Cependant, le temps de réaction est relativement important et

d'environ 36 h. Parmi les substrats actifs, il y a les anilines, imidazoles et benzimidazoles ce qui est important. Mais l'inconvénient principal de ce catalyseur est qu'il n'est pas actif envers les amines aliphatiques.

En 2014, des complexes de cuivre(II) portant un ligand de type salen furent utilisés dans le couplage de CEL par le groupe de Gogoi (Figure 1.54).⁸⁰

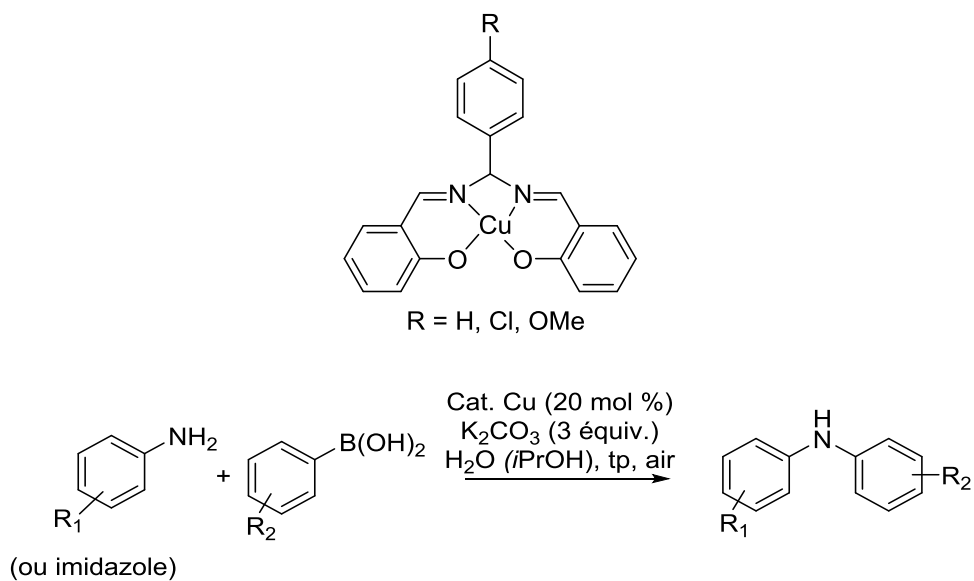


Figure 1.54 : Complexe de cuivre proposé par l'équipe de Gogoi pour la catalyse du couplage de CEL.

Les complexes sont relativement actifs avec les réactifs de types imidazoles puisqu'en quelques heures, à température ambiante, à l'air libre et avec 20 mol % du catalyseur, le couplage est terminé. Cependant, trois équivalents de base carbonatée sont nécessaires, et d'après leurs travaux, les bases organiques sont beaucoup moins efficaces. Dans le cas des anilines, la réaction dans des solvants organiques donne lieu à des rendements faibles. L'ajout d'eau fut indispensable pour parvenir au couplage ainsi qu'une quantité de catalyseur élevée. Par conséquent, ces composés de cuivre ont une activité limitée à certains substrats et ont besoin de conditions opératoires spécifiques comme la présence d'une atmosphère d'oxygène, de tamis moléculaire ou encore d'une base en quantité sub-stochiométrique.

Des complexes de cuivre(II) de type Chitosan furent également testés pour ce couplage par le groupe de Anuradha (Figure 1.55).⁸¹

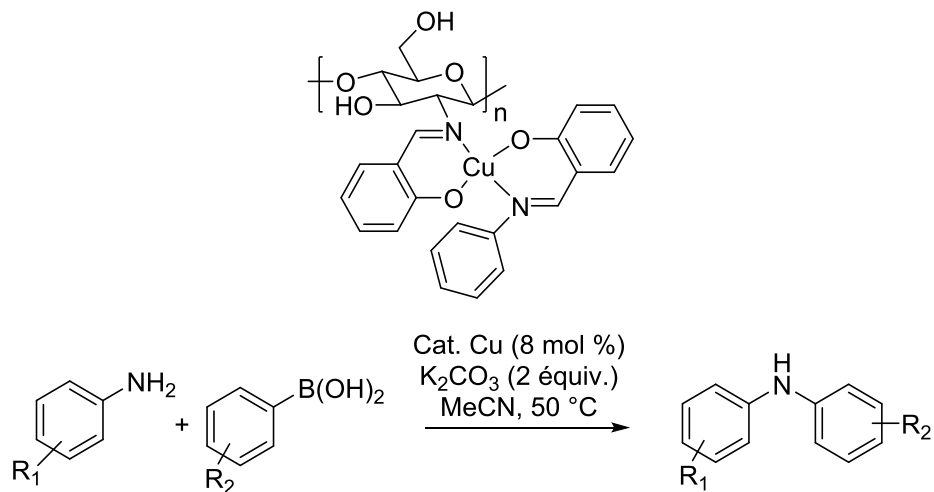


Figure 1.55 : Complexe de cuivre proposé par l'équipe de Chitosan pour la catalyse du couplage de CEL.

Avec ce polymère de cuivre, deux équivalents de base sont nécessaires ainsi qu'un apport énergétique via le chauffage de la solution. Aucune réactivité dans l'eau n'est observée, mais le catalyseur est recyclable.

Enfin, en 2016, Phukan a publié le catalyseur le plus actif existant jusqu'à présent avec des ligands de type DMAP sur le cuivre avec de l'iode comme contre-anion (Figure 1.56).⁸²

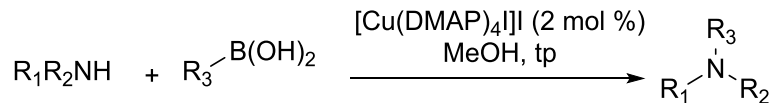


Figure 1.56 : Complexe de cuivre proposé par l'équipe de Phukan pour la catalyse du couplage de CEL.

Le complexe est extrêmement actif et catalyse la réaction d'une large gamme de substrats en moins d'une heure, à température ambiante, dans le méthanol, à l'air libre et avec 2 mol% de catalyseur. Les substrats ciblés sont très variés : amine aliphatique et aromatique, phénol,

thiophène, toylazide et amide aromatique. Ainsi, ils ont développé un système catalytique extrêmement actif pour réaliser le couplage de Chan-Lam, en très peu de temps, avec une grande étendue réactionnelle.

D'après notre revue de la littérature, il existe donc plusieurs complexes de cuivre développés et utilisés pour le couplage de Chan-Evans-Lam. Ceux existants sont très variés allant des cyclodextrines aux catalyseurs supportés en passant par des complexes de type salen. Le choix de complexe préformé semble être avantageux en réduisant le nombre d'additifs nécessaires pour réaliser le couplage. Néanmoins avec l'exception de $[\text{Cu}(\text{DMAP})_4]\text{I}$, leur réactivité n'était montrée que pour un nombre limité de nucléophiles. Nous comparerons donc principalement nos catalyseurs à celui développé par l'équipe de Phukan.

1.3.6. C-N et C-O avec des dérivés de l'acide boronique

Boroxines, esters boronique et sel de trifluoroborate

A la place d'acide arylboronique, Chan a démontré qu'il était aussi possible d'utiliser des esters d'arylboroniques à la fois pour les réactions d'O- et N-arylation.⁸³

Certains de ces réactifs se sont avérés plus réactifs que le dérivé boré initial tandis que d'autres le sont moins, comme le catéchol ester et le pinacolate (Figure 1.57).

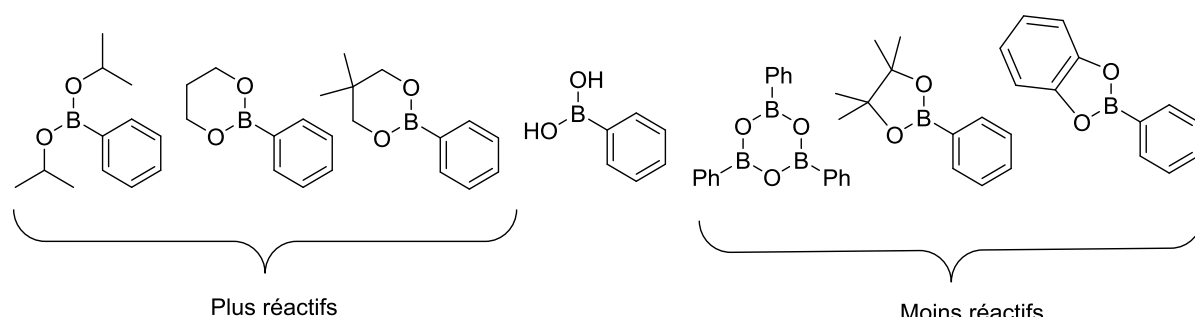


Figure 1.57 : Réactivité des dérivés borés.

Par la suite Batey et Quach ont étudié les sels de trifluoroborate d'aryle et d'alcényle comme agent de couplage (Figure 1.58).⁸⁴ Leur publication détaille un couplage croisé C-O, avec une quantité catalytique de cuivre acétate et DMAP, en présence d'oxygène et de tamis

moléculaire, donnant lieu à de meilleurs rendements que le réactif standard. Puis ils furent en mesure d'étendre cette réaction à des alcools aliphatiques primaires et secondaires ainsi que des amines aliphatiques et aromatiques.

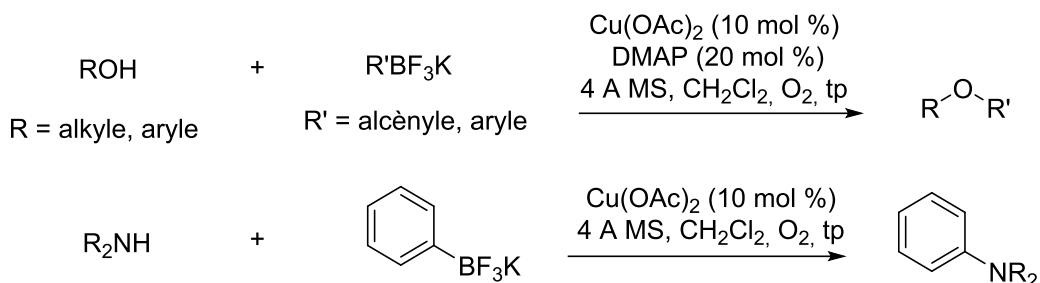


Figure 1.58 : Sels de trifluoroborate d'aryle et d'alcényle comme agent de couplage.

Cependant, les réactions avec cet agent de couplage sont longues du fait de la basse nucléophilicité du bore.

Enfin, Miyaura et son équipe développèrent un nouveau triolborate aryle de potassium pour remplacer les acides boroniques dans le couplage de Chan-Lam (Figure 1.59). Ce composé est stable à l'air et à l'eau et fortement nucléophile.⁸⁵

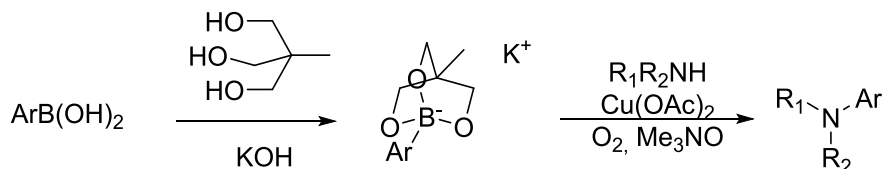


Figure 1.59 : Triolborate aryle de potassium comme agent de couplage.

Ce nouveau système catalytique est réalisé en présence d'un réoxydant (O₂, triméthylamine N-oxide) et une quantité catalytique de cuivre (10 mol%). D'après les travaux, ce composé présente une bien meilleure activité catalytique puisqu'il couple le substrat trois fois plus vite que l'acide boronique et aboutit à de meilleurs rendements que le trifluoroborate arylé de potassium. Le toluène doit être nécessairement utilisé pour éviter les réactions secondaires menant à la formation de phénol ou éther diaryle.

L'équipe d'Hartwig a travaillé sur une voie synthétique pour former des diaryles d'éther ou d'amine à partir d'arène via deux étapes (Figure 1.60) : une borylation catalysée à l'iridium suivie d'un couplage catalysé au cuivre (Chan-Evans-Lam).⁸⁶

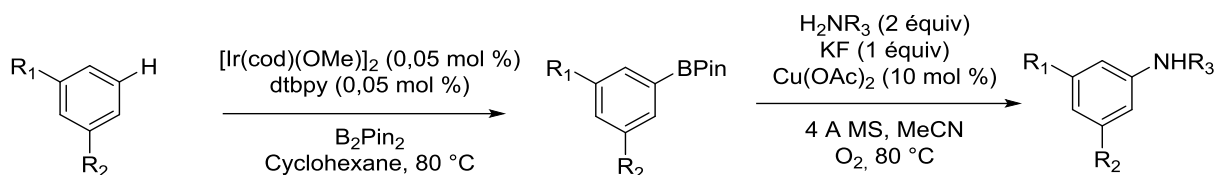


Figure 1.60 : Borylation et catalyse de CEL one-pot.

Ces travaux, en accord avec les observations faites par Batey, montrent bien que le dérivé pinacol de l'acide boronique est moins réactif puisque le couplage est fait à chaud en présence d'oxygène.

Clark et son groupe, bien plus tard en 2015 et 2016, ont étudié la synthèse ortho-aminobenzylamines et ortho-hydroxybenzylamines à partir d'ester boronate benzylamine avec des amines et des phénols (Figure 1.61).⁸⁷ Une réaction de homocouplage en compétition menant au biaryle fut observée, mais en l'absence de base il est possible d'éviter cette réaction secondaire.

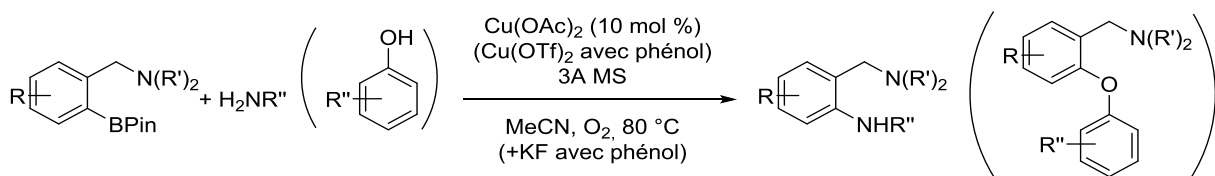


Figure 1.61 : N-arylation versus O-arylation.

En 2016, le groupe de Watson a développé un protocole catalytique général utilisant l'acide boronique arylé pinacol sur des amines arylés ou alkylés (Figure 1.62). Un mélange de solvant MeCN/EtOH est préféré dans le cas des amines arylés. De nouveau, la réaction a lieu à 80 °C.⁸⁸

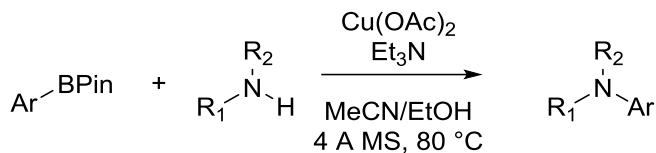


Figure 1.62 : Protocole de Watson.

L'étude de la littérature semble indiquer que le meilleur réactif pour le couplage de Chan-Lam est l'acide boronique et non un ester boronique. La raison doit être que les esters boroniques sont moins réactifs dans l'étape de transmétallation. En effet, le choix de l'acétate de cuivre et non du chlorure de cuivre n'est pas anodin, celui-ci faciliterait l'étape de transmétallation par précoordination de l'acide boronique sur le contre-anion.⁶⁹ De sorte que, utiliser un ester boronique ne permet plus à cet équilibre d'exister ou le rend moins favorable.

Acide alcényle boronique et alcynyle boronique

Lam fut le premier à utiliser les acides alcényles boroniques avec des dérivés aminés et phénols utilisant la catalyse au cuivre (Figure 1.63).⁸⁹ Cependant, des quantités catalytiques donnèrent lieu à des rendements bien plus faibles qu'en quantité stœchiométrique.

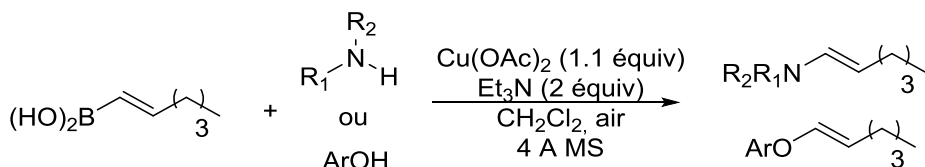


Figure 1.63 : Lam protocole pour les acides alcényles boroniques.

De plus, les acides boroniques vinyliques sont réputés instables et donc rapidement remplacés par McKinley et O'Shea par un complexe trivinylboroxine/pyridine (Figure 1.64).⁹⁰ L'inconvénient est qu'un large excès de pyridine est requis pour obtenir de hauts rendements.

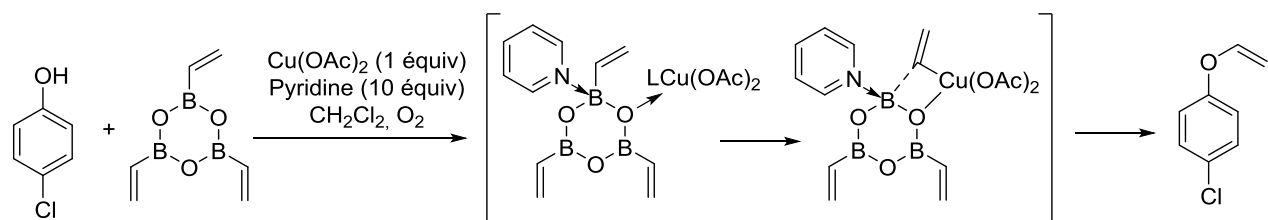


Figure 1.64 : Les complexes trivinylboroxine/pyridine dans le couplage CEL.

Une avancée significative fut le développement de réactions avec des vinyles boronates par le groupe de Merlic (Figure 1.65).⁹¹

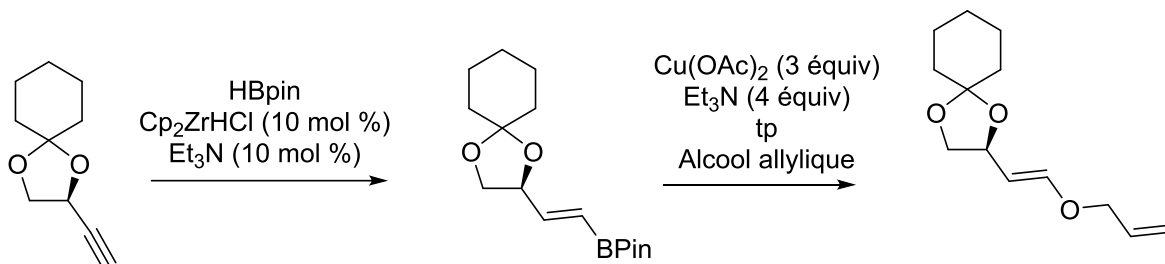


Figure 1.65 : Vinyles boronates en réaction.

Pour ce type de substrat boré, il existe uniquement des conditions opératoires requérant une quantité stœchiométrique de cuivre et une grande quantité de base coordinante.

Acide alkyle-boronique

Le groupe de Lam fut le premier à étudier l'utilisation d'acide alkyle-boronique dans cette réaction promue par le cuivre (Figure 1.66).^{50b} L'acide cyclohexyle-boronique à 70 °C réagit avec la *tert*-butylaniline dans le dichlorométhane, aboutissant après deux jours au produit désiré, avec de faibles rendements puisque plus de la moitié de l'aniline est récupérée.

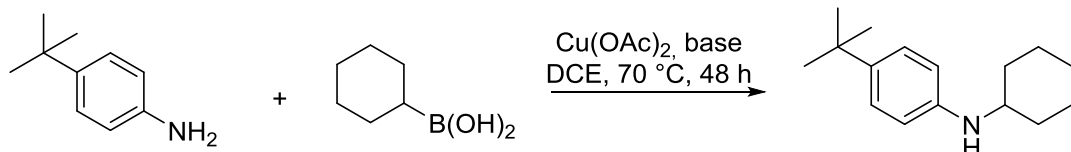


Figure 1.66 : L'acide cyclohexyle-boronique comme substrat dans le couplage de CEL.

La seconde avancée avec ce type de dérivé de bore date de 2008, avec deux groupes qui ont étudié les possibilités de N-cyclopropanation catalysé au cuivre(II) indépendamment.⁹²

Tsuritani se concentra sur les indoles et amides avec une combinaison de Cu(OAc)₂, pyridine ou DMAP et NaHMDS dans le toluène à 95 °C (Figure 1.67).

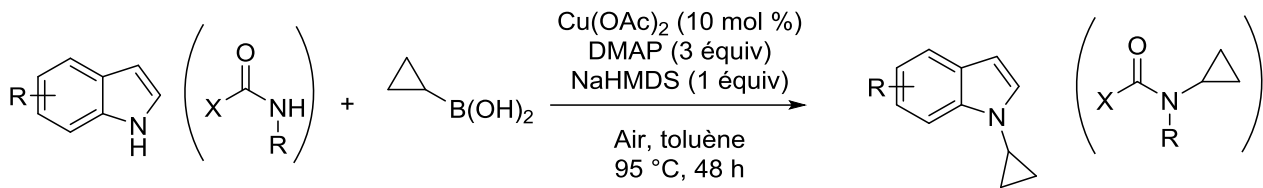


Figure 1.67 : Tsuritani protocole pour le couplage avec l'acide cyclopropyle boronique.

L'équipe de Zhu quant à elle, reporta une réactivité avec les amides, azoles et sulfonamides en présence de bipyridine, de Na_2CO_3 comme base à 70 °C dans le DCE (Figure 1.68).

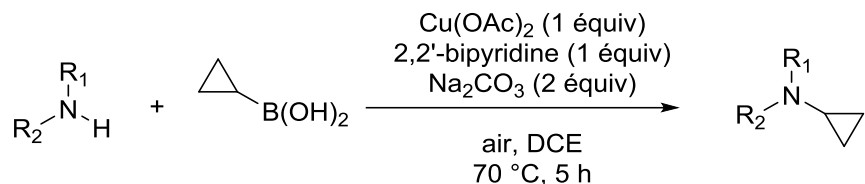


Figure 1.68 : Zhu protocole pour le couplage avec l'acide cyclopropyle boronique.

L'année suivante une méthode fut mise au point pour réaliser le couplage de Chan-Lam avec l'acide méthylboronique pour sélectivement générer la monométhylation de l'aniline (Figure 1.69).⁹³ Différents impératifs sont nécessaires dont une pré-incubation du cuivre, avant l'addition de l'acide boronique en quantité équivalente, pour obtenir de bons rendements.

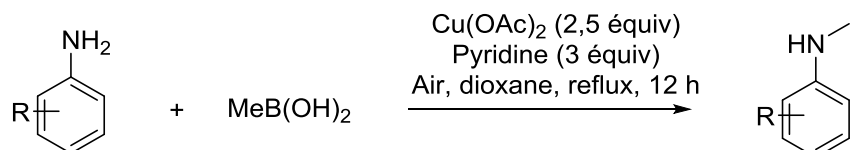


Figure 1.69 : Monométhylation de l'aniline.

Le même groupe de Cruces étendra la réaction de N-alkylation des anilines en utilisant des alkyle-boranes comme partenaire organoboré (Figure 1.70).⁹⁴ Le composé boré est synthétisé *in situ* par hydroboration du styrène correspondant.

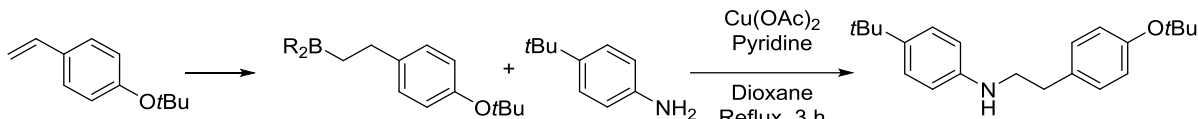


Figure 1.70 : Cruces protocole pour le couplage avec l'acide cyclopropyle boronique.

Cette réaction requiert de hautes températures et des substrats activés par un groupement électrodonneur dans le cas de l'aniline, et électrodonneur dans le cas du styrène. Il ne s'agit donc pas d'un système catalytique généralisable.

Enfin, la dernière publication avec des alkyle-boranes sur des amines et phénols date de 2013 avec un système catalytique comprenant de l'acéate de cuivre et la di-*tert*-butylperoxyde (Figure 1.71). À 100 °C dans le toluène après 24 h et deux équivalents d'oxydant, le produit du couplage croisé est obtenu avec de bons rendements.⁹⁵

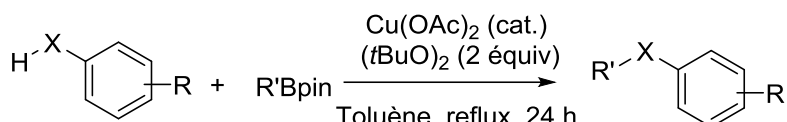


Figure 1.71 : Alkylboranes en réaction co-catalysée par du cuivre et un oxydant.

Les publications sur le couplage d'acide alkyle-boronique, toutes détaillées ci-dessus, sont d'un nombre restreint et présentent beaucoup d'inconvénients. Le premier est que le couplage nécessite des conditions opératoires extrêmement dures avec une température très élevée ainsi qu'un ou plusieurs additifs (base et/ou oxydant). De plus, les protocoles sont très spécifiques au substrat boronique pour lesquels ils sont développés. Aucune explication particulière sur le manque de réactivité de ces substrats borés n'a été proposée, c'est pourquoi il serait intéressant de comprendre où est le problème pour pouvoir y remédier.

1.3.7. Couplage C-N

L'avantage du couplage de Chan-Evans-Lam est sa grande tolérance pour les groupements fonctionnels et son applicabilité sur une large gamme de substrats due à de très douces et efficaces conditions opératoires. Parmi les nucléophiles pouvant réagir dans cette réaction, les

amines sont les plus utilisées et principalement les anilines, pour la simple raison que ce sont les plus réactives.

La première publication du groupe de Chan démontra dès le début que cette réaction est utilisable sur une grande variété de substrats amines (amine, amide, imide, urée, carbamate et sulfonamide) (Figure 1.72). L'utilisation d'une quantité stoechiométrique de cuivre permis de coupler l'acide p-tolylboronique à ces nucléophiles, pour créer des liens C-N.^{53a}

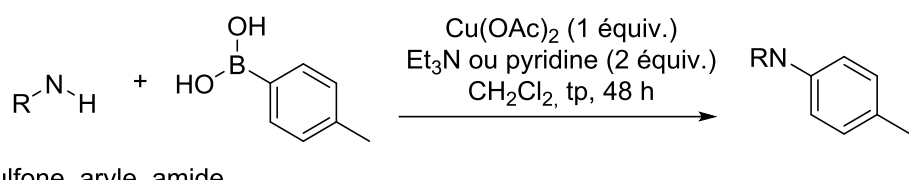


Figure 1.72 : Chan réaction avec les amines.

Lam augmenta peu après les possibilités de cette réaction en étudiant la réactivité de divers hétérocycles (imidazole, pyrazole, triazole, tétriazole, benzimidazole et pyrazole) (Figure 1.73).^{53b} Dans les conditions typiques de Chan, différentes réactivités furent observées suivant la richesse électronique du cycle et l'ajout d'un tamis moléculaire favorisa la réaction.

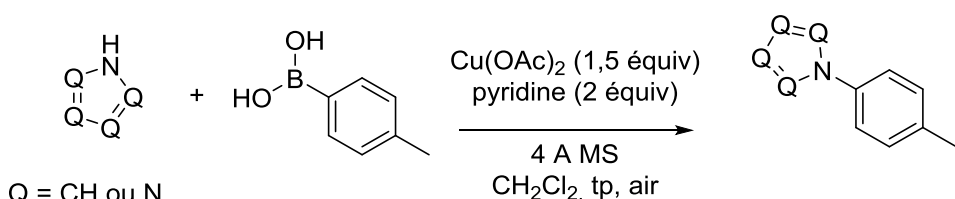


Figure 1.73 : Lam réaction avec les hétérocycles.

Ensuite, les pyrroles et indoles furent ciblés comme substrat pour cette réaction.⁹⁶

Dans les années qui suivirent la découverte de cette réaction, de nombreuses publications apparurent concernant la N-arylation de différents substrats : hétéroarylaminés, imines, amides, lactames et hydantoins.

Collman fut le premier à proposer un couplage introduisant une quantité catalytique de cuivre $[\text{Cu}(\text{OH})\cdot\text{TMEDA}]_2\text{Cl}_2$ (10 mol %) en présence d'oxygène (Figure 1.74).⁷⁶ D'après ces

observations, l'eau diminue les rendements tout comme l'avait remarqué Lam dans sa première publication.

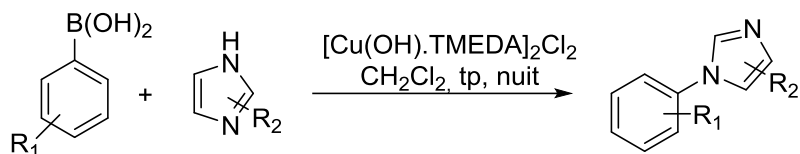


Figure 1.74 : Collman réaction avec les hétérocycles.

L'année suivante, Lam publia sa réaction en utilisant l'acétate de cuivre en quantité catalytique (10 mol %), et la pyridine N-oxide comme additif oxydant.⁹⁷ En présence d'air, la réaction fonctionne également, mais dans certains cas cet oxydant améliore les résultats.

Aujourd'hui, beaucoup de publications proposent différents protocoles pour réaliser le couplage de CEL avec une forte dépendance du substrat. L'utilisation d'une base est souvent requise, tandis que l'air ou l'oxygène est généralement un oxydant suffisant, ce qui ne nécessite pas l'ajout d'un additif complémentaire. Les deux principales limitations de ce couplage sont reliées aux substrats. Certains substrats s'avèrent difficiles à coupler en utilisant le couplage de CEL comme les amines encombrées et les amines secondaires acycliques. De plus, les protocoles utilisés divergent suivant le type de substrat, et les conditions opératoires doivent donc être optimisées suivant l'amine aliphatique ou aromatique ciblée.

1.3.8. Couplage C-O

Parmi les substrats possibles au couplage de Chan-Lam, il y a également les alcools aliphatiques ou aromatiques. Ceux-ci sont moins nucléophiles et de ce fait sont moins réactifs dans ce couplage.

L'équipe de Chan reporta également en 1998 la formation d'un lien C-O via l'intermédiaire de cuivre(II) (Figure 1.75).^{53a} La réaction originale nécessitait deux jours à température ambiante avec une quantité stoechiométrique de cuivre (Cu(OAc)_2) et d'amine (Et_3N) dans le dichlorométhane. D'après leur observation, les acides aryle-boroniques électroniquement riches sont plus réactifs dans ces conditions

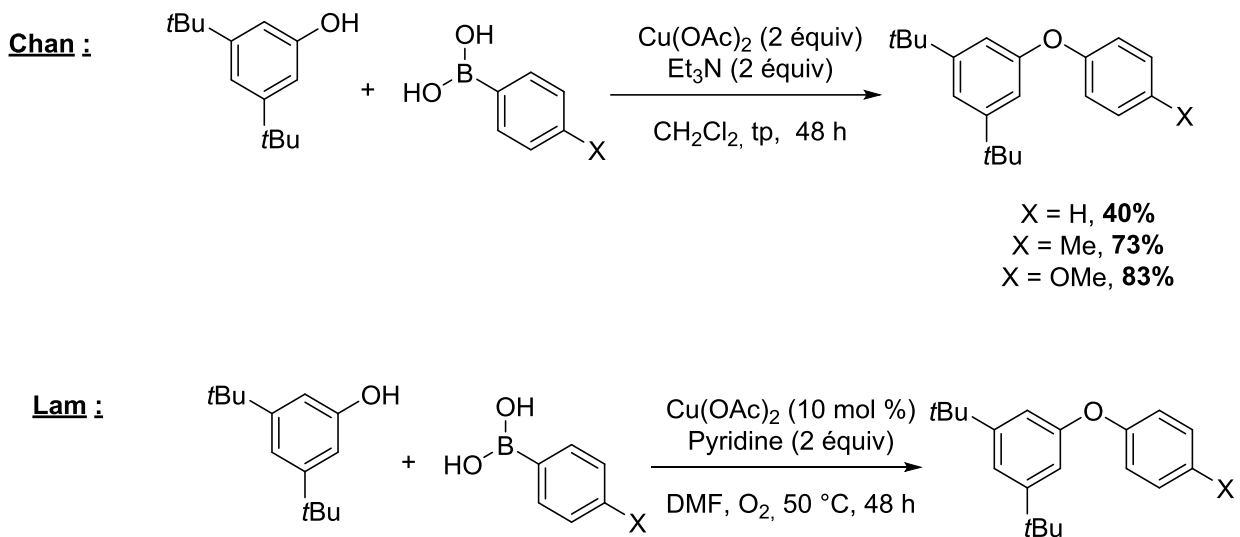


Figure 1.75 : Couplage avec les phénols.

En 2001, Lam réalisa le même couplage avec une quantité catalytique de cuivre, avec différents co-oxydants ou l'oxygène, et utilisant la pyridine comme base (Figure 1.75).⁹⁷ Pour y parvenir, il a cependant dû changer de solvant afin de chauffer le milieu réactionnel à 50 °C.

Similairement au couplage avec les amines, le groupe d'Hartwig développa une méthodologie pour préparer des éthers biarylques à partir des phénols, via une séquence de borylation catalysé à l'iridium, suivi d'une hydrolyse oxydante de l'ester boronique avec une solution aqueuse de périodate de sodium, et enfin un couplage de l'acide boronique avec un arène induit par du cuivre (Figure 1.76).⁸⁸ Pour la dernière étape, un très large excès de base est nécessaire ainsi qu'une quantité stoechiométrique de cuivre.

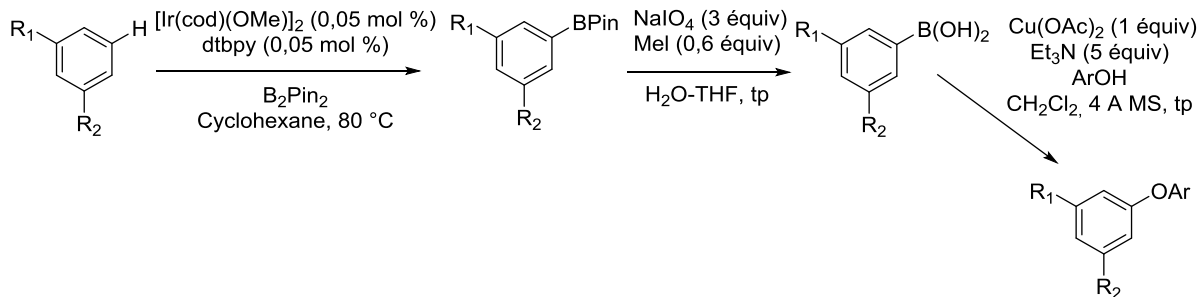


Figure 1.76 : Borylation/couplage avec les phénols.

Ce type de substrat nucléophile (phénol) s'avère donc moins réactif que les dérivés aminés envers le couplage de Chan-Lam. Le nombre de publications avec ces réactifs est beaucoup plus limité et les protocoles font intervenir un large excès de base et souvent d'un co-oxydant.

1.3.9. Couplage C-S

Le couplage avec les thiols est très peu reporté dans la littérature. La première publication date de 2000 où le groupe de Chan réalisa le couplage en présence d'une quantité substœchiométrique de catalyseur et d'une atmosphère d'oxygène (Figure 1.77).⁹⁸ Les rendements se révélèrent plutôt faibles à cause de l'oxydation du thiol menant au dithiane.

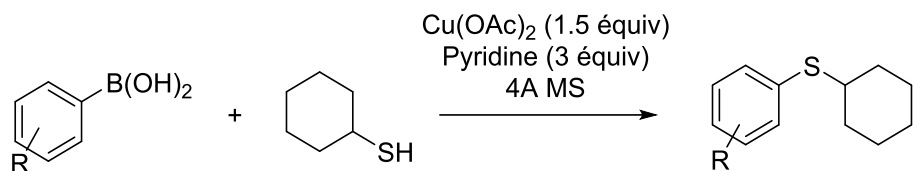


Figure 1.77 : Réaction de Chan avec les thiols.

Pour empêcher ces réactions secondaires, un thiol préactivé fut proposé, catalysé cette fois par du cuivre(I). Il ne s'agit plus d'un couplage oxydant, donc il ne peut être catégorisé dans les couplages de type.⁹⁹

D'autres se sont orientés vers l'utilisation de soufre oxydé, mais cette réaction nécessite la présence d'oxygène et forme de nombreux sous-produits dans certaines conditions (le diphenyl, le diarylether et le phénol) (Figure 1.78).¹⁰⁰

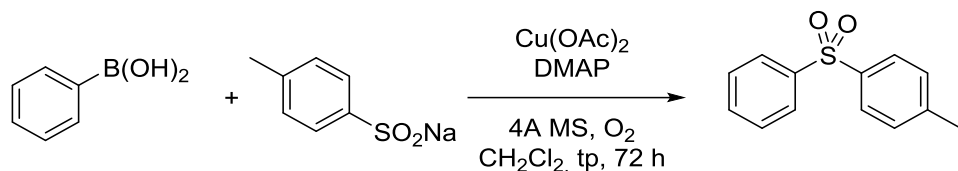


Figure 1.78 : Couplage de CEL avec les sulfinates.

Dans la même idée, plus récemment, en partant de thio-sulfonate, il est possible de faire le couplage, sans formation de sous-produit, à température ambiante (Figure 1.79).¹⁰¹

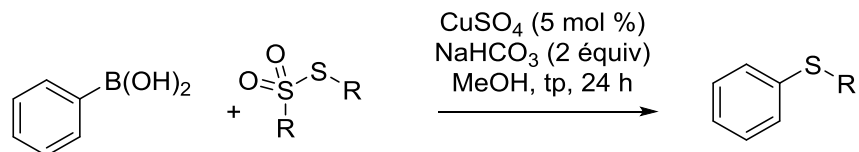


Figure 1.79 : Couplage de CEL avec les thio-sulfonates.

Par la suite, certains groupes se sont intéressés à l'utilisation de disulfide comme substrat, puisque cela semble être un sous-produit commun de la réaction (Figure 1.80).¹⁰² À la fois le cuivre(I) et (II) fonctionnent dans les conditions opératoires via un couplage oxydatif, mais il est nécessaire de chauffer de manière importante à environ 100 °C.

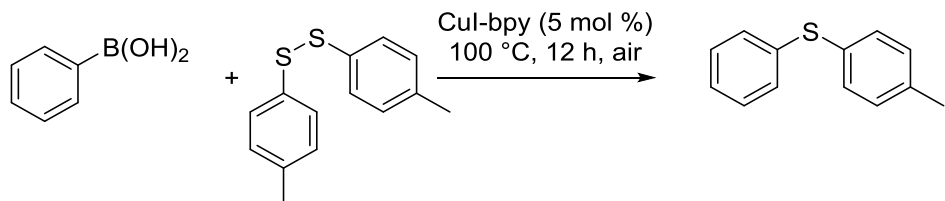


Figure 1.80 : Couplage de CEL avec les disulfides.

Pour revenir au couplage direct avec le thiol, quelques groupes sont récemment parvenus à réaliser ce couplage plus aisément.¹⁰³ D'abord, les conditions nécessitent une atmosphère d'oxygène et une base organique ($n\text{Bu}_4\text{NOH}$, car les bases inorganiques ne fonctionnent pas) (Figure 1.81). De plus, le même groupe fait aussi la réaction avec le cuivre déposé sur une surface solide.

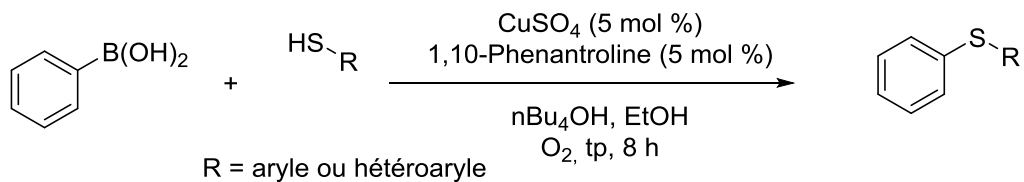


Figure 1.81 : Protocole de couplage de thiol en milieux aqueux.

Une publication, datant de l'année dernière, propose les meilleures conditions opératoires actuelles pour coupler les thiols, via l'utilisation de $[\text{Cu}(\text{DMAP})_4\text{I}]$ (Figure 1.82).¹⁰⁴ La réaction nécessite plus de temps qu'avec les amines dans les mêmes conditions, et les thiols portant un groupe électroattracteur réagissent plus vite, étonnamment.

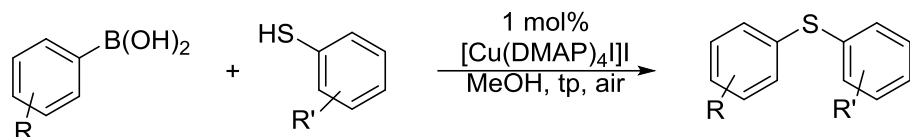


Figure 1.82 : Protocole de couplage des thiols avec un complexe de CuDMAP.

Pour finir, la dernière méthode publiée est également très efficace pour coupler le thiol, elle utilise un complexe de cuivre(II) de type salen dans des conditions douces (Figure 1.83).¹⁰⁵

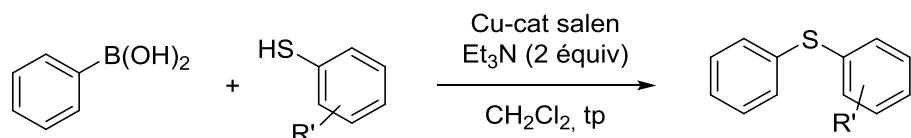


Figure 1.83 : Protocole de couplage des thiols avec un complexe portant un ligand de type salen.

En résumé, dans la littérature, les substrats thiolés s'avèrent peu étudiés, car faiblement réactifs dans ce couplage, du fait de la forte tendance à former les disulfides comme produits secondaires. Pour les dérivés du thiophénol, quelques protocoles ont tout de même pu être développés grâce à la mise au point des complexes métalliques. Quant aux thiols aliphatiques, aucun protocole avec une quantité catalytique de cuivre n'a été rapporté. Pour ce substrat nucléophile, il reste donc du travail de recherche pour permettre un couplage aisément de tous les thiols.

Pour conclure, le couplage de Chan-Evans-Lam est très attractif puisqu'il utilise un catalyseur cuivré peu cher et très répandu, et cette réaction ayant lieu dans des conditions douces donc peut être appliquée sur des substrats sensibles. Cependant, le couplage présente

encore un certain nombre de limitations, notamment autour des substrats réactifs. En effet, concernant les substrats nucléophiles, comme les amines encombrées ou secondaires, la catalyse est difficile. De même, les alcools nécessitent forcément des additifs pour les rendre plus nucléophiles et finalement, les thiols ont une forte tendance à former des disulfides produisant un intermédiaire, peu enclin à être couplé avec un acide boronique.

Une autre observation faite dans la littérature est que, généralement, les protocoles sont spécifiques aux substrats, c'est-à-dire que si le mode opératoire est très efficace pour les amines aliphatiques, il l'est beaucoup moins pour les anilines et inversement.

La dernière problématique très importante du couplage de CEL est le manque de réactivité des acides alkyle-boroniques. Ainsi, avec ce couplage, de nombreuses d'améliorations restent à développer pour proposer un mode opératoire général pour l'ensemble des substrats nucléophiles, comportant un minimum d'additifs et pouvant être actif avec les acides alkyles-boroniques.

Durant mon doctorat, j'ai donc tenté, via le développement de nouveaux complexes cuivrés, de répondre à ces points négatifs du couplage de CEL. Peu de publications proposent des complexes cuivrés pour cette réaction, ce qui cependant pourrait être fortement utile pour limiter les additifs, notamment les bases coordinantes, et augmenter la réactivité générale.

1.4. Objectif de recherche

Mes projets de recherche se sont orientés autour de l'étude de complexes de cuivre portant des ligands sulfonés (Figure 1.84 **(A)** et **(B)**). Quelques complexes carboxylés ont été étudiés à titre de comparaison (Figure 1.84 **(C)**).

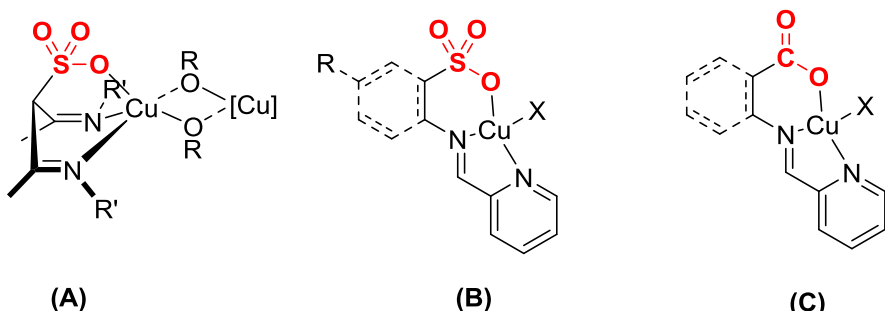


Figure 1.84 : Complexes organométalliques cuivrés ciblés.

L'idée est que le sulfonate pourrait, en se coordinant et décoordinant du centre métallique, libérer un site de coordination pour le lactide (**(A)** et **(B)**) (Figure 1.85). Ces nouveaux complexes auront une haute stabilité envers l'eau, l'oxygène et l'acide lactique même à haute température. Alternativement le lactide peut se coordonner pour former un complexe penta-coordonné avec la faible donation du sulfonate dans la position apicale (**(A)** et **(B)**) (Figure 1.85).

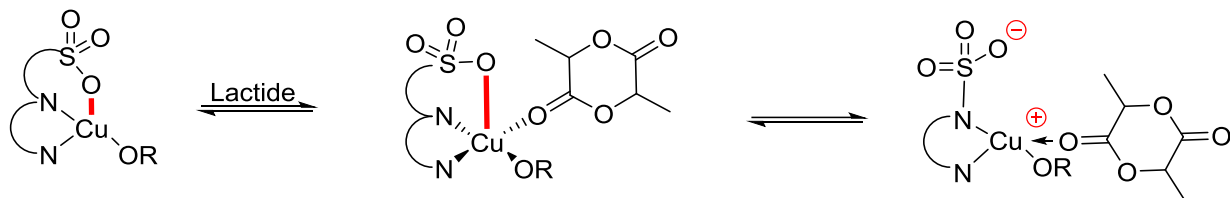


Figure 1.85 : Coordination/décoordination du groupement sulfonate du ligand du métal pour la polymérisation de lactide.

Avec cette idée et à partir des précédents travaux du laboratoire, un premier projet est mis à l'étude concernant des complexes de dikétimines sulfonatés, où principalement le sulfonate pourrait se décoordiner aisément du centre métallique pour faciliter l'insertion du lactide. Ensuite, nous envisageons de développer des complexes imino-sulfonatés toujours cuivrés pour cette application en catalyse. Et finalement, un dérivé très proche des complexes imino-sulfonatés seront étudiés où le sulfonate est remplacé par un carboxylate. Avec ces trois

différents complexes de coordination nous espérons produire des polymères à haut poids moléculaire, stéréoenrichis et dans des conditions douces.

À propos du couplage de Chan-Evans-Lam, les mêmes complexes cités ci-dessus, seront étudiés dans cette réaction. Nous évaluerons leur activité catalytique, leur étendu réactionnel et le potentiel effet du groupement sulfonate présent sur le ligand. Ces complexes pourraient s'avérer très intéressants dans cette réaction, car il est connu que l'étape limitante de ce couplage est la transmétallation. Généralement cette étape du cycle catalytique est favorisée par un contre-anion de type acétate sur le sel cuivré qui favorise le transfert par précoordination de l'acide boronique sur ce groupement. L'avantage de nos complexes est que, du fait de la structure du ligand et notamment la présence d'un groupement sulfonate ou carboxylate, la transmétallation pourrait être aisée.

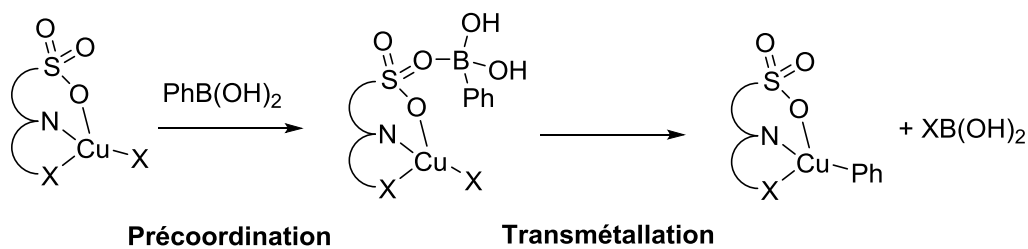


Figure 1.86 : Précoordination facilitant la transmétallation.

La précoordination de l'acide boronique avec nos complexes aurait lieu sur le ligand lui-même. L'ajout d'une base coordinante ne serait plus nécessaire pour activer le cuivre, grâce à la présence du ligand permettant de limiter les conditions opératoires à optimiser et proposer un protocole général.

En résumé, plusieurs complexes organométalliques cuivrés sont ciblés dans le but de réaliser la polymérisation de lactide et le couplage de Chan-Evans-Lam. Pour chacun des trois types de complexes nous étudierons le potentiel catalytique et nous étudierons le mécanisme de la réaction, après avoir mis au point un protocole de synthèse des complexes. Dans la littérature, plusieurs publications se contredisent notamment sur la nécessité d'oxygène pour cette réaction. Stahl le dit indispensable⁶⁸ tandis que Tromp,¹⁰⁶ lui, suggère que le cuivre est

réoxydé par voie radicalaire. Ainsi dans la littérature il manque encore quelques études mécanistiques plus approfondies pour différencier les deux possibilités.

¹ Hammond, C. R. *The Elements, in Handbook of Chemistry and Physics 81st edition. CRC press.* **2004**, ISBN 0849304857.

² Rickwood, P. C. *American Mineralogist* **1981**, 66, 885.

³ <https://pxhere.com/fr/photo/1085633> ; <https://pxhere.com/fr/photo/1031667> ;
<https://pxhere.com/fr/photo/1031667>

⁴ Fenton D. E. *Biocoord. Chem., Oxford Science Publications, 3rd Ed.* **2000**, 2.

⁵ (a) Nicholls, D. *Complexes and First-Row Transition Metal Elements.* **1992**, 201. (b) Housecroft, C. E.; Sharpe, A. G. *Inorganic Chemistry, 3rd Ed.* **2008**, 734.

⁶ <https://www.riverregionfacialplastics.com/copper/>

⁷ (a) Willert-Porada, M. A.; Burton, D. J.; Baenziger, N. C. *J. Chem. Soc., Chem. Commun.* **1989**, 1633. (b) Naumann, D.; Roy, T.; Tebbe, K.-F.; Crump, W. *Angew. Chem., Int. Ed. Engl.* **1993**, 32, 1482. (c) Furuta, H.; Maeda, H.; Osuka, A. *J. Am. Chem. Soc.* **2000**, 122, 803. (d) Ribas, X.; Jackson, D. A.; Donnadieu, B.; Mahía, J.; Parella, T.; Xifra, R.; Hedman, B.; Hodgson, K. O.; Llobet, A.; Stack, T. D. P. *Angew. Chem., Int. Ed.* **2002**, 41, 2991. (e) Santo, R.; Miyamoto, R.; Tanaka, R.; Nishioka, T.; Sato, K.; Toyota, K.; Obata, M.; Yano, S.; Kinoshita, I.; Ichimura, A.; Takui, T. *Angew. Chem., Int. Ed.* **2006**, 45, 7611.

⁸ (a) Kato, M.; Kamigaito, M.; Sawamoto, M.; Higashimura, T. *Macromolecules* **1995**, 28, 1721. (b) Wang, J.-S.; Matyjaszewski, K. *J. Am. Chem. Soc.* **1995**, 117, 5614.

⁹ Glaser, C. *Ber. Dtsc. Chem. Ges.* **1869**, 2, 422.

¹⁰ Hay, A. S. *J. Org. Chem.* **1962**, 27, 3320.

¹¹ (a) Siemsen, P.; Livingston, R. C.; Diederich, F. *Angew. Chem., Int. Ed.* **2000**, 39, 2632. (b) Shun, A. L. K. S.; Tykwiński, R. R. *Angew. Chem., Int. Ed.* **2006**, 45, 1034. (c) Valenti, E.; Pericas, M. A.; Serratosa, F. *J. Am. Chem. Soc.* **1990**, 112, 7405. (d) Liao, Y.; Fathi, R.; Yang, Z. *Org. Lett.* **2003**, 5, 909. (e) Li, D.; 69 Yin, K.; Li, J.; Jia, X. *Tetrahedron Lett.* **2008**, 49, 5918. (f) Yadav, J. S.; Reddy, B. V. S.; Reddy, K. B.; Gayathri, K. U.; Prasad, A. R. *Tetrahedron Lett.* **2003**, 44, 6493. (g) Li, J.; Jiang, H. *Chem. Commun.* **1999**, 2369. (h) Li, J.-H.; Liang, Y.; Xie, Y.-X. *J. Org. Chem.* **2005**, 70, 4393. (i) Liu, Q.; Burton, D. J. *Tetrahedron Lett.* **1997**, 38, 4371.

¹² (a) Ullmann, F.; Bielecki, J. *Ber. Dtsch. Chem. Ges.* **1901**, 34, 2174. (b) Ullmann, F. *Ber. Dtsch. Chem. Ges.* **1903**, 36, 2382. (c) Goldberg, I. *Ber. Dtsch. Chem. Ges.* **1906**, 39, 1691.

¹³ Bohnet, M. *Ullmann's encyclopedia of industrial chemistry. 6th, completely rev. ed.*; Wiley-VCH: Weinheim, **2003**.

¹⁴ Gilman, H.; Jones, R. G.; Woods, L. A. *J. Org. Chem.* **1952**, 17, 1630.

¹⁵ Kolb, H. C.; Finn, M. G.; Sharpless, K. B. *Angew. Chem. Int. Ed.* **2001**, 40, 2004-

¹⁶ (a) Huisgen, R. *Proc. Chem Soc.* **1961**, 357. (b) Huisgen, R. *Angew. Chem. Int. Ed.* **1963**, 75, 13, 565. (c) Huisgen, R. *Angew. Chem., Int. Ed.* **1963**, 2, 633.

¹⁷ (a) Tornoe, C. W.; Christensen, C.; Meldal, M. *J. Org. Chem.* **2002**, 67, 9, 3057. (b) Rostovtsev, V. V.; Green, L. G.; Fokin, V. V.; Sharpless, K. B. *Angew. Chem. Int. Ed.* **2002**, 41, 14, 2596.

¹⁸ a) Xie, X. ; Chen, Y.; Ma, D. *J. Am. Chem. Soc.* **2006**, 128, 16050. b) Cai, Q.; Zou, B.; Ma, D. *Angew. Chem., Int. Ed.* **2006**, 45, 1276. c) Shafir, A.; Buchwald, S. L. *J. Am. Chem. Soc.* **2006**, 128, 8742. d) Zou, B.; Yuan, Q.; Ma, D. *Angew. Chem. Int. Ed.* **2007**, 46, 2598. e) Monnier, F.; Taillefer, M. *Angew. Chem. Int. Ed.* **2009**, 48, 6954.

¹⁹ WERTZ, J.-L. (2011). *L'amidon et le PLA : deux biopolymères sur le marché*. Document ValBiom – Gembloux Agro-Bio Tech ; WERTZ, J.-L. (2016). *Polymères biobasés : amidon, PLA, PHA, PE et PET*. Document ValBiom – Gembloux Agro-Bio Tech.

²⁰ Martien van den Oever, Karin Molenveld, Maarten van der Zee, Harriëtte Bos (2017) *Bio-based and biodegradable plastics – Facts and Figures Focus on food packaging in the Netherlands*. © Wageningen Food & Biobased Research, institute within the legal entity Stichting Wageningen Research.

²¹ (Martien van den Oever, Karin Molenveld, Maarten van der Zee, Harriëtte Bos (2017) Bio-based and biodegradable plastics – Facts and Figures Focus on food packaging in the Netherlands. © Wageningen Food & Biobased Research)

²² Carothers, W. H.; Dorrough, G. L.; Van Natta, F. J. *J. Am. Chem. Soc.* **1932**, 54, 761.

²³ a) Lunt, J. *Polym. Degrad. Stab.* **1998**, 59, 1-3, 145. b) Garlotta, D. *J. Polym. Environ.* **2001**, 9, 2, 63-84 c) Lunt, J.; Shafer, A.L. *J. Ind. Text.* **2000**, 29, 3, 191.

²⁴ (a) O'Keefe, B. J.; Breyfogle, L. E.; Hillmyer, M. A.; Tolman, W. B. *J. Am. Chem. Soc.* **2002**, 124, 4384. (b) Vaidya, A. N.; Pandey, R. A.; Mudliar, S.; Kumar, M. S.; Chakrabarti, T.; Devotta, S. *Crit. Rev. Environ. Sci. Technol.* **2005**, 35, 429.

-
- ²⁵ <https://www.togotopinfos.com/2018/05/10/lansat-reste-engage-a-soutenir-paysans-togolais-80-tonnes-de-achetes/>; <http://french.foodgradeenzyme.com/sale-10715114-fast-acting-bulk-enzyme-powder-fungus-amylase-starch-into-sugars.html>.
- ²⁶ Biron, M. *Thermosets and Composites: Technical Information for Plastics Users*, Elsevier Ltd., 1st edn. **2003**, ch. 2, p. 32.
- ²⁷ (a) Gruber, P. R.; Hall, E. S.; Kolstad, J. J.; Iwen, M. L.; Benson, R. D.; Borchardt, R. L. US Pat., 5 142 023, 1992. (b) Gruber, P. R.; Hall, E. S.; Kolstad, J. J.; Iwen, M. L.; Benson, R. D.; Borchardt, R. L. US Pat., 5 247 058, 1992.
- ²⁸ Drumright, R. E.; Gruber, P. R.; Henton, D. E. *Adv. Mater.* **2000**, 12, 1841.
- ²⁹ Dechy-Cabaret, O.; Martin-Varca, B.; Bourissou, D. *Chem. Rev.* **2004**, 104, 6147.
- ³⁰ Kamber, N. E.; Jeong, W.; Waymouth, R. M. *Chem. Rev.* **2007**, 107, 5813.
- ³¹ (a) Sarazin, Y.; Schormann, M.; Bochmann, M. *Organometallics* **2004**, 23, 3296. (b) Bourissou, D.; Martin-Varca, B.; Dumitrescu, A.; Graullier, M. Lacombe, F. *Macromolecules* **2005**, 38, 9993.
- ³² Hild, F.; Brelot, L.; Dagorne, S. *Organometallics* **2011**, 30, 5457.
- ³³ (a) Nakano, K.; Kosaka, N.; Hiyama, T.; Nozaki, K. *Dalton Trans.* **2003**, 4039. (b) Wu, J.; Yu, T. L.; Chen, C. T.; Lin, C. C. *Coord. Chem. Rev.* **2006**, 250, 602.
- ³⁴ (a) Paukkeri, R.; Vaananen, T.; Lehtinen, A. *Polymer* **1993**, 34, 2488. (b) Coates, G. W. *J. Am. Chem. Soc.* **1996**, 112, 11583.
- ³⁵ Gao, B. ; Zhao, D. ; Li, X. ; Cui Y. ; Duanb, R. ; Pang, X. *RSC Adv.* **2015**, 5, 440.
- ³⁶ Kleine, J.; Kleine, H. H. *Makromol. Chem.* **1959**, 30, 23.
- ³⁷ (a) Kowalski, A. D.; Penczek, S. *Macromol. Rapid Commun.* **1998**, 19, 567. (b) Kowalski, A. D.; Penczek, S. *Macromolecules* **2000**, 33, 20, 7359.
- ³⁸ Liang, C.; Sun, J.; Shi, W.; Chen, D. *J. Appl. Polym. Sci.* **2002**, 86, 3312.
- ³⁹ John, A.; Katiyar, V.; Pang, K.; Shaikh, M. M.; Nanavati, H.; Ghosh, P. *Polyhedron* **2007**, 26, 4033.
- ⁴⁰ Bhunora, S.; Mugo, J.; Bhaw-Luximon, A.; Mapolie, S.; Wyk, J. V.; Darkwa, J.; Nordlander, E. *Appl. Organometal. Chem.* **2011**, 25, 133.

-
- ⁴¹ Mandal, M.; Oppelt, K.; List, M.; Teasdale, I.; Chakraborty, D.; Monkowius, U. *Monatsh Chem* **2016**, 147, 1883.
- ⁴² Chen, L.-L.; Ding, L.-Q.; Zeng, C.; Long, Y.; Lu, X.-Q.; Song, J.-R.; Fan, D.-D.; Jin, W.-J. *Appl. Organometal. Chem.* **2011**, 25, 310.
- ⁴³ Routaray, A.; Nath, N.; Mantri, S.; Maharana, T.; Sutar, A., K. *Chin. J. Catal.* **2015**, 36, 764.
- ⁴⁴ Chakraborty, D; Gowda, R.-R. *J. Mol. Catal. A: Chem.* **2011**, 349, 86.
- ⁴⁵ Schaper, F.; Whitehorne, T. J. *J. Chem. Commun.* **2012**, 48, 10334.
- ⁴⁶ Schaper, F.; Whitehorne, T. J. *J. Inorg. Chem.* **2013**, 52, 13612.
- ⁴⁷ Chen, Y. L.; Hsu, S. J.; Kin, C.-L.; Tsai, C.-Y.; Wang, J.-H.; Ko, B.-T.; Lin, C.-H.; Huang, H.-Y. *J. Polym. Sci., Part A: Polym. Chem.* **2013**, 51, 3840.
- ⁴⁸ Darkwa, J.; Appavoo, D.; Omondi, B.; Guzei, L.-A.; Wyk, J. L.; ZInyemba, O. *Polyhedron* **2014**, 60, 55.
- ⁴⁹ Kwon, K. S.; Cho, J.; Navab, S.; Jeong, J. H. *Inorg. Chem. Com.* **2015**, 55, 36.
- ⁵⁰ Cho, J.; Nayab, S.; Jeong, J. H. *Polyhedron* **2016**, 113, 81.
- ⁵¹ Schaper, F.; Fortun, S.; Daneshmand, P. *Angew. Chem. Int. Ed.* **2015**, 54, 13669.
- ⁵² Ahn, S H.; Chun, M. K.; Kim, E.; Jeong, J. K.; Nayab, S.; Lee, H. *Polyhedron* **2017**, 127, 51.
- ⁵³ (a) Chan, D. M. T.; Monaco, K. L.; Wang, R.- P.; Winteres, M. P. *Tetrahedron Lett.* **1998**, 39, 2933. (b) Lam, P. Y. S.; Clark, C.- G.; Saubern, S.; Adams, J.; Winters, M. P.; Chan, D. M. T.; Combs, A. *Tetrahedron Lett.* **1998**, 39, 2941. (c) Evans, D. A.; Katz, J. L.; West, T. R. *Tetrahedron Lett.* **1998**, 39, 2937.
- ⁵⁴ Ullmann, F. *Chem. Ber.* **1905**, 38, 2211.
- ⁵⁵ Hartwig, J. F.; Louie, J. *Tetrahedron Lett.* **1995**, 36, 3609.
- ⁵⁶ Kiyomori, A.; Marcoux, J.-F.; Buchwald, S. L. *Tetrahedron Lett.* **1999**, 40, 2657.
- ⁵⁷ (a) Klapars, A.; Antilla, J.; Huang, X.; Buchwald, S. L. *J. Am. Chem. Soc.* **2001**, 123, 7727.
- ⁵⁸ Antilla, J. C.; Klapars, A.; Buchwald, S. L. *J. Am. Chem. Soc.* **2002**, 124, 11684.

⁵⁹ Kwong, F.; Klapars, A.; Buchwald, S. *Org. Lett.* **2002**, 4, 581.

⁶⁰ Altman, R. A.; Anderson, K.; Buchwald, S. L. *J. Org. Chem.* **2008**, 73, 5167.

⁶¹ Kwong, F. Y.; Buchwald, S. L. *Org. Lett.* **2003**, 5, 793.

⁶² Stahl, S. S.; Brunold, T. C.; King, A. E. *J. Am. Chem. Soc.* **2009**, 131, 5044.

⁶³ Huffman, L. M.; Stahl, S. S. *J. Am. Chem. Soc.* **2008**, 130, 9196.

⁶⁴ Lam, P. Y. S.; Bonne, D.; Vincent, G.; Clark; C. G.; Combs, A. P. *Tetrahedron Lett.* **2003**, 44, 1691.

⁶⁵ (a) Terent'ev, A. P.; Mogilianskii, D. J. *Gen. Chem. USSR* **1958**, 28, 2002. (b) Lu, W.; Xi, C. *Tetrahedron Lett.* **2008**, 49, 4011. (c) Zhang, C.; Jiao, N. *Angew. Chem., Int Ed.* **2010**, 49, 6174. (d) Zhang, M.; Zhang, R.; Zhang, A.-Q.; Li, X.; Liang, H. *Synth. Commun.* **2009**, 39, 3428.

⁶⁶ (a) Kinoshita, K. *Bull. Chem. Soc. Jpn.* **1959**, 32, 780. (b) Terent'ev, A. P.; Mogilyanskii, Ya. D. *J. Gen. Chem. USSR* **1961**, 31, 298.

⁶⁷ Lu, W.; Xi, C. *Tetrahedron Lett.* **2008**, 49, 4011.

⁶⁸ Zhang, C.; Jiao, N. *Angew. Chem., Int Ed.* **2010**, 49, 6174.

⁶⁹ (a) Minakata, S.; Ohshima, Y.; Takemiya, A.; Ryu, I.; Komatsu, M.; Ohshiro, Y. *Chem. Lett.* **1997**, 311. (b) Uemura, S. *Bull. Chem. Soc. Jpn.* **2003**, 76, 2399.

⁷⁰ (a) Adimurthy, S.; Patil, R. D. *Adv. Synth. Catal.* **2011**, 353, 1695. (b) Itoh, S.; Tabuchi, K.; Sugimoto, H.; Kunishita, A.; Fujieda, N. *Inorg. Chem.* **2011**, 50, 5, 1633. (c) Kerton, F. M.; Hu, Z. *Org. Biomol. Chem.* **2012**, 10, 1618. (d) Gu, H.; Wang, J.; Lu, S.; Cao, X. *Chem. Commun.* **2014**, 50, 5637. (e) Marui, K. ; Nomoto, A. ; Ueschima, M. ; Ogawa, A. *Tetrahedron Lett.* **2015**, 56, 1200.

⁷¹ Li, W.; Fan, Y.; Xia, Y.; Rocchi, P.; Zhu, R.; Qu, F.; Neyts, J.; Iovanne, J. L.; Peng, L. *Helv. Chim. Acta* **2009**, 92, 1503.

⁷² King, A. E.; Ryland, B. L.; Brunold, T. C.; Stahl, S. S. *Organometallics* **2012**, 31, 7948.

⁷³ (a) Collman, J. P.; Zhong, M. *Org. Lett.* **2000**, 2, 1233. (b) Collman, J. P.; Zhong, M.; Zhang, C.; Costanzo, S. *J. Org. Chem.* **2001**, 66, 7892.

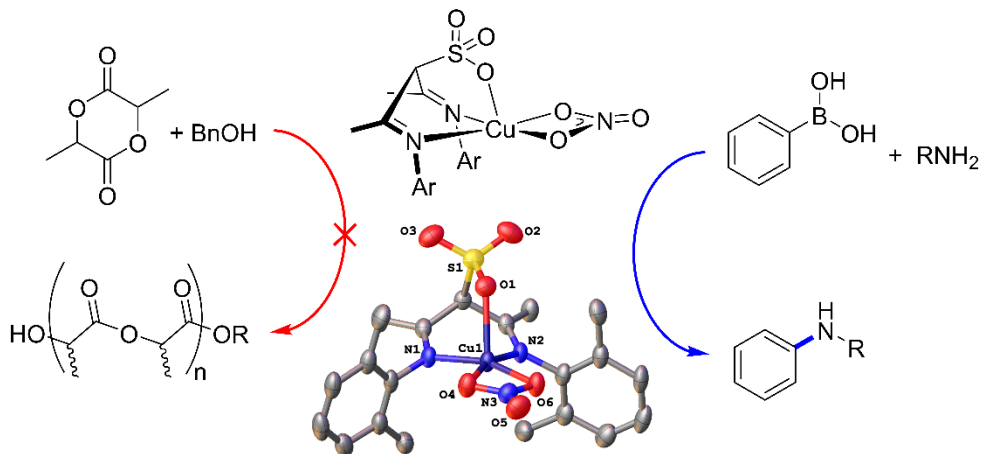
⁷⁴ Van Berkel, S. S.; Van den Hoogenband, A.; Terpstra, J. W.; Tromp, M.; Van Leeuwen, P. W. N. M.; Van Strijdonck, G. P. F. *Tetrahedron Lett.* **2004**, 45, 7659.

-
- ⁷⁵ Chiang, G.; Olsson, T. *Org. Lett.* **2004**, 6, 18, 3079.
- ⁷⁶ Choudary, B. M.; Kantam, M. L.; Venkanna, G. T.; Sridhar, C.; Sreedhar, B. *J. Org. Chem.* **2006**, 71, 9522.
- ⁷⁷ Lin, Y.; Cai, M.; Fang, Z.; Zhao, H. *Tetrahedron* **2016**, 72, 3335.
- ⁷⁸ Kaboutin, B.; Abedi, Y.; Yokomatsu, T. *Eur. J. Org. Chem.* **2011**, 6656.
- ⁷⁹ Chen, W.; Zhou, Y.; Liu, B.; Liu, B. *Organometallics* **2010**, 29, 1457.
- ⁸⁰ Gogoi, A.; Sarmah, G.; Dewan, A.; Bora, U. *Tetrahedron Lett.* **2014**, 55, 31.
- ⁸¹ Anuradha, S.; Kumari, S.; Pathak, D. D. *Tetrahedron Lett.* **2015**, 56, 4135.
- ⁸² Phukan, P.; Kashyap, B.; Sarma, M. J.; Roy, S. *Chem. Commun.* **2016**, 52, 1170.
- ⁸³ Chan, D. M. T.; Monaco, K. L.; Bonne, D.; Li, R.; Clark, C. G.; Lam, P. Y. S. *Tetrahedron Lett.* **2003**, 44, 3863.
- ⁸⁴ (a) Batey, R. A.; Quach, T. A. *Org. Lett.* **2003**, 5, 1381. (b) Batey, R. A.; Quach, T. A. *Org. Lett.* **2003**, 5, 4397. (c) Batey, R. A.; Bolshan, Y. *Angew. Chem. Int. Ed.* **2008**, 47, 2109.
- ⁸⁵ (a) Miyaura, N.; Yu, X. Q.; Takizawa, M.; Yamamoto, Y. *Angew. Chem. Int. Ed.* **2008**, 47, 928. (b) *Chem. Asian J.* **2008**, 3, 1517.
- ⁸⁶ Hartwig, J. F.; Murphy, J.; Tzschucke, C. *Org. Lett.* **2007**, 9, 5, 761.
- ⁸⁷ (a) Clark, T. B.; Duenas, A. A.; McGarry, K. A. *J. Org. Chem.* **2015**, 80, 7193. (b) Clark, T. B.; Ferber, C. J.; McGarry, K. A.; Marcum, J. S. *J. Org. Chem.* **2016**, 81, 7963.
- ⁸⁸ Watson, A. J. B.; Atkinson, S. J.; Isidro-Llobet, A.; Law, R. P.; Vantourout, J. C. *J. Org. Chem.* **2016**, 81, 3942.
- ⁸⁹ Lam, P. Y. S.; Clark, C. G.; Saubern, S. A.; Averill, K. M.; Chan, D. M. T.; Combs, A. *Synlett* **2000**, 674.
- ⁹⁰ McKinley, N. F.; O'Shea, D. F. *J. Org. Chem.* **2004**, 69, 5087.
- ⁹¹ Merlic, C. A.; Olsen, J.-C.; Hyde, A. M.; Shade, R. E. *J. Am. Chem. Soc.* **2010**, 132, 1202.

-
- ⁹² (a) Tsuritani, T.; Strotman, N. A.; Yamamoto, Y.; Kawasaki, M.; Yasuda, N.; Mase, T. *Org. Lett.* **2008**, 10, 1653. (b) Zhu et al. *J. Org. Chem.* **2008**, 73, 6441.
- ⁹³ Cruces, J.; Rodriguez, R.; Guerrero, C.; Mosquera, J.; Gonzalez, I. *J. Org. Lett.* **2009**, 11, 1677.
- ⁹⁴ Cruces, K. Rodriguez, R.; Larrosa, M.; Naya, L. *Tetrahedron Lett.* **2012**, 53, 769.
- ⁹⁵ Kuninobu Y.; Sueki, S. *Org. Lett.* **2013**, 15, 7, 1544.
- ⁹⁶ (a) Mederski, W. W. K. R.; Lefort, M.; Germann, M.; Kux, D. *Tetrahedron* **1999**, 55, 12757. (b) Yu et al. *Org. Chem.* **2002**, 67, 1699. (c) Bekolo H. *Can. J. Chem.* **2007**, 85, 42.
- ⁹⁷ Lam, P. Y. S.; Deudon, S.; Hauptman, E.; Clark, C. G. *Tetrahedron Lett.* **2001**, 42, 2427.
- ⁹⁸ Kiplin Guy, R.; Pendola, K. A.; Herradura, P. S. *Org. Lett.* **2000**, 2, 14, 2019.
- ⁹⁹ Savarin, C.; Srogl; J.; Liebeskind, L. S. *Org. Lett.* **2002**, 4, 24, 4309.
- ¹⁰⁰ Batey, R. A.; Huang, F. *Tetrahedron* **2007**, 63, 7667.
- ¹⁰¹ Yoshida, S.; Sugimura, Y.; Hazama, Y.; Nishiyama, Y.; Yano, T.; Shimizu, S.; Hosoya, T. *Chem. Commun.* **2015**, 51, 16613.
- ¹⁰² Taniguchi, N. *J. Org. Chem.* **2007**, 72, 1241.
- ¹⁰³ (a) Xu, H.- J.; Zhao, Y.- Q.; Feng, T.; Feng, Y.-S. *J. Org. Chem.* **2012**, 77, 2878. (b) Zhao, H.; Fang, Z.; Cai, M.; Lin, Y. *Tetrahedron* **2016**, 72, 3335.
- ¹⁰⁴ Roy, S.; Sarma, M. J.; Kashyap, B.; Phukan, P. *Chem. Commun.* **2016**, 52, 1170.
- ¹⁰⁵ Azam, M.; Dwivedi, S.; Al-Resayes, S. I.; Shahidul, M.; Islam, S.; TRzesowska-Kruszynska, A.; Kruszynski, R.; Lee, D.-U. *Journal of Molecular Structure* **2017**, 1130, 122.
- ¹⁰⁶ Tromp, M.; van Strijdonck, G. P. F.; van Berkel, S. S.; van den Hoogenband, A.; Feiters, M. C.; de Bruin, B.; Fiddy, S. G.; van der Eerden, A. M. J.; van Bokhoven, J. A.; van Leeuwen, P. W. N. M.; Koningsberger, D. C. *Organometallics* **2010**, 29, 3085.

2. Sulfonato-diketimine Copper(II)

Complexes : Synthesis and
Application as Catalysts in
Chan–Evans–Lam Couplings



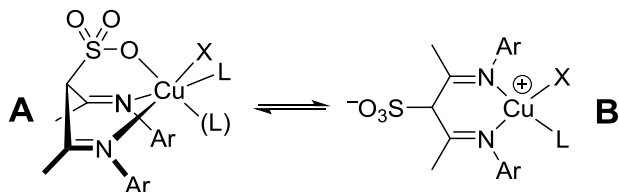
Reprinted with permission from

V. Hardouin Duparc, F. Schaper *Organometallics* **2017**, *36*, 3053–3060.

Copyright 2017 American Chemical Society.

2.1. Introduction

Diketiminate (“*nacnac*”) ligands, the nitrogen equivalent of the ubiquitous acetylacetone ligand, have been known since the 60s¹ but gained increasing popularity starting in the mid 90s,² following the success of the related diimino ligands in α -olefin polymerization.³ Copper complexes of diketiminate ligands were among the first metal complexes reported for this ligand¹ and have been since then employed, for example, as biomimetic model systems,⁴ as catalysts for a variety of organic transformations, or as ⁵CVD/ALD precursors.⁶ We had recently shown that copper diketiminates provide highly active lactide polymerization catalysts.⁷ While diketiminate ligands have several advantages, they are highly basic, sensitive to protonation or even to oxidation by oxygen at the 3-position.⁸ In 2014, Reddy published a series of metal complexes incorporating a sulfonated diketimine ligand.⁹ We postulated, based on the structures observed for Pd, Co, Ni, and Zn complexes,⁹ that copper complexes with this type of ligand might be able to interconvert between a five-coordinated ground state, **A**, and a square-planar betaine complex, **B**, in the catalytic cycle (Scheme 2-1). The latter strongly resembles the typical diketiminate ligand coordination but is stable against protonation or oxidation.



Scheme 2-1

In the present study, we report synthesis and structures of copper complexes with diketimino-sulfonate ligands and their application in catalysis. Reactivity in lactide polymerization was explored, given the structural similarity of betaine **B** to successful copper diketiminate complexes.^{7a-c} Chan–Evans–Lam couplings¹⁰ were investigated, since the sulfonate group

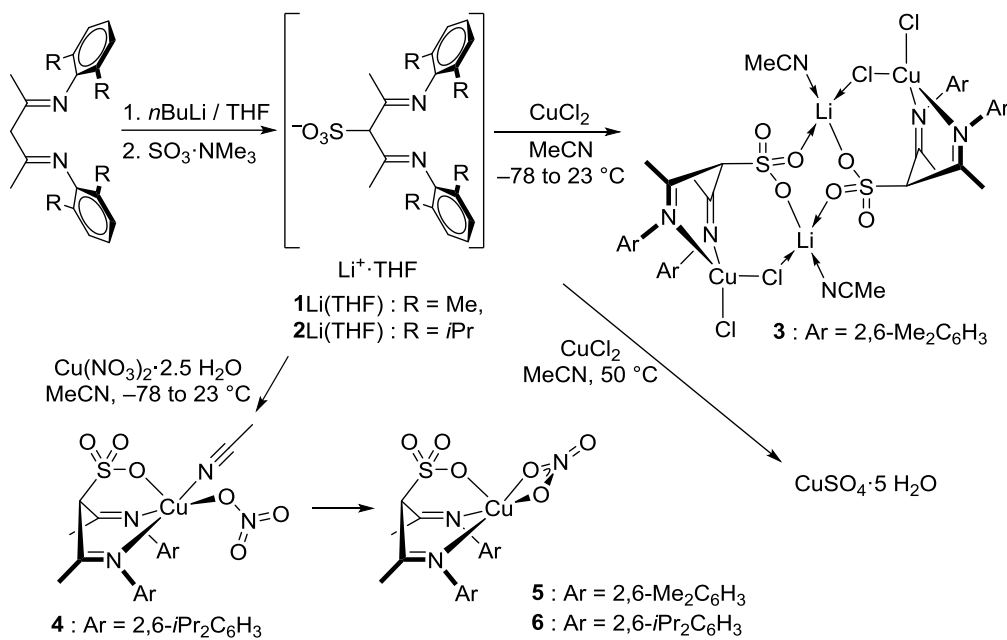
might allow coordination to boronic acid, which is normally postulated to be achieved by interaction with the counteranion or other anionic ligands.¹¹

2.2. Results and discussion

2.2.1. Synthesis

Lithiated ligands **1Li(THF)** and **2Li(THF)** were prepared according to the procedure of Reddy et al. from lithiated diketiminate and $\text{SO}_3\cdot\text{NMe}_3$ (Scheme 2-2).⁹ Preparation of similar ligands with N-alkyl groups (benzyl or methylbenzyl) was unsuccessful, however, and resulted in double sulfonation of the diketiminate salt even in the presence of excess diketiminate. Neither variation of the reaction conditions (temperature, solvent, concentrations) nor attempted sulfonation of the neutral diketimine or attempted sulfonation of a copper diketiminate complex yielded the desired products with aliphatic N-substituents.

Reaction of **1Li(THF)** with anhydrous CuCl_2 in acetonitrile yielded the cluster compound $\{(1)\text{CuCl}\cdot\text{LiCl}\cdot\text{MeCN}\}_2$, **3** (Scheme 2-2). The X-ray structure of **3** revealed that the sulfonate group is coordinated to lithium, but not to copper (Figure 2.1). An acetonitrile ligand, coordination of a sulfonate from a neighboring molecule, and a μ -chloride ligand complete the coordination geometry around lithium. Two chloride ligands around copper balance the charge of the metal center. Copper shows a coordination geometry intermediate between square-planar and tetrahedral with an angle of 55° between the CuN_2 and the CuCl_2 planes.



Scheme 2-2

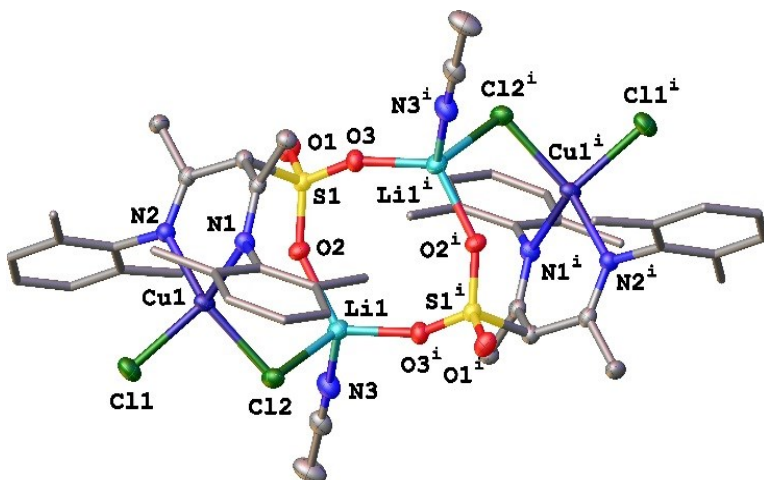


Figure 2.1 : X-ray structure of **3**. Hydrogen atoms were omitted for clarity. Thermal ellipsoids are drawn at 50% probability. Selected geometrical data: Bond distances [Å]: Cu1–Cl1: 2.2408(8), Cu1–Cl2: 2.2488(8), Cu1–N1: 1.998(2), Cu1–N2: 2.002(2), Li1–Cl2: 2.371(5), Li1–O2: 1.906(5), Li1–O3ⁱ: 1.909(5), Li1–N3: 2.030(5), S1–O1: 1.437(2), S1–O2: 1.460(2). Bond angles [°]: Cl1–Cu–Cl2: 95.48(3), N1–Cu1–N2: 92.32(9), X–Li1–Y: 96.2(2)–120.2(3).

Heating a reaction of **1** $\text{Li}(\text{THF})$ with CuCl_2 to 50 °C led to hydrolysis, desulfonation of the ligand and precipitation of $\text{CuSO}_4 \cdot 5 \text{ H}_2\text{O}$. To avoid bridging incorporation of LiCl , the counteranion was switched to nitrate. Reaction of $\text{Cu}(\text{NO}_3)_2 \cdot 2.5 \text{ H}_2\text{O}$ with **2** $\text{Li}(\text{THF})$ led to the five-coordinated complex $(\mathbf{2})\text{Cu}(\text{NO}_3)\cdot\text{NCMe}$, **4**. The crystal structure of **4** confirms that the sulfonate ligand is coordinated to copper, which requires distortion of the diketimine ligand into a boat-conformation (Figure 2.2, Table 2-1), a conformation also observed in anionic diketiminate complexes.^{2,12} The nitrate ligand is monodentate with a bonding Cu1–O1 distance of 1.967(5) Å, although a weak interaction exists with O5 (Cu1–O5 = 2.5 Å). The resulting coordination geometry around Cu is square-pyramidal ($\tau = 0.0$). The sulfonate ligand is found in the apical position with a considerably elongated Cu–O bond compared to the nitrate ligand (Cu–O1: 2.399(5) Å).

Table 2-1 : Bond Lengths (Å) in Crystal Structures of **4–6**.

	4	4·2 H₂O	5	6
Cu-N _{imine}	2.021(5), 2.021(6)	2.020(3), 2.031(3)	1.969(3), 1.972(3)	1.960(1), 1.960(1)
Cu-OSO ₂	2.399(5)	2.421(3)	2.254(3)	2.303(2)
Cu-NCMe	2.005(7)	2.319(4)		
Cu-O ^a	1.967(5), 2.503(5)	2.001(3), 2.008(3)	1.998(3), 2.012(3)	2.015(1), 2.015(1)
τ	0.0	octahedral	0.0	0.0

^a for **4–6**: Cu-ONO₂; for **5**: Cu-OH₂

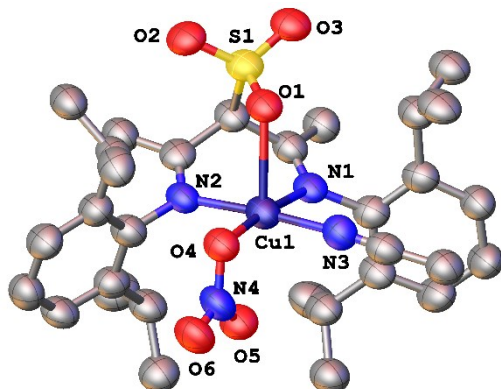


Figure 2.2 : Crystal structure of **4**. Hydrogen atoms omitted for clarity.

Recrystallization or crystallization from dry dichloromethane afforded solvent-free complexes **5** and **6**. The coordination geometry around copper remains square-pyramidal ($\tau = 0.0$) and a bidentate coordination of the nitrate ligand replaces the acetonitrile in **4** (Figure 2.3). The overlap due to the smaller bite angle, resulted in significantly shorter Cu–N and Cu–OSO₂ distances (Table 2-1).

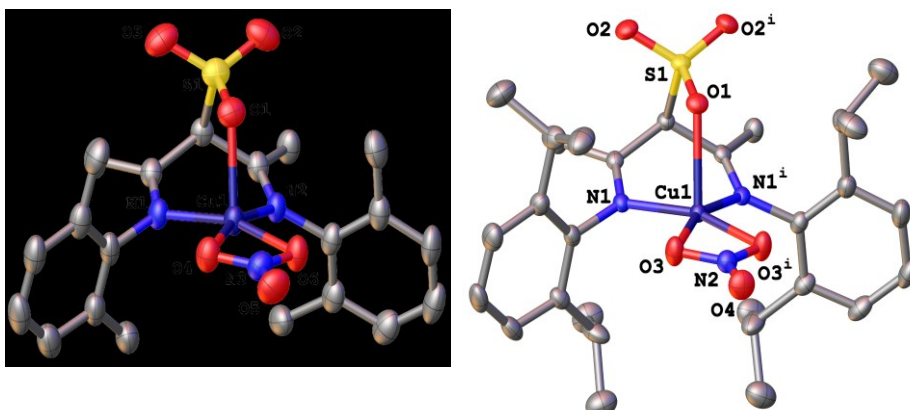


Figure 2.3 : X-ray structure of **5** (left) and **6** (right). Hydrogen atoms and co-crystallized dichloromethane in **6** are omitted for clarity. Thermal ellipsoids are drawn at 50% probability.

2.2.2. Complex Stability in the Presence of Water

Solutions of **4** in undried methanol open to ambient atmosphere showed only a slight variation of the UV-vis spectrum over a period of 24 h, and the absorption at 770 nm retained

most of its intensity. When approximately 20 equiv of water were added, the same change to an intense green solution (slight reduction of the intensity at 770 nm, slight increase around 550 nm) was observed in the first 8 h, but standing for additional 12 h led to complete disappearance of the absorption at 770 nm (Figure 2.4). From the obtained solution, crystals separated, which were identified as CuSO₄·5 H₂O by X-ray diffraction. Single crystals obtained under different conditions provide additional insight into reactions with water. Crystallization of **4** in undried dichloromethane afforded green crystals of complex **4**·2 H₂O, in which two water ligands replaced the coordinated nitrate (Figure 2.4, Table 2-1). In reactions of **4** with strong bases (*vide infra*), crystallizations yielded CuSO₄·5 H₂O as well as diketimine complex **7**, in which the sulfonate group was lost (Figure 2.4). On the basis of these results, it seems likely that **4** forms aquo or methanol complexes similar to **4**·2 H₂O, which are responsible for the minor change of the UV/vis spectra in the first hour(s). At prolonged standing in the presence of larger amounts of water (but not in undried methanol), desulfonation occurs by attack of water at the sulfonate group (Figure 2.4). Complex **4** is thus stable in undried methanol solution even in the presence of excess of water for at least several hours.

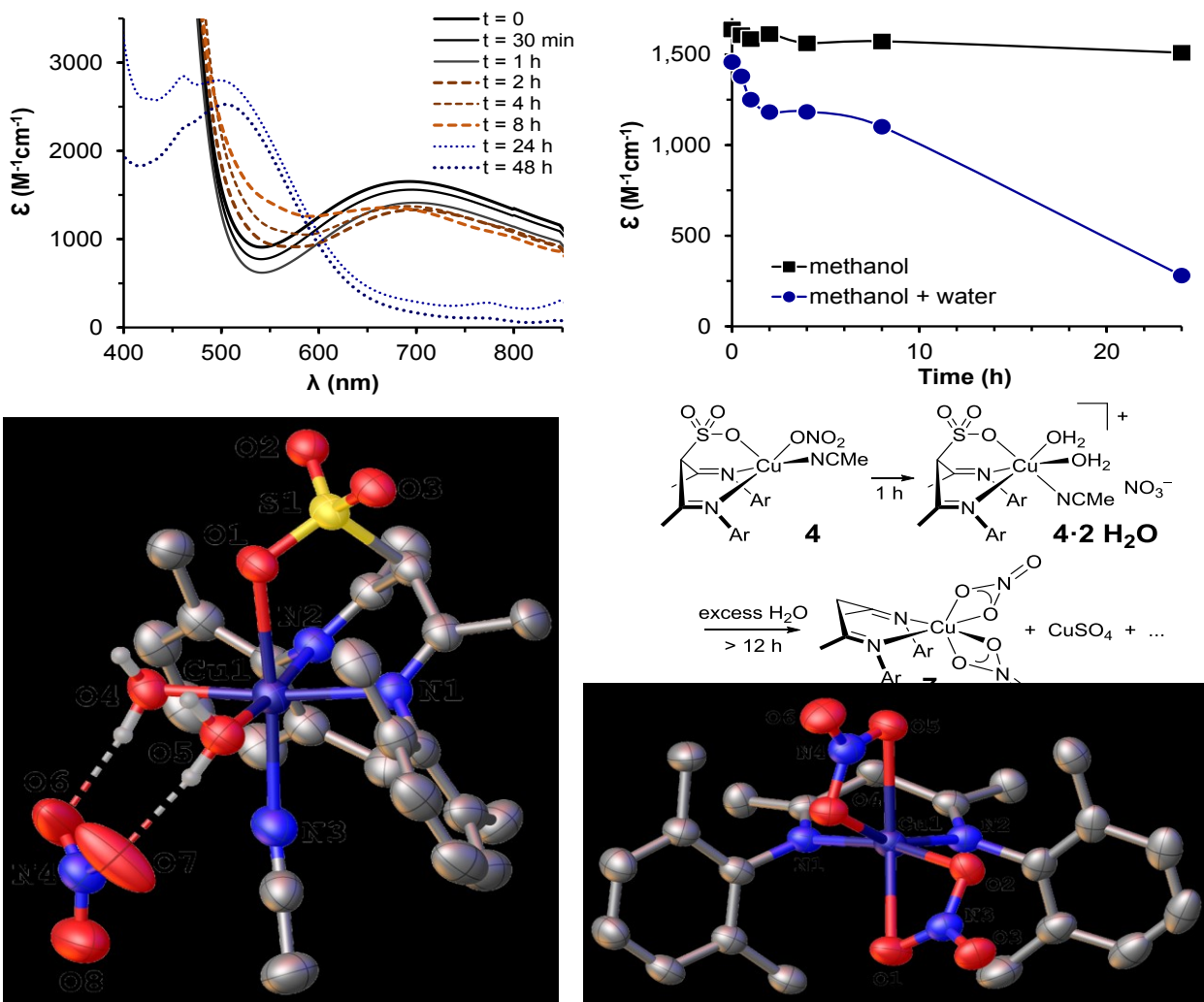


Figure 2.4 : Top left: UV/vis spectra of **4** in methanol in the presence of 20 equiv of water. Top right: Change of the intensity of absorption at 700 nm over time in the presence or absence of an excess of water. Bottom left: Crystal structure of **4**· H_2O . Bottom right: Crystal structure of **7**. Hydrogen atoms (other than those of water), cocrystallized THF (**7**), and the second, similar molecule in the asymmetric unit (**7**) omitted for clarity. Ellipsoids drawn at 50% probability.

2.2.3. Attempted rac-Lactide Polymerization

Cu(II) complexes have been used previously as catalysts for cyclic ester polymerizations.^{7c,d,13} The suitability of **5** for lactide polymerization following an activated monomer mechanism in the presence of 1 equiv of benzyl alcohol was thus briefly

investigated. At room temperature in dichloromethane or at 70 °C in toluene, **5** was inactive in lactide polymerization. In molten monomer at 130 °C, no polymer was obtained, and the color change indicated complex decomposition. Alternatively, polymerization via a coordination–insertion mechanism requires introduction of an alkoxide group. Reactions with **5** and several alkoxides (NaOMe, KO^tBu, NaOCH₂C₅H₄N) in a variety of solvents (dichloromethane, THF, toluene, acetonitrile, or methanol) and varying reaction conditions never yielded the desired copper alkoxide complex. In all cases, rapid color changes indicated complex decomposition instead of lack of reactivity. Two major decomposition pathways are indicated from single crystals obtained in some reactions (Figure 2.5, quantities insufficient for characterization other than X-ray diffraction). Reaction of **5** with 1.1 equiv of NaOMe in THF led to complex **7** (Figure 2.5, structure in Figure 2.4), indicating loss of the sulfonate group in the presence of alkoxide. In acetonitrile, desulfonation was suppressed, but only Cu(I) complex **8** was obtained (Figure 2.5), most likely by β -H elimination from a Cu(II) alkoxide complex,^{7b} followed by homolytic decomposition of copper(II) hydride. Similarly, reaction of sodium pyridyl methoxide with **4** yielded LCu(pyridyl methanol), **9** (Figure 2.5). Cu(I) complexes **8** and **9** show a trigonal-pyramidal coordination environment around the copper center. While this coordination is far less common than tetrahedral Cu(I) complexes, it can be observed with Cu(I) complexes if either the coordination geometry is enforced by the ligand, e.g., by a tetradentate tripodal ligand,¹⁴ or a weakly coordinating ligand is combined with strong (π - acceptor) ligands, e.g., in (PhCN)₃Cu(O₄Cl).¹⁵ In summary, diketimino-sulfonate copper complexes are unlikely candidates for cyclic ester polymerization catalysts. They are not sufficiently Lewis acidic for polymerization following an activated monomer mechanism, and they do not allow preparation of copper alkoxide complexes required for coordination–insertion polymerization: Either the sulfonate group is lost, likely by attack of the alkoxide, or the facial coordination of ligand **1** or **2** encourages facile β -H elimination from the alkoxide.

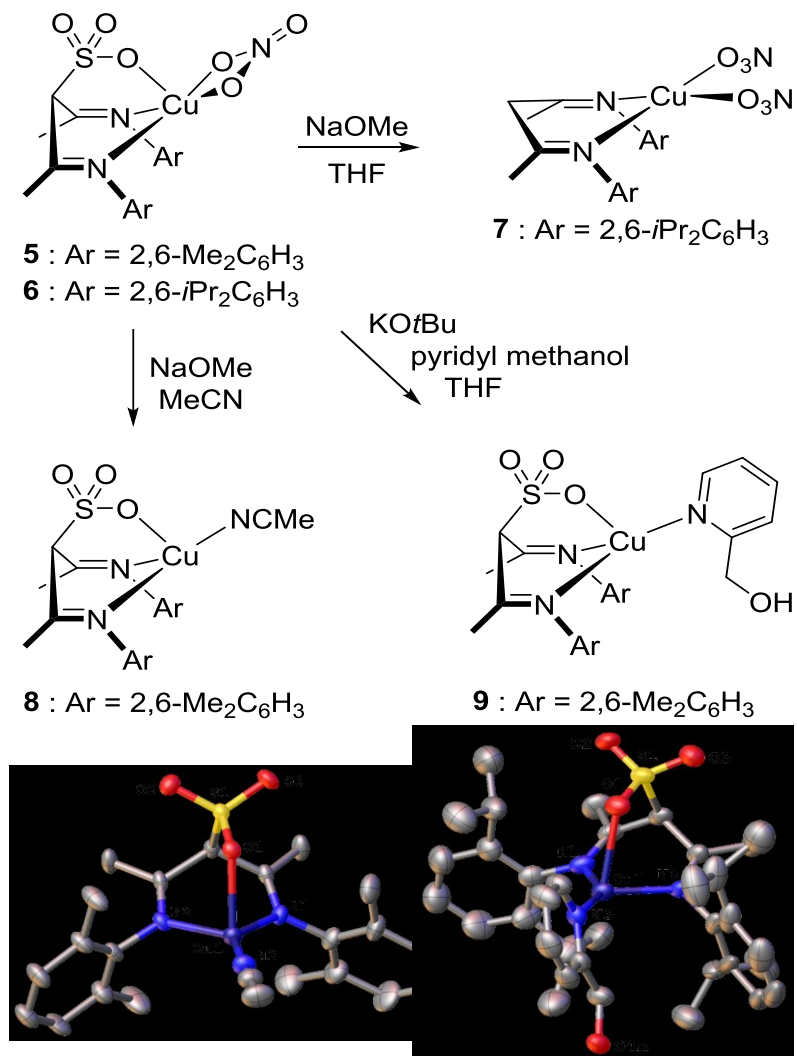
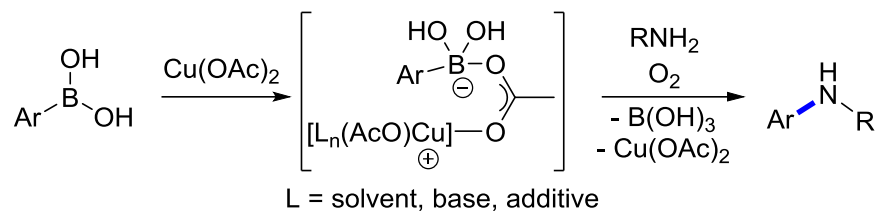


Figure 2.5 : Decomposition products identified by X-ray diffraction. Bottom left: Crystal structure of **8**, bottom right: crystal structure of **9**. Hydrogen atoms, disordered THF (**8**), co-crystallized bis(pyridylmethoxide)copper, and CH₂Cl₂ (**9**) omitted for clarity (see Figure 2.S1 for full structure). Thermal ellipsoids drawn at 50% probability.

2.2.4. Chan–Evans–Lam coupling

Chan–Evans–Lam couplings are oxidative couplings of a boronic acid with a nucleophile. Copper acetate is most commonly used, although a variety of other homogeneous and inhomogeneous systems have been employed. Qualitative evidence suggests that the

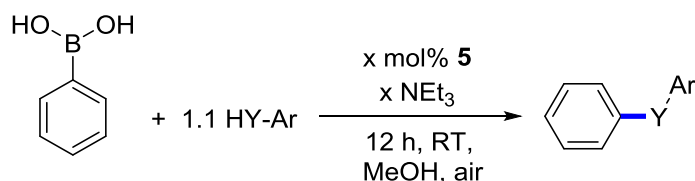
presence of an anionic group which can bridge to boron might facilitate transmetalation and that increased solubility due to ligation increases activity (Scheme 2-3).^{11,16}



Scheme 2-3

Both of these requirements would be met by sulfonatodiketimine ligands **1** and **2**, and respective complexes **5** and **6** were thus tested in Chan–Evans–Lam couplings with phenyl boronic acid. Initial screenings of complex **5** indicate only weak activity in Chan–Evans–Lam coupling of phenols or alkoxides but very high reactivity for anilines (Table 2-2) even in the absence of base or molecular sieves.

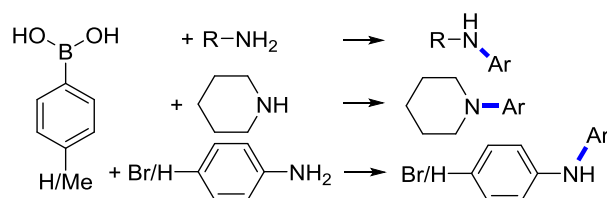
Table 2-2 : Initial Screening of Activity in Chan–Evans–Lam.



HY-Ar	mol-% 5	conditions	yield
PhNH ₂	5	no base	>95%
PhOH	5	no base	5%
p-FC ₆ H ₄ OH	5	no base	<5%
iPrOH	5	no base	0%
PhOH	5	2 equiv NEt ₃	34%
PhOH	0	2 equiv NEt ₃	0%

Chan–Evans–Lam couplings using $\text{Cu}(\text{OAc})_2$ catalyst require substrate-dependent optimizations of reaction conditions, which led to protocols which performed differently even for closely related substrates such as anilines or aliphatic amines. For example, Batey reported the successful coupling of amines under base-free conditions (Table 2-3).¹⁷ Anilines, in contrast, performed poorly under these conditions. By addition of myristic acid and 2,6-lutidine, Buchwald optimized the coupling of anilines, but yields for amines dropped below 60%.¹⁸ Since **5** was active toward aniline without addition of ancillary base/ ligand, removal of water, or heating, this removed the main variables which normally require optimization. Consequently, couplings with **5** as catalyst proceeded equally well for amines as well as anilines, even at shorter reaction times and at smaller catalyst loadings compared to $\text{Cu}(\text{OAc})_2$ (Table 2-3 reports isolated yields). Conversion to product is >95% in reactions with **5**.

Table 2-3 : Isolated yields in coupling of amines and anilines with $\text{Cu}(\text{OAc})_2$ or **5** as catalyst.



Substrate	$\text{Cu}(\text{OAc})_2^{\text{a}}$	$\text{Cu}(\text{OAc})_2^{\text{b}}$	5 ^c
$\text{C}_n\text{H}_{2n+2}\text{NH}_2$	50% ($n = 4$)	89-92% ($n = 8$)	76% ($n = 6$)
piperidine	56%	78-86%	85%
PhNH_2	79-91%		90%
$\text{BrC}_6\text{H}_4\text{NH}_2$		30-53%	81%

^a 1.5 equiv $\text{PhB}(\text{OH})_2$ or $\text{p-MeC}_6\text{H}_4\text{B}(\text{OH})_2$, 5-10 mol% $\text{Cu}(\text{OAc})_2$, 10-20 mol% myristic acid, 2,6-lutidine, mol. sieves, air, RT, toluene, 24 h (ref. ¹⁸). ^b $\text{PhB}(\text{OH})_2$ or PhBF_3K , 10 mol% $\text{Cu}(\text{OAc})_2$, mol. sieves, O_2 , RT or 40 °C, CH_2Cl_2 , 24 h (ref. ¹⁷). ^c 2.5 mol% **5**, 1.5 equiv $\text{PhB}(\text{OH})_2$, RT, air, CH_2Cl_2 , 12 h.

2.2.5. Substrate Scope

Given the good reactivity under very mild conditions, the substrate scope of **5** was investigated briefly to characterize catalyst reactivity. To enable comparisons, reactions were quenched after 320 min, where most substrates showed only partial conversion. The values in Chart II-1 thus do not represent attainable conversions but compare substrate reactivity. (For conversion at $t > 320$ min, see Table 2-S2.) Generally, weaker nucleophiles show lower reactivity in Chan–Evans–Lam coupling, and reduced activity for paranitroaniline was expected (Chart 2-1). Surprisingly, the respective fluoro- and bromo-anilines showed increased reactivity, while *para*-methoxyaniline was less reactive than aniline. The observed differences can be explained by the formation of unproductive off-cycle adducts (*vide infra*). *ortho*-Fluoroaniline reacted readily, but 2,6-dimethylaniline reacted slower than did the unsubstituted aniline. The coupling of *ortho*-disubstituted anilines is difficult,^{18,19} and only few optimized protocols report yields above 80%.^{18,19c,d,g}

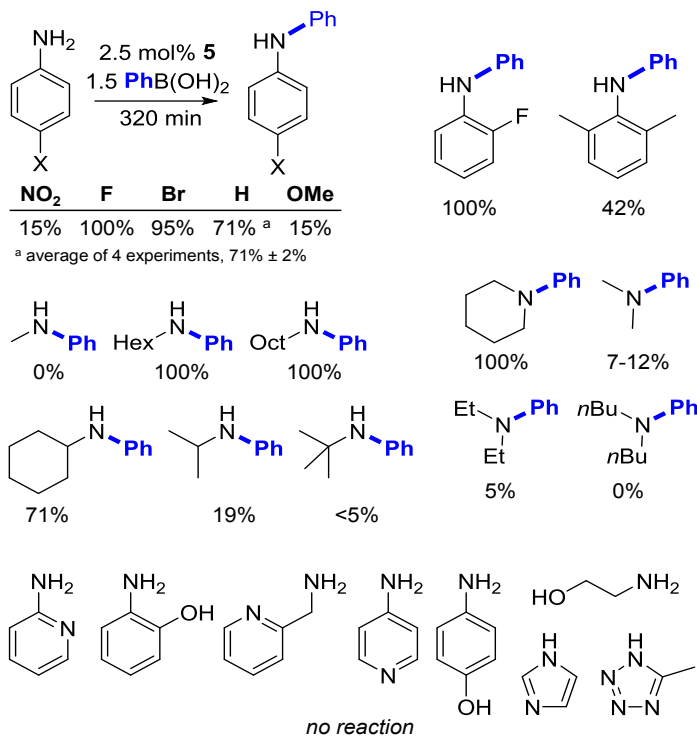


Chart 2-1 : Relative Reactivity of Different Amines and Anilines.

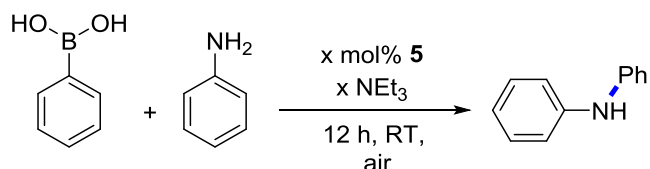
Primary aliphatic amines with undemanding substituents, such as hexylamine or octylamine, underwent facile coupling to phenyl boronic acid under the same mild conditions. Methylamine, used as an aqueous solution, was unreactive, but on the basis of the observed color changes during catalysis, this is likely related to complex decomposition. Despite the relative stability of the catalyst toward water (*vide supra*), use of a basic aqueous methylamine solution was not tolerated. The catalyst proved to be very sensitive to the steric bulk of the amine and amine activities decreased in the following order: primary alkyl > cyclic secondary alkyl > secondary alkyl > tertiary alkyl. The same trend was observed for secondary amines. Cyclic secondary amines still showed good reactivity, but acyclic secondary amines did not perform well. Low reactivity toward acyclic secondary amine is a general problem in Cu-catalyzed C–N couplings,²⁰ although yields of 40–60% have been reported using Cu(OAc)₂.^{18,21} The only high performance coupling reported for acyclic secondary amines employed a preformed [Cu(DMAP)4I]I catalyst.^{19f}

No reactivity was observed for aminopyridine, picolylamine, pyrazole or tetrazole. The lack of reactivity is most likely related due to coordination to copper and formation of off-cycle coordination complexes. Amines or anilines with hydroxyl groups are likewise unreactive. Since couplings of hexylamine in the presence of 1 equiv of ethanol reached full conversion in 320 min, the catalyst is in general stable toward alcohols, but the presence of hydroxyl groups in the substrate is not tolerated. This might be either due to the formation of chelates with copper and/or due to an unproductive esterification of the substrate with boronic acid.

2.2.6. Mechanistic Investigations.

Coupling of aniline with phenyl boronic acid was investigated in more detail to explore reaction conditions and mechanism, and in particular the effect of the sulfonato-diimine ligand. Reactions in Table 2-4 were thus conducted under identical conditions and quenched after 320 min. Catalyst **5** and **6** performed identically (Table 2-4, entries 5 and 24) and all other reactions were undertaken using **5** as a catalyst.

Table 2-4 : Coupling of Aniline with Phenylborate Using **5** as a catalyst.^a



Entry	Solvent	Modification ^a	Yield
1	MeCN	-	2%
2	THF	-	12%
3	MeOH	-	40%
4	Toluene	-	66%
5	CH ₂ Cl ₂	-	71% ± 2% ^b
6	CH ₂ Cl ₂	1.0 equiv NEt ₃	14%
7	CH ₂ Cl ₂	10 mol% NEt ₃	67%
8	CH ₂ Cl ₂	2.5 mol% NEt ₃	70%
9	CH ₂ Cl ₂	1.0 equiv Na ₂ CO ₃	28%
10	CH ₂ Cl ₂	10 mol% Na ₂ CO ₃	73%
11	CH ₂ Cl ₂	2.5 mol% H ₂ O	61%
12	CH ₂ Cl ₂	5 mol% H ₂ O	85%
13	CH ₂ Cl ₂	10 equiv H ₂ O	81%
14	CH ₂ Cl ₂	20 equiv H ₂ O	76%
15	CH ₂ Cl ₂	2.5 mol% NH ₄ Cl	83%
16	CH ₂ Cl ₂	1.0 equiv NH ₄ Cl	25%
17	CH ₂ Cl ₂	molecular sieves	35%
18	CH ₂ Cl ₂	N ₂	5%
19	CH ₂ Cl ₂	N ₂ , 2.5 mol% H ₂ O	4%
20	CH ₂ Cl ₂	2.5 mol% NaOAc	60%
21	CH ₂ Cl ₂	3.0 equiv PhB(OH) ₂	79%
22	CH ₂ Cl ₂	5.0 mol% 5	88%
23	CH ₂ Cl ₂	1.0 mol% 5	30%
24	CH ₂ Cl ₂	2.5 mol% 6	73%

^a Conditions: room temperature, air, 320 min, 1.5 equiv. PhB(OH)₂, 1.0 M aniline, 2.5 mol% **5**.

Equivalents refer to concentrations relative to amine. ^b Average of four experiments.

Investigation of solvent dependence showed decreased activity in coordinating solvents (Table 2-4, entries 1–5) with CH₂Cl₂, toluene > MeOH > THF > MeCN. This order differs notably from the empirical order found for Chan–Evans–Lam couplings with Cu(OAc)₂: CH₂Cl₂ > 1,4-dioxane, NMP, THF, DMF > EtOAc, toluene, DMSO > MeOH.²² The difference is most likely due to differences in solubility: For highly soluble **5**, polar solvents offer no major advantage and compete with substrate for coordination to copper. For less soluble Cu(OAc)₂, solvent performance is a complex equilibrium between higher availability of the catalyst in more polar solvents, activation of dimeric Cu₂(OAc)₄, and competition with substrate.

Investigation of base dependence (entries 6–10) showed that addition of a stoichiometric amount of triethylamine is deactivating, while 2.5–10 mol % do not offer any advantage over reactions in the absence of base. Addition of base had been advantageous in coupling of phenol substrates with **5** (Table 2-2) indicating that a base-assisted proton transfer is part of the mechanism. In coupling with aniline the substrate or the reaction product might catalyze proton transfer, thus eliminating the need for an external base. This differs again from couplings with Cu(OAc)₂, which often require the presence of excess base. However, the added nitrogen base might be rather required as ligand to activate the copper acetate dimer.^{11b} In agreement with this, several Chan–Evans–Lam reactions using preformed coordination complexes do not require the use of base/ligand,^{19,23} but some couplings catalyzed by simple copper salts also do not require additional base.^{11c,19a,21b} Deactivation of **5** by stoichiometric amounts of NEt₃ might indicate coordination of the latter to the active side. However, a similar deactivation is observed for insoluble Na₂CO₃. Strong bases might lead to deprotonation of Cu-coordinated aniline (or water) to form an anilide (or hydroxide) complex early in the catalytic cycle which seems to be detrimental.

The presence of water (up to 20 equiv per amine) and even small amounts of NH₄Cl are tolerated well, yielding even slightly higher conversions which are, however, close to the error margin. Stoichiometric amounts of NH₄Cl drastically reduce the observed yield (entries 11–16). Interestingly, the presence of molecular sieves, as advised in the “standard” Chan–Evans–Lam protocol, reduced conversion to 35% (entries 17). Presence of water thus seems to be

advantageous for the reaction. Increased yields in the presence of water have been reported before,²⁴ and one possible explanation is its involvement in activating boronic acid for the transmetalation step.^{11b,25} Since the same activating effect was also observed for ammonium chloride, it seems more likely, however, that for **5** the presence of small amounts of acidic protons just facilitates proton transfer steps in the mechanism.

Reactions under nitrogen atmosphere drastically reduced conversion to 4–5% (entries 18 and 19), even when water was added. Reactions with **5** thus follow an oxidative coupling mechanism with oxygen as oxidant,^{10b,11a,16,26} rather than anaerobic couplings proposed to involve boronic acid^{25,27} or oxidative addition/reductive elimination pathways proposed for the Ullmann–Goldberg reaction.²⁸ The role of the counteranion in Chan–Evans–Lam couplings is complex. Cu(OAc)₂ is the most frequently used catalyst, and Cu(OAc)₂ (or Cu(OTf)₂) often, although not always, outperforms other copper salts in catalytic activity. Stahl reported that addition of acetate accelerates reactions with Cu(ClO₄)₂ (likely by bridging coordination to boron) but inhibits reactions with Cu(OAc)₂.^{11a} Watson further outlined the involvement of acetate (or acetic acid) in the stabilization of the unreactive paddlewheel precatalyst and found that hydroxide is more effective than acetate in bridging copper and boron.^{11b} Addition of 2.5 mol % sodium acetate to the coupling reaction with **5** resulted only in slight suppression of activity (entry 20). Acetate is thus more likely to block coordination sites at copper, and any potential role it plays in boronic acid activation can be competently fulfilled by the sulfonate group incorporated in the ligand.

Reactions are pseudo-first-order and do not depend on the concentration of phenyl boronic acid (Figure 2.6, Table 2-4, entry 21). This differs from Stahl's findings for methanol arylation with Cu(OAc)₂, in which transmetalation was the rate determining step and saturation kinetics in boronic acid concentration was observed.^{11a,26} Transmetalation is thus more facile in **5** and not significantly influenced by added acetate, in agreement with an involvement of the sulfonate group in the transmetalation step. Yields increased at higher catalyst concentration (Table 2-4, entries 5, 22, and 23), but dependence on catalyst concentration was not investigated in detail.

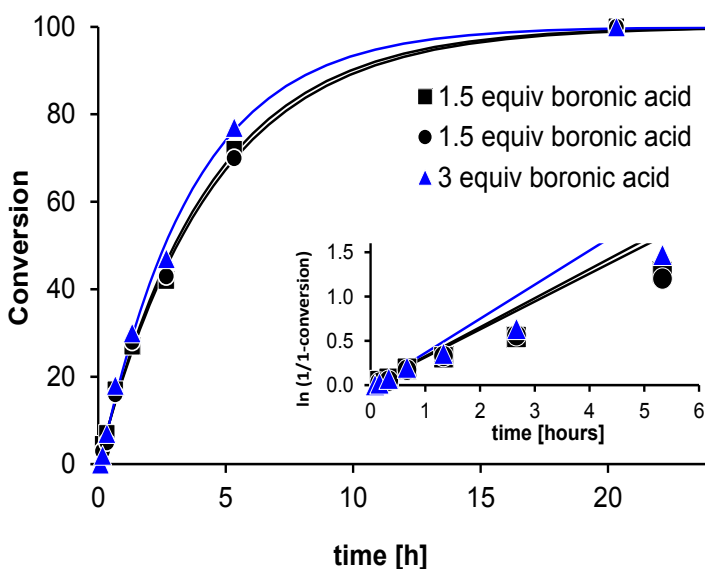


Figure 2.6 : Time–concentration profile for the coupling of aniline with phenylboronic acid. Conditions: 1 M aniline in CH_2Cl_2 , 2.5 mol % **5**, 1.5 M $\text{PhB}(\text{OH})_2$ (squares, circles) or 3.0 M $\text{PhB}(\text{OH})_2$ (triangles). The inset shows the linearized plot according to first-order kinetics.

While more nucleophilic substrates generally show higher reactivities (and did so also for **5**) the inverted reactivity for *para*-bromoaniline > aniline > *para*-methoxyaniline was puzzling. Competition experiments between these three substrates showed that more nucleophilic anilines showed in fact the expected higher relative reactivity, but that overall reactivity for both anilines was reduced in the presence of better nucleophiles (Table 2-5). General deactivation in the presence of more nucleophilic anilines can be explained by the formation of unproductive coordination complexes, such as coordination of aniline to copper (thus blocking the coordination site required for transmetalation) or coordination of aniline to boron (thus preventing bridging coordination of the sulfonate group and/or reducing availability of the nucleophile). If aniline coordination to boronic acid is involved, then it seems highly unlikely that doubling the relative concentration of boronic acid would not have any effect on reaction kinetics. Aniline thus most likely coordinates to **5** in an off-cycle coordination complex. Formation of off-cycle copper– aniline complexes would be expected to lead to an inverse relationship on substrate concentration, which was not observed in the reaction

kinetics. It is probable, however, that diphenylamines can likewise coordinate to **5** (c.f. strong deactivation in the presence of triethylamine) which would in first approximation render this equilibrium independent from conversion.

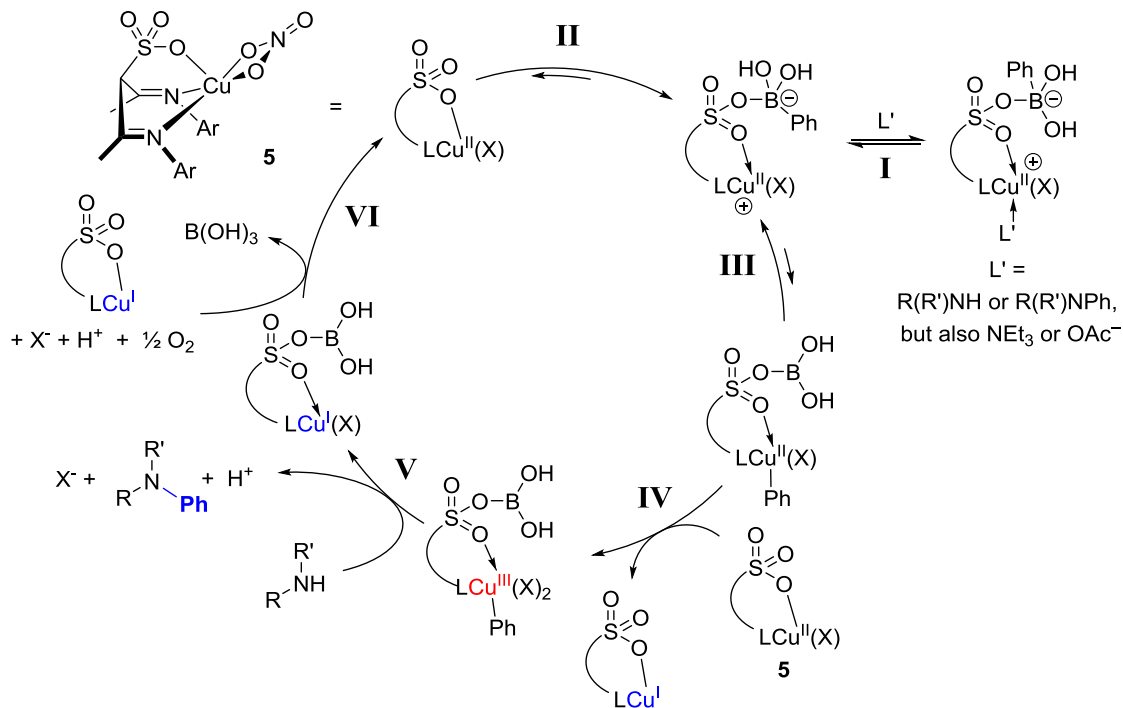
Table 2-5 : Conversions in Competition Experiments.^a

X	Y	Conversion X/Y	Total conversion
Br			95%
H			71%
Br	H	14% / 56%	70%
H	OMe	5% / 38%	43%

Conditions: rt, air, 320 min, 1.5 M PhB(OH)₂, 1.0 M of each aniline, 2.5 mol% **5**.

These findings lead us to propose the mechanism outlined in Scheme 2-4 for arylations with **5**. The reduced reactivities with electron-rich anilines indicate the formation of off-cycle adducts (**I**) and that transmetalation has to occur prior to coordination of the nucleophile. Again, arylations with **5** thus seem to follow the mechanism proposed by Collman and Stahl,^{11a,16,26} rather than that of anaerobic couplings of imidazoles in which nucleophile coordination precedes transmetalation.^{25,27} The nature of the rate-determining step is unknown: Kinetics indicate independence from boronic acid concentration and dependence on nucleophile concentration. However, saturation of the coordination equilibrium of boronic acid (**II**) would remove dependence of boronic acid concentration even if transmetalation (**III**) is rate-determining. If transmetalation is reversible, then dependence on nucleophile concentration can be observed even if transition state **III** is the rate-determining state. The available data does not allow to confirm the presence of a Cu(III) species, the way in which it is formed, or whether amine coordination occurs prior to or after oxidation. Steps **IV–VI** are

thus presumed to be identical to the mechanism proposed by Stahl for arylation of methanol.^{11a,26} While anion dissociation from Cu is possible, it should be noted that contrary to reactions with $\text{Cu}(\text{OAc})_2$ no anion transfer to boron is required. Persistent coordination of nitrate to copper would explain the good performance of **5** and **6** in nonpolar solvents.



Scheme 2-4

2.3. Conclusions

Imino-sulfonato copper complexes proved to be moderately stable toward moisture and to catalyze Chan–Evans–Lam couplings following essentially the same mechanism observed for copper acetate. The sulfonate-containing ligand fulfills the roles typically assigned to added base/ligand, counteranion, solvent, and complex **5** thus allowed the coupling of amines and anilines using an identical, nonoptimized reaction protocol for both substrates. The substrate scope is however limited by the intolerance of hydroxyl groups on the substrate and the strong decline in reactivity for sterically bulky substrates. While the strategy of employing a preformed coordination complex with a group capable of coordinating to boron thus allowed a more general reactivity, improved catalysts will require a higher stability versus hydrolysis/desulfonation and a more open ligand framework to allow for reactions with more bulky substrates.

2.4. Experimental section

General

Ligand syntheses were performed using Schlenk or glovebox techniques under nitrogen atmosphere. Complex synthesis were performed under ambient atmosphere, even when dry solvents were used. Diketimine ligands *nacnac*^{xylylH},²⁹ *nacnac*^{BnH},³⁰ *nacnac*^{MeBnH},³⁰ and **2**Li(THF)⁹ were prepared according to literature. Solvents for ligand synthesis were dried by passage through activated aluminum oxide (MBraun SPS). *rac*-Lactide (98%) was purchased from Sigma-Aldrich, purified by three recrystallizations from dry ethyl acetate, and kept at -30 °C. Phenyl boronic acid was purified by washing with dichloromethane until the filtrate turns colorless. All other chemicals were purchased from common commercial suppliers and used without further purification. ¹H and ¹³C NMR spectra were acquired on a Bruker AVX 400 spectrometer. The chemical shifts were referenced to the residual signals of the deuterated solvents (MeOD: ¹H: δ 3.31/4.78 ppm, ¹³C: δ 49.2 ppm). Elemental analyses were performed by the Laboratoire d'analyse élé mentaire (Université de Montréal).

Lithium-2,4-bis[(2,6-dimethylphenyl)imino]pentane-3-sulfonate, **1Li(THF).** In a Schlenk tube, a solution of *nacnac*^{xylylH} (2.0 g, 6.5 mmol) in anhydrous THF (20 mL) was cooled to -78 °C under N₂. *n*-BuLi in hexane (2.7 mL, 7.2 mmol) was added slowly. The mixture was stirred 15 min at -78 °C, then held for 30 min at room temperature before again being cooled to -78 °C and added via canula transfer slowly to a solution of SO₃NMe₃ (985 mg, 7.2 mmol) in anhydrous THF (20 mL) at -78 °C. The mixture was allowed to return to room temperature, stirred overnight, filtered, and concentrated under vacuum. Cooling to -30 °C resulted in a white precipitate 2.3 g (82%).

¹H NMR (CD₃OD, 400 MHz, 298 K): δ 1.88 (m, 4H, THF), 2.08 (s, 12H, ArMe), 3.34 (s, 6H, C(=N)Me), 3.74 (m, 2H, THF), 5.05 (s, 1H, CH(SO₃), 6.89 (m, 2H, Ar), 7.00 (m, 4H, Ar). ¹³C{¹H} NMR (CD₃OD, 126 MHz, 330 K): δ 169.4, 147.9, 134.7, 128.5, 127.9, 126.6, 126.3, 123.4, 67.83, 25.5. Anal. Calcd for C₂₅H₃₃N₂O₄SLi: C, 64.64; H, 7.34; N, 6.46; S, 6.90. Found: C, 64.43; H, 7.16; N, 6.03; S, 5.80.

{(1)CuCl·LiCl·MeCN}₂, 3. Copper chloride (52 mg, 0.38 mmol) and **1Li(THF)** (160 mg, 0.35 mmol) were combined and cooled to -78 °C. Dry acetonitrile (5 mL) was added slowly. The solution was allowed to return to room temperature and stirred overnight. The orange mixture was filtered and placed at -20 °C to obtain orange crystals (51 mg, 23%). Anal. Calcd for C₂₃H₂₈Cl₂CuLiN₃O₃S: C, 48.64; H, 4.97; N, 7.40; S, 5.64. Found: C, 44.14; H, 5.35; N, 4.97; S, 6.33 (decomposition on recrystallization).

(2)CuNO₃·MeCN, 4. Copper nitrate (81 mg, 0.35 mmol) and **2Li(THF)** (160 mg, 0.32 mmol) were combined and cooled to -78 °C. Dry acetonitrile (5 mL) was added slowly. The solution was allowed to return to room temperature and stirred overnight. The orange mixture was filtered and placed at -20 °C to obtain green crystals (80 mg, 50%). Anal. Calcd for C₃₁H₄₄N₄O₆SCu: C, 56.05; H, 8.43; N, 6.67; S, 4.83. Found: C, 55.81; H, 8.38; N, 6.85; S, 4.49.

(1)CuNO₃, 5. Copper nitrate (88 mg, 0.38 mmol) and **1Li(THF)** (160 mg, 0.35 mmol) were combined and cooled to -78 °C. Dry acetonitrile (5 mL) was added slowly. The solution was allowed to return to room temperature and stirred overnight. After evaporation of the solvent, the solid was recrystallized in dry dichloromethane at -20 °C to afford green crystals (130 mg, 80%). Anal. Calcd for C₂₁H₂₅CuN₃O₆S: C, 49.36; H, 4.93; N, 8.22; S, 6.27. Found: C, 49.90; H, 5.33; N, 7.65; S, 4.96.

(2)CuNO₃·CH₂Cl₂, 6. Following the same procedure as that for **4**, but with complete evaporation of the solvent, followed by recrystallization from dry dichloromethane at -20 °C afforded green crystals of **6** (117 mg, 73%). Anal. Calcd for C₂₉H₄₁CuN₃O₆S·CH₂Cl₂: C, 50.88; H, 6.12; N, 5.93; S, 4.53. Found: C, 50.59; H, 6.25; N, 6.08; S, 4.31.

General Procedure for Chan–Evans–Lam Couplings. To a stirred solution of amine (2 mmol) in dichloromethane (2 mL) was added phenyl boronic acid (3 mmol), followed by the desired copper catalyst (0.05 mmol). The reaction mixture was stirred at room temperature in a vessel open to air. After the desired time, the reaction was quenched by addition of a saturated aqueous solution of ammonium chloride.

For determination of conversion by GC-MS, the reaction mixture was diluted with ethyl acetate, an internal standard (typically anisole) added, the organic phase separated, and the solution filtered through a silica plug to remove copper catalyst. Conversion to product was determined from comparison of the product peak to that of the added standard in GC-MS analysis. Calibration factors for GC-MS analysis were obtained from simultaneous NMR and GC-MS analysis, of either isolated experiments or a mixture of standard and product obtained from commercial suppliers. For the determination of isolated yields, reaction time was 12 h, and the product was purified by column chromatography (silica/9:1 hexane/EtOAc). See the Supporting Information for product characterizations.

X-ray Diffraction Studies

Single crystals were obtained directly from isolation of the products as described above. Diffraction data were collected on a Bruker Venture METALJET diffractometer ($\text{Ga K}\alpha$ radiation) or a Bruker APEXII with a Cu microsource/Quazar MX using the APEX2 software package.³¹ Data reduction was performed with SAINT,³² absorption corrections with SADABS.³³ Structures were solved by dual-space refinement (SHELXT).³⁴ All non-hydrogen atoms were refined anisotropic using full-matrix least-squares on F2 and hydrogen atoms refined with fixed isotropic U using a riding model (SHELXL97).³⁵ Further experimental details can be found in Table 2-S1 and CCDC 1552773–1552780.

2.5. Supporting information

- **Figure 2.S1** Crystal structure of **9**
- **Characterization of isolated coupling products**
- **Table 2-S1** Coupling yields after >12h
- **Table 2-S2** Details of X-ray Diffraction Studies
- **Figure 2.S2** ^1H NMR spectrum of lithium-2,4-bis[(2,6-dimethylphenyl)imino]pentane-3-sulfonate, **1Li(THF)**.

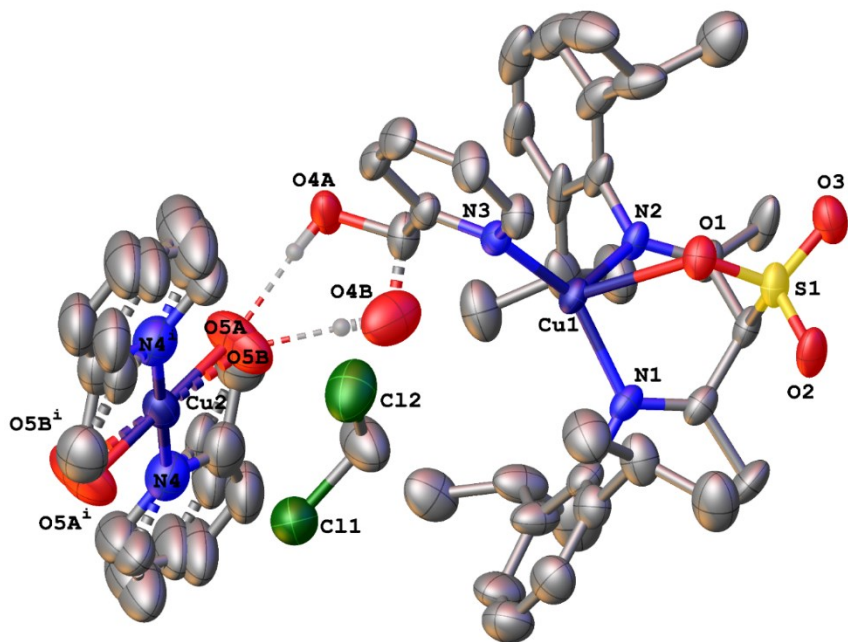


Figure 2.S1 : Crystal structure of **9**. Hydrogen atoms and the disordered hydroxy were omitted for clarity. Thermal ellipsoids drawn at 50% probability.

Characterization of isolated coupling products:

N-(n-Hexyl)aniline : from *n*-hexylamine, yellow oil, 76%.

¹H NMR (300 MHz, CDCl₃) : δ 7.13 (2H, t, J_{HH} = 7 Hz), 6.67 (1H, t, J_{HH} = 7 Hz), 6.58 (2H, d, J_{HH} = 7 Hz), 3.56 (1H, s), 3.08 (2H, t, J_{HH} = 7 Hz), 1.59 (2H, t, J_{HH} = 7 Hz), 1.38 (4H, m), 0.89 (2H, t, J_{HH} = 7 Hz).

4-Bromo-N-phenylaniline : from 4-bromoaniline, brown solid, 81%.

¹H NMR (300 MHz, CDCl₃) : δ 7.36 (2H, d, J_{HH} = 8 Hz), 7.30 (2H, t, J_{HH} = 8 Hz), 7.07 (2H, d, J_{HH} = 8), 6.95 (3H, m), 5.69 (1H, s)

Diphenylamine : from aniline, orange oil, 90%.

¹H NMR (300 MHz, CDCl₃) : δ 7.25 (4H, t, J_{HH} = 7 Hz), 7.03 (4H, d, J_{HH} = 7 Hz), 6.90 (2H, t, J_{HH} = 7 Hz), 5.60 (1H, s)

N-phenylpiperidine : from piperidine, colorless oil, 85%.

¹H NMR (300 MHz, CDCl₃) : δ 7.24 (2H, t, J_{HH} = 7 Hz), 6.93 (2H, t, J_{HH} = 7 Hz), 6.82 (1H, t, J_{HH} = 7 Hz), 3.15 (2H, t, J_{HH} = 5 Hz), 1.70 (4H, m), 1.57 (2H, m)

NMR data of isolated products (and of crude reaction mixtures) agree with literature.

- Sun, W.-B.; Zhan, P.-Z.; Jiang, T.; Li, C.-K.; An, L.-T.; Shoberu, A.; Zou, J.-P. *Tetrahedron* **2016**, 72, 6477.
- Zhang, G.; Yin, Z.; Zheng, S. *Org. Lett.* **2016**, 18, 300.
- Vantourout, J. C.; Law, R. P.; Isidro-Llobet, A.; Atkinson, S. J.; Watson, A. J. B. *J. Org. Chem.* **2016**, 81, 3942.
- Chen, Z.; Zeng, H.; Girard, S. A.; Wang, F.; Chen, N.; Li, C.-J. *Angew. Chem. Int. Ed.* **2015**, 54, 14487.

Table 2-S1 : Yields (GC) at prolonged reaction times.

Yields (from calibrated GC-MS analysis) obtained after reaction times longer than 320 min are provided in Table 2-S1 below. These yields are provided for completeness only. The substrate scope has been analyzed to characterize complex reactivity and no attempt has been made to optimize reaction conditions to achieve full conversion.

	Yield 320 min	Yield > 12 h
	15%	45%
	15%	65%
	76%	100%
	19%	87%
	<5%	6%
	7-12%	28%
	5%	10%
	0%	19% (24 h) 22% (48 h) ^a

^a Three independent experiments.

For the following substrates no conversion was observed even after 12 – 48 h, indicating reasons other than low reactivity impeding catalysis (e. g. boronic ester formation, substrate/product coordination to copper inhibiting transmetallation):

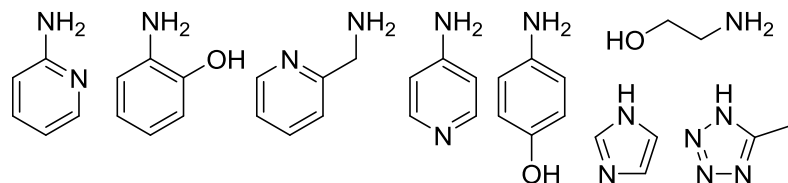


Table 2-S2 : Details of X-ray Diffraction Studies

	3	4	4·2 H₂O	5
Formula	C ₅₈ H ₇₄ Cl ₄ Cu ₂ Li ₂ N ₁₂ O ₆ S ₂	C ₃₁ H ₄₄ CuN ₄ O ₆ S	C ₂₃ H ₃₂ CuN ₄ O ₈ S	C ₂₁ H ₂₅ CuN ₃ O ₆ S
M _w (g/mol); F(000)	1382.17; 1436	664.30; 702	588.12; 2456	511.04; 2120
T (K); wavelength	100; 1.34139	100; 1.34139	100; 1.34139	100; 1.34139
Crystal System	Monoclinic	Triclinic	Monoclinic	Orthorhombic
Space Group	P2 ₁ /c	P-1	P2 ₁ /c	Pbca
Unit Cell: a (Å)	11.7897(5)	10.1655(3)	34.6493(19)	9.7956(3)
b (Å)	21.2709(9)	11.6853(4)	9.3123(5)	17.4076(6)
c (Å)	13.3963(5)	14.7099(5)	18.7620(11)	25.5629(9)
α (°)	90	80.041(2)	90	90
β (°)	101.531(2)	89.745(2)	119.870(2)	90
γ (°)	90	75.126(2)	90	90
V (Å ³)	3290.8(2)	1661.88(10)	5249.6 (5)	4358.9(3)
Z; d _{calcd.} (g/cm ³); Flack-x	2; 1.395	2; 1.328	8; 1.488	8; 1.557
μ (mm ⁻¹); Abs. Corr.	5.15; multi-scan	4.17; multi-scan	5.27; multi-scan	6.24; multi-scan
θ range (°); completeness	3.44-60.83; 1.00	2.66-60.60; 1.00	4.11-60.79; 1.00	3.01-64.74; 1.00
Collected reflections; R _σ	52480; 0.049	31550; 0.063	63187; 0.065	66669; 0.058
Unique reflections; R _{int}	7593; 0.081	7582; 0.075	6021; 0.087	5704; 0.109
Oberved Reflections; R1(F)	6169; 0.052	4588; 0.112	4882; 0.067	3603; 0.065
wR(F ²) (all data); GoF(F ²)	0.154; 1.05	0.303; 1.06	0.194; 1.03	0.183; 1.02
Residual electron density	0.89 e ⁻ /Å ³	1.20 e ⁻ /Å ³	0.66 e ⁻ /Å ³	1.66 e ⁻ /Å ³

Table 2-S2 continued. Details of X-ray Diffraction Studies

	6	7	8	9
Formula	C ₃₀ H ₄₃ Cl ₂ CuN ₃ O ₆ S	C ₂₅ H ₃₄ CuN ₄ O ₇	C ₂₇ H ₃₆ CuN ₃ O ₄ S	C ₈₄ H ₁₁₀ Cl ₄ Cu ₃ N ₈ O ₁₀ S ₂
<i>M_w</i> (g/mol); F(000)	708.17; 742	566.10; 1188	562.19; 1184	1788.33; 1874
<i>T</i> (K); wavelength	100; 1.34139	105; 1.34139	105; 1.54178	100; 1.54178
Crystal System	Monoclinic	Triclinic	Orthorhombic	Monoclinic
Space Group	<i>P</i> 2 ₁ /m	<i>P</i> -1	<i>P</i> bca	<i>P</i> 2 ₁ /n
Unit Cell: <i>a</i> (Å)	9.0439(3)	13.6149(4)	11.056(3)	17.4501(6)
<i>b</i> (Å)	18.0163(5)	15.0047(5)	15.4865(5)	11.6045(4)
<i>c</i> (Å)	10.2305(3)	15.3112(5)	17.0102(5)	21.3118(8)
<i>a</i> (°)	90	106.081(2)	90	90
<i>β</i> (°)	96.909(2)	90.513(2)	90	95.002(2)
<i>γ</i> (°)	90	111.990(2)	90	90
<i>V</i> (Å ³)	1654.83(9)	2764.47(16)	2907.09(15)	4299.2(3)
<i>Z</i> ; <i>d</i> _{calcd.} (g/cm ³); Flack-x	2; 1.421	4; 1.360	4; 1.284; 0.424(4)	2; 1.381
<i>μ</i> (mm ⁻¹); Abs. Corr.	5.16; multi-scan	4.53; multi-scan	4.67; multi-scan	2.95; multi-scan
θ range (°); completeness	3.79-60.74; 1.00	2.64-60.55; 1.00	4.16-60.71; 1.00	2.54-71.95; 1.00
Collected reflections; <i>R</i> _σ	26343; 0.028	58613; 0.048	81484; 0.025	56173; 0.041
Unique reflections; <i>R</i> _{int}	3937; 0.043	12673; 0.061	6690; 0.56	8417; 0.065
Oberved Reflections; <i>R</i> 1(<i>F</i>)	3733; 0.036	10297; 0.066	6571; 0.038	7205; 0.089
w <i>R</i> (<i>F</i> ²) (all data); GoF(<i>F</i> ²)	0.095; 1.08	0.210; 1.03	0.105; 1.17	0.280; 1.04
Residual electron density	0.66 e ⁻ /Å ³	0.98 e ⁻ /Å ³	0.69 e ⁻ /Å ³	1.47 e ⁻ /Å ³

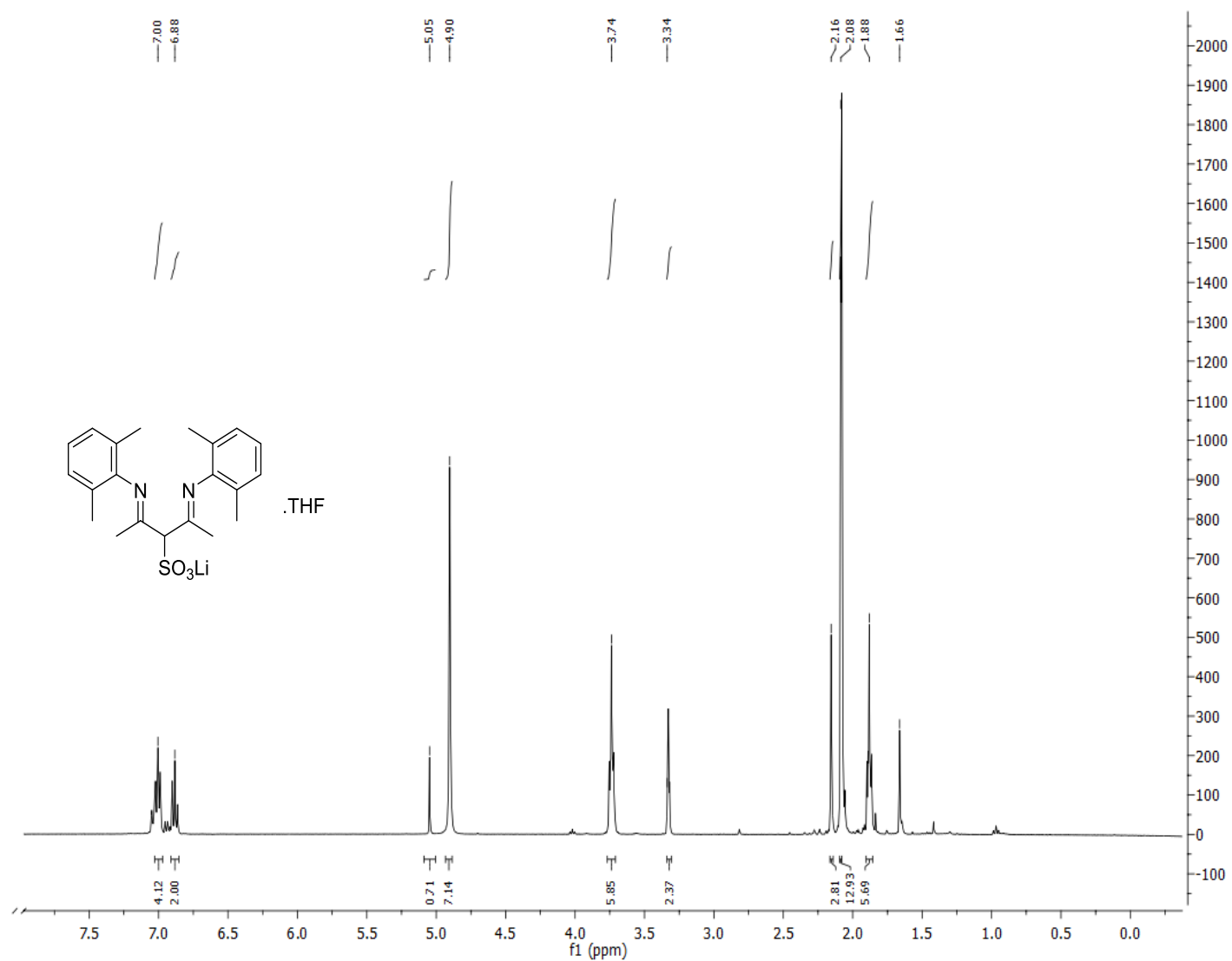


Figure 2.S2 : ^1H NMR spectrum of lithium-2,4-bis[(2,6-dimethylphenyl)imino]pentane-3-sulfonate, **1**Li(THF).

2.6. References

¹ McGeachin, S. G. *Can. J. Chem.* **1968**, *46*, 1903.

² Bourget-Merle, L.; Lappert, M. F.; Severn, J. R. *Chem. Rev.* **2002**, *102*, 3031.

³ Johnson, L. K.; Killian, C. M.; Brookhart, M. *J. Am. Chem. Soc.* **1995**, *117*, 6414.

⁴ (a) Hong, S.; Gupta, A. K.; Tolman, W. B. *Inorg. Chem.* **2009**, *48*, 6323. (b) Aboeella, N. W.; Gherman, B. F.; Hill, L. M. R.; York, J. T.; Holm, N.; Young, V. G.; Cramer, C. J.; Tolman, W. B. *J. Am. Chem. Soc.* **2006**, *128*, 3445.

⁵ (a) Salvador, T. K.; Arnett, C. H.; Kundu, S.; Sapiezynski, N. G.; Bertke, J. A.; Raghibi Boroujeni, M.; Warren, T. H. *J. Am. Chem. Soc.* **2016**, *138*, 16580. (b) Jang, E. S.; McMullin, C. L.; Käß, M.; Meyer, K.; Cundari, T. R.; Warren, T. H. *J. Am. Chem. Soc.* **2014**, *136*, 10930. (c) Wiese, S.; Badiei, Y. M.; Gephart, R. T.; Mossin, S.; Varonka, M. S.; Melzer, M. M.; Meyer, K.; Cundari, T. R.; Warren, T. H. *Angew. Chem., Int. Ed.* **2010**, *49*, 8850.

⁶ Park, K.-H.; Bradley, A. Z.; Thompson, J. S.; Marshall, W. J. *Inorg. Chem.* **2006**, *45*, 8480.

⁷ (a) Whitehorne, T. J. J.; Schaper, F. *Can. J. Chem.* **2014**, *92*, 206. (b) Whitehorne, T. J. J.; Schaper, F. *Inorg. Chem.* **2013**, *52*, 13612. (c) Whitehorne, T. J. J.; Schaper, F. *Chem. Commun. (Cambridge, U. K.)* **2012**, *48*, 10334. (d) Fortun, S.; Daneshmand, P.; Schaper, F. *Angew. Chem., Int. Ed.* **2015**, *54*, 13669.

⁸ (a) Azoulay, J. D.; Rojas, R. S.; Serrano, A. V.; Ohtaki, H.; Galland, G. B.; Wu, G.; Bazan, G. C. *Angew. Chem., Int. Ed.* **2009**, *48*, 1089. (b) Scheuermann, M. L.; Luedtke, A. T.; Hanson, S. K.; Fekl, U.; Kaminsky, W.; Goldberg, K. I. *Organometallics* **2013**, *32*, 4752. (c) Holze, P.; Corona, T.; Frank, N.; Braun-Cula, B.; Herwig, C.; Company, A.; Limberg, C. *Angew. Chem., Int. Ed.* **2017**, *56*, 2307. (d) Yokota, S.; Tachi, Y.; Itoh, S. *Inorg. Chem.* **2002**, *41*, 1342. (e) Camp, C.; Arnold, J. *Dalton Trans.* **2016**, *45*, 14462.

⁹ Rajendran, N. M.; Reddy, N. D. *Polyhedron* **2014**, *72*, 27.

¹⁰ (a) Chan, D. M. T.; Monaco, K. L.; Wang, R.-P.; Winters, M. P. *Tetrahedron Lett.* **1998**, *39*, 2933. (b) Evans, D. A.; Katz, J. L.; West, T. R. *Tetrahedron Lett.* **1998**, *39*, 2937. (c) Lam, P. Y. S.; Clark, C. G.; Saubern, S.; Adams, J.; Winters, M. P.; Chan, D. M. T.; Combs, A. *Tetrahedron Lett.* **1998**, *39*, 2941.

¹¹ (a) King, A. E.; Ryland, B. L.; Brunold, T. C.; Stahl, S. S. *Organometallics* **2012**, *31*, 7948. (b) Vantourout, J. C.; Miras, H. N.; Isidro-Llobet, A.; Sproules, S.; Watson, A. J. B. *J. Am. Chem. Soc.* **2017**, *139*, 4769. (c) Garnier, T.; Sakly, R.; Danel, M.; Chassaing, S.; Pale, P. *Synthesis* **2017**, *49*, 1223.

¹² El-Zoghbi, I.; Verguet, E.; Oguadinma, P. O.; Schaper, F. *Inorg. Chem. Commun.* **2010**, *13*, 529.

¹³ (a) Routaray, A.; Nath, N.; Maharana, T.; Sahoo, P. K.; Das, J. P.; Sutar, A. K. *J Chem Sci* **2016**, *128*, 883. (b) Cho, J.; Nayab, S.; Jeong, J. H. *Polyhedron* **2016**, *113*, 81. (c) Sun, J.; Shi, W.; Chen, D.; Liang, C. *J. Appl. Polym. Sci.* **2002**, *86*, 3312.

¹⁴ Baumeister, J. M.; Alberto, R.; Ortner, K.; Spingler, B.; August Schubiger, P.; Kaden, T. A. *J. Chem. Soc., Dalton Trans.* **2002**, 4143.

¹⁵ Bowmaker, G. A.; Lim, K. C.; Skelton, B. W.; White, A. H. *Z. Naturforsch., B* **2004**, *59b*, 1264

¹⁶ Collman, J. P.; Zhong, M.; Zhang, C.; Costanzo, S. *J. Org. Chem.* **2001**, *66*, 7892.

¹⁷ Quach, T. D.; Batey, R. A. *Org. Lett.* **2003**, *5*, 1381.

¹⁸ Antilla, J. C.; Buchwald, S. L. *Org. Lett.* **2001**, *3*, 2077.

¹⁹ (a) Quach, T. D.; Batey, R. A. *Org. Lett.* **2003**, *5*, 4397. (b) Chiang, G. C. H.; Olsson, T. *Org. Lett.* **2004**, *6*, 3079. (c) Kabalka, G. W.; Zhou, L.-L. *Letters in Organic Chemistry* **2006**, *3*, 320 . (d) McGarry, K. A.; Duenas, A. A.; Clark, T. B. *J. Org. Chem.* **2015**, *80*, 7193. (e) Bao, J.; Tranmer, G. K. *Tetrahedron Lett.* **2016**, *57*, 654. (f) Roy, S.; Sarma, M. J.; Kashyap, B.; Phukan, P. *Chem. Commun. (Cambridge, U. K.)* **2016**, *52*, 1170. (g) Rucker, R. P.; Whittaker, A. M.; Dang, H.; Lalic, G. *Angew. Chem., Int. Ed.* **2012**, *51*, 3953.

²⁰ Evano, G.; Blanchard, N.; Toumi, M. *Chem. Rev.* **2008**, *108*, 3054.

²¹ (a) Combs, A. P.; Tadesse, S.; Rafalski, M.; Haque, T. S.; Lam, P. Y. S. *J. Comb. Chem.* **2002**, *4*, 179. (b) Yu, X.-Q.; Yamamoto, Y.; Miyaura, N. *Chemistry – An Asian Journal* **2008**, *3*, 1517. (c) Benard, S.; Neuville, L.; Zhu, J. *Chem. Commun. (Cambridge, U. K.)* **2010**, *46*, 3393. (d) Debreczeni, N.; Fodor, A.; Hell, Z. *Catal. Lett.* **2014**, *144*, 1547. (e) Vantourout, J. C.; Law, R. P.; Isidro-Llobet, A.; Atkinson, S. J.; Watson, A. J. B. *J. Org. Chem.* **2016**, *81*, 3942.

²² Ley, S. V.; Thomas, A. W. *Angew. Chem., Int. Ed.* **2003**, *42*, 5400.

²³ (a) Liu, B.; Liu, B.; Zhou, Y.; Chen, W. *Organometallics* **2010**, *29*, 1457. (b) Kaboudin, B.; Abedi, Y.; Yokomatsu, T. *Eur. J. Org. Chem.* **2011**, *2011*, 6656.

²⁴ Nishiura, K.; Urawa, Y.; Soda, S. *Adv. Synth. Catal.* **2004**, *346*, 1679.

²⁵Tromp, M.; van Strijdonck, G. P. F.; van Berkel, S. S.; van den Hoogenband, A.; Feiters, M. C.; de Bruin, B.; Fiddy, S. G.; van der Eerden, A. M. J.; van Bokhoven, J. A.; van Leeuwen, P. W. N. M.; Koningsberger, D. C. *Organometallics* **2010**, *29*, 3085.

²⁶King, A. E.; Brunold, T. C.; Stahl, S. S. *J. Am. Chem. Soc.* **2009**, *131*, 5044.

²⁷van Berkel, S. S.; van den Hoogenband, A.; Terpstra, J. W.; Tromp, M.; van Leeuwen, P. W. N. M.; van Strijdonck, G. P. F. *Tetrahedron Lett.* **2004**, *45*, 7659.

²⁸Tye, J. W.; Weng, Z.; Johns, A. M.; Incarvito, C. D.; Hartwig, J. F. *J. Am. Chem. Soc.* **2008**, *130*, 9971.

²⁹Budzelaar, Peter H. M.; Moonen, Nicolle N. P.; de Gelder, R.; Smits, Jan M. M.; Gal, Anton W. *Eur. J. Inorg. Chem.* **2000**, 753.

³⁰El-Zoghbi, I.; Ased, A.; Oguadinma, P. O.; Tchiroua, E.; Schaper, F. *Can. J. Chem.* **2010**, *88*, 1040.

³¹*APEX2*, Release 2.1-0; Bruker AXS Inc.: Madison, USA, 2006.

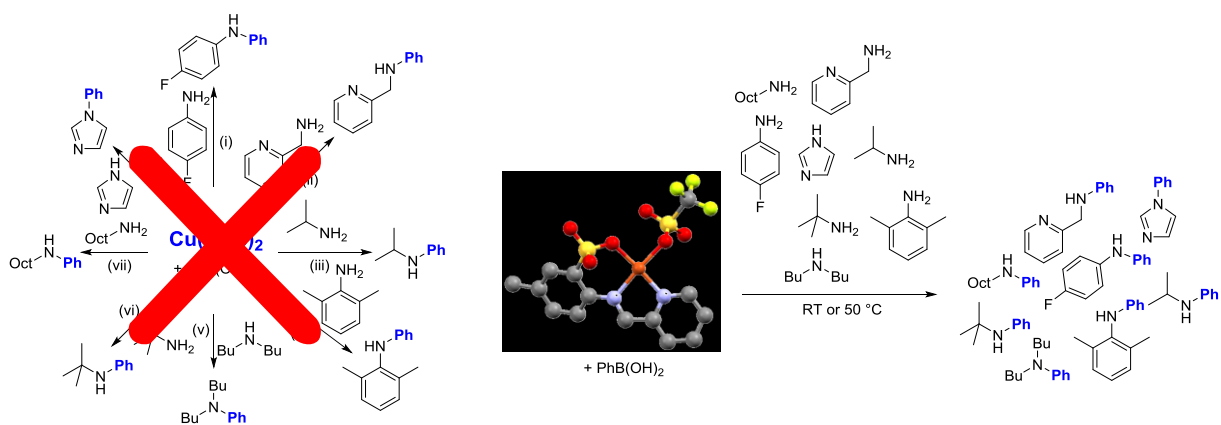
³²*SAINT*, Release 7.34A; Bruker AXS Inc.: Madison, USA, 2006.

³³Sheldrick, G. M. *SADABS*, Bruker AXS Inc.: Madison, USA, 1996 & 2004.

³⁴Sheldrick, G. *Acta Crystallographica Section A* **2015**, *71*, 3.

³⁵Sheldrick, G. M. *Acta Crystallogr.* **2008**, *A64*, 112.

3. Sulfonato-imino copper(II) complexes : fast and general Chan-Evans-Lam coupling of amines and anilines



Reprinted with permission from

V. Hardouin Duparc, F. Schaper *Dalton Trans.* **2017**, *46*, 12766-12770.

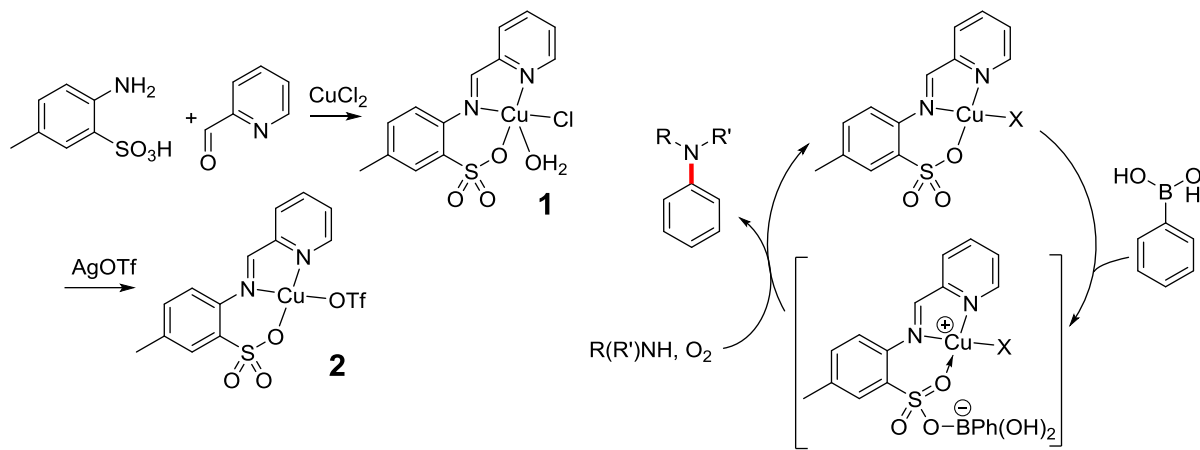
Copyright 2017 Royal Society of Chemistry.

3.1. Introduction

Palladium-catalyzed bond formations are in general without competition with regard to scope and reactivity, but the toxicity and high reactivity of trace amounts of palladium raised concerns, in particular in the pharmaceutical industry.¹ The copper-catalyzed Chan-Evans-Lam coupling of boronic acids with alcohols, amines or other nucleophiles to form carbon-heteroatom bonds provides an alternative bond-forming reaction, using milder conditions compared to the related Ullmann-Goldberg reaction² or to the analogous Buchwald-Hartwig coupling using Pd.^{3,4} Following the original work of Chan, Evans and Lam,⁵⁻⁷ a large number of studies have opened a wide substrate scope and allowed reactions using catalytic amounts of copper.⁸⁻¹⁶ With regard to catalyst performance, copper salts with acetates and or triflate counterions are often preferable over halogens or perchlorate anions,^{17,18} possibly due to pre-coordination of boronic acid to the anion.¹⁸⁻²⁰ Chan-Evans-Lam couplings also often require the addition of base, but its mechanistic implication is unclear and one of its roles might be that of a ligand activating dinuclear Cu₂(OAc)₂.¹⁹ For these reasons, Chan-Evans-Lam couplings using Cu(OAc)₂ or other simple copper salts react strongly to changes in reaction conditions such as solvent and the nature of the base used. Yields and rates can vary unpredictably, even for closely related substrates,¹² and reaction conditions have to be adapted accordingly.⁸ Even then, several substrates show only low or no reactivity.⁹

We decided to investigate copper coordination complexes with imino-sulfonate ligands (Scheme 3-1) as potential catalysts for Chan-Evans-Lam couplings. The chelating ligand removes the need for external "base" as ligand and reduces dependence of catalyst performance on the solvent. The sulfonate group incorporated in the ligand enables coordination to boronic acid (see the proposed intermediate in Scheme 3-1), which should make the choice of counter-ion less important. Although several studies reported improved catalytic performance when nitrogen ligands, such as TMEDA, were added to Chan-Evans-Lam couplings,²¹⁻²⁵ only a very limited amount of studies used preformed coordination complexes

instead of simple copper salts.²⁶⁻³² Of these, $[\text{Cu}(\text{DMAP})_4]\text{I}$, recently reported by Phukan, displayed high activity to a variety of amines and anilines.³²



Scheme 3-1

3.2. Results and discussion

Chloride complex **1** can be readily prepared in a one-pot reaction from commercially available starting materials, following protocols for similar complexes.³³ Anion exchange provided the triflate complex **2** (Scheme 3-1). The crystal structure of **2** shows a tetragonally distorted octahedral coordination geometry around copper (Fig. 3.1). The triflate anion is coordinated in the equatorial plane with a Cu-O distance comparable to that of the sulfonate ligand (1.929(1) and 2.015(1), respectively). Bridging coordination of the triflate and sulfonate ligands of neighbouring molecules to the apical positions ($d_{\text{Cu}-\text{O}} = 2.4 - 2.5 \text{ \AA}$) leads to formation of a 1D- coordination polymer along the crystallographic *b*-axis (Fig. 3.S1). The increased Lewis acidity of copper due to the weakly coordinating triflate anion is likely responsible for the octahedral coordination environment and the slightly shorter bond distances in **2** when compared to similar Cu complexes with chloride or carboxylate counteranions, which show square-pyramidal coordination geometries without bridging sulfonate groups.³³⁻³⁷ It should be

noted that the formation of the coordination polymer strongly resembles the interaction of **2** with boronic acid proposed in Scheme 3-1: bridging coordination of the sulfonate group to a Lewis-acidic centre (Cu or B, Fig. 3.1) and interaction of an anionic group on this centre with copper (triflate or Ph). Chloride complex **1** shows square-pyramidal coordination geometry ($\tau = 0.1$, Fig. 3.S2) and is very similar to that of the related complex without the 3-methyl group, in which water is replaced by a μ -chloride ligand.³⁴

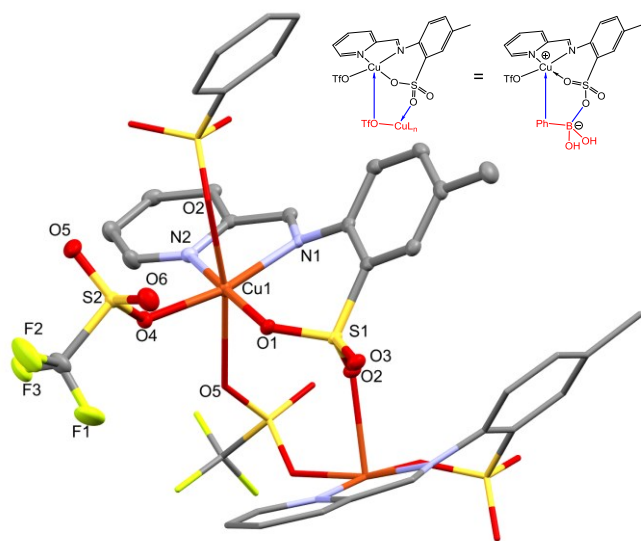


Figure 3.1 : X-ray structure of **2**. Thermal ellipsoids are drawn at 50% probability. Hydrogen atoms and co-crystallized dichloromethane were omitted for clarity. Selected bond distances (Å) and angles (°): Cu-N1 = 2.0261(13), Cu-N2 = 1.967(1), Cu-O1 = 1.929(1), Cu-O4 = 2.015(1), Cu-O2 = 2.379(1), Cu-O4 = 2.488(1), N1-Cu-N2 = 81.89(5), N2-Cu-O4 = 93.58(5), O1-Cu-O4 = 91.38(5), N1-Cu-O1 = 94.25(5), X-Cu-O2 = 82.18(4)- 94.18(5).

3.2.1. Catalytic performance

Complex **1** catalyses the Chan-Evans-Lam coupling of aniline with phenyl boronic acid in a variety of solvents (Table 3-S1). Increasing polarity led to higher activity (until deactivation in acetonitrile, probably by solvent coordination to copper), but variations were relatively small. We were delighted to note that addition of external base was indeed not necessary. To

the contrary, its presence even in catalytic amounts drastically reduced activity (Table 3-S1), in agreement with the mechanistic interpretation that nitrogen bases employed in Chan-Evans-Lam couplings act as a ligand. Presence of water was tolerated and addition of molecular sieves did not improve the reaction (Table 3-S1). Complex **2** was slightly more active than **1** with 98% and 86% conversion, respectively, after 320 min (Table 3-S1). Kinetic studies showed that this was mainly due to a longer induction period for **1** (40 min vs. 10 min for **2**), after which the reaction proceeded with very similar rates ($k_{\text{obs}}(\mathbf{1}) = 0.37(3) \text{ h}^{-1}$, $k_{\text{obs}}(\mathbf{2}) = 0.49(1) \text{ h}^{-1}$, Fig. 3.S3). Similar rates, but different induction periods indicate that the anion most likely dissociates from copper and does not further participate in the reaction mechanism. The presence of the chelating sulfonate ligand thus eliminated the requirement of an acetate or triflate counteranion, catalytic performance was good in a variety of solvents and no additional base/ligand was needed. Together with the tolerance towards water, this removed the main variables which typically need to be optimized in Chan-Evans-Lam couplings and which required different protocols even for substrates as closely related as amines and anilines.^{38, 39} Complex **2** could thus be applied in base-free Chan-Evans-Lam couplings without any optimization of reaction conditions and the arylation of anilines, primary and secondary amines proceeded with quantitative conversion (Chart 3-1, isolated yields >85%) at room temperature and in 12 h reaction time.

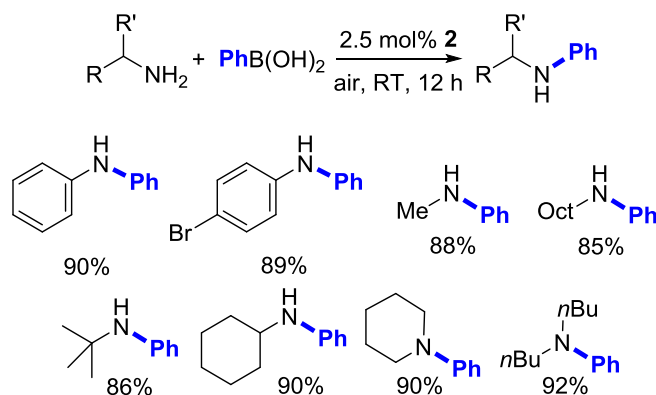


Chart 3-1 : Isolated yields for arylations with **2**.

3.2.2. Reactivity studies

Given the good reactivity towards amines and anilines in general, the reactivity of different substrates was investigated in more detail with particular attention towards substrates reported to be less reactive. Complex **2** was chosen for these studies, since its shorter induction time facilitates reactivity comparisons at short reaction times. Poorer nucleophiles are generally more difficult to react in Chan-Evans-Lam couplings,^{30,39-41} but *para*-fluoro, -bromo or -iodo anilines reacted only slightly slower than unsubstituted aniline (Chart 3-2, **A-D**). While *para*-phenoxy aniline reacted readily at room temperature (**E**), anilines carrying alkoxy substituents in *para*-position surprisingly only yielded starting material (**F-I**). Since formation of diphenyl side product was likewise suppressed in these reactions, electron-rich anilines probably coordinate to either copper or boron in an unproductive off-cycle complex. Dissociation of these complexes would be more favourable at higher temperatures and full conversion can be achieved by conducting the reaction at 50 °C (**F-I**).[‡] In the case of *para*-*tert*-butyl aniline, the reaction yielded a 1:2 mixture of the coupling product (**J**) and 4,4'-di(*tert*-butyl)azobenzene (**J'**). Cu-catalyzed formation of azabenzenes by aerial oxidation of anilines is well established,^{42,43} but has not been reported as a side reaction in Chan-Evans-Lam couplings. At 50 °C, aza-benzene formation was reduced to 10%, but could not be suppressed completely.

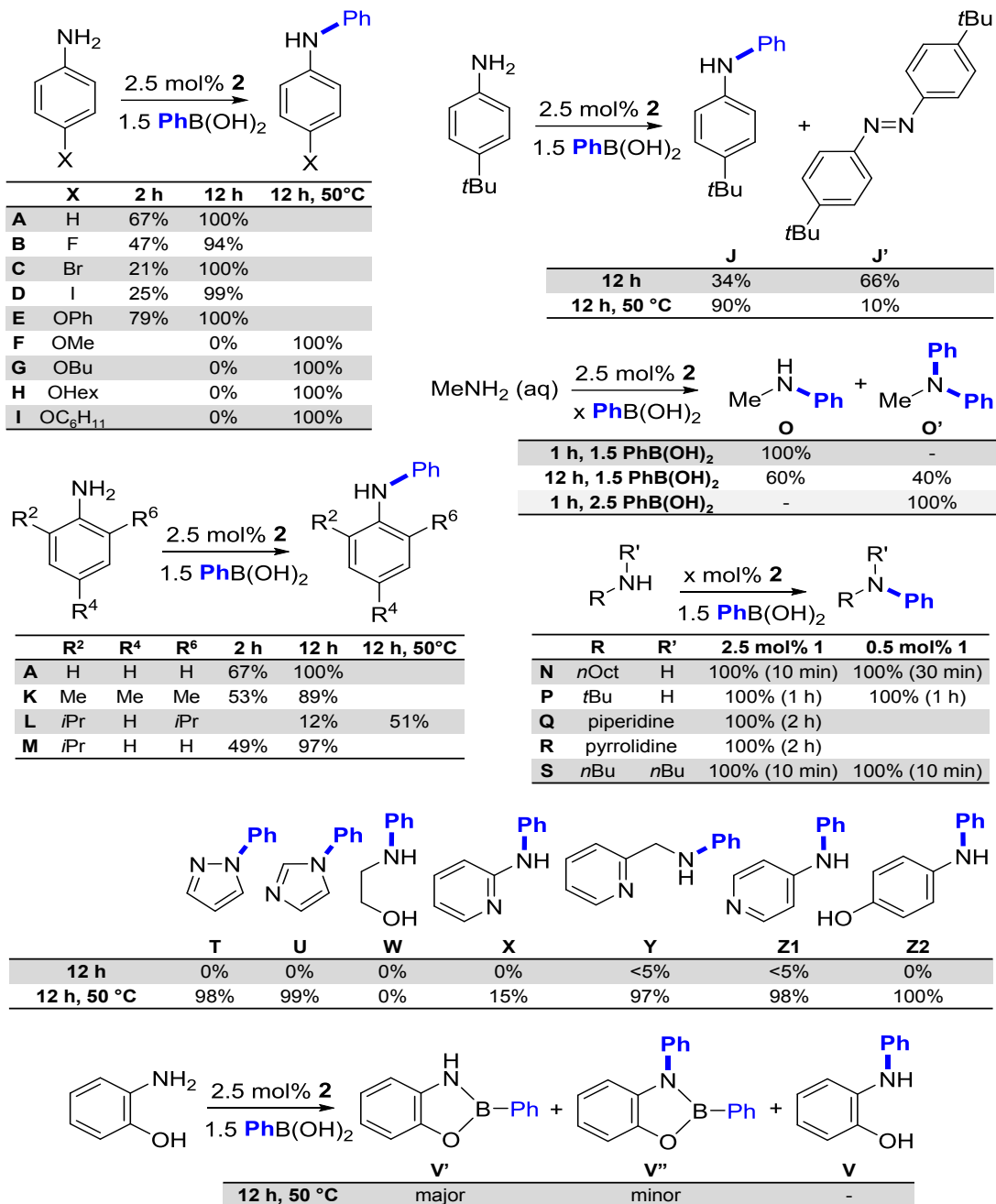


Chart 3-2 : Conversion to product (determined by GC-MS vs. internal calibrated standard) for the coupling of nitrogen nucleophiles with phenyl boronic acid.

Chan-Evans-Lam couplings of sterically demanding *ortho*-disubstituted anilines are typically difficult^{32, 38, 39, 44-48} and only few optimized protocols report yields above 80%.^{39, 45, 46}

⁴⁸ Complex **2** coupled 2,4,6-trimethylaniline (**K**) with only slightly lower activity than aniline. 2,6-Diisopropyl aniline reacted more slowly and only partial conversion of 51% was observed even after 12 h at 50 °C (**L**). We are aware of only one other Cu-catalyzed coupling of diisopropylaniline with arylboronic acid.⁴⁹ If one *i*Pr-substituent is removed, coupling proceeds readily at room temperature (**M**).

Aliphatic amines react in general faster and more easily than anilines. Primary amines typically reached full conversion in less than 2 h at ambient temperature. Catalytic activity was investigated in more detail with octylamine (**N**) and full conversion could be achieved in 30 min with a reduced catalyst loading of 0.5 mol%. The tolerance toward water in Chan-Evans-Lam couplings with **2** allowed the use of an aqueous solution of methylamine, which readily reacted in 1 h to MeN(Ph)H (**O**). To the best of our knowledge, no copper-catalyzed coupling of boronic acids with methylamine has been reported. Prolonged reaction times led in this case to the appearance of the double coupling product, MeNPh₂ (**O'**). The second coupling is, however, notably slower and formation of MeNPh₂ can be avoided by controlling reaction time or reducing the excess of phenyl boronic acid. With 2.5 equiv of phenyl boronic acid, full conversion to MeNPh₂ (**O'**) was observed after 12 h. The same product was obtained from coupling of *N*-methyl aniline.

Increased steric hindrance typically overcomes the increase in nucleophilicity and tertiary alkyl amines show very low activities in Chan-Evans-Lam couplings.³⁸ Couplings of *tert*-butyl amine have been reported with (isolated) yields of 28% – 60% using reaction temperatures of 40 – 80 °C and 20 – 24 h reaction time.⁵⁰⁻⁵² Coupling of *tert*-butyl amine with phenyl boronic acid using **2** proceeds with drastically higher activity and full conversion is achieved at room temperature in 1 h, even at lowered catalyst loadings of 0.5 mol% (**P**).

Cyclic secondary amines, such as piperidine (**Q**) and pyrrolidine (**R**), undergo Chan-Evans-Lam couplings readily,⁵ and full conversion is also obtained with **2** at room temperature in 2 h. Low reactivity of acyclic secondary amines, on the other hand, has been reported as a "major restriction" in copper-catalyzed coupling reactions.⁹ Reactions with Cu(OAc)₂ as a catalyst typically require longer reaction times at elevated temperature and yield vary

between traces to 60%.^{39, 41, 45, 50, 51, 53-56} Using (Xantphos)Cu(OtBu) as catalyst, Lalic obtained *iPr*₂NAr from benzoyloxy diisopropylamine in 94% conversion at 60 °C.⁴⁸ Phukan reported yields of 83% – 94% in 5 – 10 min for the coupling of *N*-methyl-benzylamine to various arylboronic acids using 2 mol% of a highly active [(DMAP)₄CuI]I catalyst.³² Using **2**, dibutylamine showed full conversion to *n*Bu₂NPh in 10 min at room temperature at reduced catalyst loadings of 0.5% (**S**).

Pyrazol (**T**) and imidazole (**U**) could also be successfully coupled at 50 °C, using the same reaction conditions employed for amines and anilines. *Ortho*-amino phenol, amino ethanol and *ortho*-amino pyridine did not react or only sluggishly (**V-X**), probably due to formation of phenyl boronic esters which were identified by GC-MS for *ortho*-aminophenol (**V'**, **V''**). Addition of glycol, of B(OH)₃¹⁹ or both, did not change the reaction outcome. Picolylamine (**Y**) was coupled successfully, but was the only alkylamine which required heating. Consequently, *para*-amino pyridine (**Z1**) and *para*-amino phenol (**Z2**), which cannot form chelated boronic esters, were coupled quantitatively at 50 °C. Using Cu(OAc)₂ catalyst, couplings of *para*-amino phenol were reported with up to 75% (isolated) yield, but required carefully optimized reaction conditions (dioxane, 90 °C, 12 h, CsCO₃, benzoic acid).⁵⁷ As with **2**, *ortho*-aminophenols could not be coupled.

3.3. Conclusions

In conclusion, use of a chelating ligand containing a sulfonate group able to coordinate to boronic acid afforded a highly active catalyst for Chan-Evans-Lam couplings, which does not require additional base/ligand, tolerates the presence of water and displays only slight dependence of activity on the solvent and the counter-anion. Consequently, no optimization of reaction conditions other than time and temperature was necessary to achieve full conversion to product for the coupling of a large variety of amines and anilines, including substrates generally considered challenging. In particular, sterically crowded substrates, such as 2,4,6-trimethylaniline, *tert*-butylamine and dibutylamine, react readily. Considering also the similarly high activity reported for $[\text{Cu}(\text{DMAP})_4\text{I}]$ with amines and anilines,³² the use of preformed coordination complexes can provide more universal Chan-Evans-Lam coupling protocols than simple copper salt catalysts.

3.4. Supporting information

- **Figure 3.S1.** Packing diagram showing the 1D-coordination polymer formed by **2**
- **Figure 3.S2.** Crystal structure of complex **1**.
- **Table 3-S1.** Arylation of aniline catalysed by **1**
- **Figure 3.S3.** Time-Conversion plots for the arylation of aniline with catalyst **1** or **2**
- **Experimental data and NMR spectra (Fig. 3.S4-S10)**
- **Details of the X-ray diffraction studies**

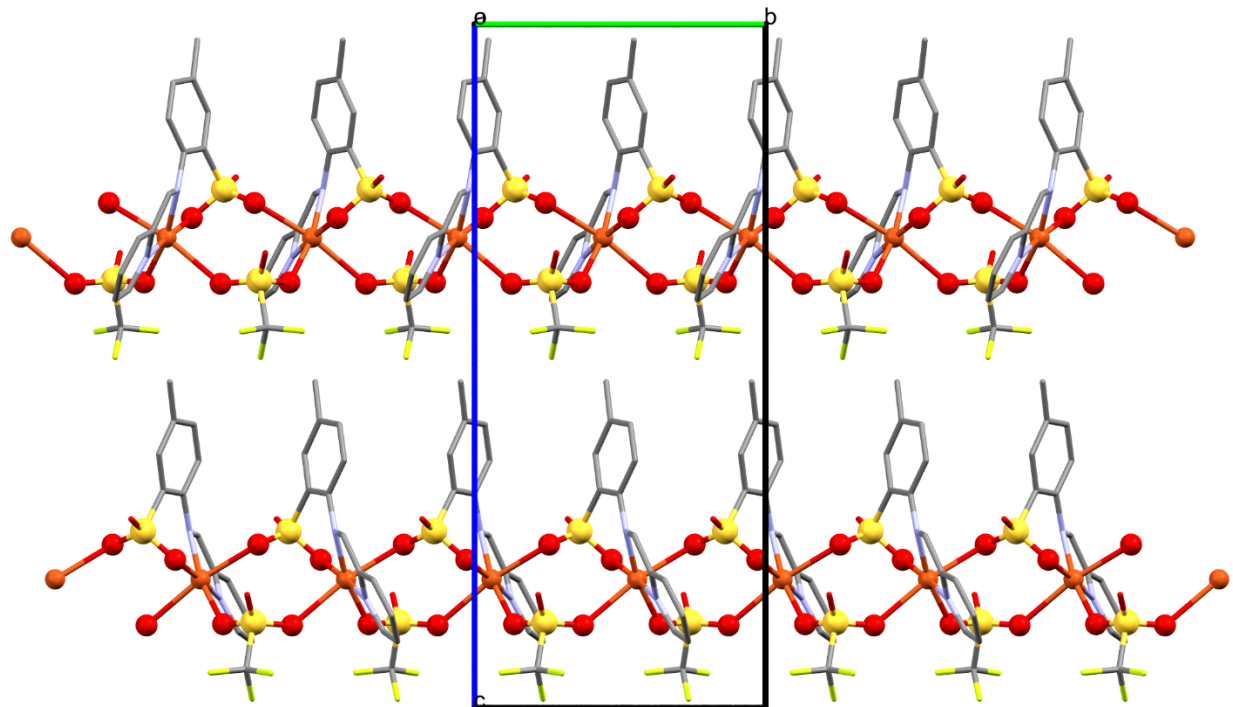


Figure 3.S1 : Packing diagram showing the 1D-coordination polymer formed by **2** along the *b*-axis due to bridging coordination of the sulfonate and triflate groups.

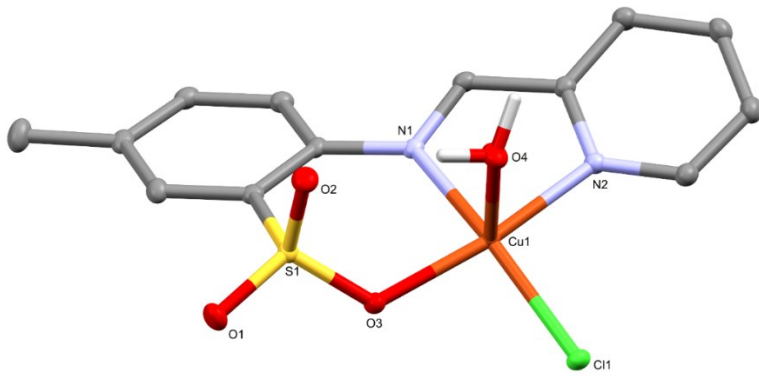
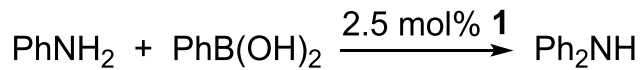


Figure 3.S2 : Crystal structure of complex **1**. Hydrogen atoms other than that of water omitted for clarity. Thermal ellipsoids are drawn at 50% probability.

Table 3-S1 : Arylation of aniline catalysed by **1**.



Entry	Solvent	Additive	Time ^a	Conversion ^b
1	MeCN		320 min	0%
2	MeOH		320 min	86%
3	THF		320 min	67%
4	CH ₂ Cl ₂		320 min	41%
5	toluene		320 min	36%
6	MeOH		320 min	86%
7	MeOH	1 equiv NEt ₃	320 min	0%
8	MeOH	2.5 mol% NEt ₃	320 min	12%
9	MeOH	molecular sieves	320 min	62%
10	MeOH	Using 2 as catalyst	320 min	98%

Conditions: room temperature, air, 1.0 M aniline, 2.5 mol% catalyst, 1.5 equiv.

PhB(OH)₂. ^a Reactions were quenched before full conversion to allow comparisons. ^b Conversion to product, determined by GC-MS and calibrated vs. internal standard.

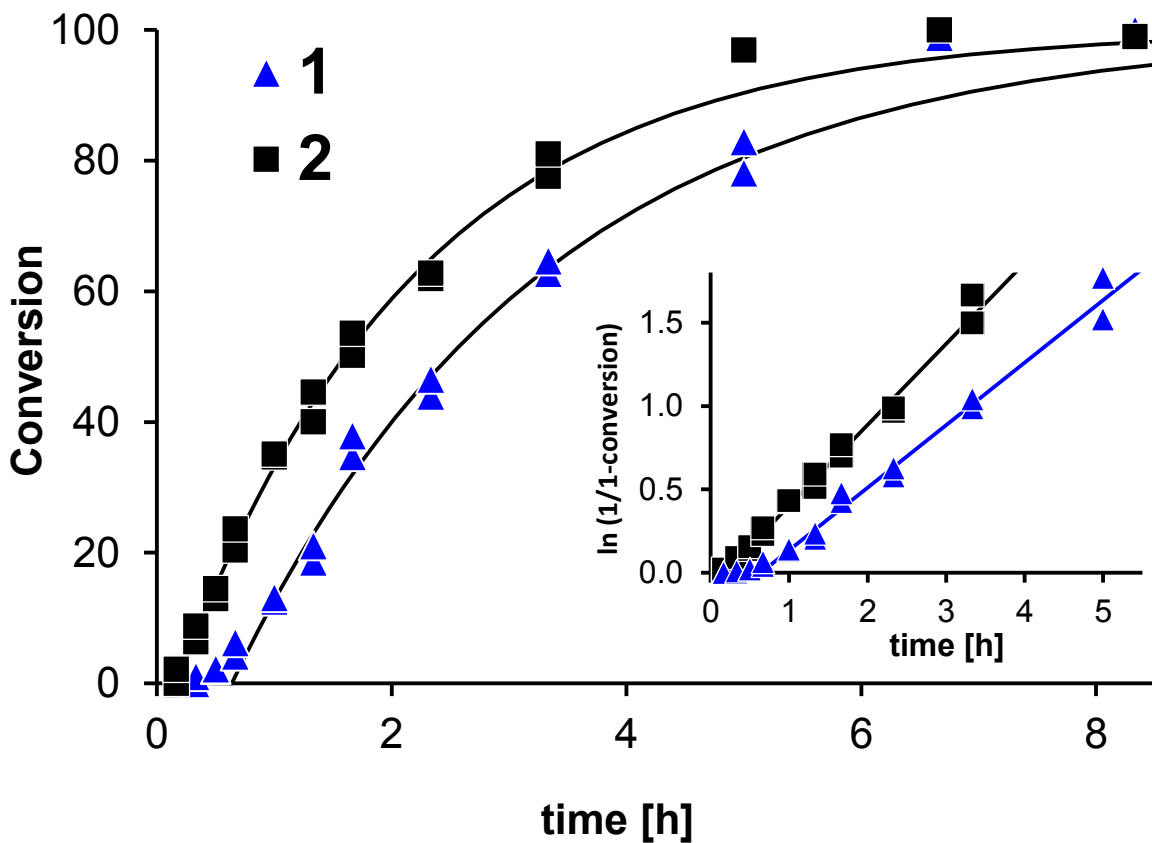
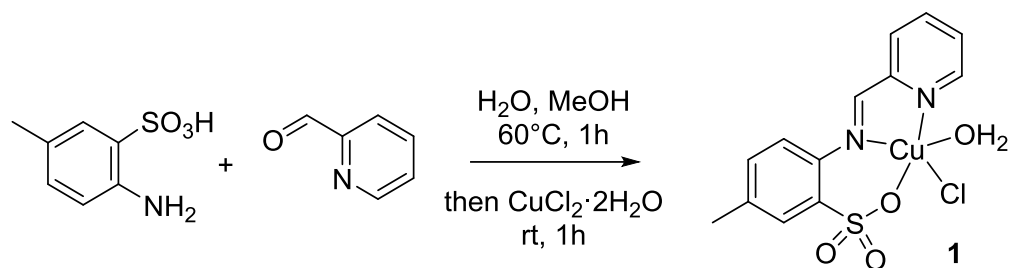


Figure 3.S3 : Time-Conversion plots for the arylation of aniline with catalyst **1** (triangles) or **2** (squares). Conditions: 1 M aniline, 1.5 PhB(OH)₂, 25 mM catalyst, ambient temperature, methanol. Conversion determined from GC-MS by comparison to (calibrated) standard either from disappearance of monomer or appearance of product (both data shown). The inset shows the linearized rate plot.

Experimental Data

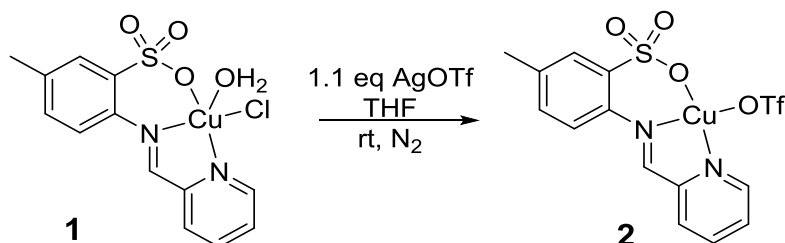
General. Phenyl boronic acid was purified by washing with dichloromethane until the filtrate stayed colorless. All other chemicals were purchased from common commercial suppliers and used without further purification. Elemental analyses were performed by the Laboratoire d'analyse élémentaire (Université de Montréal). UV/vis spectra were recorded on a Cary Series

UV-Vis-NIR spectrophotometer from Agilent Technologie. GC-MS spectra were recorded on a Agilent Technologie GC/MS.



LCuCl(H₂O), 1. To a hot solution (60 °C) of 4-aminotoluene-3-sulfonic acid (184 mg, 1.0 mmol) in water (5 mL) and methanol (10 mL) was added 2-pyridinecarboxaldehyde (95 µL, 1.0 mmol). The mixture was stirred one hour, then copper chloride hydrate (205 mg, 1.1 mmol) was added, resulting in a green solution. Heating was stopped and the solution was stirred another hour. Slow evaporation of solvent afforded green crystals of **1** (321 mg, 82%).

Anal. Calcd. for C₁₃H₁₃ClCuN₂O₄S : C, 39.80; H, 3.34; N, 7.14; S, 8.17. Found: C, 40.09; H, 3.37; N, 3.37; S, 8.47. UV-vis (DMSO, 1·10⁻² M or 1.49·10⁻⁴ M) [λ_{max}, nm (ε, M⁻¹·cm⁻¹)]: 338 (97 100), 800 (500).



LCuOTf, 2. Complex **1** (391, 1.0 mmol) was dissolved in dry THF (5 mL) under nitrogen atmosphere to give a green solution. Silver triflate (28 mg, 1.1 mmol) was added. After one hour of reaction at ambient temperature, a precipitate appeared and the colour of the solution intensified. Slow evaporation of the green solution (under N₂), afforded green crystals of **2** (263 mg, 54%).

Anal. Calcd. for $C_{14}H_{11}CuF_3N_2O_6S_2$: C, 34.46; H, 2.27; N, 5.74; S, 13.14. Found: C, 34.10; H, 2.59; N, 5.26; S, 12.61. UV-vis (DMSO, $1.2 \cdot 10^{-2}$ M or $3.35 \cdot 10^{-4}$ M) [λ_{max} , nm (ϵ , $M^{-1} \cdot cm^{-1}$)] : 338 (62 100), 730 (470).

General procedure for Chan-Evans-Lam couplings. To a solution of amine or aniline (1 mmol) and phenylboronic acid (1.5 mmol) in methanol (1 mL) was added catalyst **1** or **2** (0.025 mmol). Trimethoxybenzene was added as internal standard. The reaction was stirred open to air at ambient temperature or at 50 °C under O₂ atmosphere. After the desired time, the reaction was quenched with a saturated aqueous solution of ammonium chloride. For analysis of conversion, the organic layer was extracted three times with ethyl acetate and filtered through a short silica plug to remove copper complex. Conversion was determined by comparison to trimethoxybenzene. Calibration factors between products and trimethoxybenzene were determined from simultaneous NMR and GC-MS analysis or by analysis of stock solutions prepared from isolated or commercially available products. ¹H NMR data of all products agreed with literature data and the only observed species in the reaction mixtures were starting material (if conversion was less than 100%), product and biphenyl side-product from homocoupling reactions.

Isolation of coupling products. To a solution of amine (5 mmol) and phenylboronic acid (7.5 mmol) in methanol (5 mL) was added **2** (0.125 mmol). The reaction mixture was stirred for 12 h open to air at ambient temperature. The mixture was diluted with dichloromethane (20 mL) and washed once with a saturated solution of ammonium chloride and twice with water. Then combined aqueous phases were re-extracted two times with dichloromethane. The combined organic phases were dried, evaporated and purified by column chromatography with hexane/ethyl acetate.

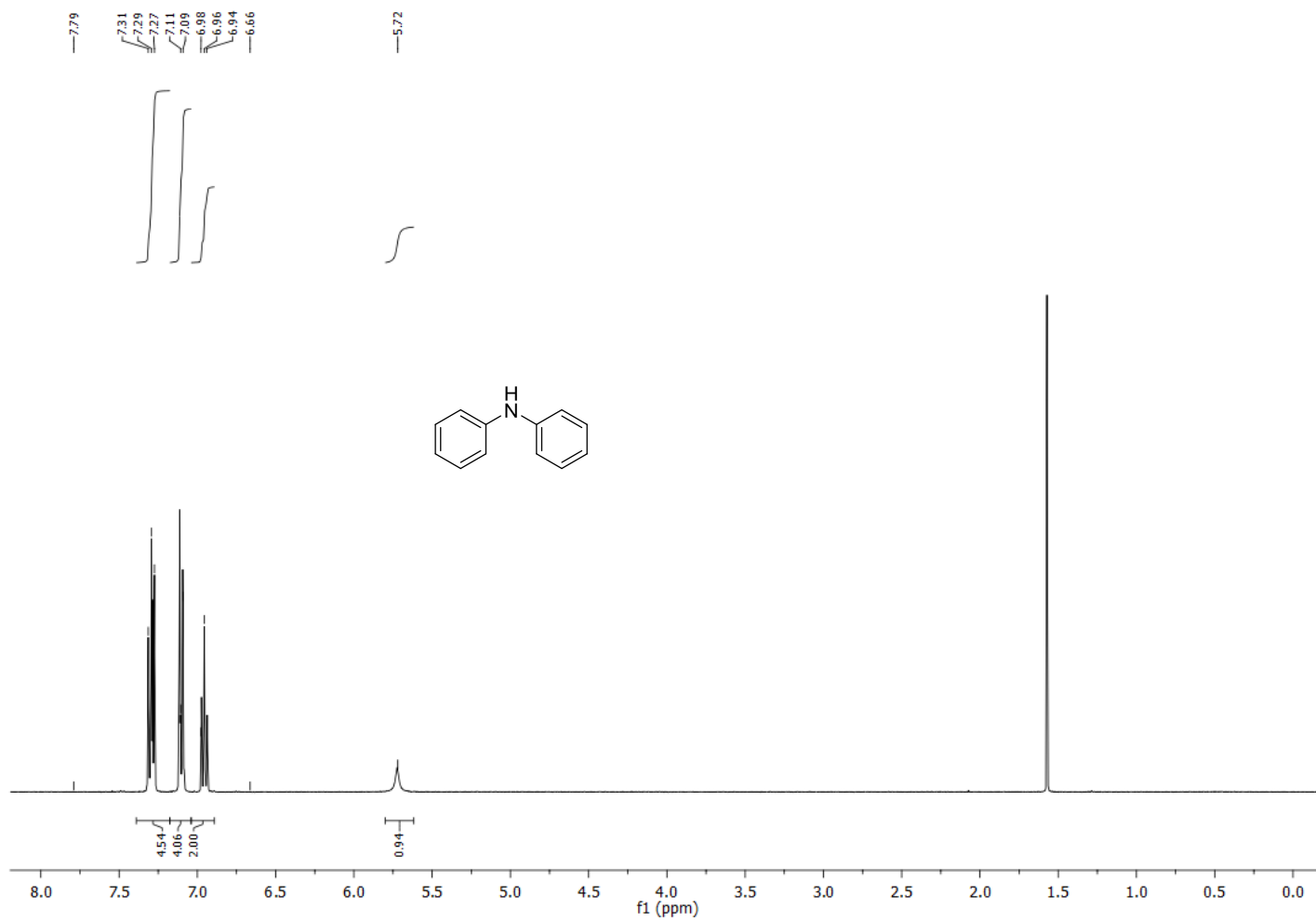


Figure 3.S4 : Diphenylamine. White powder, 761 mg, 90%

^1H NMR (400 MHz, CDCl_3): 7.25 (t, $J = 7$ Hz, 2H), 7.05 (d, $J = 7$ Hz, 2H), 6.90 (t, $J = 6$ Hz, 1H), 5.61 (s, 1H); ^{13}C NMR (400 MHz, CDCl_3): 142.8, 129.1, 121.1, 117.8

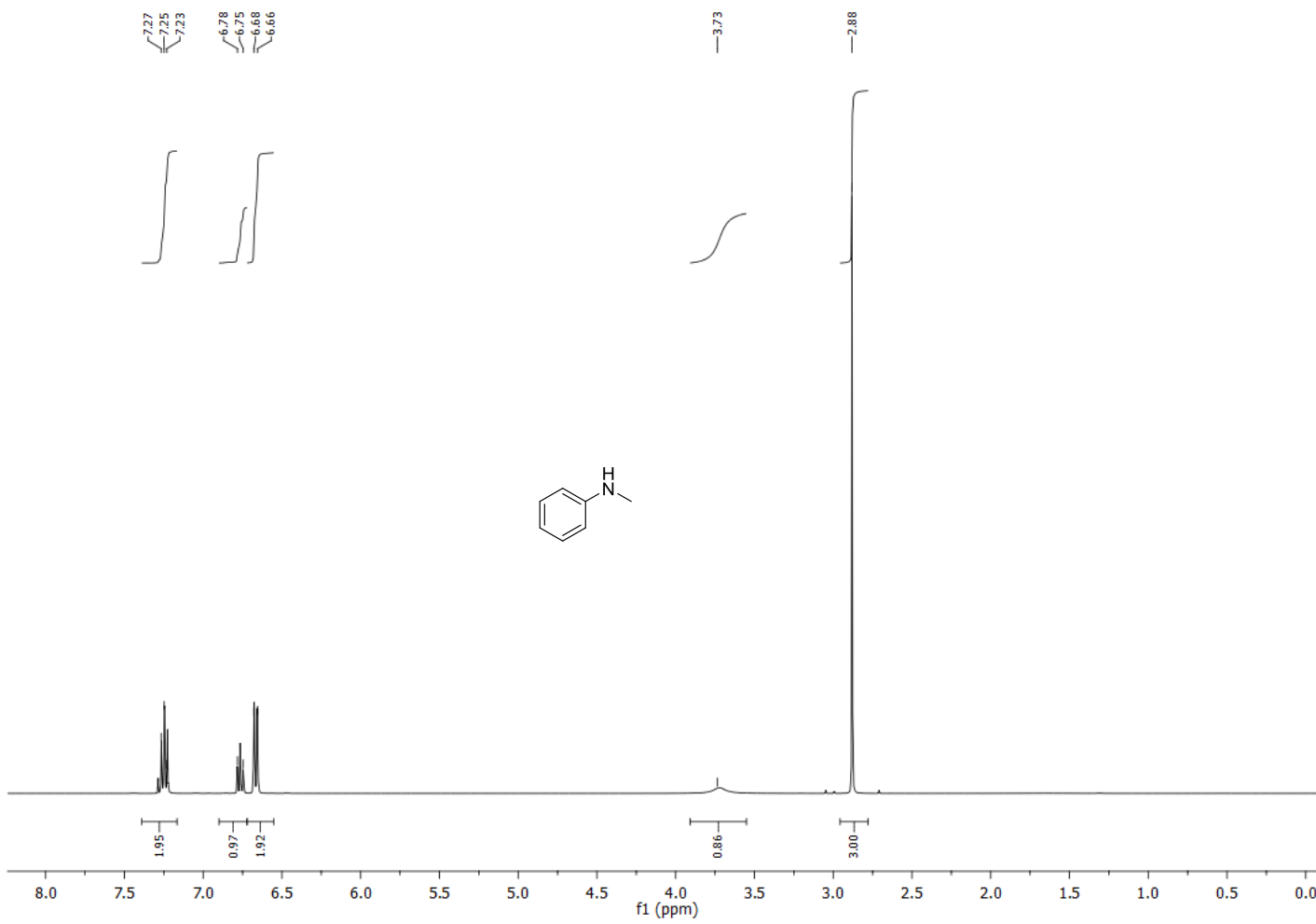


Figure 3.S5 : *N*-Methylaniline. Oil, 471 mg, 88%

^1H NMR (400 MHz, CDCl_3): 7.28 (t, $J = 7$ Hz, 2H), 6.7 (d, $J = 8$ Hz, 2H), 6.55 (t, $J = 8$ Hz, 1H), 3.69 (s, 1H), 2.75 (s, 3H); ^{13}C NMR (400 MHz, CDCl_3): 149.9, 129.5, 117.2, 112.0, 30.6

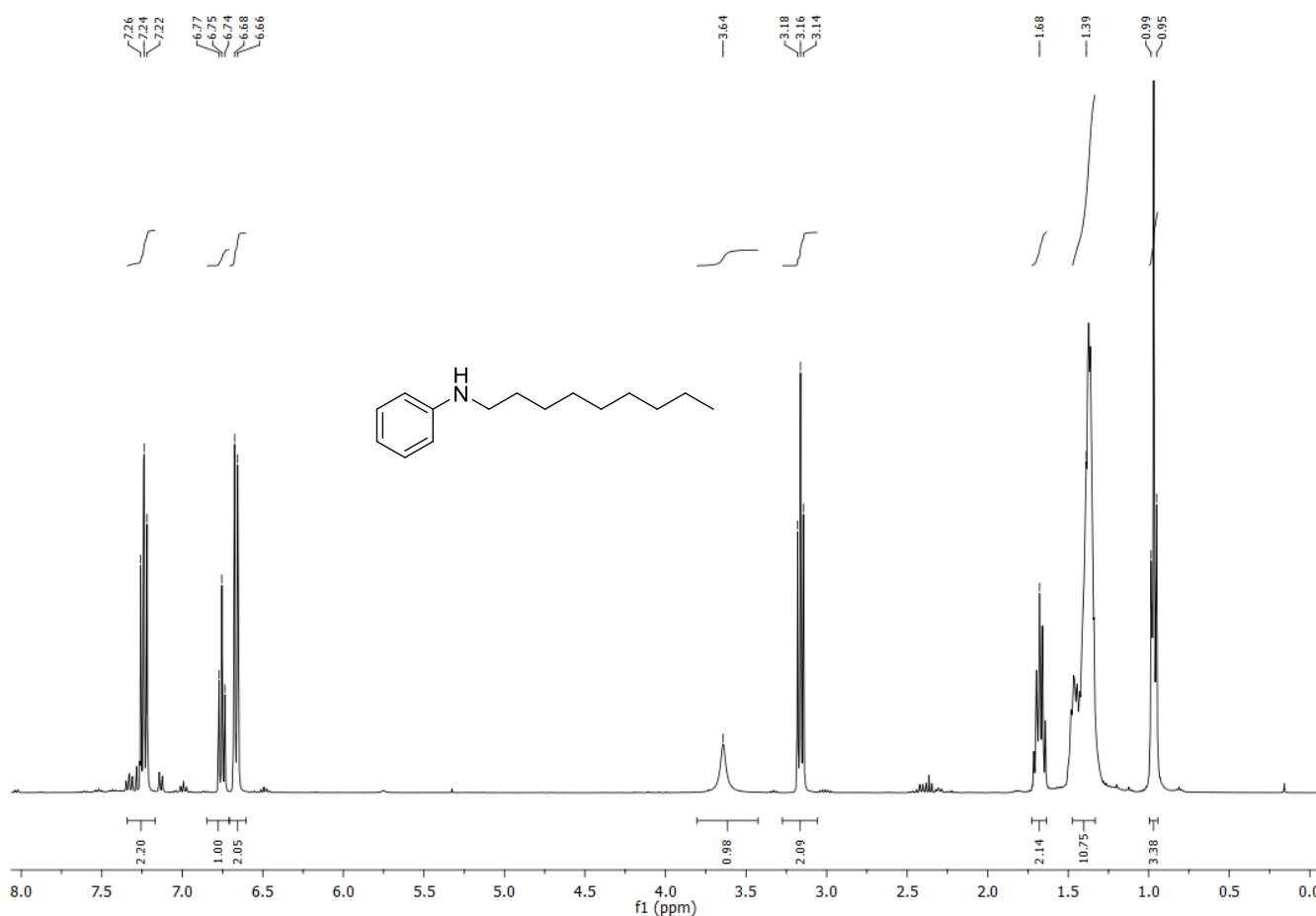


Figure 3.S6 : N-Octylaniline. Oil, 871 mg , 85%

^1H NMR (400 MHz, CDCl_3): 7.17 (t, $J = 9$ Hz, 2H), 6.70 (t, $J = 9$ Hz, 1H), 6.61 (d, $J = 8$ Hz, 1H), 3.4 (s, 1H), 3.12 (t, $J = 7$ Hz, 2H), 1.60 (m, 2H), 1.28-1.25 (m, 10H), 0.895 (t, $J = 7$ Hz, 3H); ^{13}C NMR (400 MHz, CDCl_3): 148.4, 129.1, 117.0, 112.6, 44.0, 31.8, 30.9, 29.5, 29.2, 27.1, 22.6, 14.0

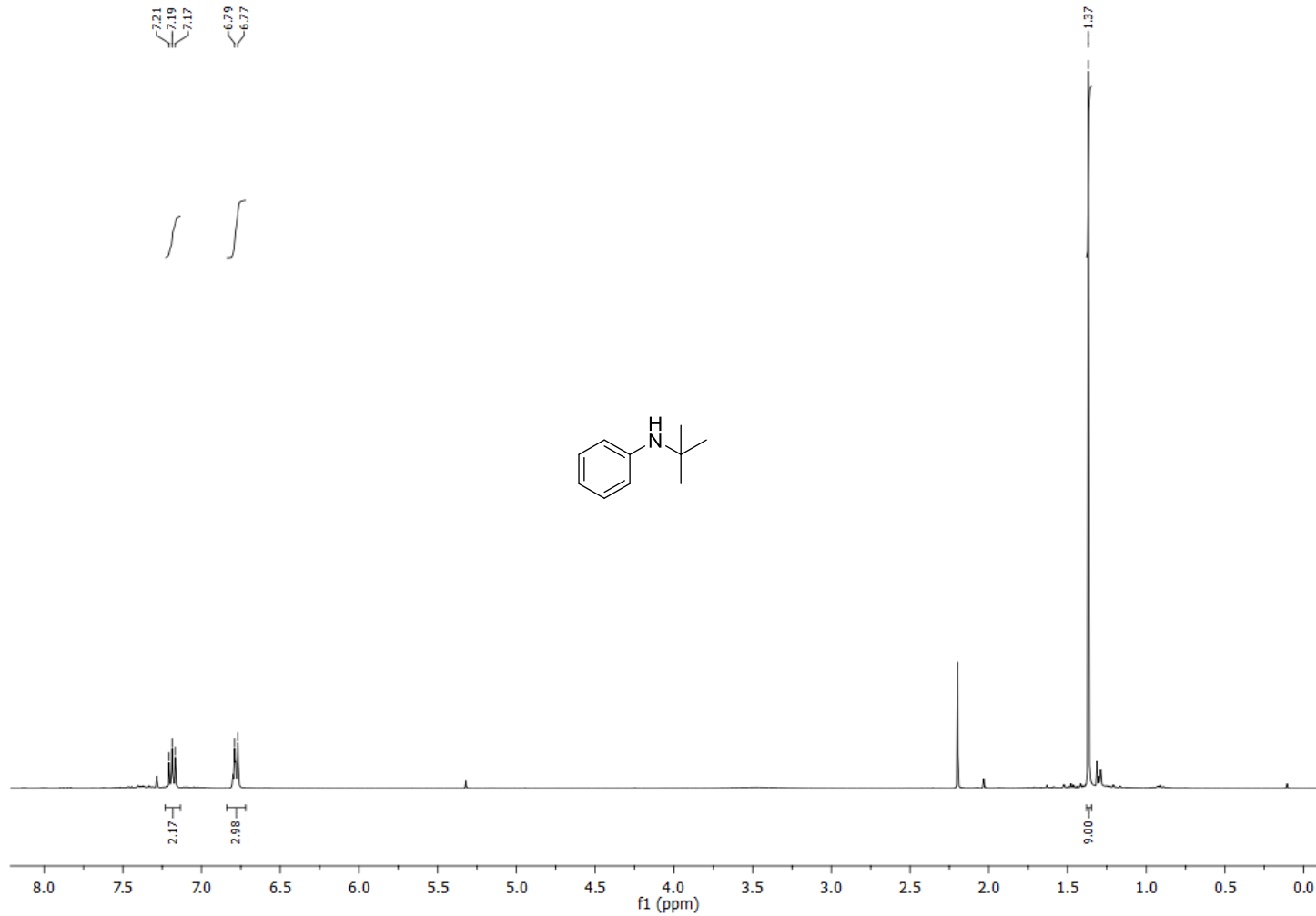


Figure 3.S7 : *N*-*tert*-butylaniline. Oil, 976 mg, 86%

^1H NMR (400 MHz, CDCl_3): 7.27 (t, $J = 8 \text{ Hz}$, 2H), 6.76 (m, 3H), 1.37 (s, 9H); ^{13}C NMR (400 MHz, CDCl_3): 146.7, 128.8, 118.3, 117.5, 51.5, 30.7

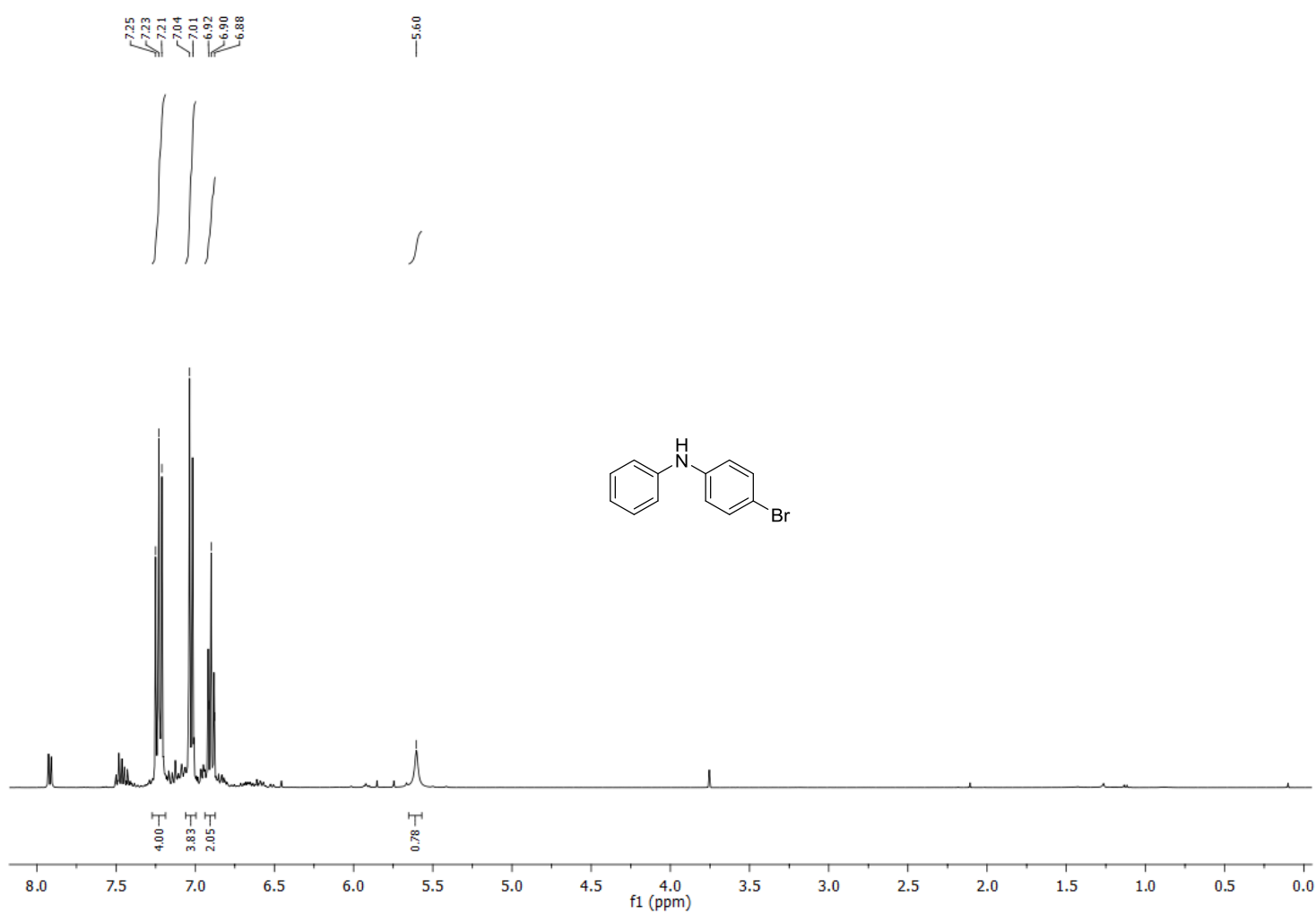


Figure 3.S8 : *N*-phenyl-(4-bromo)aniline. White powder, 1.099 mg, 89%

^1H NMR (400 MHz, CDCl_3): 7.34 (d, $J = 9$ Hz, 2H), 7.28 (d, $J = 8$ Hz, 2H), 7.05 (d, $J = 8$ Hz, 2H), 6.86 (m, 3H), 5.66 (s, 1H); ^{13}C NMR (400 MHz, CDCl_3): 142.5, 142.4, 132.2, 129.5, 121.7, 119.0, 118.3, 112.6

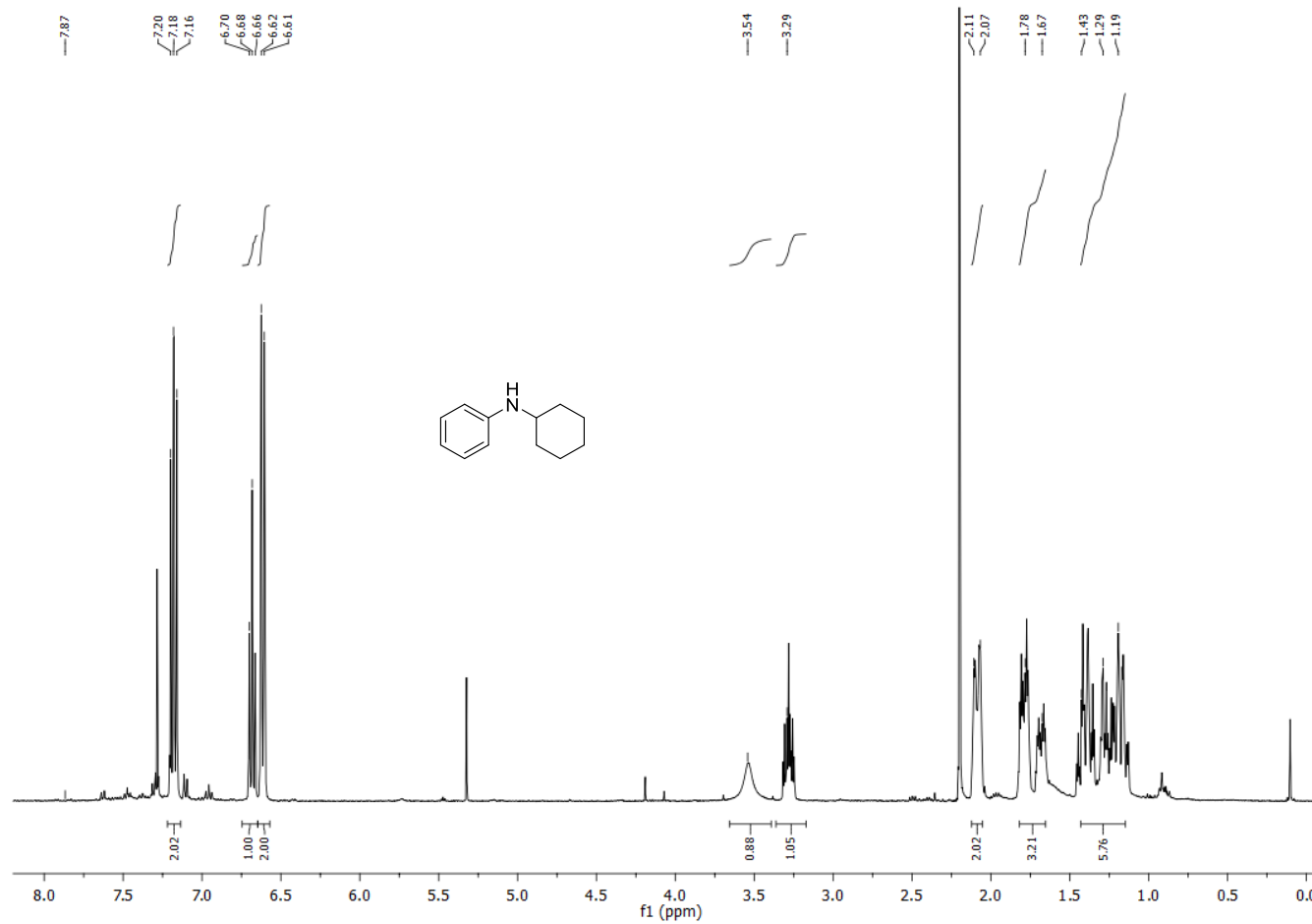


Figure 3.S9 : *N*-Cyclohexylaniline. White powder, 787 mg, 90%

^1H NMR (400 MHz, CDCl_3): 7.17 (t, $J = 7$ Hz, 2H), 6.69 (t, $J = 7$ Hz, 1H), 6.62 (d, $J = 7$ Hz, 2H), 3.39 (s, 1H), 3.25 (m, 1H), 2.07 (m, 2H), 1.78 (m, 3H), 1.43 (m, 5H); ^{13}C NMR (400 MHz, CDCl_3): 147.3, 129.1, 116.8, 113.1, 51.6, 33.4, 25.8, 24.9

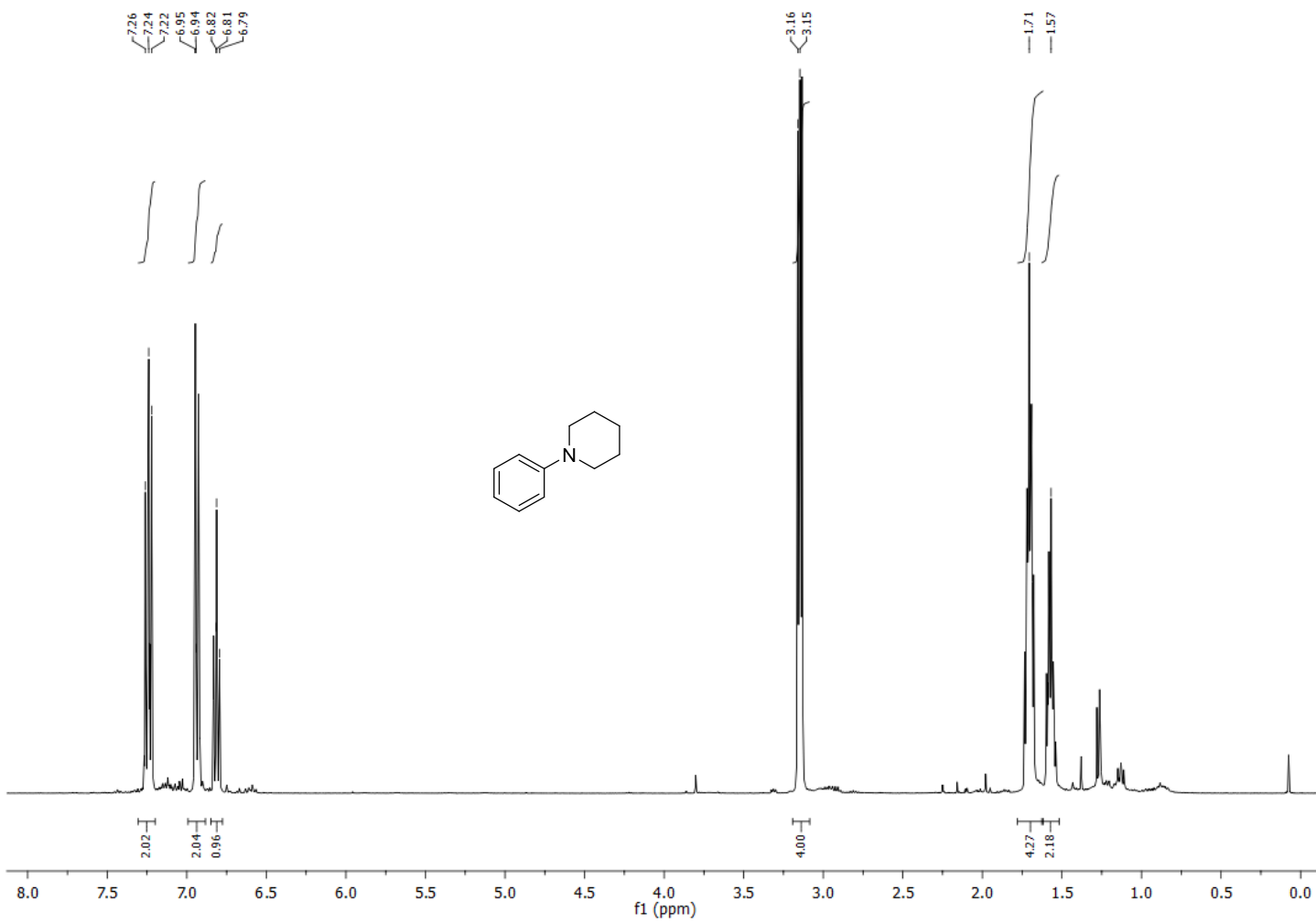


Figure 3.S10 : 1-Phenylpiperidine. White powder, 741 mg, 90%

¹H NMR (400 MHz, CDCl₃): 7.29 (t, *J* = 7 Hz, 2H), 6.98 (d, *J* = 8 Hz, 2H), 6.86 (t, *J* = 8 Hz, 1H), 3.19 (m, 4H), 1.76 (m, 4H), 1.61 (m, 2H);

¹³C NMR (400 MHz, CDCl₃): 152.2, 128.9, 119.1, 116.5, 50.6, 25.8, 24.3

X-ray diffraction studies. Single crystals were obtained directly from isolation of the products as described above. Diffraction data were collected on a Bruker Venture METALJET diffractometer (Ga K α radiation) or a Bruker APEXII with a Cu microsource/Quazar MX using the APEX2 software package.¹ Data reduction was performed with SAINT,² absorption corrections with SADABS.³ Structures were solved by dual-space refinement (SHELXT).⁴ All non-hydrogen atoms were refined anisotropic using full-matrix least-squares on F^2 and hydrogen atoms refined with fixed isotropic U using a riding model (SHELXL97).⁵ Further experimental details can be found in Table 3-S2 and in the supporting information (CIF).

Table 3-S2 : Details of X-ray Diffraction Studies

	1	2
Formula	$C_{13}H_{13}ClCuN_2O_4S$	$C_{14}H_{11}CuN_2F_3O_6S_2$
M_w (g/mol); F(000)	392.30; 796	487.91; 1960
T (K); wavelength	100; 1.34190	100; 1.34190
Crystal System	Monoclinic	Orthorombic
Space Group	$P2_1/c$	$Pbca$
Unit Cell: a (\AA)	7.9081(2)	14.6171(2)
b (\AA)	13.4568(4)	10.0602(2)
c (\AA)	14.0019(4)	23.5560(4)
β ($^\circ$)	104.2800(10)	
V (\AA^3)	1444.01(7)	3463.93(10)
Z ; $d_{\text{calcd.}}$ (g/cm 3)	4; 1.805	8; 1.871
μ (mm $^{-1}$); Abs. Corr.	10.277; multi-scan	4.698; multi-scan
θ range ($^\circ$); completeness	4.0-60.7; 0.999	4.8-72.1; 1.000
Collected reflections; R_σ	25548; 0.0274	66922; 0.0089
Unique reflections; R_{int}	3292; 0.0472	3413; 0.0238
Observed Reflections; $R1(F)$	3254; 0.0257	3332; 0.0233
wR(F^2) (all data); GoF(F^2)	0.0735; 1.058	0.0679; 1.055
Residual electron density	0.423	0.416

- (1) *APEX2*, Release 2.1-0; Bruker AXS Inc.: Madison, USA, 2006.
- (2) *SAINT*, Release 7.34A; Bruker AXS Inc.: Madison, USA, 2006.
- (3) Sheldrick, G. M. *SADABS*, Bruker AXS Inc.: Madison, USA, 1996 & 2004.
- (4) Sheldrick, G. *Acta Crystallographica Section A* **2015**, *71*, 3.
- (5) Sheldrick, G. M. *Acta Crystallogr.* **2008**, *A64*, 112.

3.5. References

- ¹ K. Koide, in *New Trends in Cross-Coupling: Theory and Applications*, The Royal Society of Chemistry, 2015, DOI: 10.1039/9781782620259-00779, pp. 779.
- ² Y. Jiang and D. Ma, in *Copper-Mediated Cross-Coupling Reactions*, John Wiley & Sons, Inc., 2013, DOI: 10.1002/9781118690659.ch1, pp. 1.
- ³ F. Paul, J. Patt and J. F. Hartwig, *J. Am. Chem. Soc.*, 1994, **116**, 5969.
- ⁴ A. S. Guram and S. L. Buchwald, *J. Am. Chem. Soc.*, 1994, **116**, 7901.
- ⁵ D. M. T. Chan, K. L. Monaco, R.-P. Wang and M. P. Winters, *Tetrahedron Lett.*, 1998, **39**, 2933.
- ⁶ D. A. Evans, J. L. Katz and T. R. West, *Tetrahedron Lett.*, 1998, **39**, 2937.
- ⁷ P. Y. S. Lam, C. G. Clark, S. Saubern, J. Adams, M. P. Winters, D. M. T. Chan and A. Combs, *Tetrahedron Lett.*, 1998, **39**, 2941.
- ⁸ S. V. Ley and A. W. Thomas, *Angew. Chem., Int. Ed.*, 2003, **42**, 5400.
- ⁹ G. Evano, N. Blanchard and M. Toumi, *Chem. Rev.*, 2008, **108**, 3054.
- ¹⁰ F. Bellina and R. Rossi, *Adv. Synth. Catal.*, 2010, **352**, 1223.
- ¹¹ J. X. Qiao and P. Y. S. Lam, in *Boronic Acids*, Wiley-VCH Verlag GmbH & Co. KGaA, 2011, DOI: 10.1002/9783527639328.ch6, pp. 315.
- ¹² I. P. Beletskaya and A. V. Cheprakov, *Organometallics*, 2012, **31**, 7753.
- ¹³ T. R. M. Rauws and B. U. W. Maes, *Chem. Soc. Rev.*, 2012, **41**, 2463.
- ¹⁴ K. Sanjeeva Rao and T.-S. Wu, *Tetrahedron*, 2012, **68**, 7735.
- ¹⁵ L. Neuville, in *Copper-Mediated Cross-Coupling Reactions*, John Wiley & Sons, Inc., 2013, DOI: 10.1002/9781118690659.ch4, pp. 113.
- ¹⁶ P. Y. S. Lam, in *Synthetic Methods in Drug Discovery: Volume 1*, The Royal Society of Chemistry, 2016, vol. 1, pp. 242.
- ¹⁷ D. N. Rao, S. Rasheed, S. Aravinda, R. A. Vishwakarma and P. Das, *RSC Adv.*, 2013, **3**, 11472.

- ¹⁸ A. E. King, B. L. Ryland, T. C. Brunold and S. S. Stahl, *Organometallics*, 2012, **31**, 7948.
- ¹⁹ J. C. Vantourout, H. N. Miras, A. Isidro-Llobet, S. Sproules and A. J. B. Watson, *J. Am. Chem. Soc.*, 2017, **139**, 4769.
- ²⁰ T. Garnier, R. Sakly, M. Danel, S. Chassaing and P. Pale, *Synthesis*, 2017, **49**, 1223.
- ²¹ J. P. Collman and M. Zhong, *Org. Lett.*, 2000, **2**, 1233.
- ²² J. P. Collman, M. Zhong, C. Zhang and S. Costanzo, *J. Org. Chem.*, 2001, **66**, 7892.
- ²³ S. S. van Berkel, A. van den Hoogenband, J. W. Terpstra, M. Tromp, P. W. N. M. van Leeuwen and G. P. F. van Strijdonck, *Tetrahedron Lett.*, 2004, **45**, 7659.
- ²⁴ M. Tromp, G. P. F. van Strijdonck, S. S. van Berkel, A. van den Hoogenband, M. C. Feiters, B. de Bruin, S. G. Fiddy, A. M. J. van der Eerden, J. A. van Bokhoven, P. W. N. M. van Leeuwen and D. C. Koningsberger, *Organometallics*, 2010, **29**, 3085.
- ²⁵ T. Onaka, H. Umemoto, Y. Miki, A. Nakamura and T. Maegawa, *J. Org. Chem.*, 2014, **79**, 6703.
- ²⁶ B. Liu, B. Liu, Y. Zhou and W. Chen, *Organometallics*, 2010, **29**, 1457.
- ²⁷ L. Wang, Z. Jiang, L. Yu, L. Li, Z. Li and X. Zhou, *Chem. Lett.*, 2010, **39**, 764.
- ²⁸ M. Islam, S. Mondal, P. Mondal, A. Roy, K. Tuhina, M. Mobarok, S. Paul, N. Salam and D. Hossain, *Catal. Lett.*, 2011, **141**, 1171.
- ²⁹ B. Kaboudin, Y. Abedi and T. Yokomatsu, *Eur. J. Org. Chem.*, 2011, **2011**, 6656.
- ³⁰ A. Gogoi, G. Sarmah, A. Dewan and U. Bora, *Tetrahedron Lett.*, 2014, **55**, 31.
- ³¹ Anuradha, S. Kumari and D. D. Pathak, *Tetrahedron Lett.*, 2015, **56**, 4135.
- ³² S. Roy, M. J. Sarma, B. Kashyap and P. Phukan, *Chem. Commun. (Cambridge, U. K.)*, 2016, **52**, 1170.
- ³³ S. Hazra, S. Mukherjee, M. F. C. Guedes da Silva and A. J. L. Pombeiro, *RSC Adv.*, 2014, **4**, 48449.
- ³⁴ Y.-M. Ou, Z.-Y. Zhao, Yue-Hua Shi, Y.-L. Zhang and Y.-M. Jiang, *Chin. J. Struct. Chem.*, 2009, **28**, 457.

- ³⁵ G.-G. Yang, M. Ou-Yang, X.-J. Meng, X.-R. Huang and Y.-M. Jiang, *Acta Crystallogr., Sect. E: Struct. Rep. Online*, 2009, **65**, m1200.
- ³⁶ S. Hazra, A. Karmakar, M. d. F. C. Guedes da Silva, L. u. Dlhan, R. Boca and A. J. L. Pombeiro, *New J. Chem.*, 2015, **39**, 3424.
- ³⁷ S. Hazra, A. P. C. Ribeiro, M. F. C. Guedes da Silva, C. A. Nieto de Castro and A. J. L. Pombeiro, *Dalton Trans.*, 2016, **45**, 13957.
- ³⁸ T. D. Quach and R. A. Batey, *Org. Lett.*, 2003, **5**, 4397.
- ³⁹ J. C. Antilla and S. L. Buchwald, *Org. Lett.*, 2001, **3**, 2077.
- ⁴⁰ S. Chen, H. Huang, X. Liu, J. Shen, H. Jiang and H. Liu, *J. Comb. Chem.*, 2008, **10**, 358.
- ⁴¹ J. C. Vantourout, R. P. Law, A. Isidro-Llobet, S. J. Atkinson and A. J. B. Watson, *J. Org. Chem.*, 2016, **81**, 3942.
- ⁴² A. P. Terent'ev and Y. D. Mogilyanskii, *Zh. Obshch. Khim.*, 1958, **28**, 1959.
- ⁴³ K. Keiz, *Bull. Chem. Soc. Jpn.*, 1959, **32**, 777.
- ⁴⁴ G. C. H. Chiang and T. Olsson, *Org. Lett.*, 2004, **6**, 3079.
- ⁴⁵ G. W. Kabalka and L.-L. Zhou, *Letters in Organic Chemistry* 2006, **3**, 320
- ⁴⁶ K. A. McGarry, A. A. Duenas and T. B. Clark, *J. Org. Chem.*, 2015, **80**, 7193.
- ⁴⁷ J. Bao and G. K. Tranmer, *Tetrahedron Lett.*, 2016, **57**, 654.
- ⁴⁸ R. P. Rucker, A. M. Whittaker, H. Dang and G. Lalic, *Angew. Chem., Int. Ed.*, 2012, **51**, 3953.
- ⁴⁹ W. Zhong, Z. Liu, C. Yu and W. Su, *Synlett*, 2008, **2008**, 2888.
- ⁵⁰ T. D. Quach and R. A. Batey, *Org. Lett.*, 2003, **5**, 1381.
- ⁵¹ X.-Q. Yu, Y. Yamamoto and N. Miyaura, *Chemistry – An Asian Journal*, 2008, **3**, 1517.
- ⁵² A. Joliton and E. M. Carreira, *Synlett*, 2015, **11**, 737.
- ⁵³ A. P. Combs, S. Tadesse, M. Rafalski, T. S. Haque and P. Y. S. Lam, *J. Comb. Chem.*, 2002, **4**, 179.

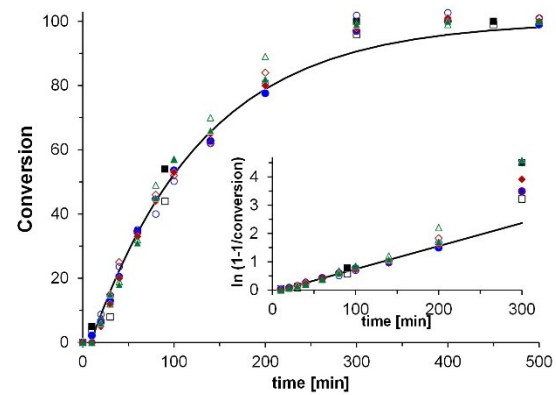
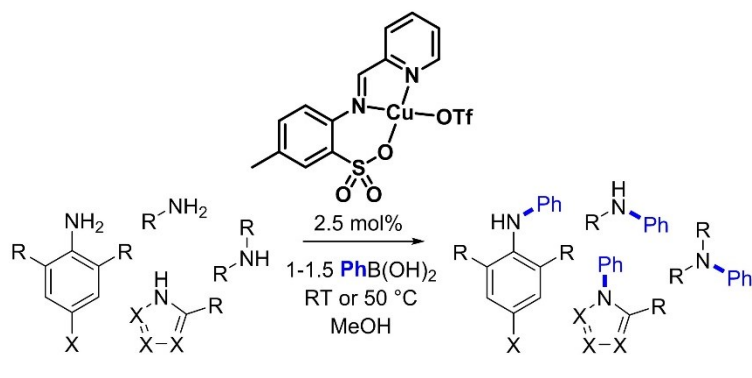
⁵⁴ S. Benard, L. Neuville and J. Zhu, *Chem. Commun. (Cambridge, U. K.)*, 2010, **46**, 3393.

⁵⁵ N. Debreczeni, A. Fodor and Z. Hell, *Catal. Lett.*, 2014, **144**, 1547.

⁵⁶ K. Singh, M. Kumar, E. Pavadai, K. Naran, D. F. Warner, P. G. Ruminski and K. Chibale, *Bioorg. Med. Chem. Lett.*, 2014, **24**, 2985.

⁵⁷ A. Siva Reddy, K. Ranjith Reddy, D. Nageswar Rao, C. K. Jaladanki, P. V. Bharatam, P. Y. S. Lam and P. Das, *Organic & Biomolecular Chemistry*, 2015

4. Chan-Evans-Lam couplings with imino-arylsulfonate copper complexes: scope and mechanism

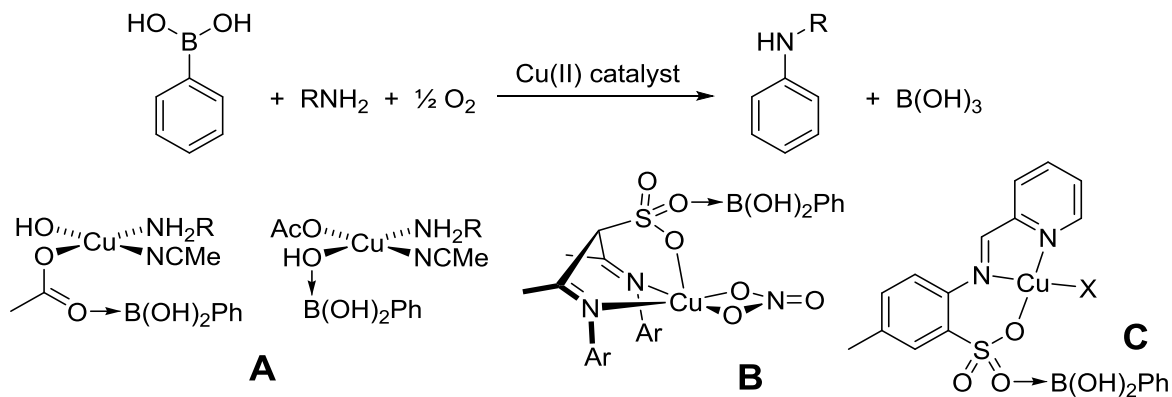


V. Hardouin Duparc, G. L. Bano, F. Schaper *ACS Catalysis* **2018**, in print.

Contributions from Guillaume Bano : Reactions and kinetic experiments with electron-deficient boronic acids.

4.1. Introduction

Over the last two decades, palladium-catalyzed coupling reactions have become a staple reaction of the pharmaceutical industry,¹ to an extend that processes to remove residual palladium from pharmaceutic products became an active area of research.² Partly due to their lower costs and higher availability, but mostly due to their significantly lower toxicity, there is thus an ongoing effort to replace catalysis with palladium-group metals by first-row transition metal alternatives for C-C, C-N, or C-O coupling reactions. Based on earlier work by Barton on couplings with aryl bismuth reagents,³ Chan, Evans and Lam reported in 1998 the oxidative coupling of amines (and other nucleophiles) with arylboronic acids by copper salts (Scheme 4-1).⁴⁻⁶



Scheme 4-1

In the following years, Chan-Evans-Lam (CEL) couplings with catalytic amounts of copper were developed and the method proved to be applicable to a wide variety of nucleophiles.⁷⁻¹⁴ Compared to the Ullmann-Goldberg reaction or Buchwald-Hartwig aminations catalyzed by palladium or copper, CEL couplings proceed under much milder conditions, often at room temperature, and are thus more attractive for complicated and sensitive substrates. While CEL couplings have now been successfully employed for a large variety of N-, O-, S-, and even C-nucleophiles, from the very beginning researchers remarked the “somewhat capricious nature of this reaction”,¹⁵ and its exceedingly high substrate-dependency. Early – and even current – work on CEL couplings thus report optimized reaction conditions which differ strongly even for closely related substrates such as amines,¹⁶ anilines,¹⁷ tetrazoles,^{18, 19} aminopyridines,²⁰ and aminophenols.²¹ In these optimized reaction protocols, water typically needs to be removed...^{5, 22} when it is not beneficial,²³⁻²⁵ the addition of base is essential...²⁶ or unnecessary,^{16, 27-}

³¹ solvent dependence is strong, but completely empirical, and copper sources with acetate or triflate anions work best,^{14, 32} with the exception of those cases where they don't.^{19, 33, 34} Only lately, more general protocols for CEL couplings of *N*-nucleophiles emerged. Watson et al. reported a modified protocol with stoichiometric amounts of copper, addition of B(OH)₃ and an excess amine, which is generally applicable to a larger variety of amines and anilines.³⁵ Phukan reported CEL couplings with [Cu(DMAP)₄I]I to proceed with high activities and to be likewise applicable to a larger variety of substrates under the same reaction conditions.³⁶

Typical catalysts in CEL couplings are simple copper salts, in most cases Cu(OAc)₂. Copper salts immobilized in resins, zeolites or other solid supports have also been employed.^{31, 37-46} Coordination complexes have been used rarely, even though the first catalytic CEL coupling by Collman employed [(tmeda)Cu(OH)]₂Cl₂ for the arylation of imidazoles.^{47, 48} A tetranuclear copper(II) carbene complex was employed for arylations of benzimidazoles, but showed low activity with amines or anilines.²⁹ Copper salen complexes have been used to enable imidazole couplings in water,^{49, 50} and likewise a cyclodextrin-based complex, which showed good activities for amines and anilines.³⁰ Recently, Phukan reported [Cu(DMAP)₄I]I as a catalyst, which showed so far the highest and most general reactivity for *N*-nucleophiles.³⁶

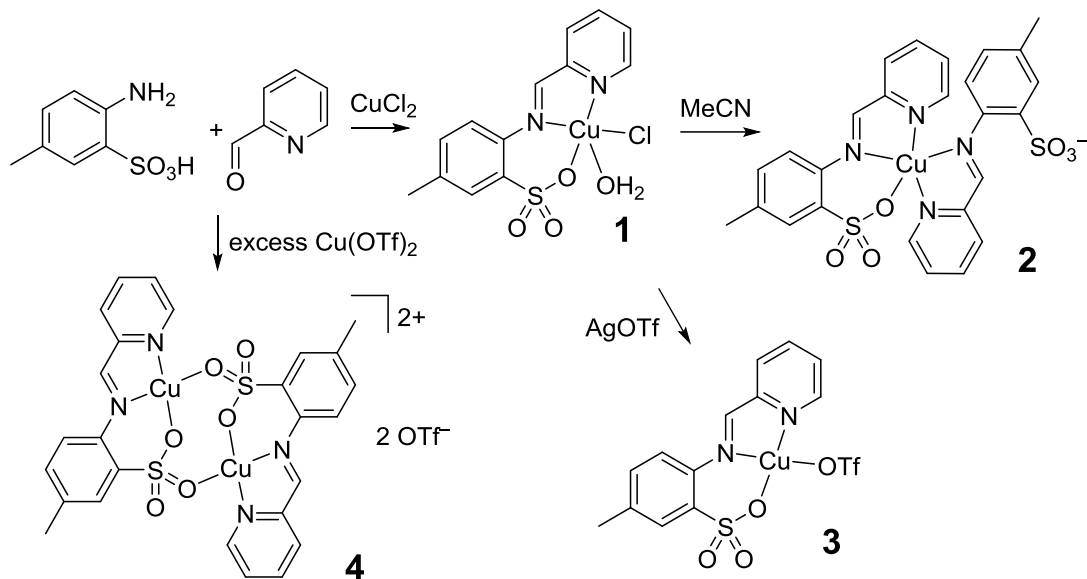
We hypothesized that the large variety of reaction conditions in CEL couplings and the strong dependence of reactivity on them is related to the use of simple copper salts as catalysts. Solvent and added base are required to solubilize and activate the copper salt, and base and counteranion play a role in the formation of dinuclear copper-boron complexes (Scheme 4-1, **A**), as a first step in the transmetallation.^{35, 51} Incorporating these features into the ligand of a coordination complex could provide catalysts with a more general reaction protocol and – hopefully – increased reactivities. Given that copper(II) tends to form square-planar or square-pyramidal complexes and that two coordination sites are required for interaction with the substrates, we targeted tridentate ligands. A sulfonate group was integrated in the ligand to enable a bridging coordination to boron and to facilitate transmetallation. We have previously reported sulfonatodiketimine complexes (Scheme 4-1, **B**), which showed indeed a more general reactivity towards amines and anilines, but proved to be unreactive even for slightly bulky substrates.²⁵ We then targeted sterically less crowded pyridylimino arylsulfonate complexes (Scheme 4-1, **C**), for which we reported a high reactivity towards amines, anilines, and *N*-heterocycles in a preliminary publication,⁵² and which showed some of the highest activities in CEL couplings, in particular

for challenging substrates. In the following, we investigate the mechanism of CEL couplings with complexes of type **C** and how to address remaining problems of reactivity.

4.2. Results and Discussion

4.2.1. Catalyst synthesis and structures

The chloride-coordinated complex **1** can be prepared in a simple one-pot procedure, following previous protocols where ligand and complex are assembled in the same reaction from commercial starting materials (Scheme 4-2).⁵³ From undried methanol, **1** crystallized as the water-coordinated, mononuclear complex (Scheme 4-2).⁵² Recrystallization of **1** in acetonitrile afforded the homoleptic complex **2** (Figure 4.1, Table 4-1).



Scheme 4-2

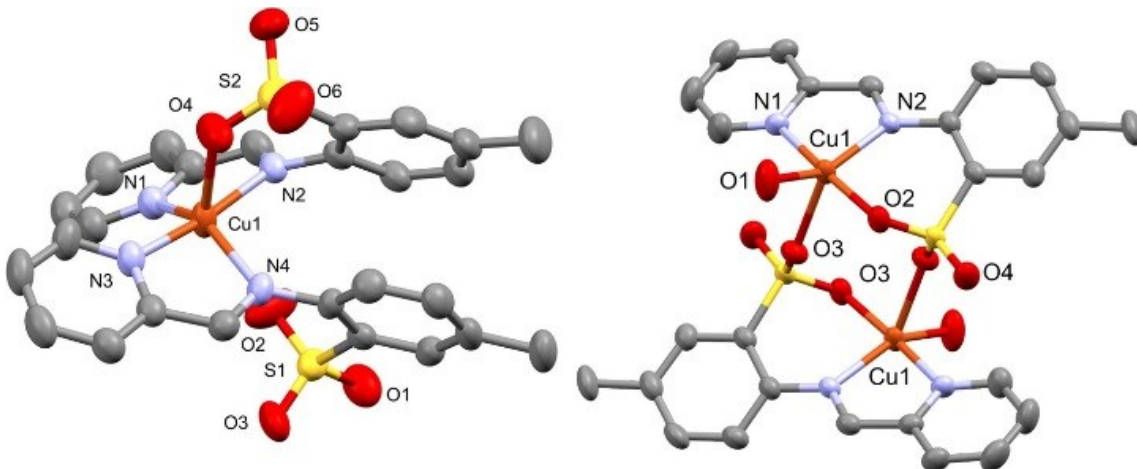


Figure 4.1: Crystal structures of **2** (left) and **4** (right). Thermal ellipsoids were drawn at the 50% probability level. Hydrogen atoms, cocrystallized water (**2**) and the anion (**4**) were omitted for clarity.

Table 4-1 : Geometrical data of complexes 1-4.

	1 ^a	3 ^a	2	4
Cu-N _{imine}	2.051(1)	2.026(1)	1.972(1), 1.986(1)	2.023(2)
Cu-N _{pyridine}	1.992(1)	1.967(1)	2.045(2), 2.073(1)	1.967(2)
Cu-O _{sulfonate}	1.969(1)	1.929(1)	2.200(1), 2.877(2)	1.934(1)
Cu-O _{bridging}		2.379(1)		2.235(1)
Cu-OH ₂	2.307(1)			1.993(1)
Cu-O _{triflate/Cl}	2.243(1)	2.015(1)		
τ	0.1		0.5	0.5

^a Taken from ref. 52

The triflate complex **3** is obtained by anion exchange with silver triflate (Scheme 4-2) and crystallizes as a coordination polymer with triflate and sulfonate interactions between neighboring molecules.⁵² **3** can also be prepared directly from the ligand precursors and Cu(OTf)₂, but required 2 equiv of the copper salt. Under these conditions a polymorph of **3**, **4**, was obtained, in which triflate dissociated from the coordination sphere and a dinuclear, dicationic complex is formed in the solid state (Figure 4.1, Table 4-1). **1** is soluble only in strongly polar solvents, such as water, DMSO or DMF and poorly soluble in methanol. The solubility of **3** is much higher and it is readily soluble in THF, CH₂Cl₂ or methanol.

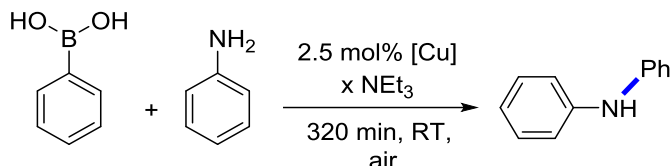
Despite τ -values⁵⁴ indicating a coordination geometry between square-pyramidal and trigonal-bipyramidal, coordination geometries around Cu are essentially square-pyramidal and contain one ligand in the apical position (water in **1**, sulfonate in **2** and **4**) with a 0.2-0.3 Å longer Cu-ligand distance. Complex **2** is essentially isostructural to its analogue lacking the *para*-methyl substituent.⁵⁵ Copper-ligand distances are otherwise in the range observed in complexes with very similar ligands (Cu-imino: 2.03(3) Å, Cu-pyridine: 2.00(2) Å, Cu-OSO₂: 1.98(6) Å based on 13 entries in the CSD).^{52, 53, 55-59}

4.2.2. Chan-Evans-Lam couplings: general reaction conditions

Typical for CEL couplings is the requirement for a careful optimization of reaction conditions. Variables are the solvent (the choice of which depends strongly on the substrate and reaction conditions), the requirement to eliminate water (presence of molecular sieves), the presence of a (Lewis) base (typically NEt₃, pyridine or other *N*-bases), potential additives/ligands and the counteranion (most often acetate or triflate). We investigated if these factors would indeed be less important for couplings with **1**. Arylation of aniline with phenylboronic acid was chosen as the standard reaction. Reactions were quenched after 5 h to provide an intermediate conversion which is sensitive to changes in conditions. Longer reaction times lead to full conversion (*vide infra*).

Solvent. Solvent dependence in CEL couplings is normally difficult to predict, since the solvent plays an activating role in solubilizing the copper catalyst and a deactivating role in saturating coordination sites required for substrate coordination. An empirical order of CH₂Cl₂ > 1,4-dioxane, THF, DMF > EtOAc, toluene > DMSO >> MeOH,¹⁴ or 1,4-dioxane, CH₂Cl₂ >> DMF > EtOAc > THF > toluene > DMSO⁹ has been claimed, but deviations from these are the rule. A more predictable dependence on solvent polarity was expected for **1**, since coordination complexes typically show less pronounced solvent interactions than simple copper salts. In fact, there is only a small dependence on the solvent in CEL couplings with **1** (Table 4-2, entries 1-5), with polar solvents working slightly better than less polar solvents. Only the use of acetonitrile was detrimental, most likely due to blocking of the copper coordination site. It is also possible that – as in recrystallizations in acetonitrile – **1** undergoes ligand exchange to the homoleptic complex **2**. The latter is not active in CEL couplings (Table 4-S1, entry 1).

Table 4-2 : Coupling of aniline and phenylboronic acid using 1 as a catalyst.^a



Entry	Solvent	Modification ^a	Yield
1	MeCN	-	0%
2	Toluene	-	36%
3	CH ₂ Cl ₂	-	41%
4	THF	-	67%
5	MeOH	-	86%
6	MeOH	Molecular sieves, 4A	62%
7	MeOH	+ 20 equiv water	90%
8	MeOH	2.5 mol% NEt ₃	12%
9	MeOH	1 equiv NEt ₃	0% (12 h)
10	MeOH	2.5 mol% NaOH	0%
11	MeOH	2.5 mol% Na ₂ CO ₃	52%
12	MeOH	1 equiv Na ₂ CO ₃	23%
13	MeOH	3 instead of 1	99%
14	MeOH	N ₂ atmosphere	0% (12 h) ^b
15	MeOH	N ₂ atmosphere, 100 mol% 1	45% (12 h)
16	MeOH	1 equiv PhB(OH) ₃	98% (12 h)

^a Conditions: room temperature, air, 320 min if not otherwise noted, 1.5 equiv. PhB(OH)₂, 1.0 M aniline, 2.5 mol% 1. Equivalents refer to concentrations relative to amine. ^b 1% conversion would have been expected from the stoichiometric reaction, but was likely not detected.

Water. The influence of water in CEL couplings is complex, contradictory and undefined. Early reports of Evans indicated that the presence of water can be detrimental due to the formation of phenol and diphenyl ether byproducts from the oxidative coupling of phenylboronic acid with water.⁵ Isotope

labeling studies by Lam confirmed that water and not oxygen is the source of phenol byproducts.⁶⁰ Water is believed to originate from condensation of boronic acids to boroxines and yields increased in the presence of molecular sieves or when boroxines instead of boronic acids were used.^{5, 22} Collman reported, however, that too high an excess of molecular sieves likewise reduces activities.⁴⁷ In other cases, the presence of water was tolerated²⁶ or even led – in the correct amounts – to improvements in reaction yields.²³⁻²⁵ Last but not least, several CEL couplings were reported in water as a solvent.^{30, 34, 40, 48-50} It is notable that in all cases where water was found to be beneficial or used as a solvent, coordination complexes or supported catalysts were employed rather than simple copper salts. In accordance with this, addition of molecular sieves slightly reduced yields in CEL couplings with **1**, while addition of 20 equiv of water (15 vol% of the solution) was well tolerated (Table 4-2, entries 6+7; Fig. 4.S1).

Base. The requirement and role of an organic or inorganic base in CEL couplings is likewise unclear. While addition of base often increases yields, other couplings proceed better under base-free conditions. The base was speculated to be involved in the formation and activation of boroxine species, in the activation of the nucleophile by deprotonation, and in the formation of copper hydroxide or alkoxide species, which allow bridging to boron or acting as a ligand for the copper catalyst. Addition of base to arylations with **1** strongly suppressed the observed yields (Table 4-2, entries 8-12)). Investigation of time-dependent conversion showed that this was indeed due to a reduction of the apparent rate constant to one half and not due to decomposition or delayed activation (Fig. 4.S2). In the case of NEt_3 , reduced activity might be related to deactivating coordination of the base to copper, but the strongly suppressed activity upon addition of NaOH or Na_2CO_3 indicates that for **1** replacement of chloride by hydroxide or methoxide is also detrimental.

Counteranion. The most commonly employed catalyst in CEL couplings is $\text{Cu}(\text{OAc})_2$, or more precisely $\text{Cu}_2(\text{OAc})_4 \cdot 2\text{H}_2\text{O}$.¹⁴ $\text{Cu}(\text{OTf})_2$ typically shows similar activities.^{61, 62} CuCl_2 , $\text{Cu}(\text{NO}_3)_2$, $\text{Cu}(\text{ClO}_4)_2$, or CuSO_4 are less active,^{14, 19, 32, 61-63} although Stahl showed that $\text{Cu}(\text{ClO}_4)_2$ can be activated by addition of one equiv of acetate.⁵¹ The anion dependence has been rationalized by formation of an acetate-bridged dinuclear copper-boron complex as an intermediate prior to transmetallation (**A**, Scheme 4-1).^{48, 51} Despite these general findings, high activities have been observed for copper salts other than acetate. For example, Collman's TMEDA/CuX catalyst showed identical activities for OTf^- and Cl^- ,⁴⁸ and coupling of hindered imidazoles worked best with $\text{Cu}(\text{NO}_3)_2$.³³ Based on the rate increase upon addition of

methoxide to Cu(OAc)₂-catalyzed reactions, Stahl proposed that a methoxide-bridged species is likewise a possible intermediate to transmetallation.⁵¹ Watson later found HRMS-evidence for the formation of acetate-bridged and hydroxide-bridged dinuclear species, of which the hydroxide-bridged complex was calculated to be of lower energy.³⁵ The influence of the anion might thus be negated if a hydroxide-containing species is formed in the catalytic cycle, as it is the case for Collman's tmeda/CuX system.^{47,48}

For CEL couplings with **1** or **3**, we proposed that coordination of phenylboronic acid to the sulfonate group precedes transmetallation (Scheme 4-1, **C**). We would thus expect that the nature of the anion, which is crucial if the anion acts as a bridging ligand, has only a minor impact on reactivity. CEL couplings with the triflate complex **3** showed, however, notably higher conversions than with the chloride complex **1** (99% vs. 86%, Table 4-2, entry 13). A closer investigation of the reaction kinetics showed that the reduced activity of **1** was due to delayed catalyst activation, while the actual reactivities were very similar with apparent first-order rate constants of $k_{app} = 0.40(2) \text{ h}^{-1}$ and $0.50(1) \text{ h}^{-1}$, respectively (Fig. 4.2).

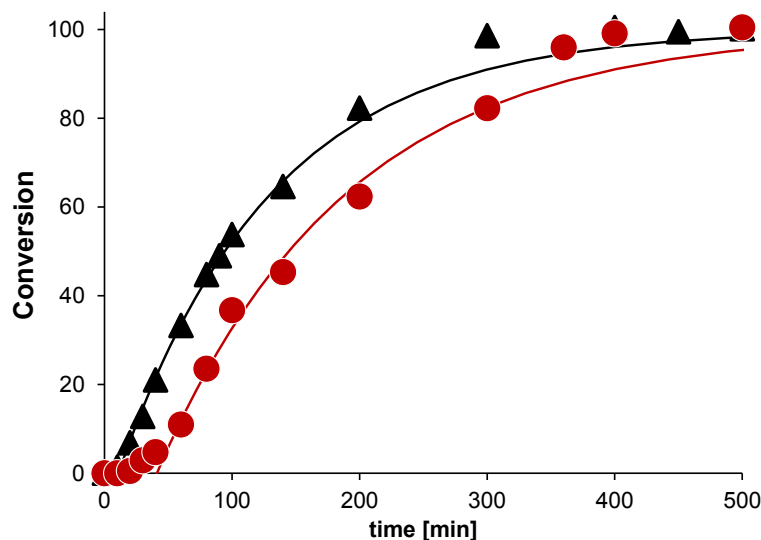


Figure 4.2 : Conversion-time profiles for the arylation of aniline with PhB(OH)₂ in methanol ([PhNH₂] = 1.0 M, [PhB(OH)₂] = 1.5 M, [Cu] = 25 mM, RT, air). Black triangles: **3**, average of 4 experiments, $k_{app} = 0.50(1) \text{ h}^{-1}$. Red circles: **1**, average of 4 experiments, $k_{app} = 0.40(2) \text{ h}^{-1}$. For the deviations at high conversion, see discussion of reaction kinetics.

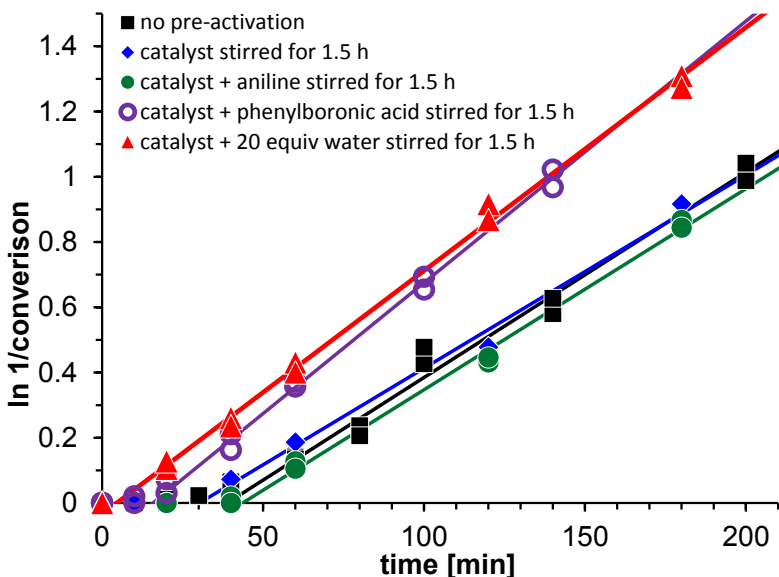


Figure 4.3 : Semi-logarithmic conversion-time profiles for the arylation of aniline with $\text{PhB}(\text{OH})_2$ catalyzed by **1** under various pre-activation conditions ($[\text{PhNH}_2] = 1.0 \text{ M}$, $[\text{PhB}(\text{OH})_2] = 1.5 \text{ M}$, $[\text{Cu}] = 25 \text{ mM}$, RT, air). The two datapoints per time indicate conversions calculated from appearance of diphenylamine and disappearance of aniline, respectively.

The significantly longer induction period observed for **1** (40 min) in comparison to triflate-coordinated **3** (10 min) was puzzling, since anion-exchange reactions in Cu(II), d^9 , complexes would be expected to be reasonably fast. Color changes during the reaction seem to point towards solubility problems as the main cause of the induction period: **3** is soluble in methanol to provide a green solution, while **1** is not, or only barely soluble. In CEL coupling reactions, the green color of **1** or **3** in solution is never observed, however: the reaction mixture turns orange after the induction period and this color persists throughout the reaction. CEL couplings with **1** were thus investigated under a variety of pre-activation conditions to clarify the origin of the induction period. Preactivation of the catalyst for 1.5 h with or without added aniline substrate before addition of phenylboronic acid did not notably influence the induction period. Preactivation with phenylboronic acid, on the other hand, reduced the induction period to one half. Finally, stirring in the presence of 20 equiv of water reduced it to <10 min, similar to that of the triflate complex **3**. It seems thus likely that water is required to solubilize the complex **1** in methanol. The analogous complex lacking the *para*-methyl group interconverts between a methanol-insoluble, dinuclear, chloride-bridged complex and a mononuclear, water-coordinated complex in the absence or presence of water.⁵⁹ In the absence of external water, the latter might be slowly taken up

from atmosphere or – in the presence of phenylboronic acid - formed during the reaction or by boroxine formation (although we did not observe boroxines when reactions were followed by NMR). To avoid complications by the long induction time of **1**, further reactivity studies were – if not otherwise mentioned – conducted with **3** as the catalyst.

Oxidant. CEL couplings are oxidative couplings and the presence of an oxidant is required in the reaction. In most cases, either air or an oxygen atmosphere is sufficient, although other oxidants have been used originally.⁶⁴⁻⁶⁶ For most CEL couplings, the accepted mechanism is the one proposed by Stahl, in which aryl copper(II) is oxidized by another copper(II) complex to aryl copper(III) prior to reductive elimination.^{51, 67} The oxidant is required solely to re-oxidize the copper(I) complexes formed. Tromp reported successful CEL couplings of imidazoles in the absence of oxidants and found evidence for the formation of boranes under anaerobic conditions.^{27, 68} To the best of our knowledge, this is the only report of successful catalytic CEL couplings in the absence of oxygen or external oxidant.

N-arylation of aniline with **1** under exclusion of oxygen did not lead to any observable formation of product. When the copper complex was added in stoichiometric amounts, 45% conversion to product was observed under exclusion of oxygen (Table 4-2, entries 14+15). CEL couplings with **1** thus require two equivalents of **1** to complete a catalytic cycle and oxygen for the regeneration of the catalyst, following the mechanism proposed by Stahl in this aspect.^{51, 67}

4.2.3. Substrate reactivity

Since CEL couplings with **3** tolerate water, can be conducted in various solvents, do not require addition of base or additional ligand and since the sulfonate group rather than the anion participates in the transmetalation step, optimization of reaction conditions was essentially limited to choosing the reaction time and temperature. Satisfyingly, **3** was active in the arylation of a variety of *N*-nucleophiles, including anilines, aliphatic amines and *N*-heterocycles. Reactions were conducted in undried methanol at room temperature or at 50 °C. In heated reactions, solvent vapor seemed to impede oxygen uptake from the atmosphere when condensers were used. Simple stirring of heated reactions open to air led to higher apparent conversions, but calibrated GC/MS-analysis showed in some cases a mass imbalance between the product formed at full conversion and the starting amine, most likely due to evaporation of the latter. Reactions at 50 °C were thus stirred in closed vessels under a supply of oxygen to ensure reproducible reaction conditions. Chart 4-1 reports the result of the reactivity study with various *N*-

nucleophiles. To best characterize substrate reactivity, conversions were obtained from calibrated GC/MS-analysis of the quenched reaction mixtures. We have shown in a preliminary communication that pure compounds can be isolated after column chromatography in yields of >85%.⁵²

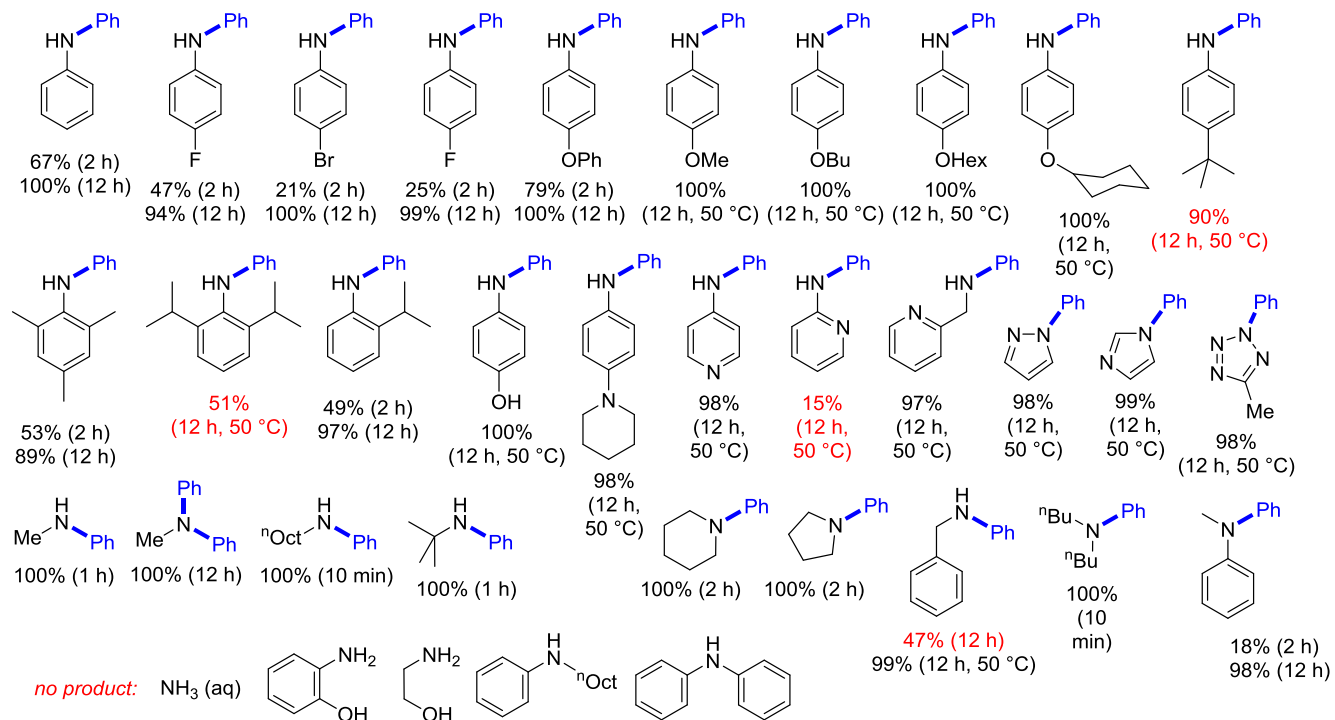
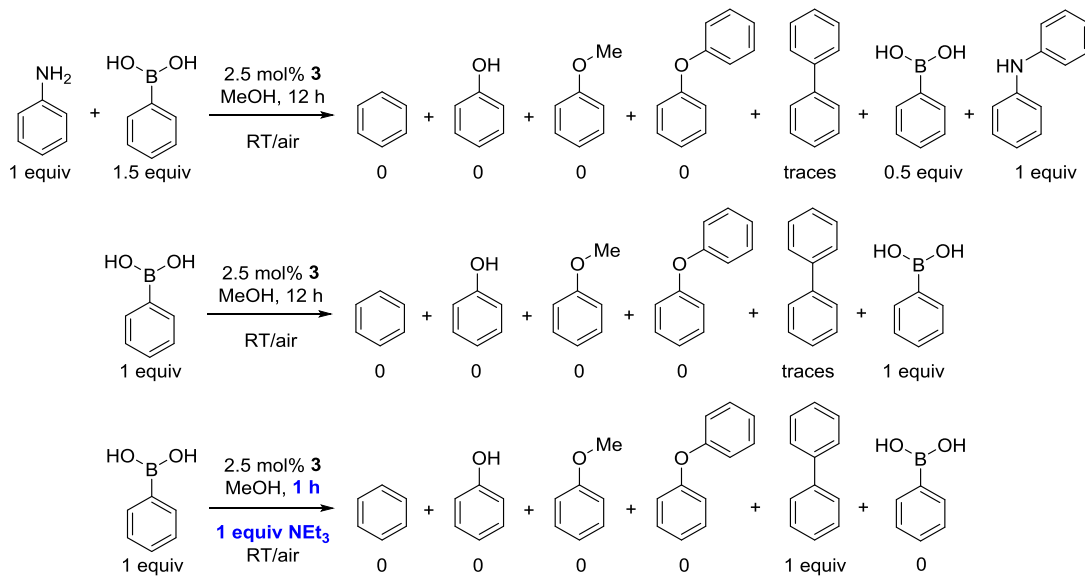


Chart 4-1

Notably, arylation proceeded well even for substrates typically reported to be difficult to arylate, such as amino-pyridines, picolylamine and *tert*-butyl amine. Coupling of acyclic secondary amines, which are considered one of the biggest challenges in C–N bond formations via CEL coupling, proceeded not only well, but with very high activity. Water was tolerated well enough that methylamine could be added as an aqueous solution. Reduced reactivity was observed for some substrates, mainly due to secondary reactions which will be discussed in the next sections.

Substrate-independent side reactions. Typical side reactions in CEL couplings are deboration to yield benzene and oxidation or coupling with water to yield phenols or diphenyl ethers if the former undergo CEL coupling. Homocoupling of two arylboronic acids to provide the respective diaryl is another common side reaction. These parasitic reactions can be competitive with the coupling reaction and are the main reason why CEL couplings typically require excess arylboronic acid or do not reach completion. Neither of these products nor coupling to the methanol solvent have been observed in CEL couplings

with **3**. Reactions in MeOD followed by NMR showed the excess amount of phenylboronic acid still present after 12 h of reaction. Neither NMR, nor GC/MS analysis provided any indication for the presence of other byproducts, although traces (<5%) of the diaryl were observed in some reactions (Scheme 4-3). Even in the absence of amine nucleophile, but under otherwise identical conditions (1.5 M PhB(OH)₂, 2.5 mol% **3**, methanol, RT/air), the only product formed was biphenyl and even this in less than 5% (Scheme 4-3). In the presence of triethylamine, complete conversion of phenylboronic acid to biphenyl occurred in 1 h (Scheme 4-3), still without evidence of any other byproducts. Targeted homocoupling of arylboronic acids with copper catalysts has been reported previously with and without external base,^{30, 69-76} the highest activity being full conversion in 15 min at room temperature.⁷⁶ Due to the complete absence of side reactions, CEL coupling with **3** is thus possible without using excess of phenylboronic acid. In the presence of a stoichiometric amount of PhB(OH)₂, 98% conversion of aniline to diphenylamine was observed after 12 h at RT (Table 4-2, entry 16). For the following mechanistic investigations, an excess of 1.5 equiv of boronic acid were continued to be used, however, to exclude any influence of side reactions on amine conversions and to ensure the reproducibility of these results.



Scheme 4-3

Substrate poisoning. Typically, more electron-rich anilines react faster in CEL couplings.^{17, 50, 63, 77} It was thus surprising that with **3** electron-poor anilines reacted with very comparable rate constants to aniline, while electron-rich anilines did not react at room temperature, but required heating (Table 4-3). We had previously observed catalyst poisoning by the substrate in CEL couplings with related sulfonate-

diketimine complexes (Scheme 4-1, **B**),²⁵ and this provides a likely explanation for the observed reactivities. Competition experiments between aniline and bromoaniline with a limiting amount of phenylboronic acid confirmed the expected higher reactivity of the more electron-rich aniline (Table 4-3). In the presence of methoxyaniline, on the other hand, arylation of *both* substrates was suppressed, indicating that electron-rich anilines, such as methoxyaniline, deactivate the catalyst by formation of an inactive aniline-copper complex.

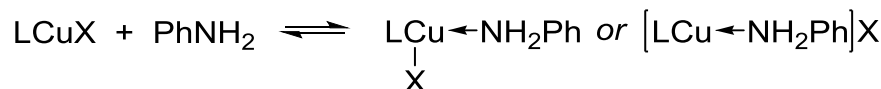
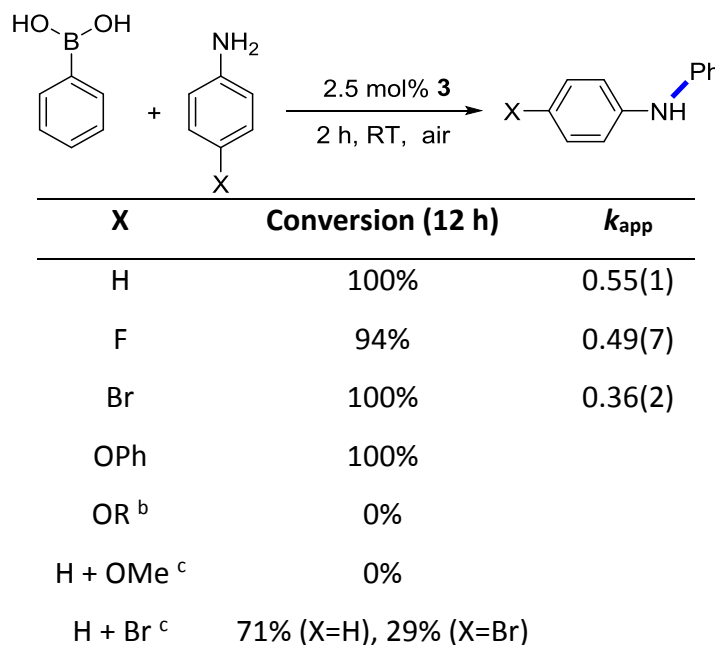


Table 4-3 : Coupling of para-substituted anilines and phenylboronic acid with **3**.^a



a Conditions: room temperature, air, 320 min if not otherwise noted, 1.5 equiv PhB(OH)_2 , 1.0 M aniline, 2.5 mol% **3**. Equivalents refer to concentrations relative to amine. b R = Me, nBu, nHex, cyclohexyl. c 1.0 M aniline, 1.0 M p-X-aniline, 1.0 equiv PhB(OH)_2 , 2.5 mol% **3**.

Formation of an aniline adduct **3**· NH_2Ph was confirmed by UV/vis spectroscopy. Upon addition of aniline to a green methanol solution of **3**, a color change to orange is observed. An isosbestic point persists up to an aniline concentration of 25 mM, indicating a simple aniline coordination to yield the putative **3**(NH_2Ph) complex. Upon further addition of aniline up to reaction concentrations of 1.0 M, new peaks appear which were assigned to a higher **3**(NH_2Ph)_n complex. Simultaneous regression of the spectral changes at 347, 450, 540, 625, and 750 nm showed best agreement with the reaction of two additional aniline to form **3**(NH_2Ph)₃ with equilibrium constants of $K_1 \approx 50 \text{ M}^{-1}$ and $K_2 \approx 10 \text{ M}^{-2}$ (Fig. 4.4).

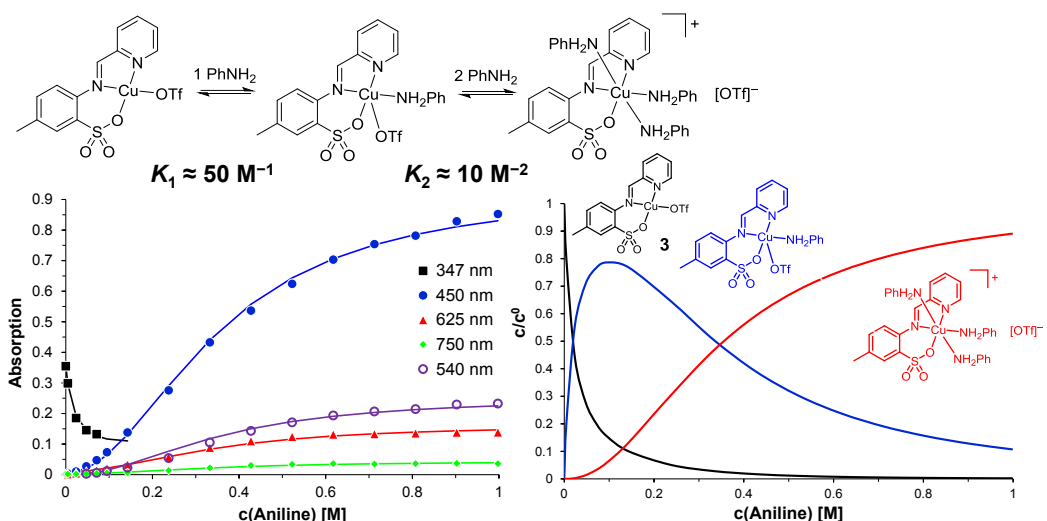
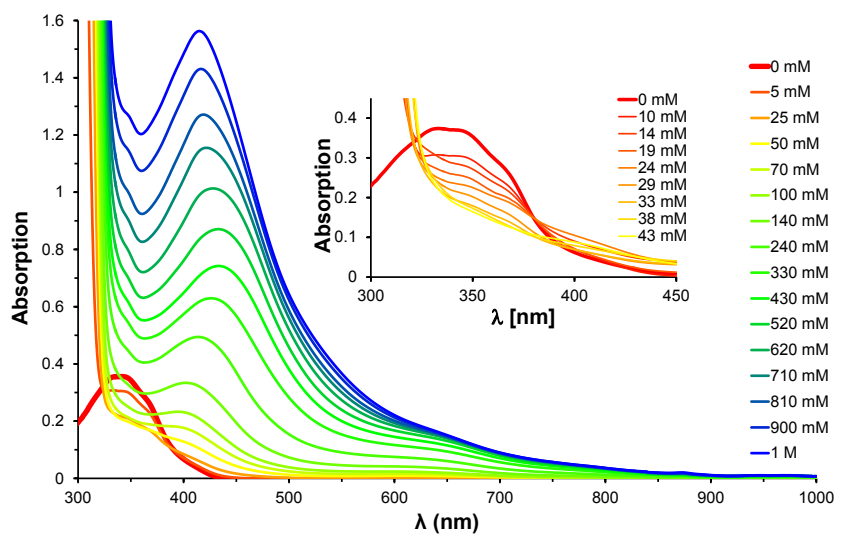


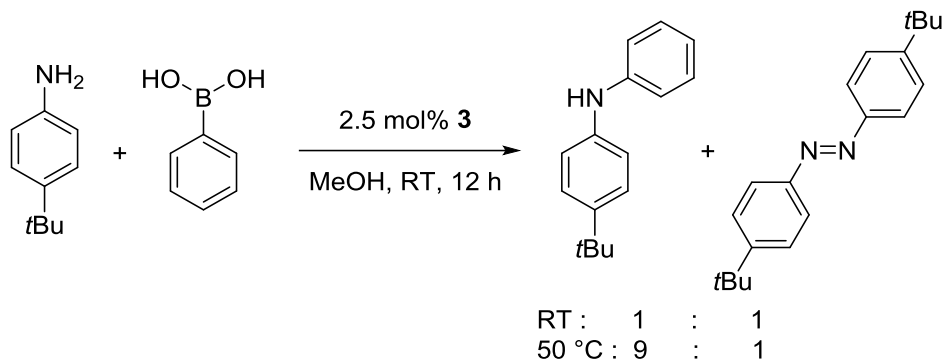
Figure 4.4 : Left: UV/vis titration of **3** (58 μ M) in MeOH with aniline. The inset shows the isosbestic point obtained until 25 mM aniline. Middle: Absorption at different wavelengths vs aniline concentration. The lines indicate the results of the simultaneous non-linear regression presuming reaction with 2 aniline in the second equilibrium. Right: Concentration of **3** and its aniline adducts at different aniline concentrations, calculated from $K_1 = 50 \text{ M}^{-1}$ and $K_2 = 10 \text{ M}^{-2}$.

tert-Butyl aniline. A different reason was responsible for the reduced conversion with *tert*-butyl aniline. Reaction at room temperature led to complete conversion of *tert*-butyl aniline after 12 h, but the obtained product was a 1:1 mixture of the coupling product and 4,4'-di-*tert*-butylazobenzene (Scheme 4-4). The oxidative coupling of anilines by copper to azobenzenes is known since the '50s,^{10,78} but has, to the best of our knowledge, not been reported to interfere with CEL couplings. The mechanism of azobenzene formation most likely proceeds via an aniline radical, generated by oxidation of aniline either directly by Cu(II) or by a peroxocopper complex formed upon reaction of Cu(I) with oxygen.⁷⁹ Reactions under different conditions showed that oxygen as well as PhB(OH)₂ were required for azobenzene formation (Table 4-4) and a Cu(I)/O₂ reaction product is thus most likely responsible for generating the aniline radical. Consequently, azobenzene formation was strongly reduced to 8% if couplings were performed in the presence of tetramethylpiperidine to trap oxygen radicals (Table 4-4). However, the presence of a nitrogen base also suppressed CEL coupling and conversion to product was limited to 25%. At 50 °C formation of azobenzene could be mostly suppressed, even without tetramethylpiperidine, in favor of the CEL coupling product (Scheme 4-4).

Table 4-4 : Oxidation of *tert*-butyl aniline catalyzed by **3**.^a

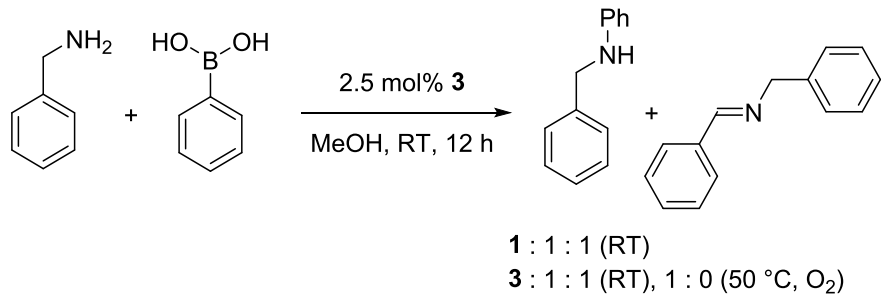
Temperature	PhB(OH) ₂	Conditions	Yield of azobenzene ^b
RT	1.5 equiv	Air	66%
RT	1.5 equiv	N ₂	0%
RT	0 equiv	O ₂	0%
50 °C	0 equiv.	O ₂	0%
50 °C	1.5 equiv	O ₂	10%
RT	1.5 equiv	Air ^c	8% ^c

^a Conditions: MeOH, [tBuC₆H₄NH₂] = 1.0 M, 12 h, 2.5 mol% **3**. ^b Based on percentage of aniline which reacted to azobenzene. Molar ratios of coupling product to azobenzene were 1:1 at RT and 20:1 at 50 °C. ^c In the presence of 0.5 equiv tetramethylpiperidine.



Scheme 4-4

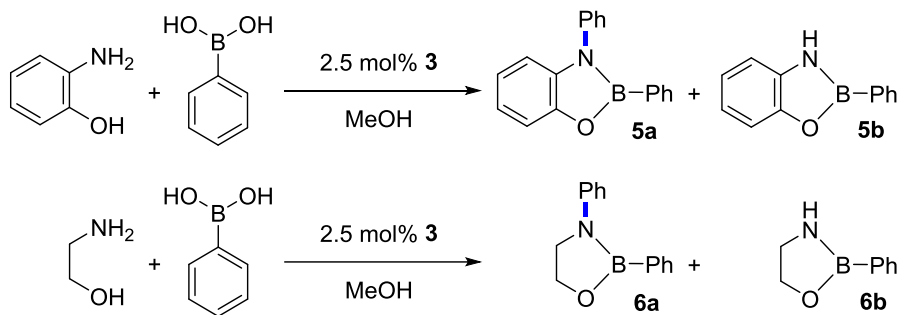
Benzylamine. Arylations of benzylamine likewise suffered from oxidative side reactions, in this case the formation of *N*-benzylidene benzylamine in an equimolar amount with the desired coupling product (Scheme 4-5). The side product is most likely the consequence of amine oxidation to the imine, followed by hydrolysis and condensation with benzylamine. The rate-determining step in aerobic copper-catalyzed amine oxidations is considered to be the abstraction of an α -H atom to form an amine radical.¹⁰ The latter might explain why this side reaction was only observed for benzyl amine. Amine oxidation was avoided at 50 °C and only coupling product was observed.



Scheme 4-5

Ammonia. While an aqueous solution of methylamine reacted fast, aqueous solutions of ammonia were unreactive. From the unusual blue color of the reaction mixture and the fact that no diphenyl was produced, catalyst decomposition/deactivation is most likely responsible for this lack of reactivity.

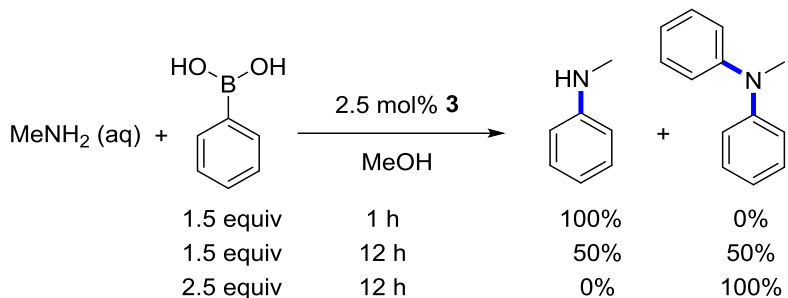
Aminophenols and aminopyridines. CEL coupling of amines capable of chelating coordination was reported to be difficult.²¹ Using **3**, 4-pyridyl amine, 4-hydroxyaniline and 2-picolyamine were coupled readily at 50 °C, although picolyamine was the only alkyl amine substrate which required heating. 2-Pyridylamine reacted sluggishly and the reaction did not reach completion. 2-Hydroxyaniline and ethanolamine could no be coupled. In both of the latter cases, analysis of the reaction mixture showed the presence of arylated (**5a**, **6a**) and non-arylated boronic esters (**5b**, **6b**, Scheme 4-6). In the presence of 3 equiv of PhB(OH)₃, reactions with ethanolamine provided only the arylated boronic ester **6a** as the single observed product. Ester formation thus leads to deactivation of phenylboronic acid, rather than of the amine. Reactions with 2-hydroxyaniline, however, did not proceed to full arylation even under excess of phenylboronic acid.



Scheme 4-6

Double arylation. Since **1** and **3** were active in CEL couplings of amines and anilines under the same reaction conditions, the question of chemoselectivity arises, i. e. if the reaction is complicated by double arylation. In fact, methylamine can be doubly arylated at prolonged reaction times and with 2.5 equiv PhB(OH)₂ present (Scheme 4-7). The same product was obtained by arylation of *N*-methylaniline (Chart IV-1). In the presence of 1.5 equiv PhB(OH)₂, selective and quantitative monoarylation was observed after one hour. If the reaction is continued over night, a 1:1 mixture of PhN(H)Me and Ph₂NMe was obtained. (Scheme 4-7). No double arylation was observed in any other reaction. Diphenylamine or *N*-octylaniline, when reacted independently, could not be further arylated (Chart 4-1). Reactions of aniline or octylamine with 2.5 equiv of PhB(OH)₂ consequently yielded selective conversion to the monoarylation products, even at 50 °C and upon addition of water to reproduce the reaction

conditions with methylamine, where an aqueous solution of the amine was used (Table 4-S1, entries 2-9). CEL couplings with **3** are thus highly selective for monoarylation.



Scheme 4-7

4.2.4. Mechanism of CEL couplings with **1** and **3**

The kinetics of CEL couplings with **3** were investigated for the *N*-arylation of aniline. Calibration of the GC-MS detector response and the use of internal standard allowed the determination of absolute quantities of unreacted aniline and the diphenylamine product. Both methods provided essentially identical conversion values, indicating that no aniline was lost in secondary reactions or due to evaporation (Fig. 4.5). After a short induction period of appr. 10 min, the reaction followed pseudo-first order kinetics. Conversions above appr. 80% were consistently higher than expected on the basis of a pseudo-first-order rate law (Fig. 4.5, solid line). Kinetics with **1** showed the same behavior (Fig. 4.S3). A possible explanation for this deviation is formation of an inactive, aniline-coordinated complex as discussed above. In the concentration profiles calculated from the equilibrium constants determined in UV/vis-titrations of **3** with aniline, the concentration of the active LCuX species sharply increases at aniline concentrations below 0.2 M (Fig. 4.4), in good agreement with the observed increase in activity above 80% conversion (Fig. 4.5). If catalyst poisoning by substrate is taken into account, agreement with the observed conversions improved notably (Fig. 4.5, dashed line). It should be noted that the value for $K_1 = 1 \text{ M}^{-1}$ obtained in non-linear regression of the kinetic data was one order of magnitude lower than the value determined via UV/vis spectroscopy. If the coordination of two further aniline to yield $[\text{LCu}(\text{NH}_2\text{Ph})_3]\text{X}$ (K_2) is included in the fitting of the kinetic data, the value for K_2 refined to nearly zero. Inclusion of inhibition by substrate thus agrees with the kinetic

data, but quantitative values differ significantly from those determined independently. This is not surprising, given that we neglected the presence of any other Lewis acids and bases in the reaction mixture.

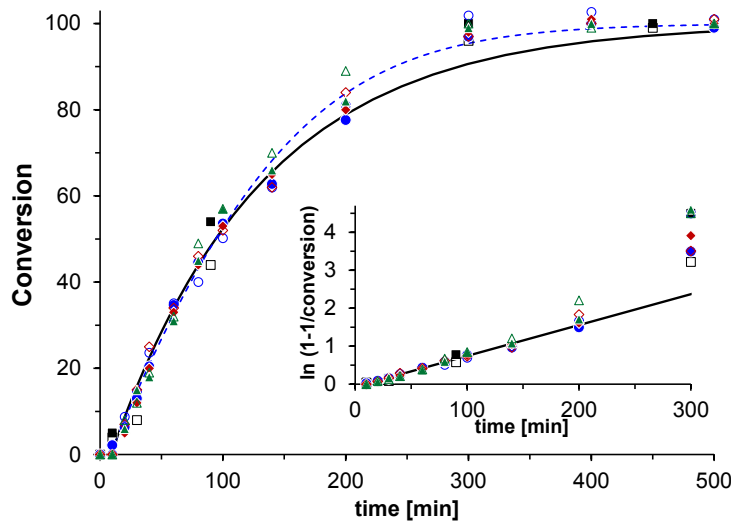


Figure 4.5 : Conversion vs time profile for the *N*-arylation of aniline. Four independent reactions under identical conditions are shown (MeOH, RT, 1.0 M aniline, 1.5 equiv PhB(OH)₂, 2.5 mol% **3**). Filled symbols: conversion determined from remaining aniline. Hollow symbols: conversion determined from diphenyl amine product. The solid, black line is calculated from the pseudo-first-order rate constant $k_{\text{app}} = 0.50(1) \text{ h}^{-1}$, determined from all datapoints in the range of 30-140 min. The blue, dashed line is the best-fit conversion trace with a pseudo-first-order rate constant $k_{\text{app}} = 0.82 \text{ h}^{-1}$ and an equilibrium constant of $K_1 = 1 \text{ M}^{-1}$ for the coordination of aniline to **3**. The inset shows the linearized $\ln(c^0/c)$ plot.

The pseudo-first-order rate constant was essentially independent from phenylboronic acid concentration. Tripling the phenylboronic acid concentration from 1.0 to 3.0 equiv led only to a small increase in the pseudo-first-order rate constant of appr. 40% (Fig. 4.6, Table 4-5). Stahl had observed for the arylation of methanol that the reaction displayed saturation kinetics in boronic acid concentration.⁵¹ The small increase of k_{app} indicates a similar situation here, i. e. that transmetallation is not the rate-determining step.

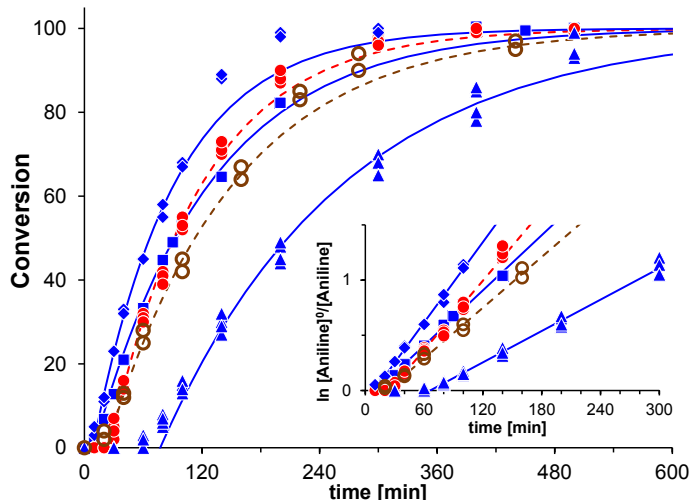


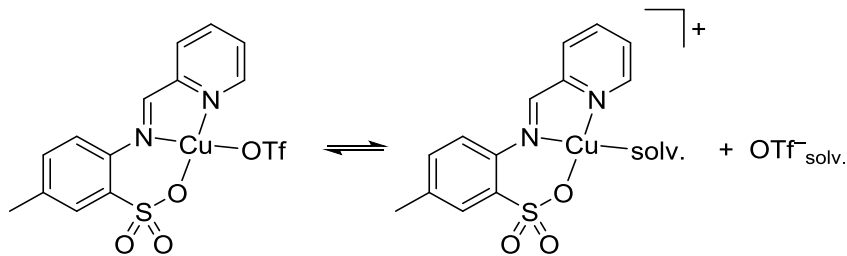
Figure 4.6 : Conversion vs time profile for the *N*-arylation of aniline under different reactant concentrations (MeOH, RT, 1.0 M aniline). Squares, 1.5 M PhB(OH)₂, 2.5 mol% **3**, average of 4 experiments; red circles, 3.0 M PhB(OH)₂, 2.5 mol% **3**, 2 experiments; brown, hollow circles: 1.0 M PhB(OH)₂, 2.5 mol% **3**; diamonds, 1.5 M PhB(OH)₂, 5.0 mol% **3**; triangles, 1.5 M PhB(OH)₂, 1.0 mol% **3**, 2 experiments. The inset shows the linearized $\ln (c^0/c)$ plot.

Table 4-5 : Apparent First-Order Rate Constants for the *N*-Arylation of Aniline with **3**.^a

Catalyst	[Catalyst]	[PhB(OH) ₂]	k_{app}
3	0.025 M	1.0 M	0.46(2) h ⁻¹
3	0.025 M	1.5 M	0.50(2) h ⁻¹ ^b
3	0.025 M	3.0 M	0.65(1) h ⁻¹ ^c
3	0.010 M	1.5 M	0.28(1) h ⁻¹ ^c
3	0.050 M	1.5 M	0.73(2) h ⁻¹
1	0.025 M	1.5 M	0.40(2) h ⁻¹
1/[NEt ₄]Cl	0.025 M	1.5 M	0.15(1) h ⁻¹

^a Conditions: 1.0 M Aniline, 1.5 M PhB(OH)₂, 2.5 mol% catalyst, MeOH, RT, air. ^b Rate constant determined from datapoints of product appearance and aniline disappearance in 4 independent experiments. ^c Rate constant determined from datapoints of 2 independent experiments.

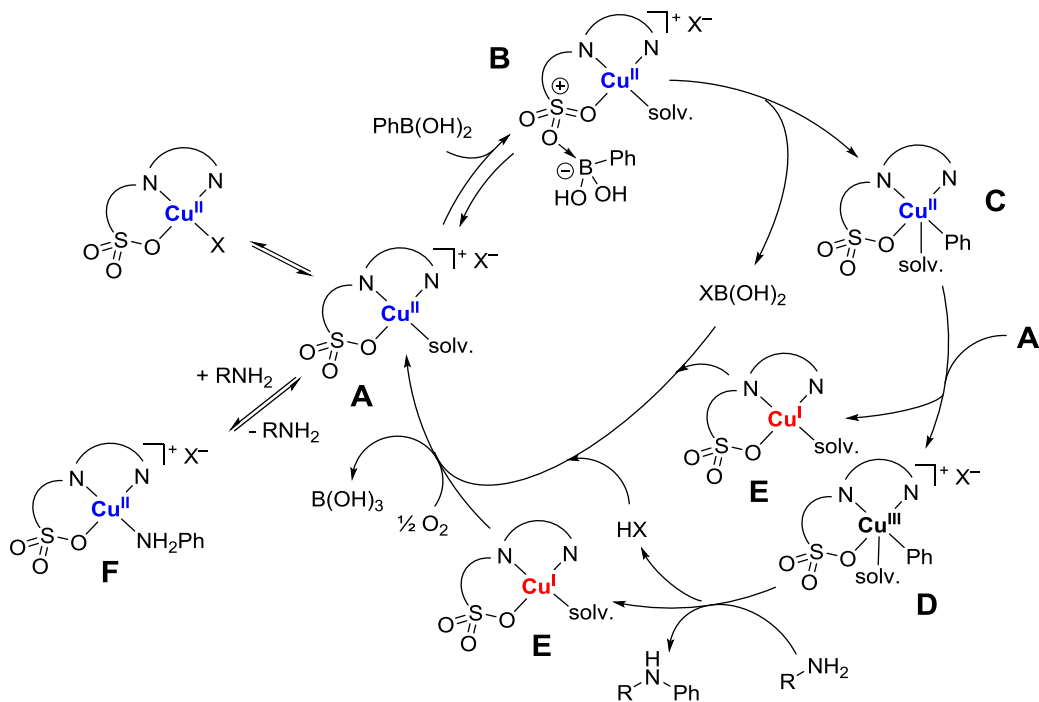
Arylation of aniline at 1.0 or 5.0 mol% of catalyst loading followed similar kinetics (Fig. 4.6, Table 4-5). The apparent rate constants and the initial rates of the reaction indicate a half-order dependence on catalyst concentration (Fig. 4.S4). A half-order dependence is typically associated with association/dissociation equilibria and **3** shows indeed bridging sulfonate coordination in the solid state. However, in the presence of water **1** forms solvated, mononuclear complexes in the solid state and both complexes show very similar UV/vis spectra (Fig. 4.S5 and 4.S6).⁵² It is thus unlikely that **3** would be present as a sulfonate-bridged dimer in undried methanol solution. An alternative explanation for a half-order dependence on catalyst concentration would be formation of an active, cationic species by dissociation of the anion (Scheme 4-8). In the presence of such an equilibrium, the concentration of the active, cationic species would be dependent on anion concentration. Indeed, addition of an equimolar amount of [NEt₄]Cl to CEL couplings with **1** reduced the apparent rate constant to half its value (Table 4-5, Fig. 4.S7). A similar anion dissociation equilibrium has been proposed by Stahl for the arylation of methanol with Cu(OAc)₂, where half-order dependence on catalyst concentration and deactivation by additional anion has likewise been observed.⁵¹



Scheme 4-8

CEL couplings with copper iminosulfonates thus follow the mechanism proposed by Stahl (Scheme 4-9).⁵¹ Formation of the active catalyst requires displacement of the anion, most likely by solvent. Transmetallation occurs from a dinuclear Cu-B-complex **B** to form the copper-aryl complex **C**. Oxidation by another complex **A** to the Cu(III) complex **D** is followed (or preceded) by coordination of the amine substrate, which then leads to product formation by reductive elimination. The catalytic cycle is closed by re-oxidation of the Cu(I) complexes **E** by oxygen. Modifications consist in our proposal that the sulfonate group and not hydroxide or the anion is bridging to boron in **B** (in agreement with the observations above) and the existence of the off-

cycle, aniline-coordinated complex **F**, which was indicated by UV-vis and kinetic data. Substrate inhibition, i. e. **F** being off-cycle, also supports that transmetallation precedes interaction with the nucleophile in the catalytic cycle. If transmetallation would occur after aniline coordination, there is no reason why complex **F** should be unfavorable. (The alternative scenario, that aniline coordinates before transmetallation and that the off-cycle intermediate **F** contains more than one aniline cannot be excluded, but agrees less well with the kinetic data.)



Scheme 4-9

The proposed mechanism is, however, inconsistent with the observed rate-law. The (near-) independence of the reaction rate from phenylboronic acid concentration and its first-order dependence on aniline concentration indicate that the catalyst resting state is located after transmetallation, but before reaction with the aniline. Neither **C** nor **D** are stable species, however. With the exception of Warren's isolation of a Cu(II)-perfluoroaryl complex⁸⁰ and Tilley's mixed-valence μ -aryl complex,⁸¹ the few isolated organocopper(II) aryl complexes stabilize the aryl group as part of a rigid macrocyclic ligand.⁸²⁻⁸⁹ Accumulation of the catalyst in the Cu(II) aryl species **C** would lead to extensive aryl homocoupling. The unstabilized Cu(III) aryl species **D**, on the other hand, will undergo rapid reductive elimination.⁹⁰ In the absence of amine this would

lead to arylation and thus destruction of the catalyst or to arylation of solvent, both of which is not observed. **D** is thus likewise an improbable catalyst resting state.

Alternatively, saturation of a pre-equilibrium would lead to zero-order-dependence on phenylboronic acid concentration. In this case, the catalyst resting state would be the dinuclear copper-boron complex **B** and transmetallation can remain the rate-determining transition state. Dinuclear copper-boron complexes have been proposed as intermediates in couplings with $\text{Cu}(\text{OAc})_2$ by Collman and Stahl.^{48, 51} Stahl found EPR-evidence for the formation of an adduct between phenylboronic acid and copper acetate, which he proposed as the catalyst resting state. Watson later found mass-spectroscopic evidence for the presence of bridged species in the catalytic cycle.³⁵ However, UV-vis titrations of solutions containing **3** with phenylboronic acid up to a concentration of 1.1 M, did not show notable changes of the absorption spectrum (Fig. 4.7). While this does not disprove the formation of a dincular **3**-boronic acid adduct (Scheme 4-9, **B**) in small equilibrium amounts, there is no indication that the latter can be the major catalyst species present in the reaction mixture.

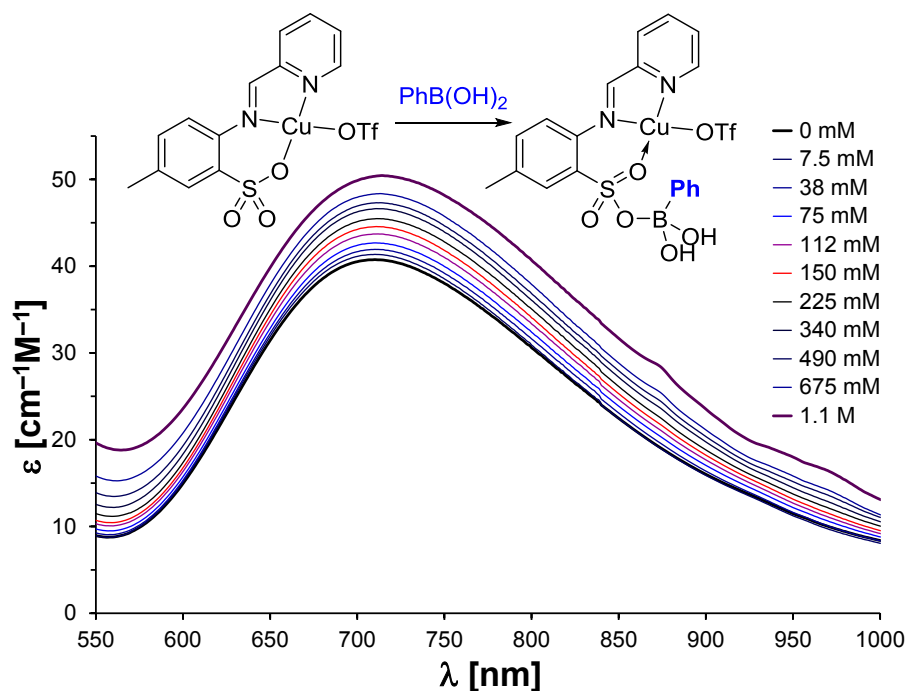
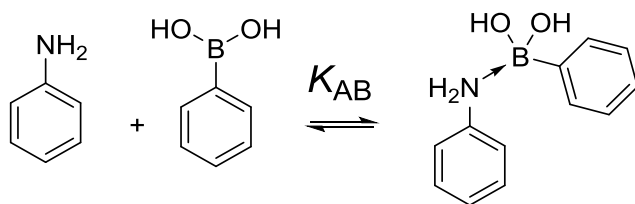


Figure 4.7 : UV/vis spectra of **3** in methanol upon addition of phenylboronic acid. The slight apparent increase in ϵ is due to uncorrected trailing absorption of the phenylboronic acid added.

In the absence of a plausible mechanism which would accommodate a fast transmetallation step, we considered possibilities which would provide an apparent zero-order dependence on the phenylboronic acid concentration despite slow transmetallation. Dependence on aniline concentration can be first-order, even if interaction with the aniline takes place after transmetallation as long as the latter is reversible. This is not unlikely, if transmetallation occurs in a dinuclear intermediate such as **B**. Should transmetallation remain the highest activation barrier, the rate law is expected to be:

$$v = k[\text{PhB(OH)}_2][\text{PhNH}_2][\text{LCuX}]^{0.5} \quad (\text{equation 1})$$

To explain the apparent independence of the rate law from phenylboronic acid concentration, we propose that aniline is involved in a Lewis acid-Lewis base adduct equilibrium with phenylboronic acid, similar to aniline coordination to **3**.



Incorporation of this equilibrium in rate law (1), provides,

$$v = \frac{k[\text{PhNH}_2]^t[\text{PhB(OH)}_2][\text{LCuX}]^{0.5}}{1 + [\text{PhB(OH)}_2]K_{AB}} \quad (\text{equation 2})$$

where $[\text{PhNH}_2]^t$ is the total concentration of unreacted aniline (see supp. information). For $[\text{PhB(OH)}_2]K_{AB} \gg 1$, the rate law becomes independent from $[\text{PhB(OH)}_2]$.

The existence of aniline-phenylboronic acid adducts was investigated by NMR spectroscopy in MeOD. An equimolar solution of phenylboronic acid and aniline showed signals displaced from the positions of the pure compounds, indicative of interaction of the two species in solution. A reliable determination of the equilibrium constant was not possible, however, since saturation of the equilibrium was barely occurring even at a 12 M concentration of one compound. At these high concentrations it is not possible to distinguish between the effect of the coordination

equilibrium or changes due to the solvent composition. Nevertheless, from the concentration-dependent shifts between 1 M and 12 M concentration, a value of $K_{AB} \approx 1 \text{ M}^{-1}$ was estimated (Fig. 4.8).

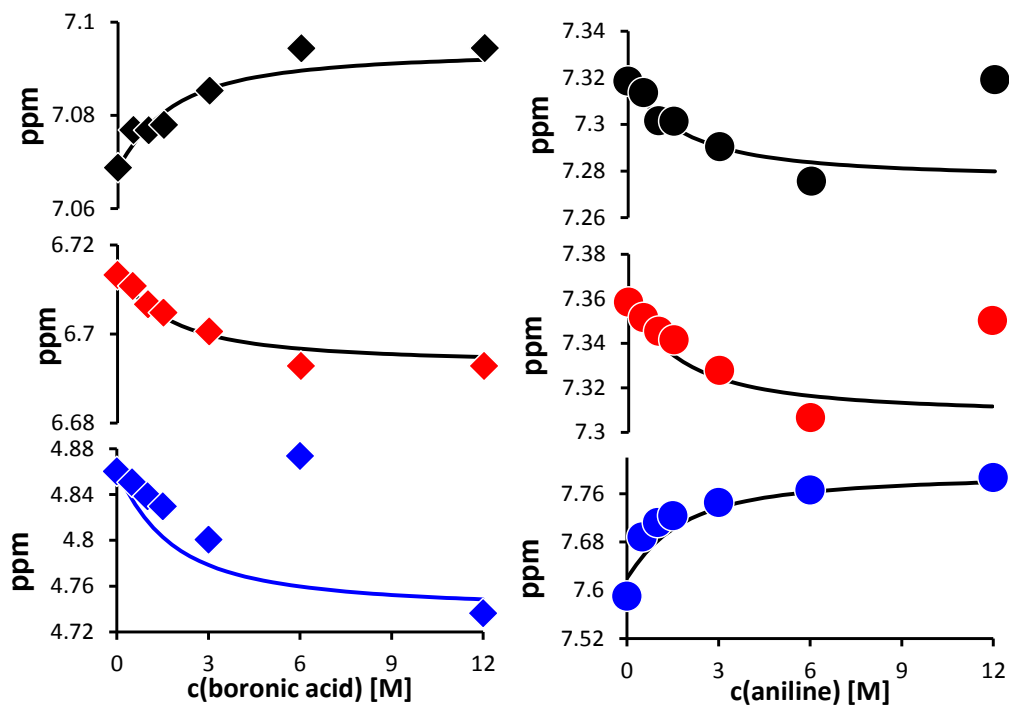


Figure 4.8 : Displacement of chemical shifts in the NMR spectra of aniline upon addition of phenylboronic acid (left) or of phenylboronic acid upon addition of aniline (right). The solid line represents the theoretical displacement assuming an equilibrium constant of $K_{AB} \approx 1 \text{ M}^{-1}$.

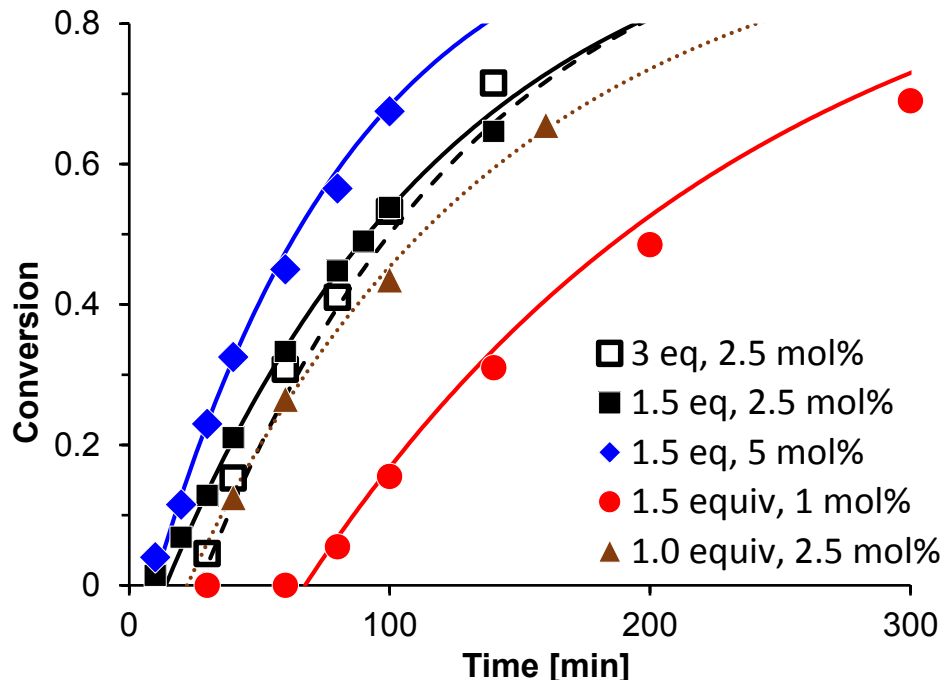


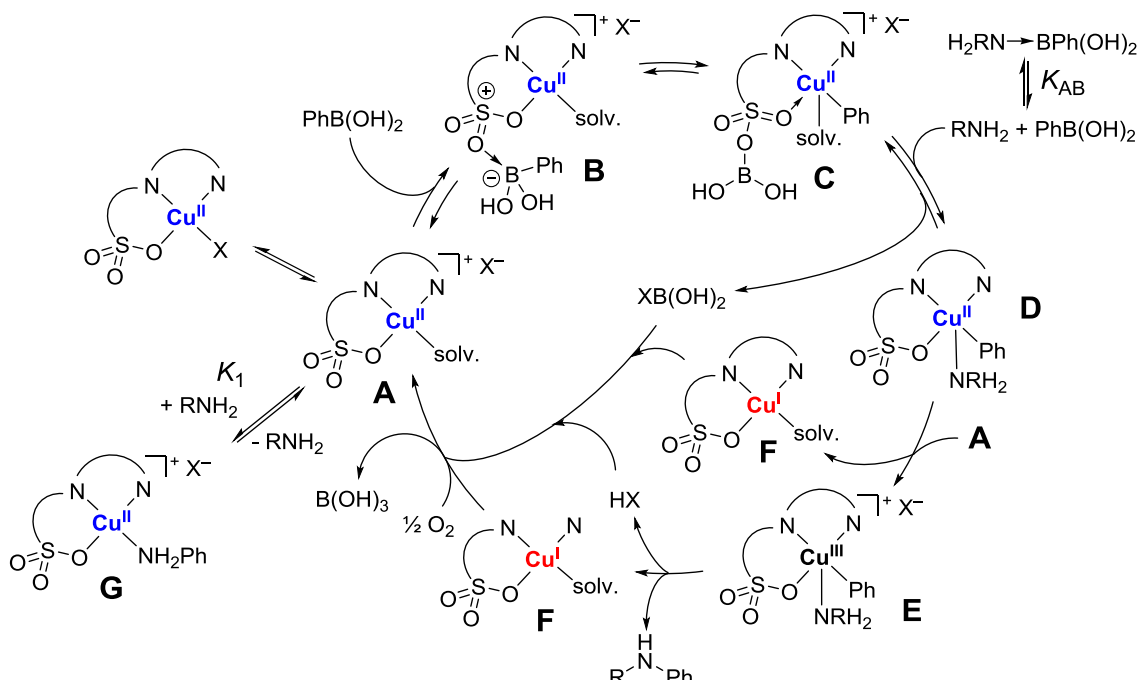
Figure 4.9 : Conversion vs time profiles for the *N*-arylation of aniline under different reactant concentrations (MeOH, RT, 1.0 M aniline). Solid lines are the simulated conversions based on $\nu = k[\text{PhB}(\text{OH})_2][\text{PhNH}_2][\text{LCuX}]^{0.5}$ under consideration of aniline coordination to phenylboronic acid. K_{AB} and k refined to best-fit values of $k = 0.4 \text{ M}^{-1.5}\text{min}^{-1}$ and $K_{\text{AB}} = 5 \text{ M}^{-1}$ (see supp. information).

The observed reaction kinetics are well reproduced using rate law (1) and equilibrium K_{AB} (Fig. 4.9). Due to the overparametrization of the problem, aniline-coordination to **3** (equilibria K_1 and K_2) were ignored and only datapoints below 80% conversion were employed in the kinetic fit (c.f. Fig. 4.5). Free refinement of both parameters provided $k = 0.4 \text{ M}^{-1.5}\text{min}^{-1}$ and $K_{\text{AB}} = 5 \text{ M}^{-1}$, in reasonable agreement with the value of $K_{\text{AB}} = 1 \text{ M}^{-1}$ estimated from NMR investigations of the equilibrium (c. f. Fig. 4.8). Since the apparent rate law is nearly independent from phenylboronic acid concentration, K_{AB} and k are strongly correlated and nearly identical fits can be obtained in the range of $K_{\text{AB}} = 1 - 10 \text{ M}^{-1}$ (supp. information). Since the kinetic model also ignores the formation of $\text{B}(\text{OH})_3$ and Ph_2NH (or assumes that their formation cancels each other out), values obtained from the kinetic fit should only be considered *apparent* equilibrium or kinetic values of a strongly simplified model. More important than quantitative values, the good agreement with the kinetic data in Fig. 4.9 shows that apparent saturation behavior in phenylboronic acid

concentration is well explained by formation of an aniline-phenylboronic acid adduct and does not need to involve fast transmetallation or saturation of a pre-equilibrium.

Based on the above, we now propose the following adapted mechanism for CEL couplings with **3** (Scheme 4-10): the reversible transmetallation from the dinuclear complex **B** is rate-determining and yields the Cu(II)-aryl complex **C**. Warren recently reported a Cu(II)-perfluorophenyl complex, which undergoes oxidation to Cu(III) and reductive elimination when reacted with a nucleophile.⁸⁰ It seems thus more likely that coordination of the amine (**D**) occurs before oxidation. Amine coordination is in competition with the back-reaction of the transmetallation **C**→**B**. Product formation thus depends on both steps and is dependent on amine concentration, even if reaction with amine occurs after the rate-determining step. If phenylboronic acid is present in excess, any enhancement in the transmetallation reaction by increased boronic acid concentration is counterbalanced by a reduction in the concentration in free amine due to the Lewis acid-Lewis base complex formed. Due to its aryl substituent and the coordinated amine, complex **D** is significantly more electron-rich and can be oxidized by the original copper(II) species **A** to form the copper(III) complex **E**.

If transmetallation is slow, either Cu(II) complex **A**, amine-adduct **G**, or the Cu(I) complexes **F** might be catalyst resting states. We did not observe any accumulation of Cu(I) species when the reaction was followed by NMR, but they might be obscured by remaining paramagnetic Cu(II). The color of the reaction mixture, however argues in favor of species **G** as the resting state: a methanol solution of **3**, i. e. species **A**, is green. Under reaction conditions, the green catalyst powder dissolves to provide an orange solution, which is reminiscent of the color of the amine adduct observed in UV/vis titrations with aniline. For Cu(I) species, we would expect them to be re-oxidized at the end of the reaction, but the orange color remains stable for hours after the reaction reached completeness. While **G** is thus the most likely resting state (probably as an adduct with the product at the end of the reaction), we could not obtain any evidence for such as species in HRMS spectra of the reaction mixture.



Scheme 4-10

C-O and C-S couplings. The absence of coupling to methanol solvent and the tolerance of water already indicated that **1** and **3** are not highly reactive towards *O*-nucleophiles. Attempts of CEL couplings to phenol either in dichloromethane or methanol required the addition of base, either because this role is fulfilled by substrate in CEL couplings of amines and anilines, or because deprotonation is required to increase the nucleophilicity of phenol. However, even under these conditions reactions with phenols were sluggish at best and thiols did not react at all. This chemoselectivity of **3** was also indicated by the selective arylation of aminophenols (*vide supra*). While **3** outperforms near all catalyst systems in the coupling of *N*-nucleophiles, even simple copper salts show better reactivity towards weaker nucleophiles such as phenols. Hydroxy- and thiol substituents should thus be considered tolerated functional groups rather than potential reaction sites, and we did not further attempt to optimize reaction conditions for C-O or C-S couplings.

Electron-deficient boronic acid reagents. CEL couplings of aniline with *para*-ethoxyphenylboronic acid, catalyzed by **3**, proceeded smoothly with an activity 4 times higher than that observed with phenylboronic acid (Fig. 4.S8). Electron-deficient boronic acids, on the

other hand, are typically more difficult to couple.^{51, 91} Indeed, couplings with *para*-iodophenylboronic acid did not yield any coupling product after 12 h at room temperature or at 50 °C. *Para*-fluorophenylboronic acid reacted likewise very sluggishly with less than 10% conversion (Table 4-6). For the first time, we noticed formation of the parent aryl from deboration side reactions. More important, however, was the notable amount of homocoupling. While homocoupling normally is only observed in trace amounts, the diaryl was the main product in these reactions.

The formation of diaryl species indicated that transmetallation is unlikely to be the problematic step. The lack of reactivity with electron-deficient boronic acid reagents probably stems from a slower oxidation to the Cu(III) species **E** (Scheme 4-10). Since the copper(II) aryl species **C** or **D** would be more difficult to oxidize with more electron-deficient aryl substituents, C-C homocoupling from **C** now becomes competitive.¹⁰ Oxidation to **E** would be facilitated by more nucleophilic amines. Reaction with *n*-octylamine indeed provided the coupling product in modest yields (Table 4-6). Similarly, we attempted to increase the nucleophilicity of aniline by addition of triethylamine, but without effect. This is consistent with the mechanistic proposal that deprotonation occurs after oxidation (Scheme 4-10). Addition of boric acid was proposed by Watson to be beneficial, in particular in the reoxidation of Cu(I) species.³⁵ Reaction conditions following Watson's protocol, i. e. 1 equiv B(OH)₃ and excess amine, which were beneficial for Cu(OAc)₂, strongly reduced conversions in couplings with catalytic amounts of **3** (Table 4-S1, entries 10-13). Addition of stoichiometric amounts of boronic acid, however, increased the yield of couplings with *para*-fluorophenylboronic acid, but did not exceed 50% conversion (Table 4-6).

Photoredox catalysis. Light-induced electronic transitions, in particular charge-transfer transitions, can be considered intramolecular redox reactions and in recent years photocatalytic reactions have proved very useful in promoting otherwise difficult redox chemistry.^{92, 93} We thus investigated if irradiation by light would facilitate the oxidation to Cu(III) species **E**. CEL couplings of aniline with *para*-fluorophenylboronic acid were conducted under irradiation with white, green (525 nm) or blue (452 nm) light (Table 4-7). While irradiation with white or green light was

not effective, irradiation with blue light afforded the coupled product in moderate yields. Heating to 35 °C or 50 °C did not notably improve conversions.

Table 4-6 : CEL couplings of aniline with electron-deficient phenylboronic acids catalyzed by **3**.^a

X	RNH ₂	Conditions ^a	Conversion
OEt	PhNH ₂	RT, air	100%
NO ₂	PhNH ₂	RT, air	0%
I	PhNH ₂	RT, air or O ₂	0%
I	PhNH ₂	50 °C, O ₂	0%
I	<i>n</i> OctNH ₂	RT, air	30%
F	PhNH ₂	RT, O ₂	4%
F	PhNH ₂	50 °C, O ₂	10%
I	PhNH ₂	RT, air, 10 mol% NEt ₃	0%
I	PhNH ₂	RT, air, 10 mol% NEt ₃	0%
F	PhNH ₂	RT, air, 2.5 mol% B(OH) ₃	33%
F	PhNH ₂	RT, air, 10 mol% B(OH) ₃	47%
F	PhNH ₂	50 °C, O ₂ , 10 mol% B(OH) ₃	50%

^a 1.0 M RNH₂, 1.5 M ArB(OH)₂, 2.5 mol% **3**, MeOH, 12 h.

Table 4-7 : Coupling of aniline or RR'NH and *para*-fluorophenylboronic acid with **3** under photoredox conditions

Light source	T, time	Conditions ^a	Conversion
-	20 °C, 12 h		no reaction
white	20 °C, 12 h		no reaction
green	20 °C, 12 h		no reaction
blue	20 °C, 12 h		50%
blue	35 °C, 12 h		69%
blue	50 °C, 8 h		50%
blue	50 °C, 8 h	O ₂	54%
-	35 °C, 12 h	1 mol% PC1	no reaction
blue	35 °C, 12 h	1 mol% PC1	59%
blue	35 °C, 12 h	1 mol% PC1, O ₂	50%
blue	35 °C, 12 h	1 mol% PC2	50%
blue	50 °C, 12 h	1 mol% PC1	59%
blue	20 °C, 8 h	2.5 mol% B(OH) ₃	54%
blue	20 °C, 8 h	10 mol% B(OH) ₃	60%
blue	50 °C, 8 h	2.5 mol% B(OH) ₃	50%
blue	50 °C, 12 h	2.5 mol% B(OH) ₃ , O ₂	100%
blue	20 °C, 12 h	RR'NH = nHexNH ₂	100%
blue	20 °C, 12 h	RR'NH = nOctNH ₂	100%
blue	20 °C, 12 h	RR'NH = (nBu) ₂ NH	no reaction
blue	20 °C, 8 h	RR'NH = Imidazole	no reaction
blue	50 °C, 12 h	RR'NH = Imidazole, 2.5 mol% B(OH) ₃	no reaction
blue	50 °C, 12 h	O ₂ NC ₆ H ₄ B(OH) ₂ , 2.5 mol% B(OH) ₃	no reaction

^a 1.0 M aniline or RR'NH, 1.5 M ArB(OH)₂, 2.5 mol% **3**.

The UV/vis spectrum of **3** shows a charge-transfer transition centered at 337 nm and a *d-d* transition at 730 nm (Fig. 4.S5 and 4.S6). If the methyl group in the *para*-position of the arylsulfonate in **1** or **3** is replaced by hydrogen, the charge-transfer transition is displaced slightly hypsochromic (appr. 10 nm). This would agree with an assignment as a ligand-to-metal charge-transfer transition. For photoredox catalysis, **3** seem to require irradiation of the LMCT band. Since an LMCT transition increases the electron density at the metal center in the excited state, it is unlikely that excitation directly enables reductive elimination from the excited state. Irradiation thus seems to facilitate the oxidation of **D** by **A**, but from the available data it is impossible to judge whether this occurs through oxidative quenching of an excited copper aryl species **D** or by reductive quenching of a photoexcited oxidant **A** (Scheme 4-10).

Kobayashi reported photoredox catalysis of CEL couplings using the typical Cu(OAc)₂ catalyst and an Iridium photocatalyst,⁹⁴ to the best of our knowledge the only other report of photocatalytic CEL coupling. We briefly investigated if electron transfer from dedicated photocatalysts is more efficient than direct excitation of **3**, but addition of 1 mol% of either [Ir(ppy)₂(bipy)][PF₆], **PC1**, or [Ru(bipy)₃][PF₆]₂, **PC2** (see exp. section), did not show any remarkable improvement (Table 4-7). It has to be noted that the performance of Kobayashi's **PC1**/Cu(OAc)₂ system showed a strong solvent dependence, which we did not optimize. The results presented here should thus *not* be considered a limitation of the reported **PC1**/Cu(OAc)₂ system.

Addition of boric acid again improved reaction yields and at 50 °C and in the presence of 2.5 mol% B(OH)₃, we observed quantitative CEL coupling between aniline and fluorophenylboronic acid. The scope of the photocatalytic reaction was investigated briefly. Substrate reactivity is similar to catalysis without irradiation: hexylamine and octylamine showed complete conversion to the coupling product under photocatalytic conditions, while methoxyaniline and imidazole, which required heating in the reaction with phenylboronic acid, did not show any reactivity with *para*-fluorophenylboronic acid, even under heating and irradiation (Table 4-7). *Para*-nitrophenylboronic acid remained unreactive. While photoredox catalysis thus improved conversions and further supported that oxidation to Cu(III) became the

reaction's bottleneck, it did not provide a generally applicable solution for electron-deficient phenylboronic acids.

Chemical oxidation. Addition of stoichiometric amounts of external oxidants, such as 4-phenylpyridine-oxide (PPO),⁶⁴⁻⁶⁶ *t*Bu₂O₂, or TEMPO,^{64, 65} did not lead to product formation in the coupling of *para*-fluorophenylboronic acid with aniline. Curiously, in the presence of oxidants the main product was the deborated product instead of the diaryl. When the same oxidants were used in CEL couplings with phenylboronic acid, these reactions did not improve either (Table 4-S1, entries 14-17). In the case of PPO, coupling was in fact suppressed. In agreement with Stahl's mechanistic proposal, an external oxidant thus does not participate directly in the Cu(II)/Cu(III) oxidation and is only required to re-oxidize the Cu(I) species formed.

We thus attempted to encourage the formation of the Cu(III) with a catalytic amount of a copper-based oxidant. Cyclic voltammograms of Cu(OAc)₂ and **3** are difficult to interpret due to the irreversibility of the Cu(II)/Cu(III) oxidation step and complications due to copper deposition on the cathode with Cu(OAc)₂, but they qualitatively provide that coordination of the imino-arylsulfonate ligand lowers the reduction potential for oxidation and reduction steps in **3** (Fig. 4-S9). We thus conducted couplings with **3** in the presence of 2.5 mol% of Cu(OAc)₂ as oxidation aid. Under these conditions aniline as well as octylamine could be coupled quantitatively with *para*-fluorophenylboronic acid at room temperature. In fact, the reaction was complete in 3 h. Surprisingly, Cu(OAc)₂ itself is reactive under these conditions, but unlikely to be the active species in the **3**/Cu(OAc)₂ system: its activity in the coupling of aniline with *para*-fluorophenylboronic acid was only half that of **3**/Cu(OAc)₂ (Table 4-8). In addition, couplings with Cu(OAc)₂ alone showed induction periods of 30 – 110 min (Fig. 4.10), while the **3**/Cu(OAc)₂ system showed the same 10 min induction period observed in couplings with **3** alone. These differences were even more pronounced in coupling of aniline with phenylboronic acid: while **3**/Cu(OAc)₂ coupled aniline and phenylboronic acid with a rate constant similar to that of **3** alone (Tables 4-5, 4-8) and with short induction periods, couplings with Cu(OAc)₂ were an order of magnitude slower, induction periods were above 1 h and the reaction was incomplete even after 12 h (Table 4-8, Fig. 4.10). Despite the surprisingly high activity of Cu(OAc)₂ in couplings with fluorophenylboronic acid, the active catalyst is thus **3**. Copper acetate acts as an oxidation aid in

reactions with electron-deficient arylboronic acids, while it does barely increase rate constants for phenylboronic acid.

Table 4-8 : CEL couplings of aniline with electron-deficient phenylboronic acids catalyzed by **3/Cu(OAc)₂.^a**

X	RNH ₂	Conditions ^a	k _{obs} [h ⁻¹]	Conversion
F	nOctNH ₂	RT		100% (2 h)
I	nOctNH ₂	RT		100% (2 h)
F	aniline	RT	1.10(8)	100%
I	aniline	RT		97%
H	aniline	RT	0.43(3)	100%
F	imidazole	50°C, O ₂		0%
NO ₂	nOctNH ₂	RT		0%
F	aniline	Cu(OAc) ₂ only	0.60(1), 0.64(1)	95%, 99% ^b
H	aniline	Cu(OAc) ₂ only	0.06(1)	62%, 66% ^b

^a 1.0 M RNH₂, 1.5 M ArB(OH)₂, 2.5 mol% **3**, MeOH, 12 h. ^b Two experiments.

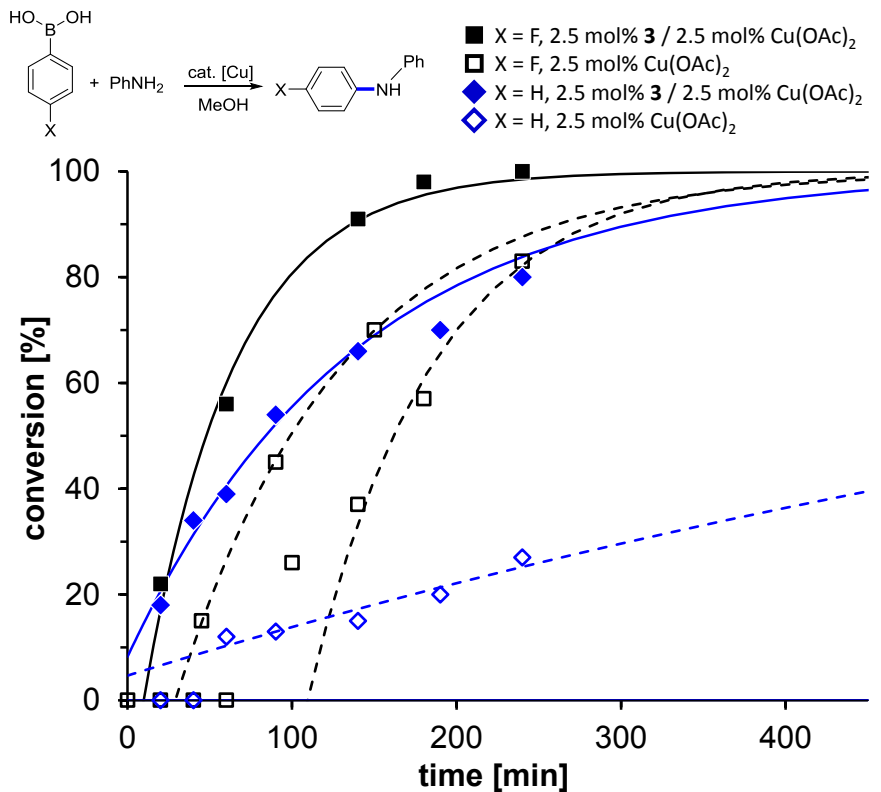


Figure 4.10 : Conversion vs time profile for the *N*-arylation of aniline with **3**/Cu(OAc)₂ or Cu(OAc)₂ only. solid squares: **3**/Cu(OAc)₂, FC₆H₄B(OH)₂; hollow squares: Cu(OAc)₂, FC₆H₄B(OH)₂, two independent reactions with different induction periods shown; solid diamonds: **3**/Cu(OAc)₂, PhB(OH)₂; hollow diamonds: Cu(OAc)₂, PhB(OH)₂. (MeOH, RT, 1.0 M aniline, 1.5 equiv ArB(OH)₂). Solid lines are the simulated conversions calculated from the rate constants and induction periods determined by linear regression (Table 4-8, Fig. 4.S10).

While addition of copper acetate gratifyingly solved the bottleneck of slow oxidation to Cu(III) for amines and anilines, the protocol was unfortunately not generally applicable. Imidazoles, which required heating for coupling with phenylboronic acid, did not couple to electron-poor phenylboronic acids even under heating. Likewise, *para*-nitrophenylboronic acid could not be coupled even with the reactive *n*-octylamine.

4.3. Conclusions

Use of **1** and **3** as catalysts in Chan-Evans-Lam couplings avoided common side reactions such as deboration or homocoupling. As a consequence, excess phenylboronic acid is not required and reactions typically run to quantitative conversion to product. Incorporation of the functionalities commonly achieved by choice of solvent, base and counter-anion into the ligand system avoided the need for an extensive optimization of reaction conditions and provided a general protocol for the arylation of amines, anilines and *N*-heterocycles, which includes sterically difficult substrates such as *tert*-butylamine and dibutylamine. The activity of **3** is among the highest reported for CEL couplings of these class of substrates. In fact, *n*-octylamine and *tert*-butylamine can be arylated in less than 1 h using 0.5 mol% of catalyst at room temperature.

On the down side, the limited access to the metal center and its reduced Lewis acidity, which are the likely reason for the lack of typical side reactions, also limited reactivity towards weaker nucleophiles such as phenols or thiols. While we believe that well-defined coordination complexes can also provide better performance for other substrate classes, these would require a different ligand framework than used in this work.

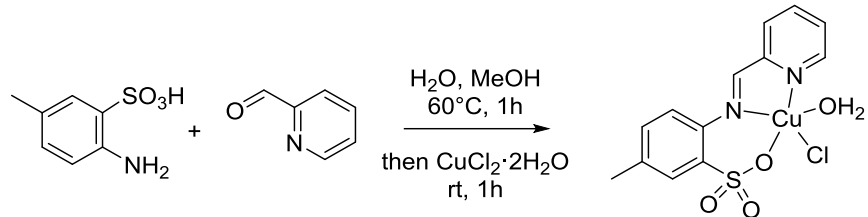
Mechanistic studies with **1** and **3** largely confirmed the general reaction mechanism established by Collman, Stahl and Watson for CEL couplings.^{35, 47, 48, 51, 67} In addition to this, we propose that formation of nucleophile-boronic acid adducts might be responsible for saturation behavior in boronic acid concentrations. Dinuclear copper-boron species are likely present only in small concentrations, even if required as intermediates to transmetallation. Based on our observations herein, the series of steps in the catalytic cycle is likely to be transmetallation – nucleophile coordination – oxidation – reductive elimination for CEL couplings with **1** and **3**. Collman proposed nucleophile coordination prior to transmetallation for $[(\text{tmida})\text{Cu}(\text{OH})]_2\text{Cl}_2$,^{47,}⁴⁸ and it is possible that the order of these two steps differ dependent on the Lewis acidity and the steric saturation of the copper complex employed. While deprotonation is required for product formation even with good nucleophiles such as amines (in no case we observed

quaternisation of tertiary amines or pyridines), its actual position in the catalytic cycle remains unclear and might depend on the nucleophile employed.

CEL couplings have been praised for their reactivity under mild conditions, but criticized for their unpredictability. Placing the copper catalyst in a well-defined ligand environment can clearly overcome these limitations.

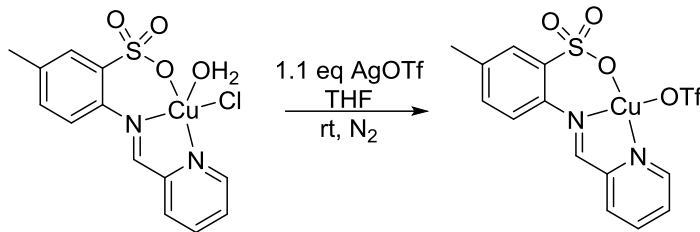
4.4. Experimental section

General. Phenylboronic acid was purified by washing with dichloromethane until the filtrate stayed colorless. All other chemicals were purchased from common commercial suppliers and used without further purification. Elemental analyses were performed by the Laboratoire d'analyse élémentaire (Université de Montréal). UV/vis spectra were recorded on a Cary Series UV-Vis-NIR spectrophotometer from Agilent Technologie. GC-MS spectra were recorded on a Agilent Technologie GC/MS.



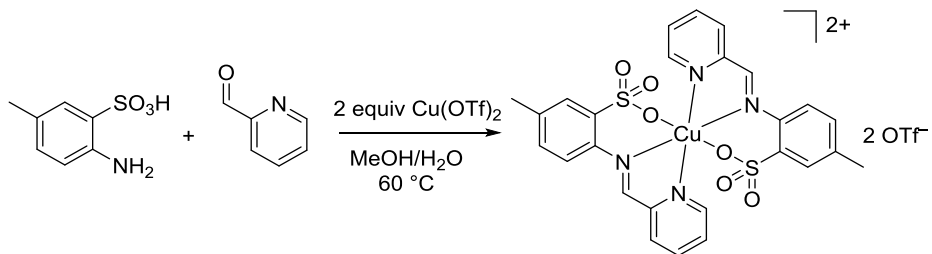
LCuCl(H₂O), 1. To a hot solution (60 °C) of 2-amino-5-methylbenzenesulfonic acid (187 mg, 1.0 mmol) in water (5 mL) and methanol (10 mL) was added 2-pyridinecarboxaldehyde (95 µL, 1.0 mmol). The mixture was stirred for one hour, then copper chloride hydrate (205 mg, 1.1 mmol) was added, resulting in a green solution. Heating was stopped and the solution was stirred another hour. Slow evaporation of the solvent afforded green X-ray quality crystals (321 mg, 82%).

Anal. Calcd. for C₁₃H₁₃ClCuN₂O₄S : C, 39.80; H, 3.34; N, 7.14; S, 8.17. Found: C, 40.09; H, 3.37; N, 3.37; S, 8.47. UV-vis (DMSO, 1·10⁻² M or 1.49·10⁻⁴ M) [λ_{max}, nm (ε, M⁻¹·cm⁻¹)] : 338 (97 000), 800 (500).



{LCu(OTf)}_n, 3. Chloride complex **1** (390 mg, 1.0 mmol) was dissolved in dry THF (5 mL) under nitrogen atmosphere to give a green solution. Silver triflate (328 mg, 1.1 mmol) was added. After one hour of reaction at ambient temperature, a precipitate appeared and the color of the solution intensified. Filtration through a syringe filter and slow evaporation of the green filtrate under N₂, afforded green X-ray quality crystals (236 mg, 54%).

Anal. Calcd. for C₁₄H₁₁CuF₃N₂O₆S₂: C, 34.46; H, 2.27; N, 5.74; S, 13.14. Found: C, 34.10; H, 2.59; N, 5.26; S, 12.61. UV-vis (DMSO, 1.2·10⁻² M or 3.35·10⁻⁴ M) [λ_{max}, nm (ε, M⁻¹·cm⁻¹)]: 338 (62 000), 730 (470).



[(LCu)₂](OTf)₂, 4. To a hot solution (60 °C) of water (5 mL) and methanol (10 mL) containing 2-amino-5-methylbenzenesulfonic acid (187 mg, 1.0 mmol) was added 2-pyridinecarboxaldehyde (95 µL, 1.0 mmol). The mixture was stirred for one hour at 60 °C, then copper triflate (724 mg, 2.0 mmol) was added. Heating was stopped and the solution was stirred another hour. After filtration, slow evaporation of the solvent provided green X-ray quality crystals (195 mg, 40%).

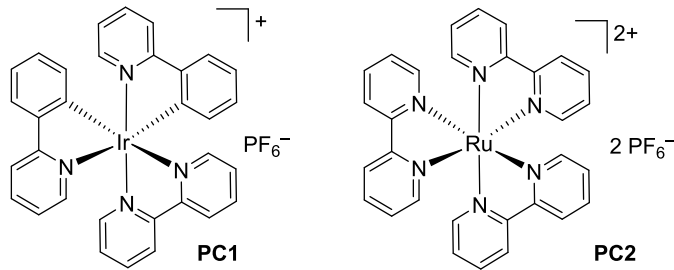
Anal. Calcd. for C₁₄H₉CuF₃N₂O₅S₂: C, 33.24; H, 2.59; N, 5.54; S, 12.67. Found: C, 33.24; H, 2.57; N, 5.10; S, 13.44. UV-vis (DMSO, 1.2·10⁻² M or 3.35·10⁻⁴ M) [λ_{max}, nm (ε, M⁻¹·cm⁻¹)]: 328 (19 000), 727 (430).

L₂Cu, 2. Recrystallization of complex **1** in a mixture of water and acetonitrile from 50 °C to RT provided to the homoleptic complex.

Anal. Calcd. for $C_{14}H_{11}CuF_3N_2O_6S_2$: C, 39.80; H, 3.34; N, 7.14; S, 8.17. Found: C, 40.09; H, 3.37; N, 7.37; S, 8.47. UV-vis (DMSO, $1.2 \cdot 10^{-2}$ M or $3.35 \cdot 10^{-4}$ M) [λ_{max} , nm (ε , $M^{-1} \cdot cm^{-1}$)] : 322 (23 000), 793 (810).

General procedure for Chan-Evans-Lam couplings. To a solution of amine or aniline (1.0 mmol) and phenylboronic acid (1.5 mmol) in methanol (1 mL) was added catalyst **1** or **2** (0.025 mmol). Trimethoxybenzene was added as internal standard. The reaction was stirred open to air at ambient temperature or at 50 °C under O₂ atmosphere. For kinetic experiments, 20 µL aliquots were taken, diluted in ethyl acetate and analyzed by GC-MS. After the desired reaction time, the reaction was quenched with 0.5 mL of a saturated aqueous solution of ammonium chloride. The organic layer was extracted and filtered through a short silica plug to remove remaining copper complex. Products and side-products were identified by the MS- and NMR-spectrum from comparison to literature. Conversion was typically analysed by GC-MS. Quantitative concentrations were determined by comparison to trimethoxybenzene standard. Calibration factors between starting materials, products, side-products and trimethoxybenzene were determined from simultaneous NMR and GC-MS analysis or by analysis of solutions prepared from isolated or commercially available products.

Photoredox catalysis. Following otherwise the general procedure, 20 mL headspace vials were used. For blue ($\lambda = 452$ nm, FWHM = 150 nm) and green light radiation ($\lambda = 525$ nm, FWHM = 170 nm), the vials were placed on a panel constituted of 90 x 1 W LED in a thermostatic bath with a Poly-Science controller set to 20 °C or 50 °C. For white light ($\lambda = 445$ and 552 nm, FWHM = 350 nm), a 10 W LED in a thermostatic bath with a A-Nova controller set to 20 °C or 50 °C was used. For reactions with additional photocatalyst, $[\text{Ir}(\text{ppy})_2(\text{bipy})][\text{PF}_6]$ (8 mg, 0.01 mmol) or $[\text{Ru}(\text{bipy})_3][\text{PF}_6]_2$ (9 mg, 0.01 mmol) were added.



Cyclic voltammetry. Electrochemical measurements were carried out in dry methanol at RT with a BioLogic-SP50 potentiostat-galvanostat interfaced to a PC on which was installed the EC-lab software. The working electrode was a glassy carbon electrode (3mm diameter) which was polished with 0.05 µm alumina paste before each sample. The counter electrode was a Pt wire and the pseudo-reference electrode was a silver wire (Ag/AgCl). The supporting electrolyte used for analysis was tetrabutylammonium perchlorate at 0.1 M in solution. The analyte concentration was about 1 mM and tetrabutylammonium hexafluorophosphate (TBAPF₆) was used as supporting electrolyte at 0.10 M. Cyclic voltammograms were obtained at scan rates of 100 mV/s.

X-ray diffraction studies. Crystal for X-ray diffraction were produced from synthesis as described above. Diffraction data were collected on a Bruker Venture METALJET diffractometer (Ga K α radiation).⁹⁵ Data reduction was performed with SAINT,⁹⁶ absorption corrections with SADABS.⁹⁷ Structures were solved by dual-space refinement (SHELXT).⁹⁸ All non-hydrogen atoms were refined anisotropic using full-matrix least-squares on F^2 and hydrogen atoms refined with fixed isotropic U using a riding model (SHELXL97).⁹⁹ Further experimental details can be found in

Table 4-9 : Experimental details of X-ray diffraction studies.

	2	4
Formula	$C_{26}H_{24}CuN_4O_7S_2$	$C_{14}H_{13}CuF_3N_2O_7S_2$
M_w (g/mol); F(000)	632.5; 2600	505.92; 510
T (K); wavelength	100; 1.34190	150; 1.34190
Crystal System	Orthorhombic	Triclinic
Space Group	$Pbca$	$P-1$
Unit Cell:		
a (Å)	17.7588(4)	7.9814(3)
b (Å)	13.9390(3)	11.0894(4)
c (Å)	20.7682(4)	11.1020(4)
α (°)	90	96.4610(10)
β (°)	90	100.1760(10)
γ (°)	90	110.0070(10)
V (Å ³)	5140.96(19)	892.77(6)
Z; $d_{\text{calcd.}}$ (g/cm ³)	8; 1.639	2; 1.882
μ (mm ⁻¹); Abs. Corr.	5.89; multi-scan	8.50; multi-scan
Extinction coefficient	-	0.120(3)
θ (°); completeness	3.7-60.7; 0.997	7.2-121.3; 1.000
Collected reflections; R_σ	66841; 0.023	21646; 0.023
Unique reflections; R_{int}	5895; 0.051	4095; 0.037
Observ. reflections; $R1(F)$	5566; 0.033	4073; 0.036
wR(F^2) (all data); GoF(F^2)	0.0894; 1.05	0.0933; 1.18
Residual electron density	0.64	0.45

4.6. References

- ¹ Gildner, P. G.; Colacot, T. J., Reactions of the 21st Century: Two Decades of Innovative Catalyst Design for Palladium-Catalyzed Cross-Couplings. *Organometallics* **2015**, *34*, 5497-5508.
- ² Garrett, C. E.; Prasad, K., The Art of Meeting Palladium Specifications in Active Pharmaceutical Ingredients Produced by Pd-Catalyzed Reactions. *Adv. Synth. Catal.* **2004**, *346*, 889-900.
- ³ Barton, D. H. R.; Finet, J.-P.; Khamsi, J., Metallic copper catalysis of N-arylation of amines by triaryl bismuth diacylates. *Tetrahedron Lett.* **1986**, *27*, 3615-3618.
- ⁴ Chan, D. M. T.; Monaco, K. L.; Wang, R.-P.; Winters, M. P., New N- and O-arylations with phenylboronic acids and cupric acetate. *Tetrahedron Lett.* **1998**, *39*, 2933-2936.
- ⁵ Evans, D. A.; Katz, J. L.; West, T. R., Synthesis of diaryl ethers through the copper-promoted arylation of phenols with arylboronic acids. An expedient synthesis of thyroxine. *Tetrahedron Lett.* **1998**, *39*, 2937-2940.
- ⁶ Lam, P. Y. S.; Clark, C. G.; Saubern, S.; Adams, J.; Winters, M. P.; Chan, D. M. T.; Combs, A., New aryl/heteroaryl C-N bond cross-coupling reactions via arylboronic acid/cupric acetate arylation. *Tetrahedron Lett.* **1998**, *39*, 2941-2944.
- ⁷ Bhunia, S.; Pawar, G. G.; Kumar, S. V.; Jiang, Y.; Ma, D., Selected Copper-Based Reactions for C-N, C-O, C-S, and C-C Bond Formation. *Angew. Chem., Int. Ed.* **2017**, *56*, 16136-16179.
- ⁸ Lam, P. Y. S., Chapter 7 Chan-Lam Coupling Reaction: Copper-promoted C-Element Bond Oxidative Coupling Reaction with Boronic Acids. In *Synthetic Methods in Drug Discovery: Volume 1*, The Royal Society of Chemistry 2016; Vol. 1, pp 242-273.
- ⁹ Neuville, L., Alternative and Emerging Reagents for the Arylation of Heteronucleophiles. In *Copper-Mediated Cross-Coupling Reactions*, John Wiley & Sons, Inc. 2013; pp 113-185.
- ¹⁰ Allen, S. E.; Walvoord, R. R.; Padilla-Salinas, R.; Kozlowski, M. C., Aerobic Copper-Catalyzed Organic Reactions. *Chem. Rev.* **2013**, *113*, 6234-6458.
- ¹¹ Beletskaya, I. P.; Cheprakov, A. V., The Complementary Competitors: Palladium and Copper in C-N Cross-Coupling Reactions. *Organometallics* **2012**, *31*, 7753-7808.
- ¹² Qiao, J. X.; Lam, P. Y. S., Recent Advances in Chan-Lam Coupling Reaction: Copper-Promoted C-Heteroatom Bond Cross-Coupling Reactions with Boronic Acids and Derivatives. In *Boronic Acids*, Wiley-VCH Verlag GmbH & Co. KGaA 2011; pp 315-361.

¹³ Evano, G.; Blanchard, N.; Toumi, M., Copper-Mediated Coupling Reactions and Their Applications in Natural Products and Designed Biomolecules Synthesis. *Chem. Rev.* **2008**, *108*, 3054-3131.

¹⁴ Ley, S. V.; Thomas, A. W., Modern Synthetic Methods for Copper-Mediated C(aryl)-O, C(aryl)-N, and C(aryl)-S Bond Formation. *Angew. Chem., Int. Ed.* **2003**, *42*, 5400-5449.

¹⁵ Cundy, D. J.; Forsyth, S. A., Cupric acetate mediated N-arylation by arylboronic acids: A preliminary investigation into the scope of application. *Tetrahedron Lett.* **1998**, *39*, 7979-7982.

¹⁶ Quach, T. D.; Batey, R. A., Ligand- and Base-Free Copper(II)-Catalyzed C–N Bond Formation: Cross-Coupling Reactions of Organoboron Compounds with Aliphatic Amines and Anilines. *Org. Lett.* **2003**, *5*, 4397-4400.

¹⁷ Antilla, J. C.; Buchwald, S. L., Copper-Catalyzed Coupling of Arylboronic Acids and Amines. *Org. Lett.* **2001**, *3*, 2077-2079.

¹⁸ Li, Y.; Gao, L.-X.; Han, F.-S., Efficient synthesis of 2,5-disubstituted tetrazoles via the Cu₂O-catalyzed aerobic oxidative direct cross-coupling of N-H free tetrazoles with boronic acids. *Chem. Commun. (Cambridge, U. K.)* **2012**, *48*, 2719-2721.

¹⁹ Liu, C.-Y.; Li, Y.; Ding, J.-Y.; Dong, D.-W.; Han, F.-S., The Development of Copper-Catalyzed Aerobic Oxidative Coupling of H-Tetrazoles with Boronic Acids and an Insight into the Reaction Mechanism. *Chem.-Eur. J.* **2014**, *20*, 2373-2381.

²⁰ Chen, J.; Natte, K.; Man, N. Y. T.; Stewart, S. G.; Wu, X.-F., Convenient copper-mediated Chan-Lam coupling of 2-aminopyridine: facile synthesis of N-arylpyridin-2-amines. *Tetrahedron Lett.* **2015**, *56*, 4843-4847.

²¹ Siva Reddy, A.; Ranjith Reddy, K.; Nageswar Rao, D.; Jaladanki, C. K.; Bharatam, P. V.; Lam, P. Y. S.; Das, P., Copper(ii)-catalyzed Chan-Lam cross-coupling: chemoselective N-arylation of aminophenols. *Organic & Biomolecular Chemistry* **2017**, *15*, 801-806.

²² Moon, P. J.; Halperin, H. M.; Lundgren, R. J., Oxidative Coupling of Aryl Boron Reagents with sp³-Carbon Nucleophiles: The Enolate Chan–Evans–Lam Reaction. *Angew. Chem., Int. Ed.* **2016**, *55*, 1894-1898.

²³ Nishiura, K.; Urawa, Y.; Soda, S., N-Arylation of Benzimidazole with Arylboronate, Boroxine and Boronic Acids. Acceleration with an Optimal Amount of Water. *Adv. Synth. Catal.* **2004**, *346*, 1679-1684.

²⁴ Yue, Y.; Zheng, Z. G.; Wu, B.; Xia, C. Q.; Yu, X. Q., Copper-Catalyzed Cross-Coupling Reactions of Nucleobases with Arylboronic Acids: An Efficient Access to N-Arylnucleobases. *Eur. J. Org. Chem.* **2005**, *2005*, 5154-5157.

²⁵ Hardouin Duparc, V.; Schaper, F., Sulfonato-diketimine copper(II) complexes : synthesis and application as catalysts in base-free Chan-Evans-Lam couplings. *Organometallics* **2017**, *36*, 3053-3060.

²⁶ Lan, J.-B.; Chen, L.; Yu, X.-Q.; You, J.-S.; Xie, R.-G., A simple copper salt catalysed the coupling of imidazole with arylboronic acids in protic solvent. *Chem. Commun. (Cambridge, U. K.)* **2004**, 188-189.

²⁷ van Berkel, S. S.; van den Hoogenband, A.; Terpstra, J. W.; Tromp, M.; van Leeuwen, P. W. N. M.; van Strijdonck, G. P. F., Base-free anaerobic Cu(II) catalysed aryl-nitrogen bond formations. *Tetrahedron Lett.* **2004**, *45*, 7659-7662.

²⁸ Yu, X.-Q.; Yamamoto, Y.; Miyaura, N., Aryl Triolborates: Novel Reagent for Copper-Catalyzed N Arylation of Amines, Anilines, and Imidazoles. *Chemistry – An Asian Journal* **2008**, *3*, 1517-1522.

²⁹ Liu, B.; Liu, B.; Zhou, Y.; Chen, W., Copper(II) Hydroxide Complexes of N-Heterocyclic Carbenes and Catalytic Oxidative Amination of Arylboronic Acids. *Organometallics* **2010**, *29*, 1457-1464.

³⁰ Kaboudin, B.; Abedi, Y.; Yokomatsu, T., Cull- β -Cyclodextrin Complex as a Nanocatalyst for the Homo- and Cross-Coupling of Arylboronic Acids under Ligand- and Base-Free Conditions in Air: Chemoselective Cross-Coupling of Arylboronic Acids in Water. *Eur. J. Org. Chem.* **2011**, *2011*, 6656-6662.

³¹ Garnier, T.; Sakly, R.; Danel, M.; Chassaing, S.; Pale, P., Chan–Lam-Type C–N Cross-Coupling Reactions under Base- and Ligand-Free Cul-Zeolite Catalysis. *Synthesis* **2017**, *49*, 1223-1230.

³² Molaei, H.; Ghanbari, M. M., Practical copper-catalyzed N-arylation of amines with 20% aqueous solution of n-Bu₄NOH. *Chinese Chemical Letters* **2012**, *23*, 301-304.

³³ Wentzel, M. T.; Hewgley, J. B.; Kamble, R. M.; Wall, P. D.; Kozlowski, M. C., Copper-Catalyzed N-Arylation of Hindered Substrates Under Mild Conditions. *Adv. Synth. Catal.* **2009**, *351*, 931-937.

³⁴ Jiang, Z.; Wu, Z.; Wang, L.; Wu, D.; Zhou, X., Preparation of aromatic amines by copper-catalyzed coupling of boronic acids with aqueous ammonia. *Can. J. Chem.* **2010**, *88*, 964-968.

³⁵ Vantourout, J. C.; Miras, H. N.; Isidro-Llobet, A.; Sproules, S.; Watson, A. J. B., Spectroscopic Studies of the Chan–Lam Amination: A Mechanism-Inspired Solution to Boronic Ester Reactivity. *J. Am. Chem. Soc.* **2017**, *139*, 4769-4779.

³⁶ Roy, S.; Sarma, M. J.; Kashyap, B.; Phukan, P., A quick Chan-Lam C-N and C-S cross coupling at room temperature in the presence of square pyramidal [Cu(DMAP)4I]I as a catalyst. *Chem. Commun. (Cambridge, U. K.)* **2016**, *52*, 1170-1173.

³⁷ Chiang, G. C. H.; Olsson, T., Polymer-Supported Copper Complex for C–N and C–O Cross-Coupling Reactions with Aryl Boronic Acids. *Org. Lett.* **2004**, *6*, 3079–3082.

³⁸ Kantam, M. L.; Venkanna, G. T.; Sridhar, C.; Sreedhar, B.; Choudary, B. M., An Efficient Base-Free N-Arylation of Imidazoles and Amines with Arylboronic Acids Using Copper-Exchanged Fluorapatite. *J. Org. Chem.* **2006**, *71*, 9522–9524.

³⁹ Islam, M.; Mondal, S.; Mondal, P.; Roy, A.; Tuhina, K.; Mobarok, M.; Paul, S.; Salam, N.; Hossain, D., An Efficient Recyclable Polymer Supported Copper(II) Catalyst for C–N Bond Formation by N-Arylation. *Catal. Lett.* **2011**, *141*, 1171–1181.

⁴⁰ Mostafalu, R.; Kaboudin, B.; Kazemi, F.; Yokomatsu, T., N-arylation of amines: C–N coupling of amines with arylboronic acids using Fe₃O₄ magnetic nanoparticles-supported EDTA-Cu(ii) complex in water. *RSC Adv.* **2014**, *4*, 49273–49279.

⁴¹ Anuradha; Kumari, S.; Pathak, D. D., Synthesis and development of Chitosan anchored copper(II) Schiff base complexes as heterogeneous catalysts for N-arylation of amines. *Tetrahedron Lett.* **2015**, *56*, 4135–4142.

⁴² Lin, Y.; Cai, M.; Fang, Z.; Zhao, H., A highly efficient heterogeneous copper-catalyzed Chan-Lam coupling between thiols and arylboronic acids leading to diaryl sulfides under mild conditions. *Tetrahedron* **2016**, *72*, 3335–3343.

⁴³ Khosravi, A.; Mokhtari, J.; Naimi-Jamal, M. R.; Tahmasebi, S.; Panahi, L., Cu₂(BDC)₂(BPy)-MOF: an efficient and reusable heterogeneous catalyst for the aerobic Chan-Lam coupling prepared via ball-milling strategy. *RSC Adv.* **2017**, *7*, 46022–46027.

⁴⁴ Dutta, M. M.; Phukan, P., Cu-doped CoFe₂O₄ nanoparticles as magnetically recoverable catalyst for CN cross-coupling reaction. *Catal. Commun.* **2018**, *109*, 38–42.

⁴⁵ Sharma, H.; Mahajan, H.; Jamwal, B.; Paul, S., Cu@Fe₃O₄-TiO₂-L-dopa: A novel and magnetic catalyst for the Chan-Lam cross-coupling reaction in ligand free conditions. *Catal. Commun.* **2018**, *107*, 68–73.

⁴⁶ Debreczeni, N.; Fodor, A.; Hell, Z., Coupling of Boronic Acids with Amines in the Presence of a Supported Copper Catalyst. *Catal. Lett.* **2014**, *144*, 1547–1551.

⁴⁷ Collman, J. P.; Zhong, M., An Efficient Diamine-Copper Complex-Catalyzed Coupling of Arylboronic Acids with Imidazoles. *Org. Lett.* **2000**, *2*, 1233–1236.

⁴⁸ Collman, J. P.; Zhong, M.; Zhang, C.; Costanzo, S., Catalytic Activities of Cu(II) Complexes with Nitrogen-Chelating Bidentate Ligands in the Coupling of Imidazoles with Arylboronic Acids. *J. Org. Chem.* **2001**, *66*, 7892–7897.

⁴⁹ Wang, L.; Jiang, Z.; Yu, L.; Li, L.; Li, Z.; Zhou, X., Cross Coupling of Arylboronic Acids with Imidazoles by Sulfonatocopper(II)(salen) Complex in Water. *Chem. Lett.* **2010**, 39, 764-765.

⁵⁰ Gogoi, A.; Sarmah, G.; Dewan, A.; Bora, U., Unique copper–salen complex: an efficient catalyst for N-arylations of anilines and imidazoles at room temperature. *Tetrahedron Lett.* **2014**, 55, 31-35.

⁵¹ King, A. E.; Ryland, B. L.; Brunold, T. C.; Stahl, S. S., Kinetic and Spectroscopic Studies of Aerobic Copper(II)-Catalyzed Methoxylation of Arylboronic Esters and Insights into Aryl Transmetalation to Copper(II). *Organometallics* **2012**, 31, 7948-7957.

⁵² Hardouin Duparc, V.; Schaper, F., Sulfonato-imino copper(II) complexes : fast Chan-Evans-Lam coupling of amines and anilines. *Dalton Trans.* **2017**, 46, 12766 - 12770.

⁵³ Hazra, S.; Mukherjee, S.; Guedes da Silva, M. F. C.; Pombeiro, A. J. L., A cyclic tetranuclear cuboid type copper(ii) complex doubly supported by cyclohexane-1,4-dicarboxylate: molecular and supramolecular structure and cyclohexane oxidation activity. *RSC Adv.* **2014**, 4, 48449-48457.

⁵⁴ Addison, A. W.; Rao, T. N.; Reedijk, J.; van Rijn, J.; Verschoor, G. C., Synthesis, structure, and spectroscopic properties of copper(II) compounds containing nitrogen-sulphur donor ligands; the crystal and molecular structure of aqua[1,7-bis(N-methylbenzimidazol-2[prime or minute]-yl)-2,6-dithiaheptane]copper(II) perchlorate. *J. Chem. Soc., Dalton Trans.* **1984**, 1349-1356.

⁵⁵ Yang, G.-G.; Ou-Yang, M.; Meng, X.-J.; Huang, X.-R.; Jiang, Y.-M., Bis[2-(2-pyridylmethyleneamino)benzenesulfonato]-[kappa]3N,N',O;[kappa]2N,N'-copper(II). *Acta Crystallogr., Sect. E: Struct. Rep. Online* **2009**, 65, m1200.

⁵⁶ Groom, C. R.; Bruno, I. J.; Lightfoot, M. P.; Ward, S. C., The Cambridge Structural Database. *Acta Crystallogr., Sect. B: Struct. Sci.* **2016**, 72, 171-179.

⁵⁷ Ou, Y.-M.; Zhao, Z.-Y.; Yue-Hua Shi; Zhang, Y.-L.; Jiang, Y.-M., *Chin. J. Struct. Chem.* **2009**, 28, 457.

⁵⁸ Hazra, S.; Karmakar, A.; Guedes da Silva, M. d. F. C.; Dlhan, L. u.; Boca, R.; Pombeiro, A. J. L., Sulfonated Schiff base dinuclear and polymeric copper(ii) complexes: crystal structures, magnetic properties and catalytic application in Henry reaction. *New J. Chem.* **2015**, 39, 3424-3434.

⁵⁹ Paul, A.; Hazra, S.; Sharma, G.; Guedes da Silva, M. F. C.; Koch, B.; Pombeiro, A. J. L., Unfolding biological properties of a versatile dicopper(II) precursor and its two mononuclear copper(II) derivatives. *Journal of Inorganic Biochemistry* **2017**, 174, 25-36.

⁶⁰ Lam, P. Y. S.; Bonne, D.; Vincent, G.; Clark, C. G.; Combs, A. P., N-Arylation of α -aminoesters with p-tolylboronic acid promoted by copper(II) acetate. *Tetrahedron Lett.* **2003**, 44, 1691-1694.

⁶¹ Rao, D. N.; Rasheed, S.; Aravinda, S.; Vishwakarma, R. A.; Das, P., Base and ligand free copper-catalyzed N-arylation of 2-amino-N-heterocycles with boronic acids in air. *RSC Adv.* **2013**, 3, 11472-11475.

62 Sanjeeva Rao, K.; Wu, T.-S., Chan-Lam coupling reactions: synthesis of heterocycles. *Tetrahedron* **2012**, 68, 7735-7754.

⁶³ Zhu, X.; Zhang, Q.; Su, W., Solvent-free N-arylation of amines with arylboronic acids under ball milling conditions. *RSC Adv.* **2014**, 4, 22775-22778.

⁶⁴ Lam, P. Y. S.; Vincent, G.; Clark, C. G.; Deudon, S.; Jadhav, P. K., Copper-catalyzed general C • N and C • O bond cross-coupling with arylboronic acid. *Tetrahedron Lett.* **2001**, 42, 3415-3418.

⁶⁵ Lam, P. Y. S.; Vincent, G.; Bonne, D.; Clark, C. G., Copper-promoted/catalyzed C-N and C-O bond cross-coupling with vinylboronic acid and its utilities. *Tetrahedron Lett.* **2003**, 44, 4927-4931.

⁶⁶ Strouse, J. J.; Jeselnik, M.; Tapaha, F.; Jonsson, C. B.; Parker, W. B.; Arterburn, J. B., Copper catalyzed arylation with boronic acids for the synthesis of N1-aryl purine nucleosides. *Tetrahedron Lett.* **2005**, 46, 5699-5702.

⁶⁷ King, A. E.; Brunold, T. C.; Stahl, S. S., Mechanistic Study of Copper-Catalyzed Aerobic Oxidative Coupling of Arylboronic Esters and Methanol: Insights into an Organometallic Oxidase Reaction. *J. Am. Chem. Soc.* **2009**, 131, 5044-5045.

⁶⁸ Tromp, M.; van Strijdonck, G. P. F.; van Berkel, S. S.; van den Hoogenband, A.; Feiters, M. C.; de Bruin, B.; Fiddy, S. G.; van der Eerden, A. M. J.; van Bokhoven, J. A.; van Leeuwen, P. W. N. M.; Koningsberger, D. C., Multitechnique Approach to Reveal the Mechanism of Copper(II)-Catalyzed Arylation Reactions. *Organometallics* **2010**, 29, 3085-3097.

⁶⁹ Demir, A. S.; Reis, Ö.; Emrullahoglu, M., Role of Copper Species in the Oxidative Dimerization of Arylboronic Acids: Synthesis of Symmetrical Biaryls. *J. Org. Chem.* **2003**, 68, 10130-10134.

⁷⁰ Kirai, N.; Yamamoto, Y., Homocoupling of Arylboronic Acids Catalyzed by 1,10-Phenanthroline-Ligated Copper Complexes in Air. *Eur. J. Org. Chem.* **2009**, 2009, 1864-1867.

⁷¹ Cheng, G.; Luo, M., Homocoupling of Arylboronic Acids Catalyzed by CuCl in Air at Room Temperature. *Eur. J. Org. Chem.* **2011**, 2011, 2519-2523.

⁷² Mulla, S. A. R.; Chavan, S. S.; Pathan, M. Y.; Inamdar, S. M.; Shaikh, T. M. Y., Ligand-, base-, co-catalyst-free copper fluorapatite (CuFAP) as a versatile, ecofriendly, heterogeneous and reusable catalyst for an efficient homocoupling of arylboronic acid at ambient reaction conditions. *RSC Adv.* **2015**, 5, 24675-24680.

⁷³ Wang, Y.-H.; Xu, M.-C.; Liu, J.; Zhang, L.-J.; Zhang, X.-M., Three-coordinate copper(I) 2-hydroxy-1,10-phenanthroline dinuclear complex catalyzed homocoupling of arylboronic acids towards biphenyls under air condition. *Tetrahedron* **2015**, *71*, 9598-9601.

⁷⁴ Parshamoni, S.; Telangae, J.; Sanda, S.; Konar, S., A Copper-Based Metal–Organic Framework Acts as a Bifunctional Catalyst for the Homocoupling of Arylboronic Acids and Epoxidation of Olefins. *Chemistry – An Asian Journal* **2016**, *11*, 540-547.

⁷⁵ Agrahari, B.; Layek, S.; Kumari, S.; Anuradha; Ganguly, R.; Pathak, D. D., Synthesis, characterization and crystal structure of Cu(II) complex of trans-cyclohexane-1,2-diamine: Application in synthesis of symmetrical biaryls. *Journal of Molecular Structure* **2017**, *1134*, 85-90.

⁷⁶ Cao, Y.-N.; Tian, X.-C.; Chen, X.-X.; Yao, Y.-X.; Gao, F.; Zhou, X.-L., Rapid Ligand-Free Base-Accelerated Copper-Catalyzed Homocoupling Reaction of Arylboronic Acids. *Synlett* **2017**, *28*, 601-606.

⁷⁷ Chen, S.; Huang, H.; Liu, X.; Shen, J.; Jiang, H.; Liu, H., Microwave-Assisted Efficient Copper-Promoted N-Arylation of Amines with Arylboronic Acids. *J. Comb. Chem.* **2008**, *10*, 358-360.

⁷⁸ Terent'ev, A. P.; Mogilyanskii, Y. D., Pyridine-cuprous chloride complex as an autoxidation catalyst. I. Preparation of azo compounds from primary aromatic amines. *Zh. Obshch. Khim.* **1958**, *28*, 1959-62.

⁷⁹ Lu, W.; Xi, C., CuCl-catalyzed aerobic oxidative reaction of primary aromatic amines. *Tetrahedron Lett.* **2008**, *49*, 4011-4015.

⁸⁰ Kundu, S.; Greene, C.; Williams, K. D.; Salvador, T. K.; Bertke, J. A.; Cundari, T. R.; Warren, T. H., Three-Coordinate Copper(II) Aryls: Key Intermediates in C–O Bond Formation. *J. Am. Chem. Soc.* **2017**, *139*, 9112-9115.

⁸¹ Ziegler, M. S.; Levine, D. S.; Lakshmi, K. V.; Tilley, T. D., Aryl Group Transfer from Tetraarylborato Anions to an Electrophilic Dicopper(I) Center and Mixed-Valence μ -Aryl Dicopper(I,II) Complexes. *J. Am. Chem. Soc.* **2016**, *138*, 6484-6491.

⁸² Chmielewski, P. J.; Łatos-Grażyński, L.; Schmidt, I., Copper(II) Complexes of Inverted Porphyrin and Its Methylated Derivatives. *Inorg. Chem.* **2000**, *39*, 5475-5482.

⁸³ Furuta, H.; Ishizuka, T.; Osuka, A.; Uwatoko, Y.; Ishikawa, Y., Metal Complexes of an N-Confused Calix[4]phyrin Derivative—The First X-ray Structure of an Organometallic Compound of Divalent Copper. *Angew. Chem., Int. Ed.* **2001**, *40*, 2323-2325.

⁸⁴ Kinoshita, I.; James Wright, L.; Kubo, S.; Kimura, K.; Sakata, A.; Yano, T.; Miyamoto, R.; Nishioka, T.; Isobe, K., Design and synthesis of copper complexes of novel ligands based on the pyridine thiolate group. *Dalton Trans.* **2003**, 1993-2003.

⁸⁵ Maeda, H.; Osuka, A.; Ishikawa, Y.; Aritome, I.; Hisaeda, Y.; Furuta, H., N-Confused Porphyrin-Bearing meso-Perfluorophenyl Groups: A Potential Agent That Forms Stable Square-Planar Complexes with Cu(II) and Ag(III). *Org. Lett.* **2003**, *5*, 1293-1296.

⁸⁶ Miyamoto, R.; Hamazawa, R. T.; Hirotsu, M.; Nishioka, T.; Kinoshita, I.; Wright, L. J., A two-dimensional clathrate hydrate sandwiched by planar arrays of a copper complex. *Chem. Commun. (Cambridge, U. K.)* **2005**, 4047-4049.

⁸⁷ Miyamoto, R.; Santo, R.; Matsushita, T.; Nishioka, T.; Ichimura, A.; Teki, Y.; Kinoshita, I., A complete series of copper(ii) halide complexes (X = F, Cl, Br, I) with a novel Cu(ii)-C(sp³) bond. *Dalton Trans.* **2005**, 3179-3186.

⁸⁸ Pawlicki, M.; Kańska, I.; Łatos-Grażyński, L., Copper(II) and Copper(III) Complexes of Pyrrole-Appended Oxacarbaporphyrin. *Inorg. Chem.* **2007**, *46*, 6575-6584.

⁸⁹ Grzegorzek, N.; Pawlicki, M.; Szterenberg, L.; Łatos-Grażyński, L., Organocopper(II) Complex of 21-Diphenylphosphoryl-Carbapolactone Hybrid: A Side-On Coordination Mode of Copper(II). *J. Am. Chem. Soc.* **2009**, *131*, 7224-7225.

⁹⁰ Casitas, A.; Ribas, X., The role of organometallic copper(iii) complexes in homogeneous catalysis. *Chem. Sci.* **2013**, *4*, 2301-2318.

⁹¹ Grimes, K. D.; Gupte, A.; Aldrich, C. C., Copper(II)-Catalyzed Conversion of Aryl/Heteroaryl Boronic Acids, Boronates, and Trifluoroborates into the Corresponding Azides: Substrate Scope and Limitations. *Synthesis* **2010**, *2010*, 1441-1448.

⁹² Prier, C. K.; Rankic, D. A.; MacMillan, D. W. C., Visible Light Photoredox Catalysis with Transition Metal Complexes: Applications in Organic Synthesis. *Chem. Rev.* **2013**, *113*, 5322-5363.

⁹³ Tucker, J. W.; Stephenson, C. R. J., Shining Light on Photoredox Catalysis: Theory and Synthetic Applications. *J. Org. Chem.* **2012**, *77*, 1617-1622.

⁹⁴ Yoo, W. J.; Tsukamoto, T.; Kobayashi, S., Visible-Light-Mediated Chan–Lam Coupling Reactions of Aryl Boronic Acids and Aniline Derivatives. *Angew. Chem., Int. Ed.* **2015**, *54*, 6587-6590.

⁹⁵ APEX2, Release 2.1-0; Bruker AXS Inc.: Madison, USA, 2006.

⁹⁶ SAINT, Release 7.34A; Bruker AXS Inc.: Madison, USA, 2006.

⁹⁷ Sheldrick, G. M. *SADABS*, Bruker AXS Inc.: Madison, USA, 1996 & 2004.

⁹⁸ Sheldrick, G., SHELXT - Integrated space-group and crystal-structure determination. *Acta Crystallogr. Sect. A: Found. Crystallogr.* **2015**, *71*, 3-8.

⁹⁹ Sheldrick, G. M., A short history of SHELX. *Acta Crystallogr. 2008, A64*, 112-122.

4.7. Supporting information

- **Figure 4.S1 :** Arylation of aniline with **1** and with **1** in the presence of 20 equiv of water.
- **Figure 4.S2 :** Arylation of aniline with $\text{PhB}(\text{OH})_2$ catalyzed by **1** in the absence and in the presence of triethylamine.
- **Figure 4.S3 :** Conversion-time profiles for the arylation of aniline with $\text{PhB}(\text{OH})_2$ catalyzed by **1**.
- **Figure 4.S4 :** Left: Linear dependence of apparent first-order rate constants on the square-root of the catalyst concentration. Top right: Double-logarithmic plot of initial rates. Bottom right: Double-logarithmic plot of apparent first-order rate constants.
- **Figure 4.S5 :** LMCT-transition in the UV/vis-spectrum in methanol of **1** and **3** and the respective complexes without a *para*-methyl group.
- **Figure 4.S6 :** d-d Transition in the UV/vis-spectrum in methanol of **1** and **3** and the respective complexes without a *para*-methyl group.
- **Figure 4.S7 :** Arylation of aniline with **1** and with **1** + $[\text{NEt}_4]\text{Cl}$.
- **Figure 4.S8 :** Conversion-time profiles for the arylation of aniline with catalyzed with $\text{PhB}(\text{OH})_2$ or with $\text{EtO}_{\text{C}_6\text{H}_4}\text{B}(\text{OH})_2$.
- **Figure 4.S9 :** Cyclic voltammograms of $\text{Cu}(\text{OAc})_2$ and **3** in methanol.
- **Figure 4.S10 :** Semi-logarithmic conversion vs time plot for the *N*-arylation of aniline with **3**/ $\text{Cu}(\text{OAc})_2$ or $\text{Cu}(\text{OAc})_2$ only.
- **Table 4-S1 :** Additional CEL couplings.

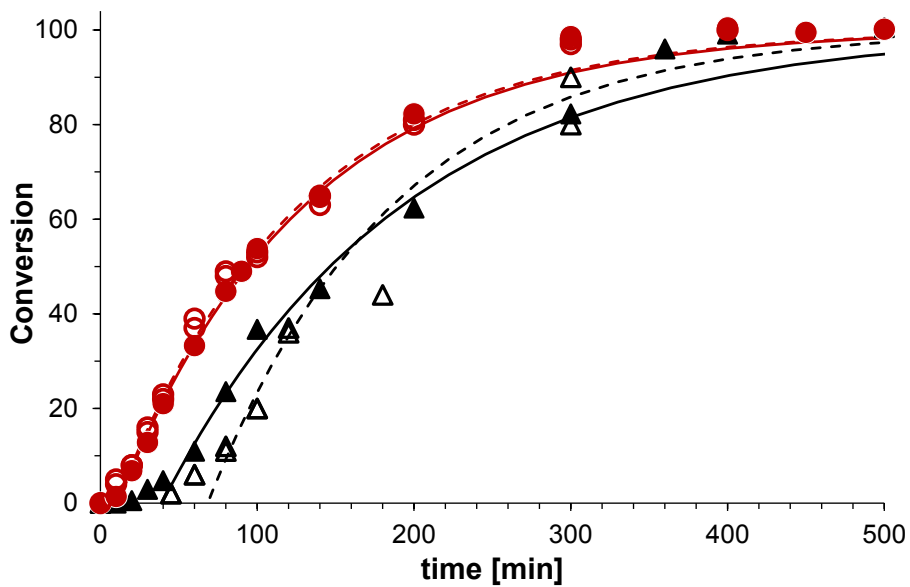


Figure 4.S1 : Arylation of aniline with **1** (black triangles) and with **1** in the presence of 20 equiv of water (hollow triangles, datapoint at 180 min ignored in linear regression analysis), as well as with **3** without (red circles) and with 20 equiv of water added (hollow circles). Conditions: 1.0 M aniline, 1.5 M PhB(OH)₂, 25 mM **1**, MeOH, RT.

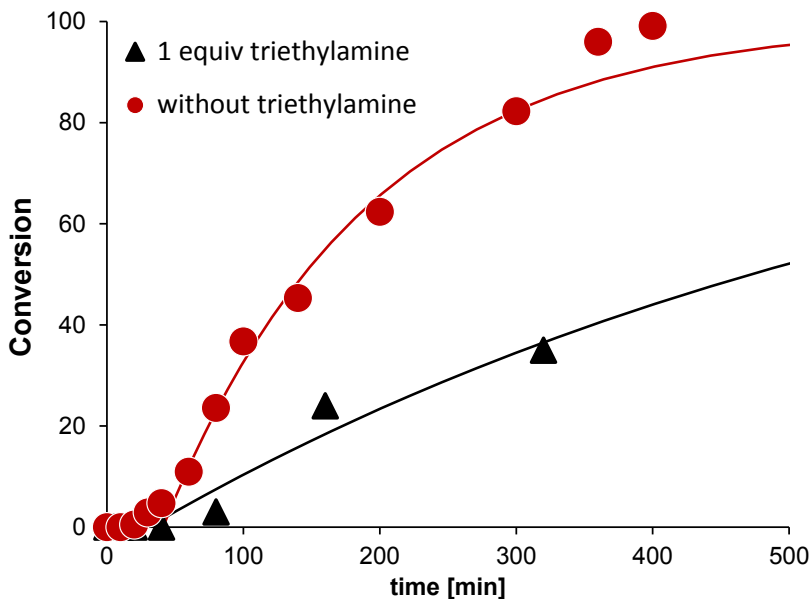


Figure 4.S2 : Arylation of aniline with PhB(OH)₂ catalyzed by **1** in the absence (red circles) and in the presence of triethylamine (black triangles). Both reactions reached 100% conversion after 12 h. Conditions: 1.0 M aniline, 1.5 M PhB(OH)₂, 25 mM **1**, MeOH, RT.

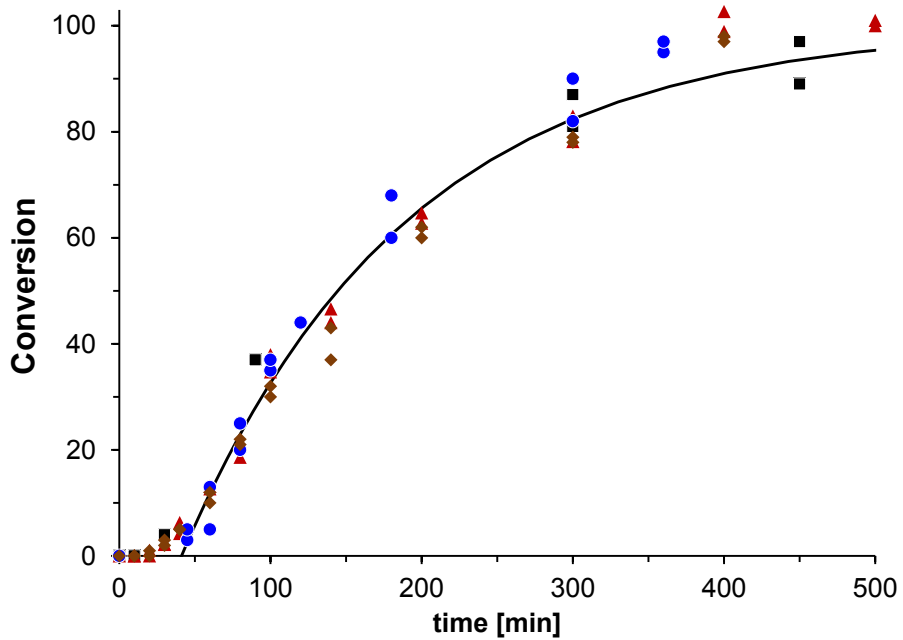


Figure 4.S3 : Conversion-time profiles for the arylation of aniline with $\text{PhB}(\text{OH})_2$ catalyzed by **1**. Four different experiments, conversion points calculated from disappearance of aniline and appearance of product shown. The solid line indicates the simulated conversion with $k_{\text{app}} = 0.40(2) \text{ h}^{-1}$ and $t_0 = 40 \text{ min}$, determined from linear regression of all data points between 80 and 300 minutes in the semi-logarithmic plot. For the deviations at high conversions, see discussion of reaction kinetics. Conditions: 1.0 M aniline, 1.5 M $\text{PhB}(\text{OH})_2$, 25 mM **1**, MeOH, RT.

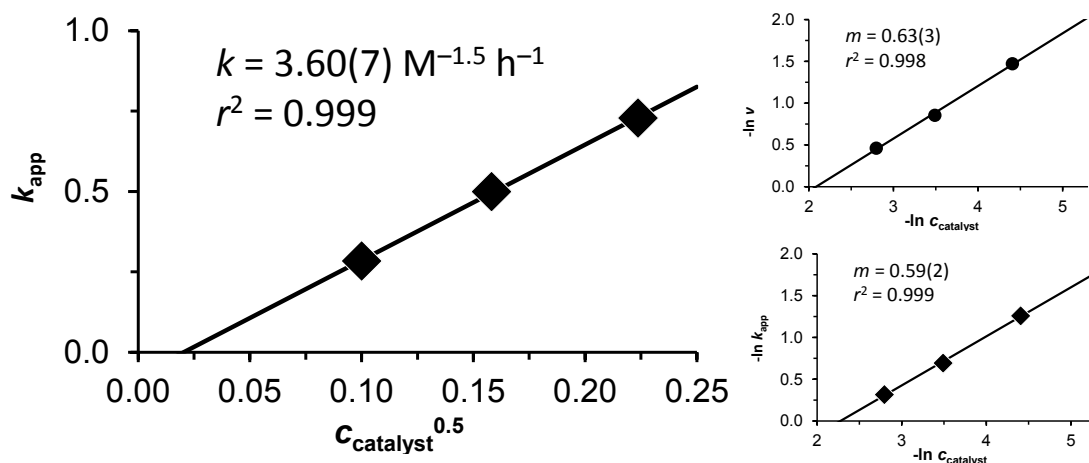
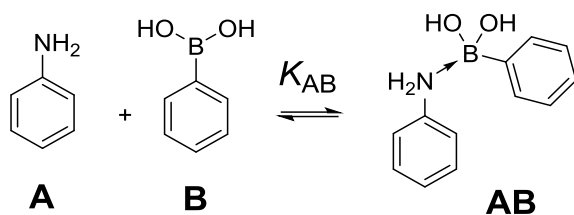


Figure 4.S4 : Left: Linear dependence of apparent first-order rate constants on the square-root of the catalyst concentration. Top right: Double-logarithmic plot of initial rates (less than 30% conversion) at different catalyst concentrations indicate a order in catalyst concentration of

0.63(3). Bottom right: Double-logarithmic plot of apparent first-order rate constants at different catalyst concentration indicate an order in catalyst concentration of 0.59(2). In all cases datapoints are the average of 2 or 4 experiments, respectively.

Independence of the rate law from phenylboronic acid concentration



The equilibrium constant for the formation of a simple Lewis-acid-base adduct (AB) between aniline (A) and phenylboronic acid (B) is given by:

$$K_{AB} = \frac{[AB]}{[A][B]} \quad (1)$$

With $[A]^t$ being the total concentration of unreacted aniline, we can substitute

$$[A]^t = [A] + [AB] \Leftrightarrow [AB] = [A]^t - [A] \quad (2)$$

$$\text{which yields : } K_{AB} = \frac{[A]^t - [A]}{[A][B]} \Leftrightarrow [A] = \frac{[A]^t}{1 + [B]K_{AB}} \quad (3)$$

Starting from a rate-law of : $v = k[A][B][cat.]^{0.5}$

$$\text{substitution with (3) provides : } v = \frac{k[A]^t[B][cat.]^{0.5}}{1 + [B]K_{AB}}$$

The latter simplifies to $v = \frac{k}{K_{AB}} [A]^t [cat.]^{0.5}$ (4), under the condition that $[B]K_{AB} \gg 1$.

Simulation of polymerization kinetics

Given the complicated nature of the rate-law, possible values were determined by fitting numerically simulated conversion curves to observed data without integration of the rate law. From the rate law

$$v = k[A][B][cat.]^{0.5}$$

conversion profiles were iteratively calculated from

$$\Delta[product] = -\Delta[A] = -\Delta[B] = k[A][B][cat.]^{0.5} \Delta t$$

Concentration of free aniline is obtained from (1) and

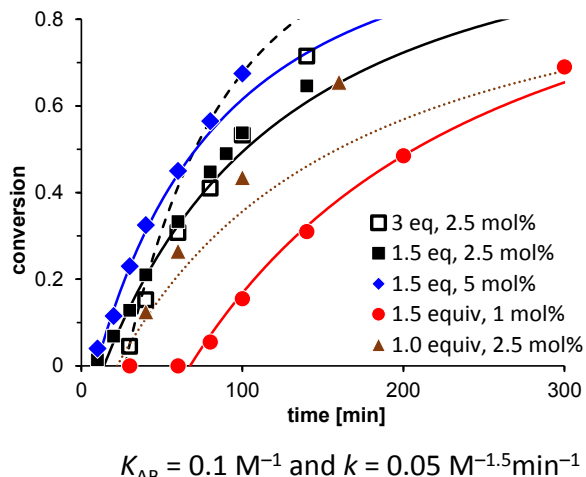
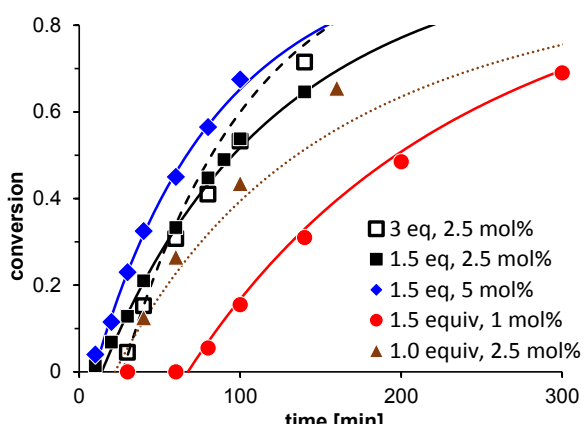
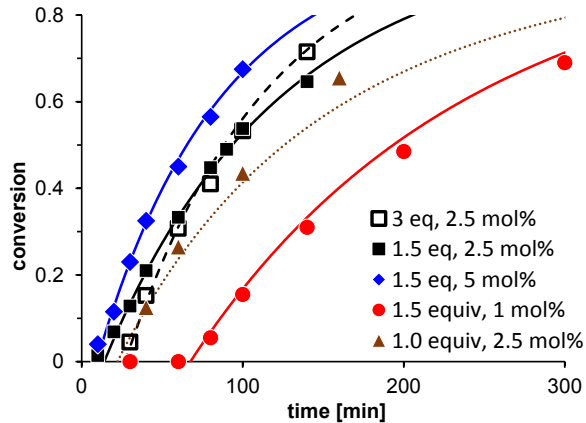
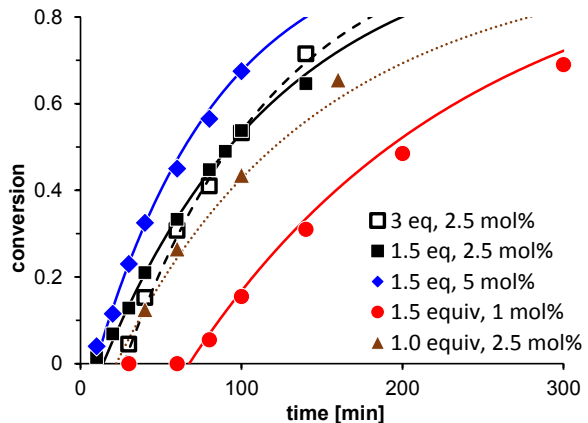
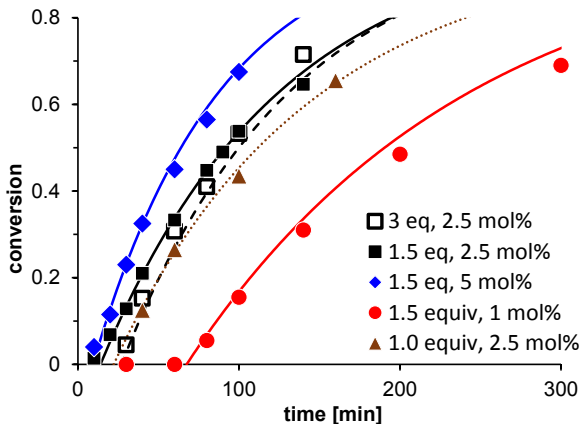
$$[A]^t = [A] + [AB] \text{ and } [B]^t = [A]^t + [B]^{ex}$$

where $[B]^{ex}$ is the excess of phenylboronic acid and $[A]^t$ and $[B]^t$ are the total concentrations of unreacted aniline and phenylboronic acid. This yielded :

$$[A] = \frac{\sqrt{4[A]^t K_{AB} + (1 + K_{AB}[B]^{ex})^2} - 1 - K_{AB}\Delta[B]^{ex}}{2K_{AB}}$$

Equilibrium constants and rate constants determined by fitting of the kinetic data with this model should *not* be considered absolute values to describe elemental reactions or equilibria! The current model neglects the presence of other Lewis acids ($B(OH)_3$ formed during the reaction) and other Lewis bases (diphenylamine formed during the reaction) and represents the *apparent* rate law and equilibria of a more complicated situation.

In addition to this, the reaction proved to be close to the simplified rate law (4) (independence from phenylboronic acid concentration), with the apparent, observed rate constant $k_{obs} = k[cat]^{0.5}/K_{AB}$. K_{AB} and k were thus strongly correlated and a large number of essentially identical solutions can be found (see graphic next page). Free refinement provided $K_{AB} = 5 \text{ M}^{-1}$, but essentially identical solutions were found for $K_{AB} = 1 - 10 \text{ M}^{-1}$. When K_{AB} was set to $K_{AB} = 0.1 \text{ M}^{-1}$ or 20 M^{-1} , the observed increase in activity with 3.0 M PhB(OH)_2 was either under- or overestimated.



UV/vis spectra of **1** and **3**

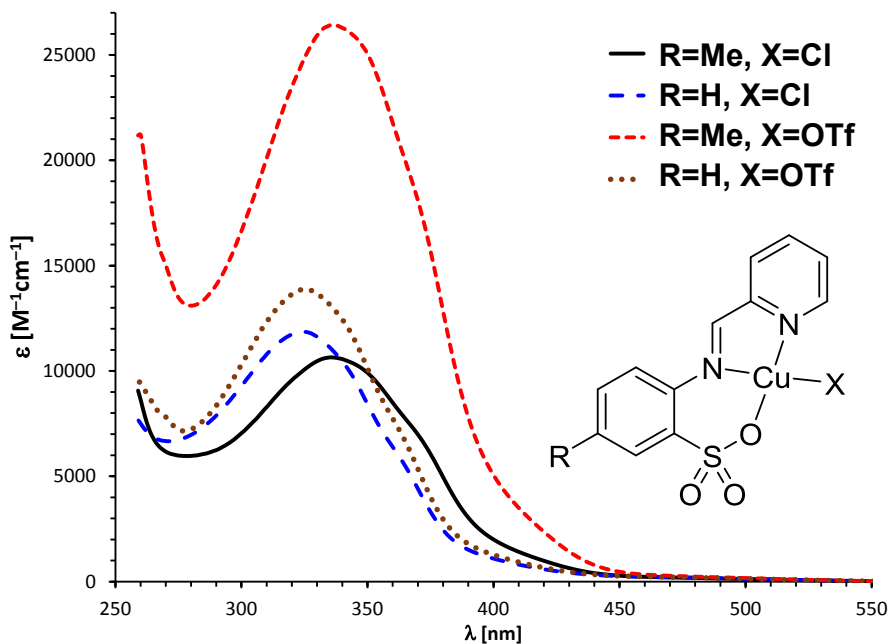


Figure 4.S5 : LMCT-transition in the UV/vis-spectrum in methanol of **1** and **3** and the respective complexes without a *para*-methyl group.

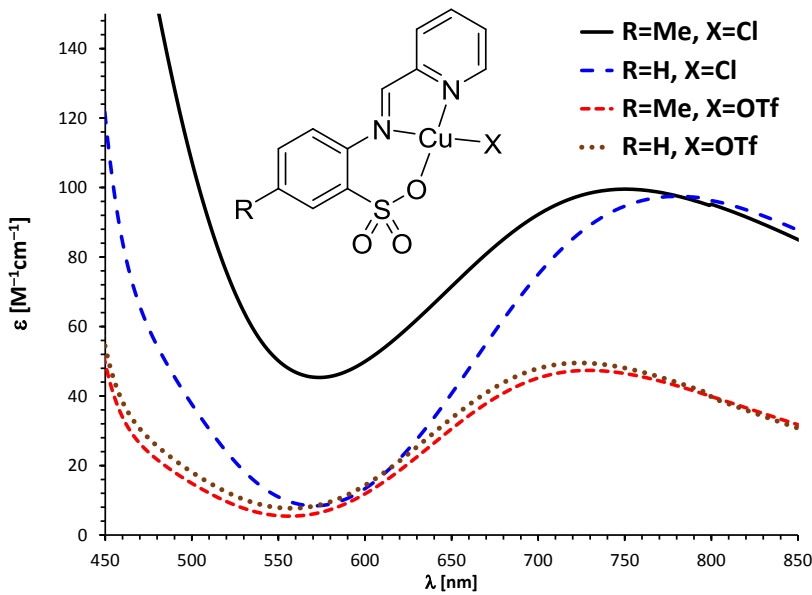


Figure 4.S6 : d-d Transition in the UV/vis-spectrum in methanol of **1** and **3** and the respective complexes without a *para*-methyl group.

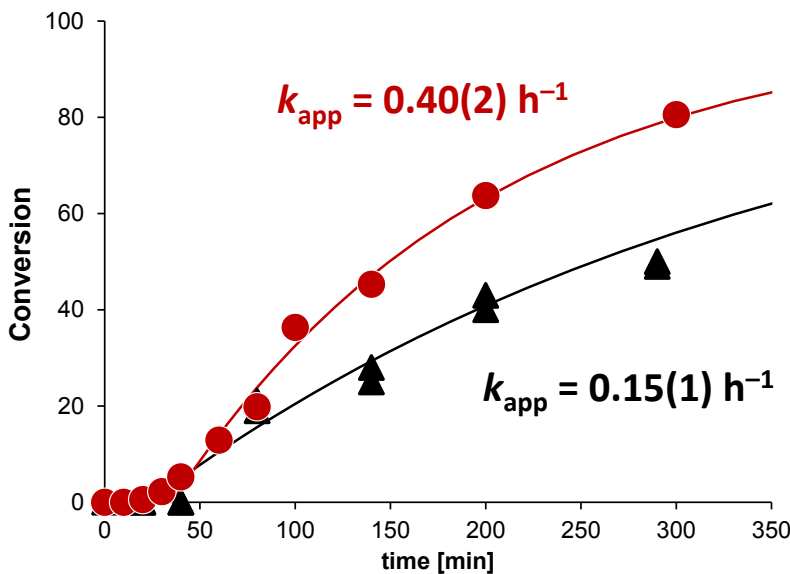


Figure 4.S7 : Arylation of aniline with **1** (red circles) and with **1** + $[\text{NEt}_4]\text{Cl}$ (black triangles). Both reactions reach completion after 12 h.

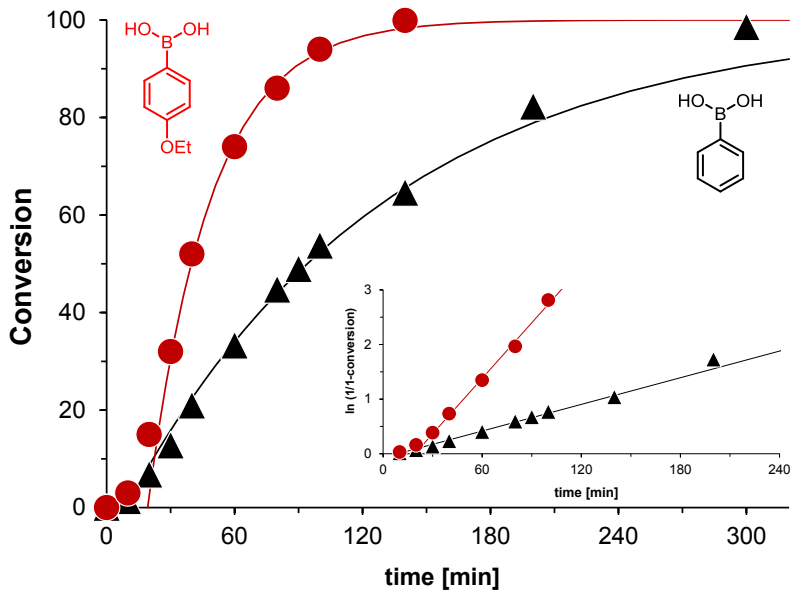


Figure 4.S8 : Conversion-time profiles for the arylation of aniline with catalyzed with $\text{PhB}(\text{OH})_2$ (black triangles, $k_{\text{app}} = 0.50(1) \text{ h}^{-1}$) or with $\text{EtOC}_6\text{H}_4\text{B}(\text{OH})_2$ (red circles, $k_{\text{app}} = 2.03(8) \text{ h}^{-1}$). Conditions: 1.0 M aniline, 1.5 M $\text{ArB}(\text{OH})_2$, 25 mM **3**, MeOH, RT.

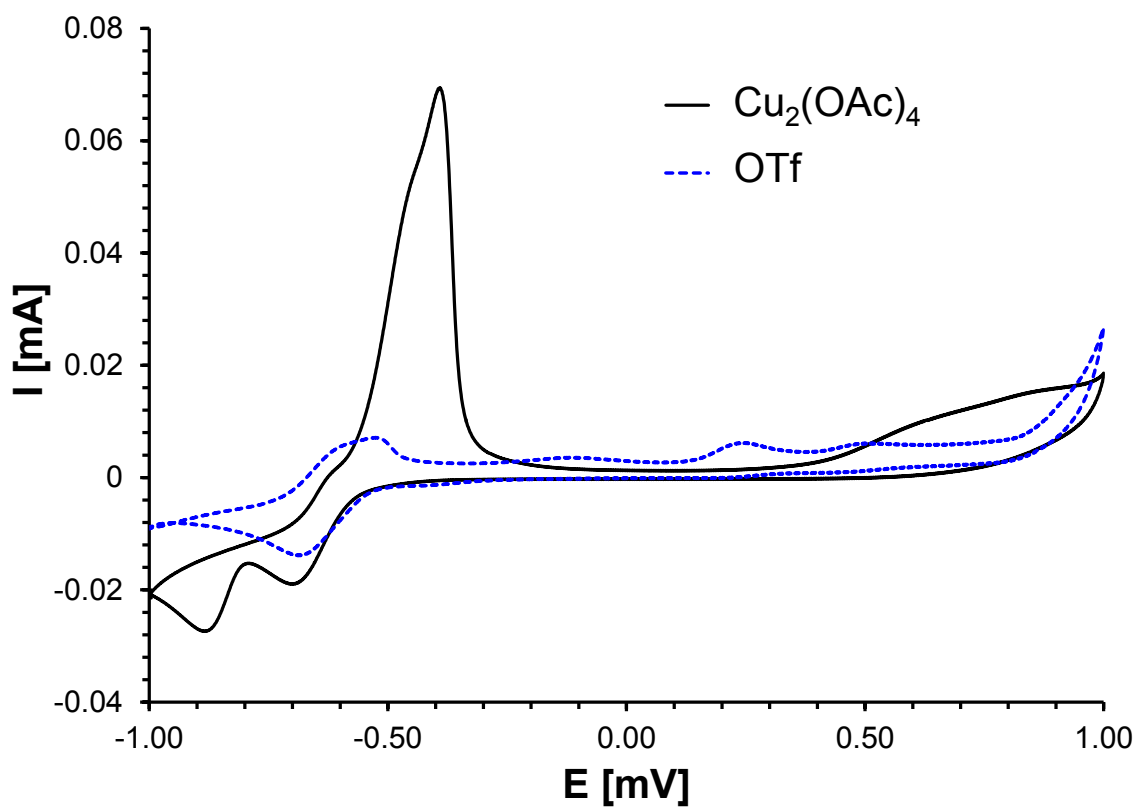


Figure 4.S9 : Cyclic voltammograms of $\text{Cu}(\text{OAc})_2$ (black, solid line) and **3** (broken, blue line) in methanol. The $\text{Cu}_2(\text{OAc})_4$ paddlewheel dimer shows two $\text{Cu}(\text{II})/\text{Cu}(\text{I})$ reduction peaks. The respective oxidation peak is overshadowed by a large peak attributed to copper-deposition on the electrode. Oxidation is, as expected, ill defined and non-reversible.

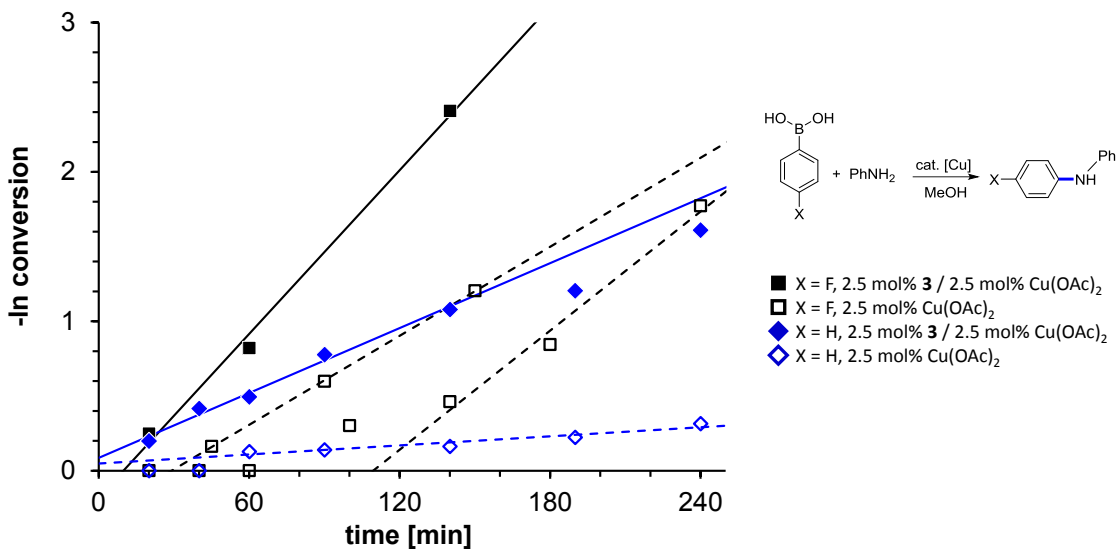


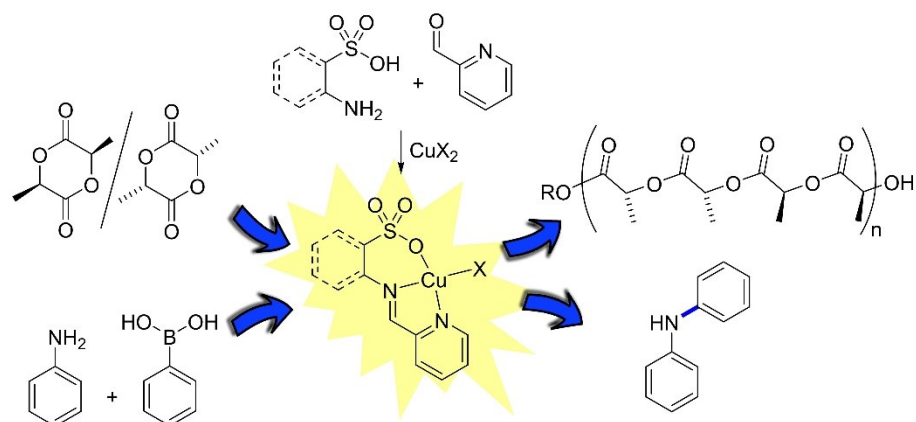
Figure 4.S10 : Semi-logarithmic conversion vs time plot for the *N*-arylation of aniline with **3**/Cu(OAc)₂ or Cu(OAc)₂ only. solid squares: **3**/Cu(OAc)₂, FC₆H₄B(OH)₂; hollow squares: Cu(OAc)₂, FC₆H₄B(OH)₂; solid diamonds: **3**/Cu(OAc)₂, PhB(OH)₂; hollow diamonds: Cu(OAc)₂, PhB(OH)₂. (MeOH, RT, 1.0 M aniline, 1.5 equiv ArB(OH)₂).

Table 4-S1 : Additional CEL couplings

	ArB(OH)₂	RNH₂	Conditions ^a	T	time	conversion
1	PhB(OH) ₂	Aniline	2 as catalyst	RT	12 h	no reaction
2	PhB(OH) ₂	Ph ₂ NH		RT	12 h	no reaction
3	PhB(OH) ₂	Ph ₂ NH	O ₂	50 °C	12 h	no reaction
4	PhB(OH) ₂	(<i>n</i> Oct)PhNH		RT	12 h	no reaction
5	PhB(OH) ₂	(<i>n</i> Oct)PhNH	O ₂	50 °C	12 h	no reaction
6	PhB(OH) ₂	Aniline	2.5 equiv PhB(OH) ₂	RT	12 h	100% monoarylation
7	PhB(OH) ₂	<i>n</i> OctNH ₂	2.5 equiv PhB(OH) ₂	RT	12 h	100% monoarylation
8	PhB(OH) ₂	Aniline	2.5 equiv PhB(OH) ₂ , 50 µL water	50 °C	12 h	100% monoarylation
9	PhB(OH) ₂	<i>n</i> OctNH ₂	2.5 equiv PhB(OH) ₂ , 50 µL water	50 °C	12 h	100% monoarylation
10	PhB(OH) ₂	Aniline	2 equiv PhNH ₂ , 1 equiv PhB(OH) ₂ , 1 equiv B(OH) ₃	RT	2 h	9%
11	PhB(OH) ₂	Aniline	2 equiv PhNH ₂ , 1 equiv PhB(OH) ₂ , 1 equiv B(OH) ₃	RT	12 h	15%
12	PhB(OCH ₂) ₂	Aniline	2 equiv PhNH ₂ , 1 equiv PhB(OCH ₂) ₂ , 1 equiv B(OH) ₃	RT	2 h	5%
13	PhB(OCH ₂) ₂	Aniline	2 equiv PhNH ₂ , 1 equiv PhB(OCH ₂) ₂ , 1 equiv B(OH) ₃	RT	12 h	12%
14	PhB(OCH ₂) ₂	Aniline	+ 1.2 equiv <i>t</i> BuOO <i>t</i> Bu	RT	12 h	100%
15	PhB(OCH ₂) ₂	Aniline	+ 1.2 equiv TEMPO	RT	12 h	100%
16	PhB(OCH ₂) ₂	Aniline	+ 1.2 equiv 4-phenylpyridine-oxide	RT	12 h	50%
17	IC ₆ H ₄ B(OH) ₂	<i>n</i> OctNH ₂	+ 1.2 equiv <i>t</i> BuOO <i>t</i> Bu or TEMPO or 4-phenylpyridine-oxide	RT	12 h	no reaction

^a Methanol, air, 1.0 M nucleophile, 1.5 M ArB(OH)₂, 2.5 mol% **3**

5. Anion influences on the structures of pyridyl-iminosulfonate copper(II) complexes and their reactivity in *rac*-lactide polymerization and Chan-Evans-Lam couplings

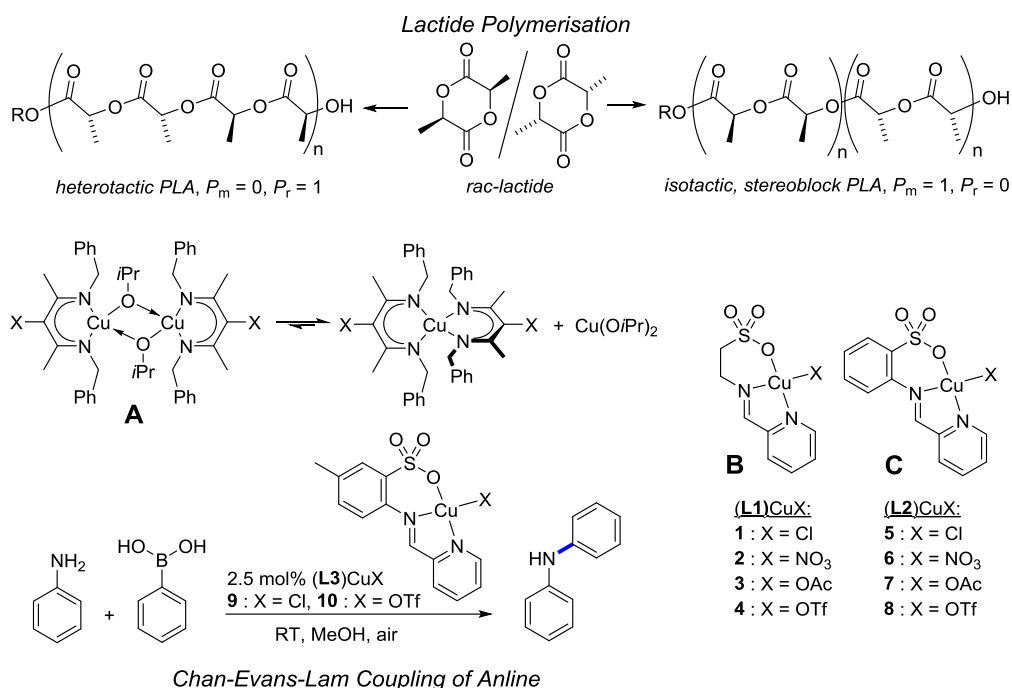


V. Hardouin Duparc, A. Thouvenin, F. Schaper *Dalton Trans.* **2018**, submitted.

Contributions from Alexandre Thouvenin : Several experiments of lactide polymerization and Chan-Evans-Lam coupling with complexes having an aliphatic backbone.

5.1. Introduction

Copper complexes have found very widespread use as catalysts,^{1, 2} in particular due to their rich oxidation chemistry, which allows Cu(I)/Cu(III) two-electron transfer mechanisms as well as Cu(I)/Cu(II)/Cu(III) single electron transfers to participate in catalysis. We have in recent years studied the application of copper catalysts in *rac*-lactide polymerisation³⁻¹⁰ and in Chan-Evans-Lam couplings.¹¹⁻¹³ Isotactic stereocontrol in *rac*-lactide polymerisation is still a challenge,¹⁴⁻³³ despite several highly promising catalytic systems,³⁴⁻⁴³ in particular when combined with high activity and good polymer molecular weight control. Diketiminate copper alkoxides (Scheme 5-1, **A**) proved to be among the most active lactide polymerisation catalysts, without any evidence for transesterification or chain-transfer side reactions, even under monomer-starved conditions.^{3, 4} The complexes were, however, highly susceptible to forming homoleptic copper diketiminate complexes in the Schlenk equilibria whenever stabilization via a dimeric species was not possible. We decided to investigate pyridyliminosulfonate copper complexes (Scheme 5-1, **B+C**) as potential catalytic systems. The latter should provide higher stability against ligand exchange and a higher stability against oxidation and protic substrates.



Scheme 5-1

Chan-Evans-Lam couplings are oxidative, copper-catalyzed couplings between a boronic acid and a second nucleophile, with copper(II) acetate being the most widely employed catalysts.⁴⁴⁻⁵⁸ We have recently shown that copper pyridyliminosulfonates (Scheme 5-1, **9+10**) are potent catalysts for CEL couplings with *N*-nucleophiles.^{12, 13} The presence of a dinuclear copper-boron complex, bridged by acetate, methoxide or hydroxide has been proposed as an intermediate prior to transmetallation.⁵⁹⁻⁶¹ We hypothesized that the sulfonate group in the ligand can likewise act as bridging ligand, which – in combination with the solubilisation and controlled environment provided by the rest of the ligand – would provide a more general reaction protocol.¹¹ Indeed, complexes **9** and **10** provided high and general reactivity for CEL couplings of primary amines, cyclic or acyclic secondary amines, anilines, imidazole, pyrazole and tetrazole.^{12, 13} At the same time, they did not show evidence of common side reactions in CEL couplings, such as deboration, coupling with water or homocoupling. To provide further support that the sulfonate group rather than the counteranion coordinates to boron, we will investigate here the reactivity of pyridyliminosulfonate copper complexes **C** and taurylimino-pyridine complexes of type **B** with different counteranions to address the influence of potential sulfonate dissociation.

Complexes of the general type **B** or **C** have been well-reported in the literature. Copper complexes with a pyridylmethylenetaurate ligand, **L1**, have been investigated by Jiang and Li, as well as by others. Heteroleptic complexes (**L1**)CuX have been reported for X = dicyanamide,⁶² Cl,⁶³ N₃⁻,^{64, 65} as well as ClO₄⁻.^{66, 67} The azide and perchlorate complexes crystallize as dimers, all others formed coordination polymers in the solid state. The respective complexes with the more rigid pyridylmethylenebenzenesulfonate ligand **L2** have been studied by Pombeiro and others. Complexes (**L2**)CuX with chloride,^{68, 69} carboxylate,^{69, 70} thiocyanate,⁷¹ azide,⁷¹ or cyanamide⁷¹ were prepared, as well as the homoleptic complex (**L2**)₂Cu.⁷² The chloride complex crystallized as a chloride-bridged dimer, but monomeric complexes were obtained with additional coordination of pyridine or water.⁷³ With an azide, thiocyanate or carboxylate anion, the complexes likewise crystallized as anion-bridged dimers, but a monomeric complex was obtained in one case.⁶⁴ (**L1/L2**)CuX complexes were mostly investigated with respect to the formation of coordination polymers and their magnetic properties, although Pombeiro also investigated their application as catalyst for alkane oxidation and the Henry reaction.^{69, 71}

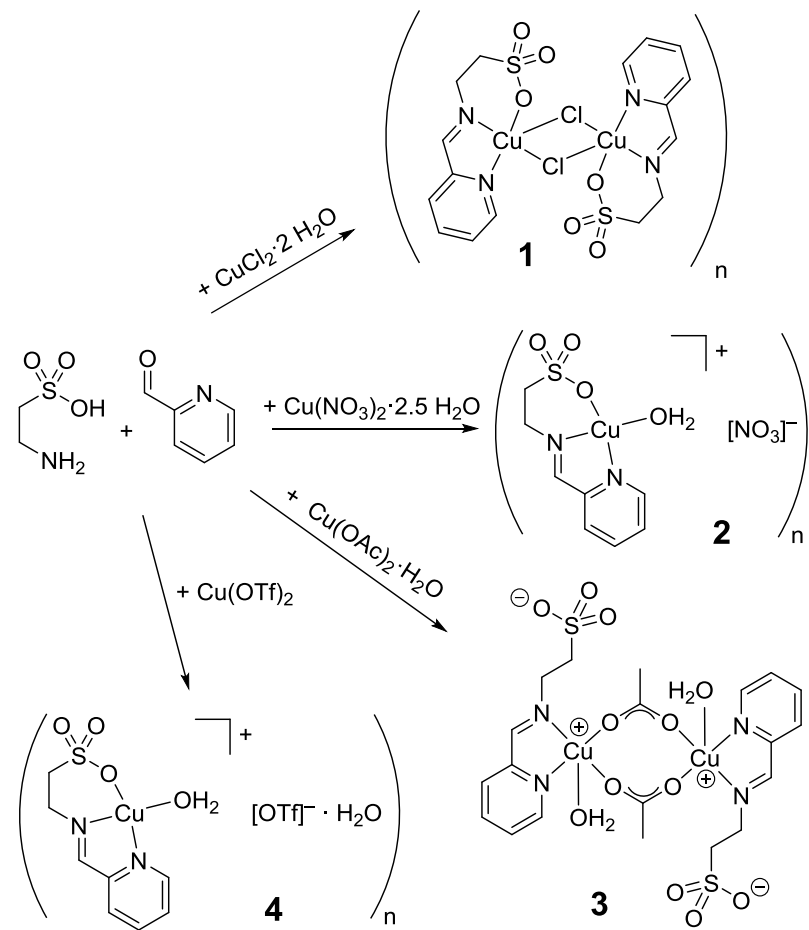
5.2. Results and discussion

5.2.1. Ligand and complex syntheses and structures

Taurine-based ligands and complexes. Preparations of the potassium and the sodium salts of **L1H** have been reported,^{62, 64, 65} but the product was either used without characterization or characterized only by slightly divergent elemental analyses and IR-spectroscopy. In our hands, all attempts to prepare **L1H** or **L1K** by condensation of taurine and pyridylaldehyde following either literature conditions or modified reaction protocols (azeotropic water removal, molecular sieves, EtOH/HCl, or others) failed to produce clean products. Instead, either starting material, side products (such as the pyridylcarbaldehyde-ketal from reactions in alcohol) or unseparable mixtures were obtained. Vittal noted that analyses were complicated/hindered by the high hygroscopy of **L1** and prepared the ligands *in situ* “due to their inherent instability”.⁶⁶ Nitschke investigated the reaction of taurine with pyridinecarboxaldehyde by NMR and found that in aqueous solution the condensation

product $[\text{L1}]^-$ is formed only to 34%, but that upon addition of a metal salt, in Nitschke's case Cu(I), the stabilization of the resulting complex led to quantitative conversion into the iminosulfonate ligand.⁷⁴ To test if this was a thermodynamic effect or a metal-catalyzed template reaction, a copper(II) salt was added in catalytic quantities (5 mol%) in our attempts to prepare **L1H** or **L1K**, but the free ligand was still not obtained. We thus concluded that **L1H** or **L1K** hydrolyze readily, which prevented the isolation of pure products in our case. It is possible that in preparations reported for $[\text{L1}]^-$, mixtures were also obtained, which assembled into the ligand only upon subsequent reaction with the metal cation.

Copper complexes (**L1**)CuX were thus prepared by *in-situ* condensation of the ligand on the complex, in slight adaptation of the preparations employed by Vittal for **1** and Pombeiro for **5**:^{66, 69} after a short pre-reaction of taurine and pyridinealdehyde, a suitable copper salt was added to provide directly the respective copper complexes (Scheme 5-2). In addition to the previously reported chloride complex (**L1**)CuCl,^{63, 66} complexes with nitrate, acetate or triflate anions were prepared (Scheme 5-2). The chloride complex **1** surprisingly did not undergo anion exchange when reacted with AgOTf, most likely due to the low solubility of the chloride complex. Triflate complex **4** was thus prepared directly from Cu(OTf)₂ (Scheme 5-2).



Scheme 5-2

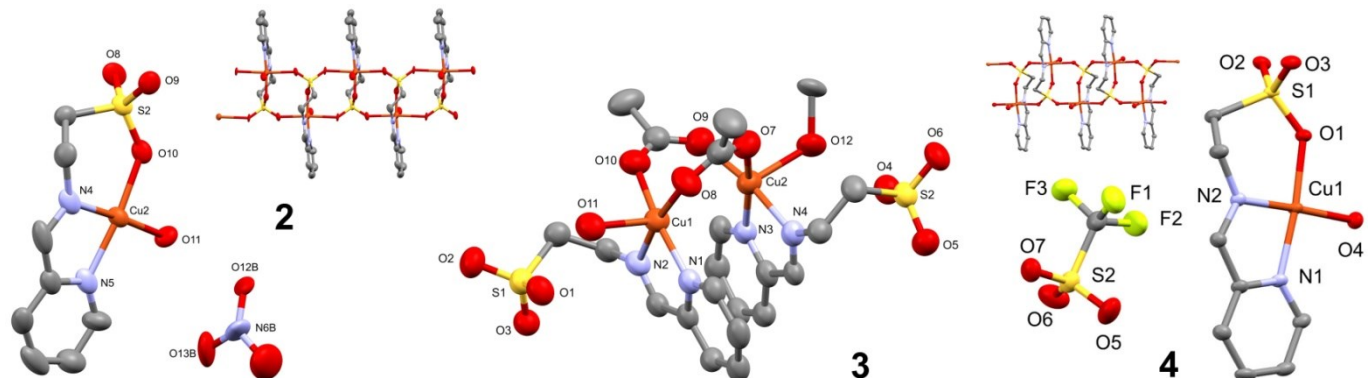


Figure 5.1 : X-ray structures of **2** (left), **3** (middle), and **4** (right). Hydrogen atoms, second molecule in the asymmetric unit (**2**) and anion disorder (**2**) omitted for clarity. Thermal ellipsoids are drawn at the 50% probability level. The insets show the 1D-coordination polymers formed by **2** and **4**.

Chloride complex **1** crystallizes under these conditions in the same structure as reported in the literature: a chloride bridged dimer, which forms a coordination polymer by

bridging coordination of the sulfonate groups.⁶³ Nitrate complex $\{[(\mu-\textbf{L1})\text{Cu}(\text{OH}_2)][\text{NO}_3]\}_n$, **2**, likewise forms a 1D-coordination polymer by bridging coordination of the sulfonate groups of two neighbouring molecules. The nitrate anion is dissociated from the metal center and water completes the Jahn-Teller distorted octahedral geometry around copper. The ligand occupies equatorial positions, while the bridging oxygen atoms occupy axial positions (Fig. 5.1, Table 5-1). Triflate complex **4** is essentially isostructural with the nitrate complex (Fig. 5.1, Table 5-1).

The acetate anion prefers a bridging coordination between two copper centers and **3** crystallizes as a dimeric complex with both copper centers in a square-pyramidal environment (Fig. 5.1, Table 5-1). The sulfonate group is dissociated from the metal center and disordered water/methanol solvent completes the coordination sphere by coordination in the apical position. The structure seems to be stabilized by a π -stacking arrangement of the iminopyridyl moieties, which bend by 13–15° out of the equatorial plane of the respective copper complex to achieve a coplanar arrangement (angle between planes = 7°, 3.2 Å distance).

Ligand-copper bond distances are in the range expected for square-pyramidal or octahedral copper(II) complexes and are in general similar to those of other (**L1**)CuX complexes (Cu-N(=C): 1.97 – 2.01 Å, Cu-N_{Py}: 2.00 – 2.02 Å, Cu-OSO₂: 1.97 – 1.99 Å).^{62–64, 66, 67, 75} The cationic complexes **2** and **4** show slightly shorter copper-ligand bond lengths (0.03 – 0.06 Å) than neutral complexes **3** and **1**. Ligands in the “weaker” apical coordination sites of the square-pyramidal or distorted octahedral complexes show 0.2 – 0.4 Å longer bond distances to copper (c. f. water in **3** compared to water in **2** or **4**. The same is observed for the Cu-sulfonate bond distances.)

Table 5-1 : Ligand-copper bond distances for taurine-based complexes.

	2	3	4	1^a
Cu-OSO ₂	1.976(10), 1.952(10)		1.999(3), 2.304(3), 2.352(3)	1.966(2), 2.735(2)
Cu-N(=C)	1.979(4), 1.970(15)	2.042(10), 2.028(10)	1.984(3)	2.005(2)
Cu-	2.016(13),	2.002(10),	2.019(3)	2.014(3)
N _{Pyridine}	2.002(13)	2.017(10)		
Cu-O ^b	1.982(10); 1.985(12)	2.202(10) - 2.230(10)	1.973(3)	
Cu-X		1.933(10) - 1.963(10)		2.260(1), 2.777(1)
Geometry	octahedral	square pyramidal	octahedral	octahedral
τ		0.0, 0.0		

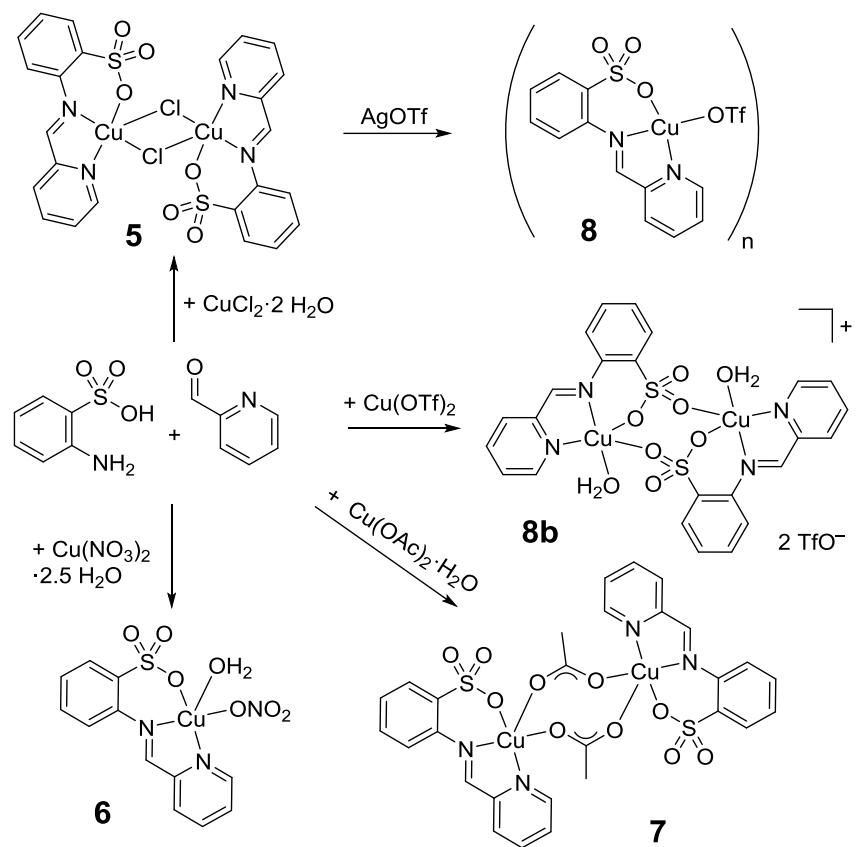
^a Taken from ref. ⁶³ ^b **4, 2:** H₂O, **3:** Water and methanol disordered at these two positions. Bond lengths should not be considered to be more accurate than ±0.1 Å

Orthanilic acid-based ligands and complexes. As for the taurine-based ligands, we were unable to isolate pure samples of the ligand either in the acidic form **L2H** or as a potassium salt **L2K**. Complexes **5, 6, 7** and **8** carrying different anions were thus also prepared by *in-situ* condensation of the ligand on the complex (Scheme 5-3), in slight adaptation of the procedure reported for **5**.⁶⁹

Complex **5** crystallized as the water-free, chloride bridged dimer reported earlier.^{68, 73} Under the conditions employed, **6** crystallized as a water-coordinated, mononuclear complex with square-pyramidal geometry (Fig. 5.2, Table 5-2). The nitrate anion is monocoordinated and water is found in the apical position. The structure resembles closely that of the respective water-coordinated chloride complex.⁷³ As for the taurine-based complexes, the acetate anion prefers a bridging coordination between two copper centres. **7** thus crystallizes as a dimer with bridging acetate anions and a square-pyramidal coordination geometry around copper. The complex is highly unsymmetrical, with one acetate being coordinated in the equatorial

position of both complexes, the other in the equatorial position of one, but the apical position of the other complex. Consequently, the sulfonate group is found either in the equatorial position with a low torsion angle of 31° between the two aryl rings or in the apical position, which forced a near-perpendicular orientation of the aryl rings (82°). A similar coordination geometry has been observed in the respective cyclohexylenedicarboxylate complex.⁶⁹

Reaction of **5** with Ag[OTf] yielded the triflate complex **8**. As in **6**, copper is found in a square-pyramidal coordination geometry formed by coordination of an additional ligand in the apical position. Instead of water, a bridging sulfonate plays this role in **8**, resulting in a 1D-coordination polymer. **8** can also be prepared directly from Cu(OTf)₂. For the respective methyl substituted complex, **10** (Scheme 5-1), an excess of triflate was required via this pathway.¹³ Reaction with excess Cu(OTf)₂ yielded in this case, however, only very small amounts of crystalline material, which was identified as **(8)₂·Cu(OTf)₂·10 H₂O** (Fig. 5.S1). Reactions with stoichiometric amounts of Cu(OTf)₂ afforded **8**, which crystallized under these conditions as the dimeric compound **(8·H₂O)₂**, **8b**, again with bridging sulfonate groups. The triflate anion was replaced by a water ligand in the copper coordination sphere. Although a τ -value of 0.4 indicates a geometry intermediate between square-pyramidal and bipyramidal, **8b** displays four short Cu-L distances of 1.9 – 2.0 Å and one elongated Cu-L distance of 2.3 Å and is thus best described as distorted square-pyramidal.



Scheme 5-3

Table 5-2 : Ligand-copper bond distances for orthanilic acid-based complexes.

	9^a	5^b	6	7	8	8b	10^a	10b^c	15
Cu-OSO ₂	1.969(1)	1.964(2)	1.954(2)	1.953(2), 2,443(2)	1.935(2), 2.249(2)	1.941(2), 2.281(2)	1.929(1), 2.379(1)	1.934(1), 2.235(1)	1.986(1)
Cu-N(=C)	2.051(1)	2.068(2)	2.030(2)	2,042(2), 1.994(2)	2.005(2)	2.016(2)	2.026(1)	2.023(2)	2.020(1)
Cu-N _{Pyridine}	1.992(1)	2.002(2)	1.973(3)	1.977(2), 2.008(2)	1.972(2)	1.967(3)	1.967(1)	1.967(2)	1.996(1)
Cu-L	2.307(1)		2.254(2)			1.987 (2)		1.993(2)	2.020(1) (Pyr.) 2.362(1) (OH ₂)
Cu-X ^a	2.243(1)	2.276(1), 2.678(1)	1.977(2)	1.931(2), 2.166(2)	1.952(2)		2.015(1)		2.390(1)
Geometry	square- pyramidal	square- pyramidal	square- pyramidal	square- pyramidal	square- pyramidal	square- pyramidal	octahedral	square- pyramidal	octahedral
τ	0.1	0.0	0.1	0.1, 0.1	0.1	0.4		0.5	
δ	27°	20°	28°	30°, 82°	34°	36°	36°	27°	30°
Phenyl/pyridyl									

^aTaken from ref. ¹². ^bTaken from ref. ⁷⁶. ^cTaken from ref. ¹³

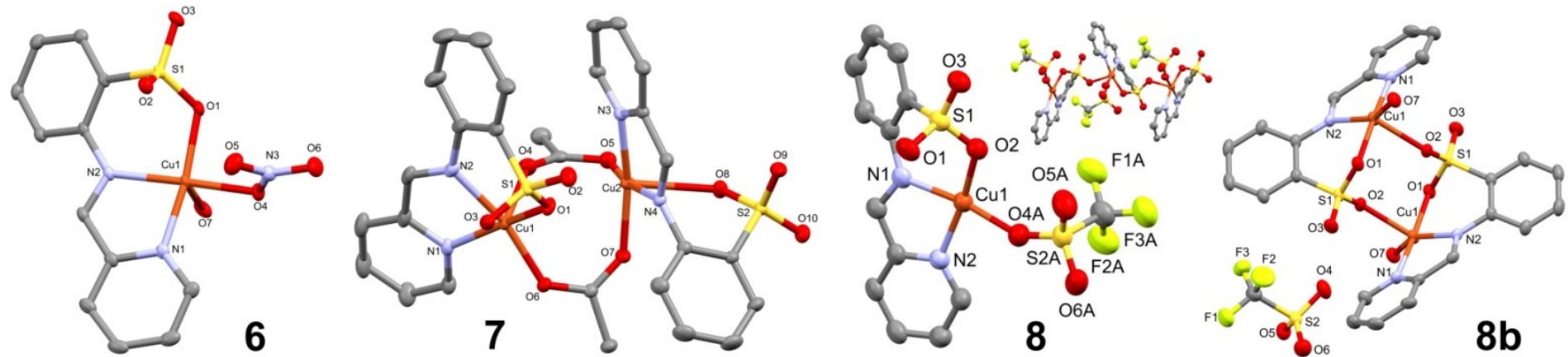


Figure 5.2 : X-ray structures of **6** (left), **7** (middle), and **8** (middle) and **8b** (right). Hydrogen atoms and anion disorder in **8** omitted for clarity. Thermal ellipsoids are drawn at the 50% probability level. The inset shows the 1D-coordination polymers formed by **8**.

Ligand-copper bond distances in all complexes are again similar to those of other (**L2**)CuX or (**L3**)CuX complexes (Cu-N(=C): 1.97 – 2.11 Å, Cu-N_{Py}: 1.97 – 2.03 Å, Cu-OSO₂: 1.93 – 2.00 Å. For definition of L3 see Scheme 5-1). As expected, chloride and acetate derivatives show a higher tendency to coordinate to the metal centre than nitrate or triflate. This is supported in the formation of the respective pyridine adduct complexes: for **5**, Paul et al. reported the existence of a dinuclear $\{(\text{L2})\text{Cu}(\mu\text{-Cl})\}_2$ structure, which can be converted to the respective neutral mononuclear complexes (**L2**)Cu(OH₂)Cl or (**L2**)Cu(py)Cl (py = pyridine).⁷³ Similarly, we obtained **9** as a monomeric, water-coordinated neutral complex (**L3**)Cu(OH₂)Cl (Scheme 5-1),¹² which in the presence of DMAP replaced water to form (**L3**)Cu(DMAP)Cl, **11** (DMAP = dimethylaminopyridine, Fig. 5.S2, Table 5-S1). When the anion is nitrate, however, crystallization of **2** in the presence of DMAP replaced the *anion* from the coordination sphere and retained a methanol solvent to form the cationic complex $[(\text{L2})\text{Cu}(\text{DMAP})(\text{MeOH})][\text{NO}_3]$, **12** (Fig. 5.S2, Table 5-S1).

In comparison, complexes with ligand **L1** have a higher tendency to form cationic complexes, either by dissociation of the anion (**2**, **4**) or by dissociation of the sulfonate ligand moiety (**3**). In **L2**-based complexes, dissociation of the sulfonate group is disfavoured due to the more rigid ligand backbone and dissociation of the anion is likewise less pronounced. Only **8b** crystallized as a cationic complex upon dissociation of the anion, and even for this complex the polymorph **8** with a coordinated triflate anion was obtained under slightly different conditions.

UV-vis spectroscopy. UV-vis spectra of the copper complexes in DMSO show a d-d transition with $\lambda_{\max} = 692 - 731$ nm (**1-4**) or $\lambda_{\max} = 716 - 779$ nm (**5-8**), respectively. In the high-energy end of the spectrum, a broad transition with several maxima (shoulders) is observed at $\lambda_{\max} = 288$ nm (**1-4**) or $\lambda_{\max} = 305 - 325$ nm (**5-8**), respectively (Fig. 5.3), which is most likely mixture of ligand-centered transitions and LMCT(s). Addition of a methyl-substituent on the benzene sulfonate ring causes a slight bathochromic shift of 10 nm of this transition (**5** and **8** vs. **9** and **10**, Scheme 5-1),¹³ which is in agreement with a charge transfer transition from the aminobenzenesulfonate to either the metal centre or the pyridine ring. While UV-vis-spectra of **L1** or **L2** have not been reported, 2-iminomethylene-pyridines show UV-vis-transitions at 270 nm if the substituent on N is alkyl, and at 325 nm, if the substituent

is an aryl,^{77, 78} in good agreement with the differences between **L1**-based **1-4** and **L2**-based **5-8**.

There is no (< 2nm) variation in the transition at 288 nm or 324 nm, respectively upon variation of the anion. Only in **7** is a significant variation in λ_{max} , form and intensity of the transition observed. The crystal structure of **7** shows an unsymmetrical dimer, in which the benzenesulfonate rings display drastically different torsion angles of either 30°, comparable to **5, 6** and **8**, or close to 90°. It is thus highly likely that the dimeric structure observed in the crystal structure of **7** is retained in solution and that the broadened transition is caused by the different degrees of electronic communication in the two ligand moieties. For the d-d transition a distinct effect of the anion is observed and indicates some interaction with the anion in solution. For CEL couplings with **9** and **10**, anion dissociation equilibria were found to participate in the catalytic cycle,¹³ which would be in agreement with the observations herein.

There is no clear correlation between the nature of the anion and the position of the d-d transition, but relative values of λ_{max} and ϵ are very similar in the series **1-4** and **5-8** (e. g. acetate complexes **1** and **5** show the highest ϵ , triflate complexes **4** and **8** the lowest ϵ , and chloride complexes **1** and **5** the most bathochromic transition). Taurine- and orthanilic acid-based complexes thus likely show similar structures in solution. Polymorphs **8** and **8b** have essentially identical spectra and thus show, unsurprisingly, the same structure in solution.

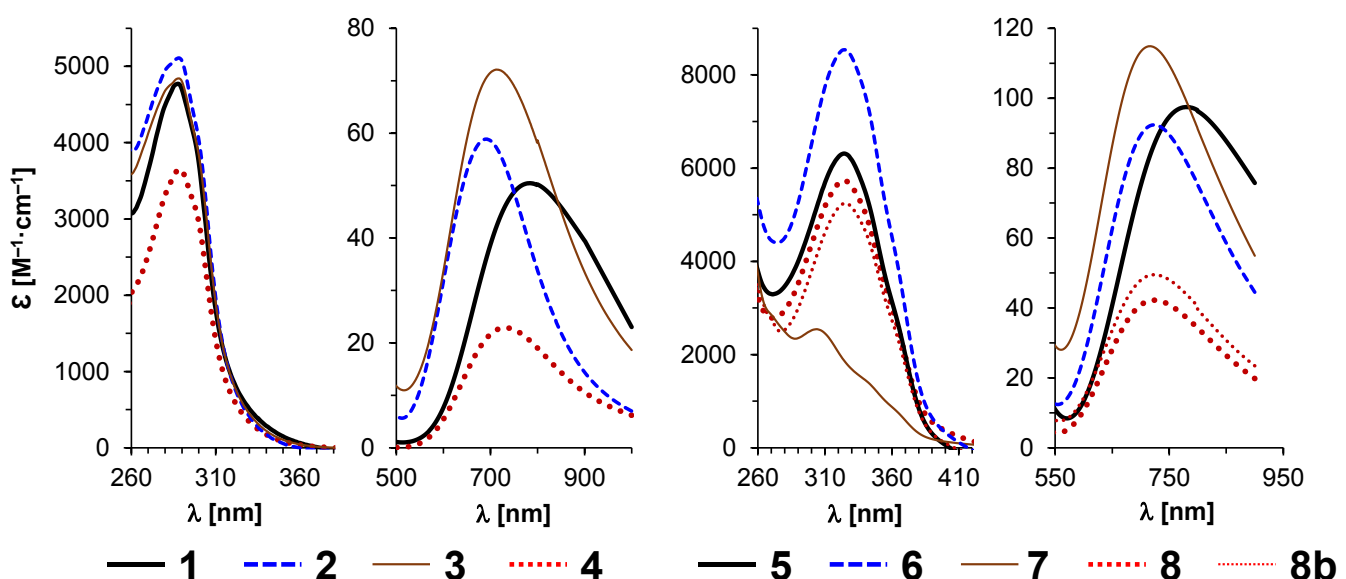
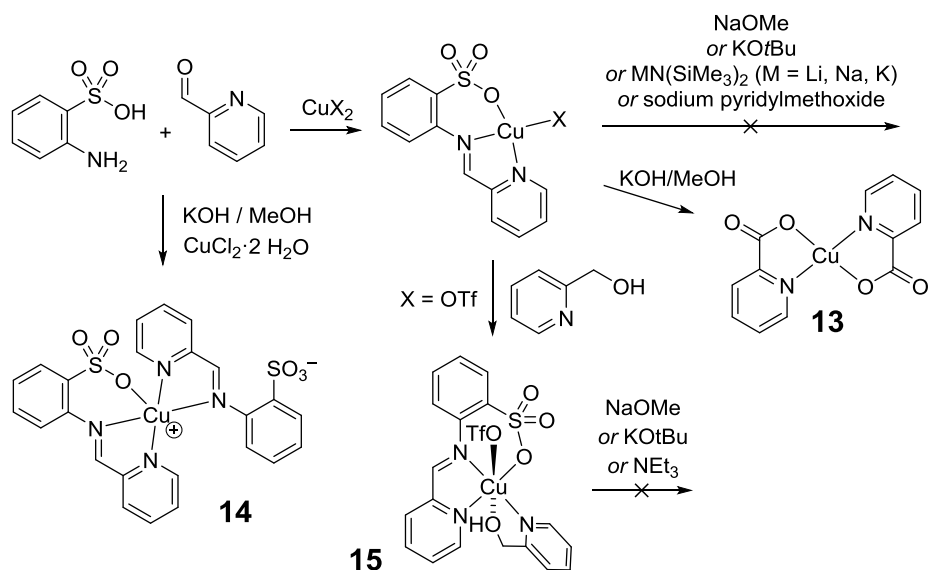


Figure 5.3 : UV/vis spectra of **1-4** (left) and **5-8** (right).

Lactide polymerisation studies

Attempted preparation of LCuOR complexes. Lactide polymerisation via a coordination-insertion mechanism requires a copper alkoxide catalyst. All of our attempts to generate such a species with ligands **L1** or **L2** failed, however. Reactions of **1-8** with alkoxide salts, such as NaOMe, KOtBu, or NaOCH₂C₅H₄N (sodium pyridylmethoxide) did not lead to the desired products. Attempts to prepare the alkoxide via an intermediate copper bis(trimethylsilyl)amide complex, an approach often successful for zinc-based alkoxide complexes, likewise failed,⁷⁹ as did an attempt to react the respective Cu(I) complex with *tert*-butylperoxide.⁸⁰ In several reactions under basic conditions, the known copper salt of picolinic acid, **13** (Scheme 5-4),⁸¹ was obtained. Crystallized yields of **13** could reach up to 60-70% in some reactions. We are aware of only one other reported oxidation of a picolyl imine to picolinic acid,⁸² but given the doubtful synthetic utility of this oxidation, we did not investigate it further. When synthesis of **5** was conducted in methanol and in the presence of base, the product was either a mixture of **5** and **13**, or the (previously reported)⁷² homoleptic complex (**L2**)₂Cu, **14** (Scheme 5-4). Ligand exchange following the Schlenk equilibrium to homoleptic complexes is a typical and often encountered obstacle in the preparation of heteroleptic copper alkoxides, but homoleptic **14** was only rarely observed in our attempts here and the respective taurine-based complex (**L1**)₂Cu was not obtained at all.



Scheme 5-4

To favor formation of an alkoxide complex and to prevent potential β -H elimination, we pre-coordinated pyridylmethanol to **8** to form the respective adduct complex **8·NC₅H₄CH₂OH**, **15** (Scheme 5-4). **15** crystallises in Jahn-Teller distorted octahedral geometry, with the triflate anion and the alcohol in the apical position and 0.4 Å longer bond distances to copper than the sulfonate ligand in the equatorial position (Fig. 5.4, Table 5-2). The alcohol hydrogen forms a weak hydrogen bridge with the sulfonate group on the ligand, but is sterically easily accessible from the outside of the complex. It is not clear why deprotonation of the pre-coordinated alcohol should be difficult to achieve, but reactions of **15** with bases such as NaOMe, KOtBu or NEt₃ did not yield any isolable products. We thus suspect a thermodynamic lability, rather than a kinetic challenge, in the preparation of (**L1**)CuOR or (**L2**)CuOR complexes.

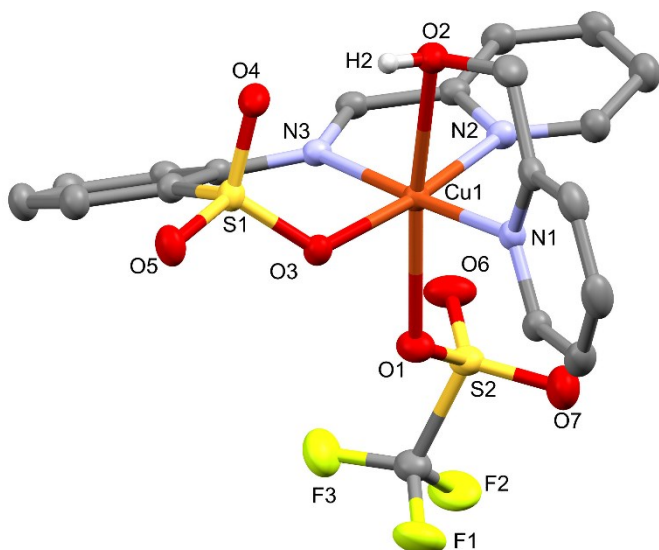


Figure 5.4 : Crystal structure of **15**. Hydrogen atoms other than H2 were omitted for clarity. Thermal ellipsoids are drawn at the 50% probability level.

5.2.2. *rac*-Lactide Polymerisation

Since heteroleptic copper alkoxide were not accessible, we undertook to test their reactivity for lactide polymerisation by preparing the alkoxide complex *in situ*. Jeong and coworkers achieved remarkably high activities with an LCuCl₂/NaOEt catalyst systems.⁸³⁻⁸⁷ Given the tendency of **1-8** to coordinate solvent or Lewis bases, these complexes might also

serve as catalysts in polymerisations following an activated monomer mechanism, where the complex acts as a Lewis acid to activate the lactide for the attack of external alcohol. Initial polymerisation tests were conducted with aryl-based catalysts **5-8**. Table 5-3 lists individual activities, but since no clear correlation of the anion with reactivity or selectivity was observed, we will use averaged values for these four catalysts in the discussion to facilitate comparison. Solution polymerisation at room temperature in combination with 1 equiv NaOMe per catalyst showed only mediocre activity for complexes **5-8** (Table 5-3). Most importantly, activities after 1 h and 12 h were nearly identical, indicative of catalyst decomposition. No activity at all was observed in the absence of sodium methoxide co-initiator for any of the catalysts. Polymerisations at 130 °C in molten monomer showed somewhat higher activities (19% on average), but reactions were sluggish and no conversion higher than 30% was observed after 12 h. In the absence of a co-catalyst, insertion either has to incur into the sulfonate or pyridine ligands, both unlikely events. Alternatively, water present in the complex or as impurity in the monomer can serve as initiator in an activated monomer mechanism.

Table 5-3 : *rac*-Lactide polymerisation with copper pyridyliminosulfonate complexes.

Catalyst	[Cu] : [lactide]	[NaOMe] : [lactide]	[BnOH] : [lactide]	Temperature / solvent	Conversion (1 h)	Conversion (12 h)	P _r	M _w /M _n	M _n (GPC)	M _n (calc.) (# chains) ^a
5	1:300	1:300		RT / CH ₂ Cl ₂	28	35	0.62	2.2	3300	7600 (5)
6	1:300	1:300		RT / CH ₂ Cl ₂	7	9				
7	1:300	1:300		RT / CH ₂ Cl ₂	18	18				
8	1:300	1:300		RT / CH ₂ Cl ₂	26	33	0.62	2.0	1400	4800 (10)
1	1:300	1:300		RT / CH ₂ Cl ₂	16	24	0.63			
2	1:300	1:300		RT / CH ₂ Cl ₂	0	0				
15	1:300	1:300		RT / CH ₂ Cl ₂	7	9				
5	1:300	1:300	1:300	RT / CH ₂ Cl ₂	17	19				
6	1:300	1:300	1:300	RT / CH ₂ Cl ₂	9	11				
7	1:300	1:300	1:300	RT / CH ₂ Cl ₂	10	15				
8	1:300	1:300	1:300	RT / CH ₂ Cl ₂	40	62	0.62	1.84	1800	6700 (15)
1	1:300	1:300	1:300	RT / CH ₂ Cl ₂	12	19	0.64	1.8	1100	2800 (8)
2	1:300	1:300	1:300	RT / CH ₂ Cl ₂	0	0				
15	1:300	1:300	1:300	RT / CH ₂ Cl ₂	8	9				
5	1:100			130 °C / neat	0	0				
6	1:100			130 °C / neat	0	23	0.75	1.6	600	1700 (6)
7	1:100			130 °C / neat	0	21	0.76	1.1	400	3100 (8)
8	1:100			130 °C / neat	0	33	0.61	1.2	900	2400 (5)
1	1:100			130 °C / neat	0	0				
2	1:100			130 °C / neat	0	0				
15	1:100			130 °C / neat	0	20	0.80			
NaOMe	-	2:100		130 °C / neat	10	50	0.50			
5	1:100	1:100		130 °C / neat	14	70	0.80	1.5	1000	5100 (10)
6	1:100	1:100		130 °C / neat	13	66	0.75	1.5	900	3200 (11)
7	1:100	1:100		130 °C / neat	13	39	0.61	1.1	800	2800 (7.1)
8	1:100	1:100		130 °C / neat	18	80	0.77	1.5	1000	3900 (12)
1	1:100	1:100		130 °C / neat	17	78	0.74	1.5	900	5700 (12)
2	1:100	1:100		130 °C / neat	-	40	0.66			
15	1:100	1:100		130 °C / neat	17	79	0.76	1.2	3100	3800 (4)
5	1:100		2:100	130 °C / neat	0	79	0.69	1.1	400	3800 (29)
6	1:100		2:100	130 °C / neat	2	58	0.85	1.1	300	2100 (28)
7	1:100		2:100	130 °C / neat	36	68	0.79	1.1	400	3300 (25)
8	1:100		2:100	130 °C / neat	0	53	0.63	1.2	400	1900 (19)
1	1:100		2:100	130 °C / neat	0	16				
2	1:100		2:100	130 °C / neat	17	87	0.62			
15	1:100		2:100	130 °C / neat	0	59	0.65	1.2	400	2200 (21)
5	1:100	2:100		130 °C / neat	24	73	0.67	1.4	900	3500 (12)
6	1:100	2:100		130 °C / neat	26	92	0.63	1.7	700	3300 (19)
7	1:100	2:100		130 °C / neat	29	94	0.60	1.4	700	4600 (19)
8	1:100	2:100		130 °C / neat	28	60	0.69	1.7	600	2200 (15)
1	1:100	2:100		130 °C / neat	17	100	0.57	1.6	1000	4800 (14)
2	1:100	2:100		130 °C / neat	25	95	0.56			
15	1:100	2:100		130 °C / neat	31	100	0.57	1.6	1000	3600 (14)
17	1:300			RT / CH ₂ Cl ₂	0	0				
17	1:300			70 °C / toluene	0	0				
17	1:300			130 °C / neat	12	33	0.67	1.1	900	7200 (16)
17	1:100			130 °C / neat	30	50	0.65	1.1	1000	3600 (7)
17	1:300		1:300	130 °C / neat	17	45	0.69	1.1	800	6500 (24)

^a Expected polymer molecular weight calculated for the lowest expected molecular weight, presuming that all water and alcohol present in the respective complexes initiate chain growth. The number of chains per copper center is calculated from # chains = (conversion*[lactide]/[catalyst]*M_{lactide})/M_n(GPC).

With sodium methoxide as co-initiator, average activities increased notably from 19% to 64% average conversion. Initiation was significantly faster and all catalysts showed activity after 1 h of polymerisation. The polymerisation was moderately heterotactic in the absence (average $P_r = 0.71$) as well as in the presence of sodium methoxide as co-initiator (average $P_r = 0.73$). It is important to note that sodium methoxide itself shows variable activities under these conditions, but typically did not yield more than 40% conversion after 12 h. Polymers obtained from sodium methoxide-initiation were always atactic ($P_r = 0.50 - 0.55$). The copper complexes are thus clearly involved in polymerisation.

It was surprising that complexes **6** and **8**, which contained coordinated or co-crystallized water showed the same general reactivity as the “water-free” catalysts **5** and **7**. Under the conditions employed here, we expected **6** and **8** to form relatively inactive copper hydroxide species. The comparable activity indicates that either copper hydroxide species can be activated by alcohol present to follow a coordination-insertion mechanism or that an activated monomer mechanism is in place for all species. Polymerisations were thus conducted with two equiv BnOH per copper instead of NaOMe. The average activity in these polymerisations was comparable (65 % averaged conversion after 12 h). More importantly, stereocontrol was likewise similar with an averaged P_r of 0.74. Since it is unlikely that a coordination-insertion mechanism and an activated monomer mechanism provide the same stereocontrol, an activated monomer mechanism is most likely active for all catalysts. With sodium methoxide as co-initiator this either indicates water present as an impurity or that sodium methoxide does not react with the copper complexes via ligand exchange, but acts (similar to benzyl alcohol) as an external nucleophile. To test for this possibility, we conducted polymerisations in the presence of two equivalents of sodium methoxide. In an activated monomer mechanism a higher concentration of nucleophile would increase the reaction rate, but should not have any other impact on polymerisation. Reactions with two equiv of sodium methoxide per copper led indeed to increased activities (80% conversion after 12 h on average, compared to 64% for 1 equiv of sodium methoxide), but heterotacticity decreased at the same time to an average P_r of 0.65 (from $P_r = 0.73$ with one equiv of NaOMe). Given that sodium methoxide is active under these conditions and produces atactic PLA, the second equivalent of sodium methoxide most likely independently polymerizes lactide without

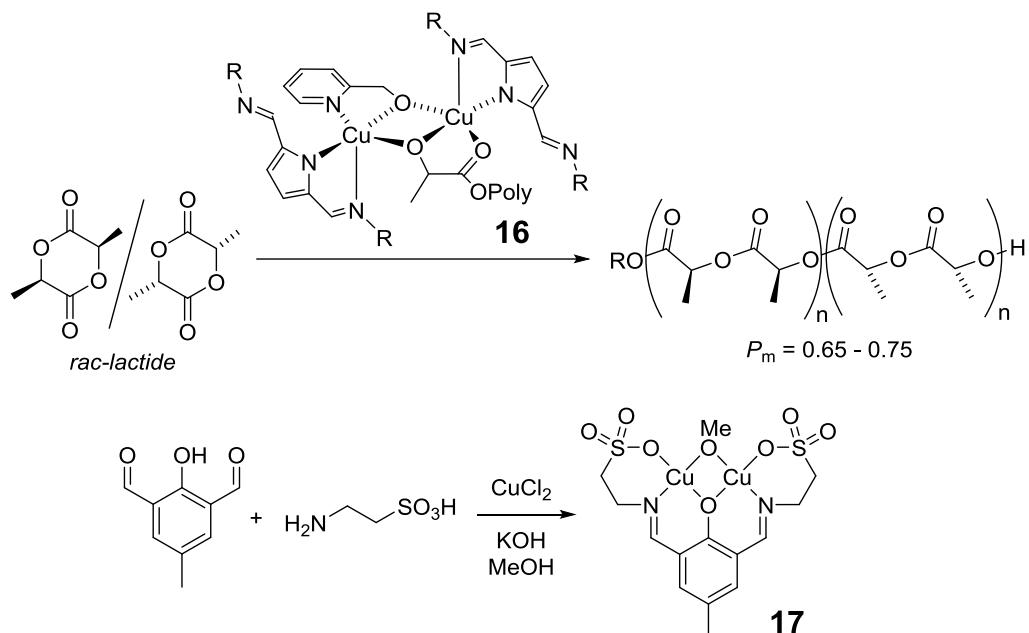
interaction with copper. Under melt conditions, catalysts **5–8** thus polymerize lactide following an activated monomer mechanism, with hydrolysis of NaOMe from adventitious water.[‡]

Taurine-based complexes **1** and **2** were employed as well. There is no general difference in reactivity or selectivity evident between the aliphatic or aromatic ligand backbone (Table 5-3). The polymerisation mechanism is thus unlikely to involve dissociation of the ligand sulfonate group. This agrees with the very comparable UV/vis spectra of **1–4** and **5–8** (Fig. 5.3). Complex **15** with a pre-coordinated pyridylmethanol group showed similar activities and moderate heterotactic stereocontrol. There is no indication that pyridylmethoxide can act as a bridging ligand in a dinuclear active species as observed in diiminopyrrolide copper complexes.^{7,8}

Last but not least, all complexes under all conditions employed show a severe lack of polymer molecular weight control. Polydispersities range from excellent to mediocre (1.1 – 1.7). In particular upon addition of benzyl alcohol polydispersities of 1.1–1.2 were obtained. However, even for polymers with narrow polydispersities, observed and expected polymer molecular weight differ strongly. In fact, with the exception of one single experiment, the highest polymer molecular weight observed is 1800, thus a polymerisation degree of 12! Again, we observe no correlation between polymer molecular weight control and the anion, the ligand backbone or the presence of pyridylmethanol. It appears that copper iminosulfonate complexes have a very high general tendency to undergo intramolecular transesterification, which accounts for the shortened chains and strongly limits the usefulness of this catalytic system for lactide polymerisation.

Dinuclear copper iminosulfonates. In previous work, we found that the active species in isotactic copper polymerisation catalysts is a dinuclear, chiral species (**16**, Scheme 5-5).^{6,7} To investigate an iminosulfonate complex of similar geometry, we prepared the dinuclear copper complex **17** by a one-pot reaction from 2,6-diformyl-4-methylphenol, taurine and copper dichloride in methanol under basic conditions. Under these conditions and from undried methanol, the copper methoxide complex was obtained readily. In the solid state, the copper center is found in square-pyramidal coordination geometry ($\tau = 0.1$) with a bridging coordination of a neighbouring sulfonate group (Fig. 5.5, Table 5-S2). The coordination

environment in the crystal structure of **17** is thus similar to the coordination environment in **16**.



Scheme 5-5

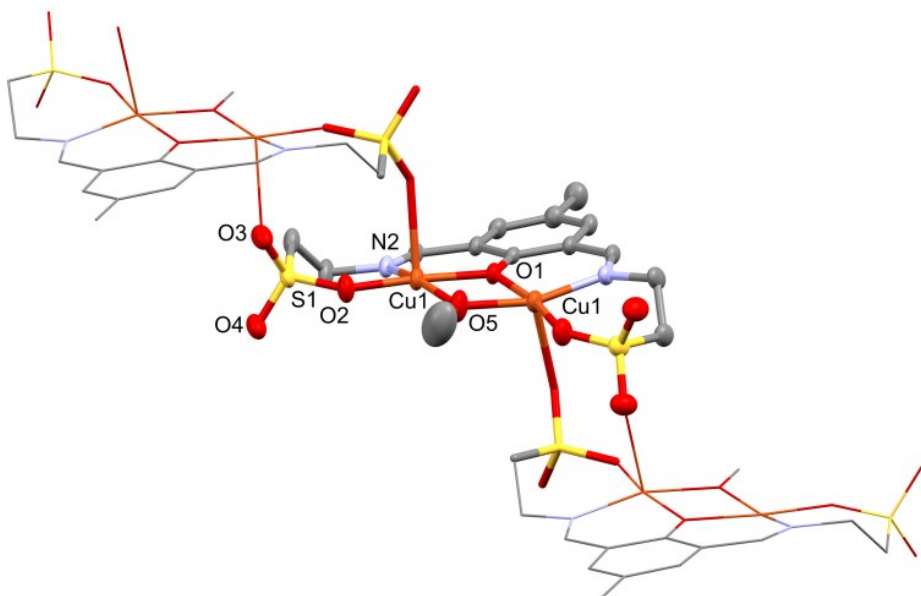


Figure 5.5 : X-ray structure of **17**. Hydrogen atoms were omitted for clarity. Thermal ellipsoids are drawn at the 50% probability level.

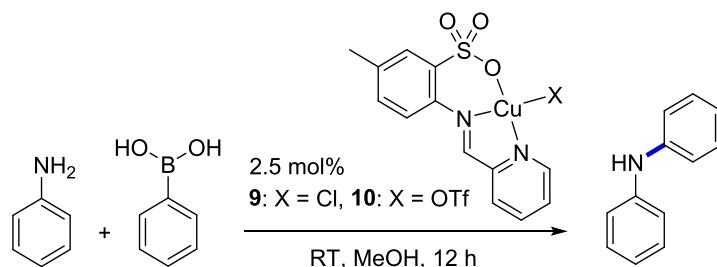
The reason for the large difference in the ease of synthesis and stability of a copper alkoxide species when comparing **1-8** and **17** is unclear. For sure, **17** does not allow the formation of homoleptic complexes, but these were observed only rarely in reactions with **1-**

8. It is possible that the bridging coordination of the methoxide and the rigid dinuclear complex prevents potential side reactions, such as β -H elimination or desulfonation.

Unfortunately, the stability of **17** extended to polymerization conditions and **17** was very unreactive in lactide polymerisation. No activity was observed at room temperature in CH_2Cl_2 solution or at 70 °C in toluene (Table 5-3). Even in molten monomer at 130 °C, **17** provided slightly heterotactic PLA ($P_r = 0.67$) in only 50% conversion after 12 h at a catalyst loading of 1:100. This is the lowest activity observed for any isolated copper alkoxide catalyst in our group. We have noticed previously that the introduction of bridging aryloxide groups is detrimental to activity.⁷ Based on EPR-results with **16**,⁷ coordination of lactide is correlated with the release of one of the Cu-O bonds of the bridging alkoxide, most likely accompanied by a deformation of the dinuclear complex. The sp^2 -hybridization of an aryloxide ligand (in contrast to alkoxide-bridged complexes which were active) might stabilize the dinuclear complex to an extend that coordination of lactide becomes too unfavourable.

5.2.3. Chan-Evans-Lam couplings

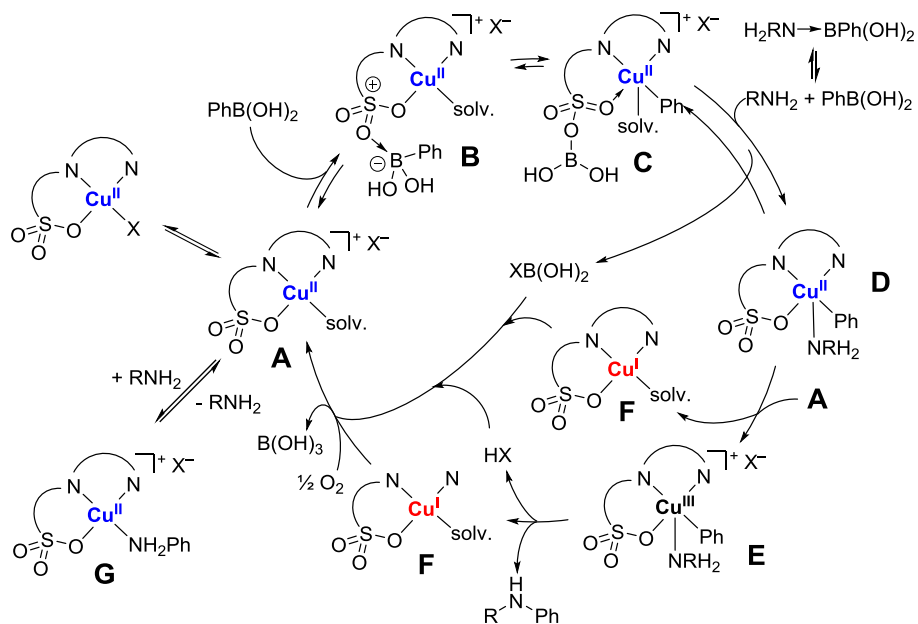
We have recently reported that iminosulfonate copper complexes **9** and **10** are excellent catalysts for Chan-Evans-Lam (CEL) couplings of *N*-nucleophiles to arylboronic acids.^{12, 13}



Since the catalyst does not require addition of base, molecular sieves or ligands and tolerated a variety of solvents, the coupling protocol was relatively general and could be applied in the same way to amine, anilines and *N*-heterocycles. With some few exceptions, conversions were quantitative. A mechanistic study provided a mechanism, similar to that established by Collman,^{59, 88} Stahl^{60, 89} and Watson,⁶¹ but with some variations specific to **9** and **10** (Scheme 5-6).¹³ One of the most important of these, is that the sulfonate group of the

ligand (instead of the counter anion) is proposed to be responsible for the formation of the dinuclear copper-boron complex (Scheme 5-6, **B**), which is considered to be an essential precursor to transmetallation (Scheme 5-6, **B**→**C**).⁵⁹⁻⁶¹ We attempted to isolate/crystallize species **B** from equimolar solutions of copper complexes and PhB(OH)₂, either in the absence or presence of DMAP (as an *N*-nucleophile inactive towards CEL-couplings). The only isolated products were, however, the DMAP adducts **11** and **12** described above, as well as a DMAP adduct of boroxine (Fig. 5.S3). To provide additional evidence for the proposed mechanism, we thus investigated the anion dependence of the performance of pyridyliminosulfonate complexes in CEL coupling of aniline to phenylboronic acid catalyzed by **5-8**.

CEL couplings were conducted under conditions identical to those used for **9** and **10**: MeOH, room temperature, exposure to air, [PhNH₂] = 1.0 M, [PhB(OH)₂] = 1.5 M, 2.5 mol% catalyst. As for **9** and **10**, no homocoupling of phenylboronic acid, deboration or coupling to water or solvent was observed. Excess phenylboronic acid is thus not necessary for reactions to reach completion, but was employed to allow comparison with data obtained with **9** and **10** under the same pseudo-first order conditions. Conversions were determined from absolute concentrations of aniline and diphenylamine, in turn determined by calibrated GC/MS-analysis relative to internal standard. There is a very good agreement of conversions determined from either the concentration of diphenylamine product or the concentration of remaining aniline, indicating that no aniline was lost to side-reactions or evaporation. Reactions were first order in aniline after a variable induction period. All reactions reached completion after 12 h, with the exception of **1**, which was the only complex showing evidence for catalyst decomposition in its kinetic profiles. Due to formation of an unreactive copper-aniline complex (Scheme 5-6, **G**),¹³ the reaction deviates positively (i. e. becomes faster than expected) at conversions > 80%. For each catalyst, two or three kinetic profiles were used to determine averaged rate constants in multiple regression analysis (Supp. Information).



Scheme 5-6

CEL couplings with iminosulfonate copper complexes show a pronounced induction period of up to 4 h, which can vary between different kinetic experiments (Table 5-4, Fig. 5-6). Qualitatively, the induction period increases in dependence of the anion in the order $\text{OTf}^- < \text{Cl}^- < \text{NO}_3^- < \text{AcO}^-$. For **9** and **10**, dissolution of the catalyst was identified as the source of the induction period,¹³ which agrees with the fact that **10** and **8** are the only complexes which show ready solubility in methanol and also show the shortest induction times. Water has been found to be beneficial in solubilizing the catalysts¹³ and differing amounts of water present in the undried reaction solvent can account for the observed variations.

The presence of an additional methyl substituent on the benzene sulfonate did not affect reactivity and very similar rate constants were obtained for **9/5**, and **10/8**, respectively. The methyl group was introduced to increase solubility of the complexes and **9** shows indeed a shorter induction period than **5**. However, given the strong dependence of induction time on reaction conditions, this might be simple happenstance. Despite its large impact on the induction period, the anion has otherwise only a small influence on reactivity and rate constants differ by less than a factor of 2 between **5-8**. For **9** and **10**, an anion dissociation equilibrium was indicated by the kinetic data as part of the catalytic cycle (Scheme 5-6, **A**). The same dissociation equilibrium was also observed for CEL couplings with $\text{Cu}(\text{OAc})_2$.⁶⁰ Such an equilibrium well accounts for the slight anion influence observed, as well as for the fact that

chloride containing **1**, **5** and **9** show overall the lowest activities. The relatively high activity of acetate-coordinated **7** is unexpected in this context, but due to the long induction time for this complex and the deviations from pseudo-first order behaviour at higher conversions, the first-order region of the concentration profile is very small for **7** and the determination of k_{obs} is less reliable for this complex. Overall, variations in reaction rates are much smaller than one would expect if the anion is actively involved in forming a bridged copper-boron species, which agrees with the mechanistic proposal that the sulfonate group occupies this role (Scheme 5-6, **C**). Complex **1** shows practically identical activities when compared to **9** and **5**. Even if the sulfonate group coordinates to boron in a dinuclear intermediate, it is thus unlikely that the mechanism involves sulfonate de-coordination from the copper center. Both kinetic runs with **1** show evidence for complex decomposition (Table 5-S3) and CEL couplings were not investigated for the other taurine-based complexes.

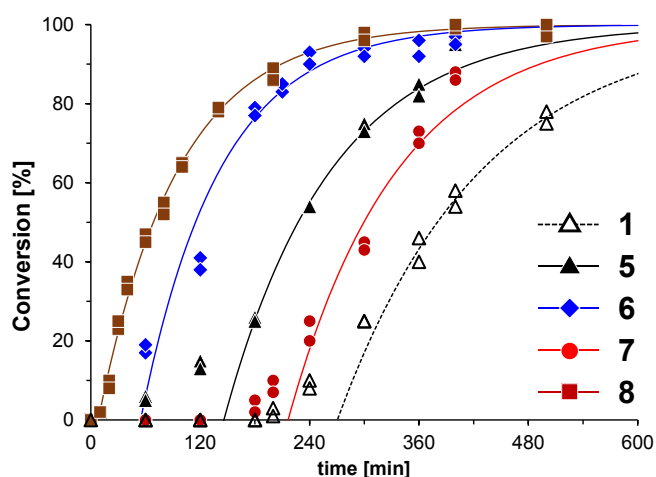


Figure 5.6: Selected kinetic traces for CEL couplings of aniline with phenylboronic acid catalysed by **1** and **5-8**. Conditions: 1.0 M aniline, 1.5 M PhB(OH)₂, 2.5 mol% [cat.], MeOH, RT. Two datapoints per time point indicate conversions determined independently from the concentration of remaining aniline and from the concentration of formed product. Solid lines are theoretical curves obtained in linear regression analysis of the semi-logarithmic plot in the pseudo-first order region of the profile (see Supp. Information for details).

Table 5-4 : Activity of iminosulfonates copper catalysts in the CEL coupling of aniline with phenylboronic acid.

Catalyst (Anion)	Final Conversion after 12 h	k_{obs}	Induction Period
9 (Cl^-) ^a	>99%	0.40(2) h^{-1}	40 min
1 (Cl^-)	95%	0.4 h^{-1}	150 – 270 min
5 (Cl^-)	>99%	0.5 h^{-1}	145 – 150 min
6 (NO_3^-)	>99%	0.7 h^{-1}	55 – 270 min
7 (AcO^-)	99%	0.7 h^{-1}	230 – 250 min
8 (TfO^-)	>99%	0.7 h^{-1}	5 – 15 min
10 (TfO^-) ^a	>99%	0.50(1) h^{-1}	10 min
17 (MeO^-)	>99%	0.2 h^{-1}	160 min
17 / $\text{MeOArNH}_2^{\text{b}}$	>99%	0.3 h^{-1}	135 min
17 / $\text{BrArNH}_2^{\text{c}}$	5% ^d	-	-

^a Taken from ref.¹³ ^b *para*-Methoxyaniline as substrate. ^c *para*-Bromoaniline as substrate. ^d At 60 °C, 15% were obtained after 12 h

We are not aware of any specific investigation targeting binuclear CEL catalysts. Although several pre-catalysts in CEL couplings are dinuclear, the active species is typically thought to be mononuclear, e. g. in Collman's tmada-based catalyst⁵⁹ or in the dimer $\text{Cu}_2(\text{OAc})_4$.⁶¹ We found it of interest to investigate the performance of dinuclear complex **17**, which is highly unlikely to dissociate under CEL coupling conditions. Complex **17** was active in CEL couplings. A notable induction period of 2.5 h (Table 5-4) is probably again related to slow solubilisation of the complex. After the induction period, **17** showed a slightly lower activity than **1-10**, but was still a competent catalyst and the reaction reached completion (Table 5-4). Substrate reactivity was briefly explored, mainly in the interest to contrast the performance of **17** with **10**.

CEL couplings with **10** showed a reactivity for electron-poor anilines comparable to that of aniline, while electron-rich anilines, such as methoxyaniline, were unreactive at room temperature and required heating to 50 °C. This was counterintuitive, since better nucleophiles typically react faster in CEL couplings and explained by the formation of an unproductive aniline coordinated complex (Scheme 5-6, **G**).¹³ CEL couplings with **17** show the

more typical reactivity order: higher activity for methoxyaniline than for aniline, while bromoaniline is unreactive. Aniline coordination to the more saturated **17** might be disfavoured or – due to the presence of two copper centers – does not preclude transmetallation.

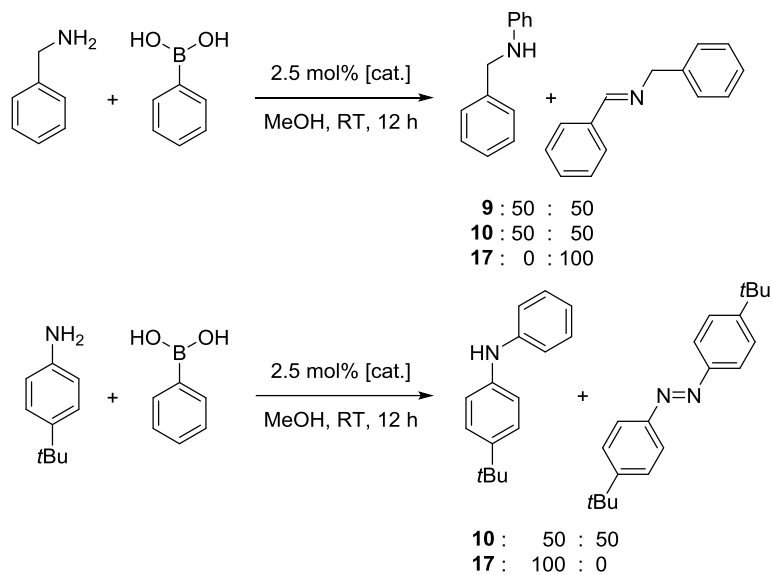
Table 5-5 : CEL couplings of phenylboronic acid with various amines catalysed by **17**

Nucleophile	Time	Conversion	Observation
Octylamine	0.5 h	0%	-
Octylamine	1 h	100%	-
Di- <i>n</i> -butylamine	1 h	0%	-
Di- <i>n</i> -butylamine	4 h	100%	-
<i>tert</i> -Butylamine	12 h	0%	Formation of Ph-Ph
Methylamine (aq)	12 h	47%	Formation of Ph-Ph
Benzylamine	12 h	0%	Formation of Ph-Ph and imine
<i>p</i> - <i>tert</i> -Butylaniline	12 h	100%	

As did **10**, **17** quantitatively coupled primary and secondary amines under the same reaction conditions as used for anilines (Table 5-5). The dinuclear catalyst is, however, more sensitive towards steric bulk. While di-*n*-butylamine and *tert*-butylamine were among the most reactive substrates for **10**,^{12,13} in couplings with **17** dibutylamine reacted slower and *tert*-butylamine was not coupled at all (Table 5-5). Methylamine, supplied as an aqueous solution, reached only 50% conversion and formation of diphenyl side product was observed. The competitive and unproductive formation of diaryls was mostly suppressed for **10**,¹³ and only observed if the oxidation step (**D** → **E**, Scheme 5-6) was slow, e. g. with electron-deficient arylboronic acids. The lower yields for *tert*-butylamine and for methylamine are thus likely related with a slower/weaker coordination of the *N*-nucleophile to copper (**C** → **D**, Scheme 5-6). Accumulation of Cu(II)-aryl species **C** then leads to homocoupling. We had initially hoped for an increased stabilization against homocoupling, since one of only two isolated copper-aryl species in which the aryl is not part of a macrocyclic ligand is a dinuclear, mixed-valence

copper aryl complex, recently published by Tilley.⁹⁰ Complex **17** might not be set up to provide the same amount of stabilization or, more likely, mixed-valence species, which could theoretically form in the reaction, are not active species in the catalytic cycle.

Although **10** successfully coupled most amines and anilines, side reactions were observed for CEL couplings with benzylamine and *p*-*tert*-butylaniline at room temperature, which could be suppressed at higher temperatures.¹³ Benzylamine partially underwent oxidation to the imine, while *p*-*tert*-butylaniline formed azobenzene at room temperature (Scheme 5-7). Both reactions are initiated by radical mechanisms, most likely from the peroxy-species formed upon oxidation of the Cu(I) species by O₂ (**F** → **A**, Scheme 5-6). The presence of two copper centers might either help or hinder re-oxidation from Cu(I) to Cu(II) and we thus investigated how **17** performed with these two substrates. The results were ambiguous, however: while formation of azobenzene was suppressed completely, benzylamine now afforded only the imine side product (Scheme 5-7, Table 5-5).



Scheme 5-7

5.3. Conclusions

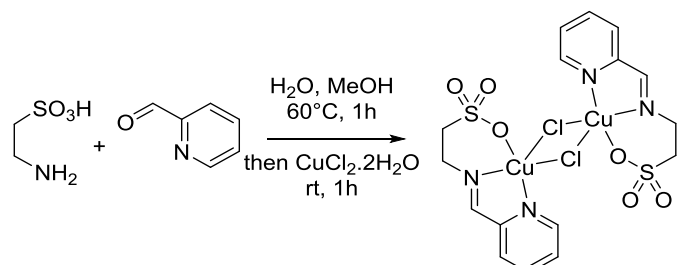
Copper pyridyliminosulfonate complexes with different anions can be prepared in simple one-pot reactions from commercial products, such as taurine or orthanilic acid without the requirement of protecting atmosphere and are thus easily accessible catalysts. In the presence of co-initiators, copper pyridyliminosulfonate complexes are moderately active in the melt polymerisation of lactide, following an activated monomer mechanism. The advantages of these catalysts, i. e. their general stability, tolerance of water, and sometimes good polydispersities, are strongly offset by the lack of stereocontrol and their high tendency to undergo intramolecular transesterification.

In Chan-Evans-Lam couplings, copper pyridyl-iminosulfonate complexes display an anion-independent reactivity which supports that in these complexes any dinuclear copper-boron intermediate is bridged by sulfonate rather than by the anion. Despite its negligible effect on activity, the choice of the anion remains highly important for practical applications due to the long induction period in the presence of some anions: after 2 h of reaction, for example, triflate-containing complex **8** reached 80% conversion, while the theoretically more active acetate complex **7** has not yet entered the catalytic cycle.

The performance of taurine-based complexes was essentially identical to that of orthanilic acid-based complexes. Neither lactide polymerisation, nor CEL couplings thus require dissociation of the sulfonate group from the metal center as an essential step in the catalytic cycle.

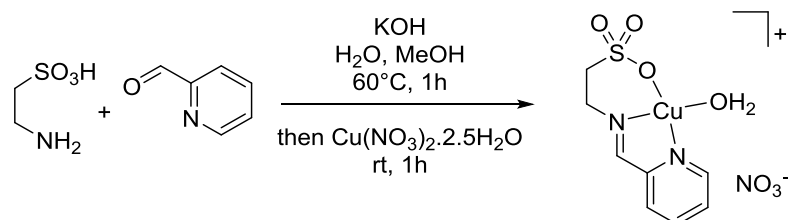
5.4. Experimental section

General. Phenylboronic acid was purified by washing with dichloromethane until the filtrate stayed colorless. *rac*-Lactide (98%) was purchased from Sigma–Aldrich, purified by 3x recrystallization from dry ethyl acetate and kept at –30 °C. All other chemicals were purchased from common commercial suppliers and used without further purification. **1** and **5** were prepared with slight modifications from the literature procedure.^{66, 69} Elemental analyses were performed by the Laboratoire d'analyse élémentaire (Université de Montreal). UV/vis spectra were recorded on a Cary Series UV-Vis-NIR spectrophotometer from Agilent Technology. GC-MS spectra were recorded on an Agilent Technology GC/MS.



{(L1)Cu(μ-Cl)}2**, 1.** 2-Pyridinecarboxaldehyde (95 µL, 1.0 mmol) was added to a hot solution (60 °C) of 2-aminoethylsulfonic acid (taurine, 125 mg, 1.08 mmol) in water/methanol (5/10 mL). The mixture was stirred for one hour at 60 °C. CuCl₂·2 H₂O (187 mg, 1.1 mmol) was added, heating was stopped and the green solution was stirred another hour. After filtration to remove trace impurities, evaporation of the solvent afforded blue-green, X-ray quality crystals (274 mg, 88%).

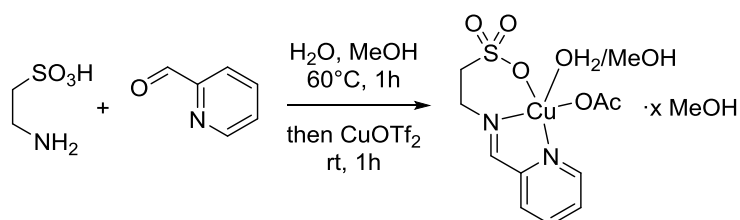
UV-vis (DMSO, 1.0·10^{−2} M or 7.22·10^{−5} M) [λ_{max}, nm (ε, M^{−1}·cm^{−1})]: 288 (4771), 783 (50). Anal. Calcd. for C₈H₉CuClN₂O₃S₁: C, 30.78; H, 2.91; N, 8.97; S, 10.27. Found: C, 31.01; H, 2.97; N, 8.87; S, 10.29.



[{L1}Cu(OH₂)][NO₃], 2.** 2-Pyridinecarboxaldehyde (95 µL, 1.0 mmol) and potassium hydroxide (56 mg, 1.0 mmol) were added to a hot solution (60 °C) of 2-aminoethylsulfonic acid (taurine,**

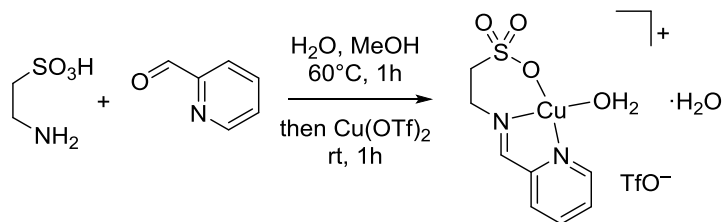
125 mg, 1.0 mmol) in water/methanol (5/10 mL). The mixture was stirred for one hour at 60 °C. Cu(NO₃)₂·2.5 H₂O (255 mg, 1.1 mmol) was added, heating was stopped and the solution was stirred another hour. After filtration to remove trace impurities, slow evaporation of the solvent afforded blue-green, X-ray quality crystals (153 mg, 43%).

UV-vis (DMSO, 1.2·10⁻² M or 6.3·10⁻⁵ M) [λ_{max}, nm (ε, M⁻¹·cm⁻¹)] : 288 (5109), 692 (59). Anal. Calcd. for C₈H₁₁CuN₃O₆S·H₂O : C, 26.93; H, 3.11; N, 17.81; S, 8.99. Found: C, 26.67; H, 3.28; 11.55; 8.40.



(L1)₂Cu₂(μ-OAc)₂(MeOH/OH₂)₂·x MeOH, 3. Equivalent to **1**, from Cu(OAc)₂·H₂O (219 mg, 1.1 mmol) was incorporated. Slow evaporation of the solvent provided blue-green, X-ray quality crystals (123 mg, 32%). The crystal structure contains disordered water and methanol in ill-defined quantities. The elemental analysis reasonably agrees with 1.5 water and 1 methanol solvent present.

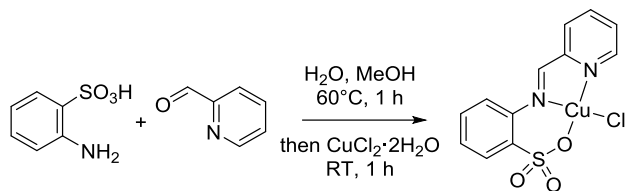
UV-vis (DMSO, 1.2·10⁻² M or 6.3·10⁻⁵ M) [λ_{max}, nm (ε, M⁻¹·cm⁻¹)] : 288 (4842), 712 (72). Anal. Calcd. for C₁₀H₁₂CuN₂O₅S·1.5 H₂O·1 MeOH : C, 33.46; H, 4.85; N, 7.09; S, 8.12. Found: C, 33.09; H, 4.30; N, 6.38; S, 6.86.



[(L1)Cu(OH₂)][OTf]·H₂O, 4. Equivalent to **1**, from Cu(OTf)₂ (398 mg, 1.1 mmol). Slow evaporation of the solvent provided blue-green, X-ray quality crystals (298 mg, 65%).

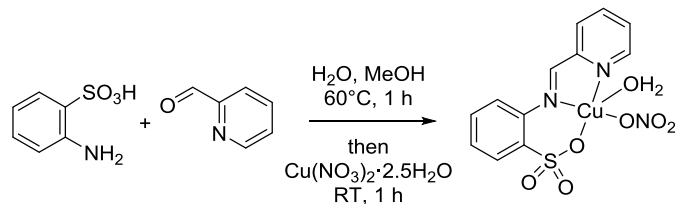
UV-vis (DMSO, 3.3·10⁻² M or 4.5·10⁻⁴ M) [λ_{max}, nm (ε, M⁻¹·cm⁻¹)] : 288 (3654), 730 (23). Anal. Calcd. for C₉H₉CuF₃N₂O₆S₂·2 H₂O: C, 23.40; H, 2.84; N, 6.07; S, 13.88. Anal. Calcd. for C₉H₉CuF₃N₂O₆S₂·H₂O: C, 24.35; H, 2.50; N, 6.31; S, 14.45. Found: C, 23.97; H, 2.75; N, 6.48; S, 13.89. Experimental values are between those calculated for the dihydrate found in the crystal

structure and a monohydrate. It is possible that (part of) the non-coordinated water in the structure was lost upon drying.



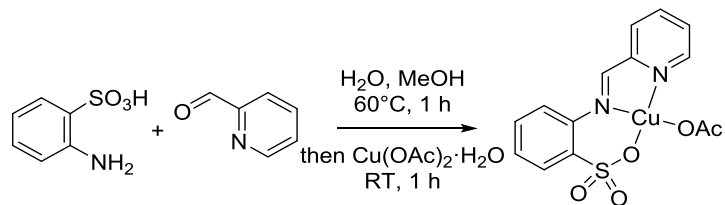
{(L1)Cu(μ-Cl)}₂, 5. Equivalent to **1**, from aniline-2-sulfonic acid (orthanilic acid, 173 mg, 1.0 mmol), 2-pyridinecarboxaldehyde (95 μL, 1.0 mmol) and CuCl₂·2 H₂O (187 mg, 1.1 mmol). Slow evaporation of the solvent yielded green, X-ray quality crystals (270 mg, 75%).

UV-vis (DMSO, 1.0·10⁻² M or 3.35·10⁻⁴ M) [λ_{\max} , nm (ε , M⁻¹·cm⁻¹)] : 322 (2311), 750 (99). Anal. Calcd. for C₁₂H₉CuN₂O₃S : C, 40.01; H, 2.52; N, 7.78; S, 8.90. Found: C, 39.97; H, 2.50; N, 7.40; S, 8.63.



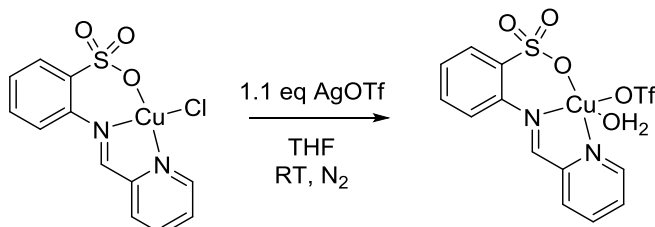
[(L2)Cu(OH₂)][NO₃], 6. Equivalent to **1**, from aniline-2-sulfonic acid (orthanilic acid, 173 mg, 1.0 mmol), 2-pyridinecarboxaldehyde (95 μL, 1.0 mmol) and Cu(NO₃)₂·2.5 H₂O (255 mg, 1.1 mmol). Slow evaporation of solvent afforded green, X-ray quality crystals (212 mg, 52%).

UV-vis (DMSO, 1.0·10⁻² M or 2.4·10⁻⁴ M) [λ_{\max} , nm (ε , M⁻¹·cm⁻¹)] : 325 (8539), 723 (92). Anal. Calcd. for C₁₂H₉CuN₃O₆S·H₂O : C, 35.60; H, 2.74; N, 10.38; S, 7.92. Found: C, 35.20; H, 2.75; N, 10.75; S, 7.63.



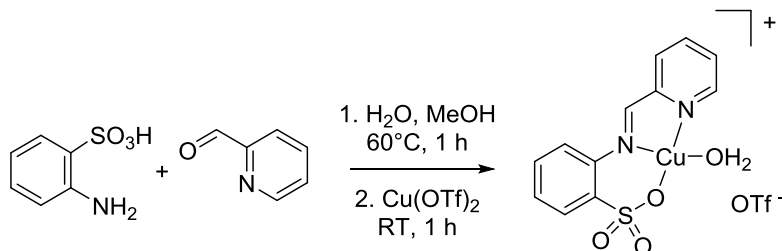
(L2)₂Cu₂(μ-OAc)₂, 7. Equivalent to **1**, from aniline-2-sulfonic acid (orthanilic acid, 173 mg, 1.0 mmol), 2-pyridinecarboxaldehyde (95 μL, 1.0 mmol), and Cu(OAc)₂·H₂O (219 mg, 1.1 mmol). Slow evaporation of the solvent yielded green, X-ray quality crystals (284 mg, 74%).

UV-vis (DMSO, $0.6 \cdot 10^{-2}$ M or $33 \cdot 10^{-4}$ M) [λ_{\max} , nm (ϵ , $M^{-1} \cdot cm^{-1}$)] : 305 (2544), 716 (115). Anal. Calcd. for $C_{14}H_{12}CuN_2O_5S \cdot 1.5 H_2O$: C, 40.92; H, 3.68; N, 6.82; S, 7.80. Found: C, 41.28; H, 3.32; N, 6.44; S, 7.01. (No water observed in the crystal structure, but compounds handled at air for elemental analysis.)

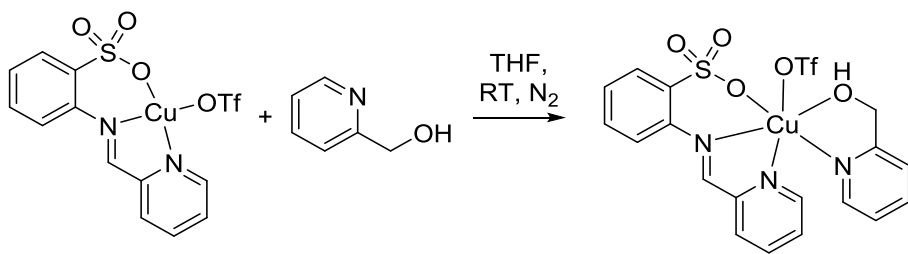


$\{(L2)Cu(OTf)\}_n$, **8**. Complex **5** (379 mg, 1.0 mmol) was put in dry THF (10 mL) under nitrogen atmosphere to give a heterogeneous mixture. Silver triflate (280 mg, 1.1 mmol) was added. After one hour of reaction at ambient temperature, a precipitate appeared and the color of the solution intensified. After filtration, slow evaporation of the green solution (under N_2), afforded green crystals of **2** (203 mg, 43%). Initial analyses differed from expected values and recrystallisation in THF proved difficult. An analytically pure sample was obtained from recrystallisation in methanol.

Anal. Calcd. for $C_{13}H_9CuF_3N_2O_6S_2 \cdot 2 MeOH$: C, 33.49; H, 3.18; N, 5.21; S, 11.92. Found: C, 33.90; H, 3.07; N, 5.10; S, 13.44. UV-vis (DMSO, $1.0 \cdot 10^{-2}$ M or $2.1 \cdot 10^{-4}$ M) [λ_{\max} , nm (ϵ , $M^{-1} \cdot cm^{-1}$)] : 325 (5245), 724 (50).

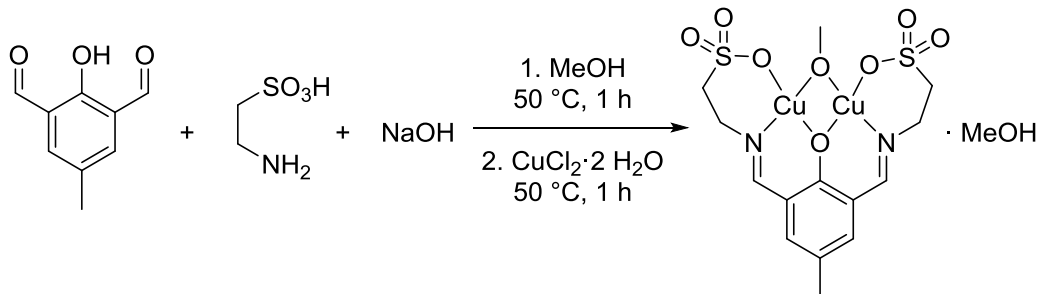


$[(L2)_2Cu_2(OH_2)_2][OTf]_2$, **8b**. Equivalent to **1**, from aniline-2-sulfonic acid (orthanilic acid, 173 mg, 1.0 mmol), 2-pyridinecarboxaldehyde (95 μ L, 1.0 mmol) and $Cu(OTf)_2$ (398 mg, 1.1 mmol). Slow evaporation of the solvent yielded green, X-ray quality crystals (350 mg, 76%). UV-vis (DMSO, $1.3 \cdot 10^{-2}$ M or $2.1 \cdot 10^{-4}$ M) [λ_{\max} , nm (ϵ , $M^{-1} \cdot cm^{-1}$)] : 325 (5747), 724 (42). Anal. Calcd. for $C_{13}H_{11}CuF_3N_2O_7S_2 \cdot H_2O$: C, 31.74; H, 2.25; N, 5.70; S, 13.04. Found: C, 31.90; H, 2.57; N, 5.50; S, 13.44.



(L2)Cu(HOCH₂C₅H₄N)(OTf), 15. To a solution of **8** (100 mg, 0.21 mmol) in THF (5 mL), pyridylmethanol (19 μ L, 0.23 mmol) was added. The solution was stirred for one hour, during which an oil separated. The supernatant solution was decanted and the remaining oil dissolved in acetonitrile. After filtration, slow evaporation afforded green crystals of **15** (78 mg, 64%).

UV-vis (DMSO, 1.0·10⁻² M or 1.5·10⁻⁴ M) [λ_{max} , nm (ϵ , M⁻¹·cm⁻¹)] : 323 (4094), 723 (63). Anal. Calcd. for C₁₉H₁₆CuF₃N₃O₇S₂: C, 39.14; H, 2.77; N, 7.21; S, 11.00. Found: C, 39.00; H, 3.07; N, 7.51; S, 10.25.



LCu₂(OMe)·MeOH, 17. Taurine (250 mg, 2.0 mmol) and 2,6-diformyl-5-methylphenol (164, 1.0 mmol) were combined in methanol (20 mL) containing sodium hydroxide (80 mg, 2.0 mmol). The mixture was stirred one hour then CuCl₂·2 H₂O (357 mg, 2.1 mmol) was added. After this addition, the heating was stopped and the solution was stirred another hour. To crystallize after filtration a slow evaporation of solvent was realized to lead to green crystal (260 mg, 49%).

UV-vis (DMSO, 1.0·10⁻² M) [λ_{max} , nm (ϵ , M⁻¹·cm⁻¹)] : 754 (123). Anal. Calcd. For C₁₄H₁₈Cu₂N₂O₈S₂·MeOH: C, 31.86; H, 3.92; N, 4.95; S, 11.34. Found : C, 31.50; H 4.12; N, 5.15; S, 11.78. (X-ray structure shows one co-crystallized methanol solvent.)

rac-Lactide polymerisation

At room temperature: The catalyst (3 µmol) was added to lactide (144 mg, 1.0 mmol) in dichloromethane (2.5 mL). If desired, benzyl alcohol (5.0×10^{-2} M in CH₂Cl₂) and/or a stock solution of sodium methoxide (5.0×10^{-2} M in CH₂Cl₂) was added to the reaction mixture in the desired quantity. Reaction mixtures were quenched at the desired polymerisation time by addition of a dichloromethane solution of acetic acid (5 mM). Polymer samples were stored in a fridge at –80 °C.

At 130°C: The catalyst (0.01 mmol) was added to lactide (144 mg, 1.0 mmol) in dichloromethane (2.5 mL) in a pressure tube. If desired, benzyl alcohol (5.0×10^{-2} M in CH₂Cl₂) and/or a stock solution of sodium methoxide (5.0×10^{-2} M in CH₂Cl₂) was added to the reaction mixture. The tube was placed in an oil bath already heated to the desired temperature. Reaction mixtures were quenched at the desired polymerisation time by addition of a dichloromethane solution of acetic acid (5 mM). Polymer samples were stored in a fridge at –80 °C.

Polymer characterization. Conversion was determined from ¹H NMR by comparison to remaining lactide. P_r values were determined from homodecoupled ¹H NMR spectra and calculated from $P_r = 2 \cdot I_1 / (I_1 + I_2)$, with $I_1 = 5.15 – 5.21$ ppm (*rnr*, *mmr/rmm*), $I_2 = 5.21 – 5.25$ ppm (*mmr/rmm*, *mmm*, *mrm*). The integration of the left multiplet and right multiplet (I_1 and I_2) required only one, very reproducible dividing point of the integration, which was always taken as the minimum between the two multiplets. P_r -values obtained this way were typically consistent to ±1% over the course of one experiment and ±3% between different experiments under identical conditions. Molecular weight analyses were performed on a Waters 1525 gel permeation chromatograph equipped with three Phenomenex columns and a refractive index detector at 35 °C. THF was used as the eluent at a flow rate of 1.0 mL·min^{–1} and polystyrene standards (Sigma–Aldrich, 1.5 mg·mL^{–1}, prepared and filtered (0.2 mm) directly prior to injection) were used for calibration. Obtained molecular weights were corrected by a Mark–Houwink factor of 0.58.⁹¹

General procedure for Chan–Evans–Lam couplings. To a solution of amine or aniline (1.0 mmol) and phenylboronic acid (1.5 mmol) in methanol (1 mL) was added the desired catalyst (0.025 mmol). Trimethoxybenzene was added as internal standard. The reaction was stirred open to air at ambient temperature. For kinetic experiments, 20 µL aliquots were taken, diluted in ethyl acetate and analyzed by GC-MS. After the desired reaction time, the reaction was quenched with 0.5 mL of a saturated aqueous solution of ammonium chloride. The

organic layer was extracted and filtered through a short silica plug to remove remaining copper complex. Products and side-products were identified by the MS- and NMR-spectrum from comparison to literature. Conversion was typically analysed by GC-MS. Quantitative concentrations were determined by comparison to trimethoxybenzene standard. Calibration factors between starting materials, products, side-products and trimethoxybenzene were determined from simultaneous NMR and GC-MS analysis or by analysis of solutions prepared from isolated or commercially available products.

X-ray diffraction studies. Crystal for X-ray diffraction were obtained from synthesis as described above. Diffraction data were collected on a Bruker Venture METALJET diffractometer (Ga K α radiation).⁹² Data reduction was performed with SAINT,⁹³ absorption corrections with SADABS.⁹⁴ Structures were solved by dual-space refinement (SHELXT).⁹⁵ All non-hydrogen atoms were refined anisotropic using full-matrix least-squares on F^2 and hydrogen atoms refined with fixed isotropic U using a riding model (SHELXL97).⁹⁶ Further experimental details can be found in Table 5-6 and the supporting information (CIF).

5.6. References

- ¹ G. Evano and N. Blanchard, *Copper-Mediated Cross-Coupling Reactions*, John Wiley & Sons, New York, 2013.
- ² W. Simon, *Angew. Chem., Int. Ed.*, 2005, **44**, 5560-5562.
- ³ T. J. J. Whitehorne and F. Schaper, *Chem. Commun. (Cambridge, U. K.)*, 2012, **48**, 10334-10336.
- ⁴ T. J. J. Whitehorne and F. Schaper, *Inorg. Chem.*, 2013, **52**, 13612-13622.
- ⁵ T. J. J. Whitehorne and F. Schaper, *Can. J. Chem.*, 2014, **92**, 206-214.
- ⁶ S. Fortun, P. Daneshmand and F. Schaper, *Angew. Chem., Int. Ed.*, 2015, **54**, 13669-13672.
- ⁷ P. Daneshmand, A. van der Est and F. Schaper, *ACS Catal.*, 2017, **7**, 6289-6301.
- ⁸ P. Daneshmand, J. L. Jiménez-Santiago, M. Aragon--Alberti and F. Schaper, *Organometallics*, 2018, **in print**, acs.organomet.8b00196.
- ⁹ P. Daneshmand, S. Fortun and F. Schaper, *Organometallics*, 2017, **36**, 3860–3877.
- ¹⁰ T. J. J. Whitehorne and F. Schaper, *Can. J. Chem.*, 2014, **92**, 206-214.
- ¹¹ V. Hardouin Duparc and F. Schaper, *Organometallics*, 2017, **36**, 3053-3060.
- ¹² V. Hardouin Duparc and F. Schaper, *Dalton Trans.*, 2017, **46**, 12766 - 12770.
- ¹³ V. Hardouin Duparc, G. Bano and F. Schaper, *ACS Catal.*, 2018, **8**, 7308–7325.
- ¹⁴ E. Le Roux, *Coord. Chem. Rev.*, 2016, **306**, 65-85.
- ¹⁵ S. Paul, Y. Zhu, C. Romain, R. Brooks, P. K. Saini and C. K. Williams, *Chem. Commun. (Cambridge, U. K.)*, 2015, **51**, 6459-6479.
- ¹⁶ J. P. MacDonald and M. P. Shaver, in *Green Polymer Chemistry: Biobased Materials and Biocatalysis*, American Chemical Society, 2015, vol. 1192, ch. 10, pp. 147-167.
- ¹⁷ S. M. Guillaume, E. Kirillov, Y. Sarazin and J.-F. Carpentier, *Chem.-Eur. J.*, 2015, **21**, 7988-8003.
- ¹⁸ A. Sauer, A. Kapelski, C. Fliedel, S. Dagorne, M. Kol and J. Okuda, *Dalton Trans.*, 2013, **42**, 9007-9023.

¹⁹ S. Dagorne, M. Normand, E. Kirillov and J.-F. Carpentier, *Coord. Chem. Rev.*, 2013, **257**, 1869-1886.

²⁰ S. Dagorne and C. Fliedel, in *Modern Organoaluminum Reagents: Preparation, Structure, Reactivity and Use*, eds. S. Woodward and S. Dagorne, Springer Berlin Heidelberg, Berlin, Heidelberg, 2013, DOI: 10.1007/3418_2012_35, pp. 125-171.

²¹ J.-F. Carpentier, B. Liu and Y. Sarazin, in *Advances in Organometallic Chemistry and Catalysis*, John Wiley & Sons, Inc., 2013, DOI: 10.1002/9781118742952.ch28, pp. 359-378.

²² I. dos Santos Vieira and S. Herres-Pawlis, *Eur. J. Inorg. Chem.*, 2012, **2012**, 765-774.

²³ C. A. Wheaton and P. G. Hayes, *Comments Inorg. Chem.*, 2011, **32**, 127-162.

²⁴ S. Inkinen, M. Hakkarainen, A.-C. Albertsson and A. Södergård, *Biomacromolecules*, 2011, **12**, 523-532.

²⁵ S. Dutta, W.-C. Hung, B.-H. Huang and C.-C. Lin, in *Synthetic Biodegradable Polymers*, eds. B. Rieger, A. Künkel, G. W. Coates, R. Reichardt, E. Dinjus and T. A. Zevaco, Springer-Verlag, Berlin, 2011, pp. 219-284.

²⁶ P. J. Dijkstra, H. Du and J. Feijen, *Polym. Chem.*, 2011, **2**, 520-527.

²⁷ S. Dagorne, C. Fliedel and P. de Frémont, in *Encyclopedia of Inorganic and Bioinorganic Chemistry*, John Wiley & Sons, Ltd, 2011, DOI: 10.1002/9781119951438.eibc2416.

²⁸ J.-C. Buffet and J. Okuda, *Polym. Chem.*, 2011, **2**, 2758-2763.

²⁹ C. M. Thomas, *Chem. Soc. Rev.*, 2010, **39**, 165.

³⁰ M. J. Stanford and A. P. Dove, *Chem. Soc. Rev.*, 2010, **39**, 486-494.

³¹ M. D. Jones, in *Heterogenized Homogeneous Catalysts for Fine Chemicals Production*, eds. P. Barbaro and F. Liguori, Springer Netherlands, 2010, vol. 33, pp. 385-412.

³² N. Ajellal, J.-F. Carpentier, C. Guillaume, S. M. Guillaume, M. Helou, V. Poirier, Y. Sarazin and A. Trifonov, *Dalton Trans.*, 2010, **39**, 8363.

³³ C. A. Wheaton, P. G. Hayes and B. J. Ireland, *Dalton Trans.*, 2009, 4832 - 4846.

³⁴ T.-Q. Xu, G.-W. Yang, C. Liu and X.-B. Lu, *Macromolecules*, 2017, **50**, 515-522.

³⁵ J. Bhattacharjee, A. Harinath, H. P. Nayek, A. Sarkar and T. K. Panda, *Chem.-Eur. J.*, 2017, **23**, 9319-9331.

³⁶ D. Myers, A. J. P. White, C. M. Forsyth, M. Bown and C. K. Williams, *Angew. Chem., Int. Ed.*, 2017, **56**, 5277-5282.

³⁷ T. Rosen, Y. Popowski, I. Goldberg and M. Kol, *Chem.-Eur. J.*, 2016, **22**, 11533-11536.

³⁸ Y. Sun, J. Xiong, Z. Dai, X. Pan, N. Tang and J. Wu, *Inorg. Chem.*, 2016, **55**, 136-143.

³⁹ P. McKeown, M. G. Davidson, G. Kociok-Kohn and M. D. Jones, *Chem. Commun. (Cambridge, U. K.)*, 2016, **52**, 10431-10434.

⁴⁰ H. Wang, Y. Yang and H. Ma, *Macromolecules*, 2014, **47**, 7750-7764.

⁴¹ Z. Mou, B. Liu, M. Wang, H. Xie, P. Li, L. Li, S. Li and D. Cui, *Chem. Commun. (Cambridge, U. K.)*, 2014, **50**, 11411-11414.

⁴² C. Bakewell, A. J. P. White, N. J. Long and C. K. Williams, *Angew. Chem., Int. Ed.*, 2014, **53**, 9226-9230.

⁴³ D. C. Aluthge, B. O. Patrick and P. Mehrkhodavandi, *Chem. Commun. (Cambridge, U. K.)*, 2013, **49**, 4295-4297.

⁴⁴ D. M. T. Chan, K. L. Monaco, R.-P. Wang and M. P. Winters, *Tetrahedron Lett.*, 1998, **39**, 2933-2936.

⁴⁵ D. A. Evans, J. L. Katz and T. R. West, *Tetrahedron Lett.*, 1998, **39**, 2937-2940.

⁴⁶ P. Y. S. Lam, C. G. Clark, S. Saubern, J. Adams, M. P. Winters, D. M. T. Chan and A. Combs, *Tetrahedron Lett.*, 1998, **39**, 2941-2944.

⁴⁷ S. Bhunia, G. G. Pawar, S. V. Kumar, Y. Jiang and D. Ma, *Angew. Chem., Int. Ed.*, 2017, **56**, 16136-16179.

⁴⁸ P. Y. S. Lam, in *Synthetic Methods in Drug Discovery: Volume 1*, The Royal Society of Chemistry, 2016, vol. 1, pp. 242-273.

⁴⁹ L. Neuville, in *Copper-Mediated Cross-Coupling Reactions*, John Wiley & Sons, Inc., 2013, DOI: 10.1002/9781118690659.ch4, pp. 113-185.

⁵⁰ A. Casitas and X. Ribas, in *Copper-Mediated Cross-Coupling Reactions*, John Wiley & Sons, Inc., 2013, DOI: 10.1002/9781118690659.ch7, pp. 253-279.

⁵¹ S. E. Allen, R. R. Walvoord, R. Padilla-Salinas and M. C. Kozlowski, *Chem. Rev.*, 2013, **113**, 6234-6458.

⁵² K. Sanjeeva Rao and T.-S. Wu, *Tetrahedron*, 2012, **68**, 7735-7754.

⁵³ T. R. M. Rauws and B. U. W. Maes, *Chem. Soc. Rev.*, 2012, **41**, 2463-2497.

⁵⁴ I. P. Beletskaya and A. V. Cheprakov, *Organometallics*, 2012, **31**, 7753-7808.

- ⁵⁵ J. X. Qiao and P. Y. S. Lam, in *Boronic Acids*, Wiley-VCH Verlag GmbH & Co. KGaA, 2011, DOI: 10.1002/9783527639328.ch6, pp. 315-361.
- ⁵⁶ F. Bellina and R. Rossi, *Adv. Synth. Catal.*, 2010, **352**, 1223-1276.
- ⁵⁷ G. Evano, N. Blanchard and M. Toumi, *Chem. Rev.*, 2008, **108**, 3054-3131.
- ⁵⁸ S. V. Ley and A. W. Thomas, *Angew. Chem., Int. Ed.*, 2003, **42**, 5400-5449.
- ⁵⁹ J. P. Collman, M. Zhong, C. Zhang and S. Costanzo, *J. Org. Chem.*, 2001, **66**, 7892-7897.
- ⁶⁰ A. E. King, B. L. Ryland, T. C. Brunold and S. S. Stahl, *Organometallics*, 2012, **31**, 7948-7957.
- ⁶¹ J. C. Vantourout, H. N. Miras, A. Isidro-Llobet, S. Sproules and A. J. B. Watson, *J. Am. Chem. Soc.*, 2017, **139**, 4769-4779.
- ⁶² Z. Qi-Ji, Y. Xue-Jun, H. Lan-Fang, O. Yan, X. Jing-Yuan, X. Cheng-Zhi and L. Jian-Shi, *Z. Anorg. Allg. Chem.*, 2010, **636**, 2487-2491.
- ⁶³ J. Li, Y. Zhao and Y. Jiang, *Synthesis and Reactivity in Inorganic, Metal-Organic, and Nano-Metal Chemistry*, 2010, **40**, 715-718.
- ⁶⁴ J. M. Li, Z. F. Shi, X. R. Huang and Y. M. Jiang, *Russian Journal of Coordination Chemistry*, 2011, **37**, 921-925.
- ⁶⁵ S. Xu and J. Li, *Asian J. Chem.*, 2012, **24**, 989-991.
- ⁶⁶ W. L. Leong and J. J. Vittal, *Journal of Inclusion Phenomena and Macrocyclic Chemistry*, 2011, **71**, 557-566.
- ⁶⁷ J.-m. Li and Z.-f. Shi, *Hecheng Huaxue (Chin. J. Syn. Chem.)*, 2013, **21**, 659-662.
- ⁶⁸ Y.-M. Ou, Z.-Y. Zhao, Y.-H. Shi, Y.-L. Zhang and Y.-M. Jian, *Chinese Journal of Structural Chemistry*, 2009, 457-460.
- ⁶⁹ S. Hazra, S. Mukherjee, M. F. C. Guedes da Silva and A. J. L. Pombeiro, *RSC Adv.*, 2014, **4**, 48449-48457.
- ⁷⁰ S. Hazra, A. P. C. Ribeiro, M. F. C. Guedes da Silva, C. A. Nieto de Castro and A. J. L. Pombeiro, *Dalton Trans.*, 2016, **45**, 13957-13968.
- ⁷¹ S. Hazra, A. Karmakar, M. d. F. C. Guedes da Silva, L. u. Dlhan, R. Boca and A. J. L. Pombeiro, *New J. Chem.*, 2015, **39**, 3424-3434.
- ⁷² G.-G. Yang, M. Ou-Yang, X.-J. Meng, X.-R. Huang and Y.-M. Jiang, *Acta Crystallogr., Sect. E: Struct. Rep. Online*, 2009, **65**, m1200.

⁷³ A. Paul, S. Hazra, G. Sharma, M. F. C. Guedes da Silva, B. Koch and A. J. L. Pombeiro, *Journal of Inorganic Biochemistry*, 2017, **174**, 25-36.

⁷⁴ N. J. R., *Angew. Chem., Int. Ed.*, 2004, **43**, 3073-3075.

⁷⁵ C. R. Groom, I. J. Bruno, M. P. Lightfoot and S. C. Ward, *Acta Crystallogr., Sect. B: Struct. Sci.*, 2016, **72**, 171-179.

⁷⁶ Y.-M. Ou, Z.-Y. Zhao, Yue-Hua Shi, Y.-L. Zhang and Y.-M. Jiang, *Chin. J. Struct. Chem.*, 2009, **28**, 457.

⁷⁷ C.-J. Qiu, Y.-C. Zhang, Y. Gao and J.-Q. Zhao, *J. Organomet. Chem.*, 2009, **694**, 3418-3424.

⁷⁸ P. Harding, D. J. Harding, N. Soponrat, K. Tinpun, S. Samuadnuan and H. Adams, *Aust. J. Chem.*, 2010, **63**, 75-82.

⁷⁹ M. Cheng, A. B. Attygalle, E. B. Lobkovsky and G. W. Coates, *J. Am. Chem. Soc.*, 1999, **121**, 11583-11584.

⁸⁰ S. Wiese, Y. M. Badiei, R. T. Gephart, S. Mossin, M. S. Varonka, M. M. Melzer, K. Meyer, T. R. Cundari and T. H. Warren, *Angew. Chem., Int. Ed.*, 2010, **49**, 8850-8855.

⁸¹ A. Takenaka, H. Utsumi, T. Yamamoto, A. Furusaki and I. Nitta, *J. Chem. Soc. Jpn. ,Pure Chem.* , 1970, **91**, 928.

⁸² N. Nasser, M. A. Fard, P. D. Boyle and R. J. Puddephatt, *J. Organomet. Chem.*, 2018, **858**, 67-77.

⁸³ K. S. Kwon, J. Cho, S. Nayab and J. H. Jeong, *Inorg. Chem. Commun.*, 2015, **55**, 36-38.

⁸⁴ J. Cho, S. Nayab and J. H. Jeong, *Polyhedron*, 2016, **113**, 81-87.

⁸⁵ S. H. Ahn, M. K. Chun, E. Kim, J. H. Jeong, S. Nayab and H. Lee, *Polyhedron*, 2017, **127**, 51-58.

⁸⁶ M. K. Chun, J. Cho, S. Nayab and J. H. Jeong, *Bull. Korean Chem. Soc.*, 2017, **38**, 1527-1530.

⁸⁷ K. S. Kwon, S. Nayab and J. H. Jeong, *Polyhedron*, 2017, **130**, 23-29.

⁸⁸ J. P. Collman and M. Zhong, *Org. Lett.*, 2000, **2**, 1233-1236.

⁸⁹ A. E. King, T. C. Brunold and S. S. Stahl, *J. Am. Chem. Soc.*, 2009, **131**, 5044-5045.

⁹⁰ M. S. Ziegler, D. S. Levine, K. V. Lakshmi and T. D. Tilley, *J. Am. Chem. Soc.*, 2016, **138**, 6484-6491.

⁹¹ M. Save, M. Schappacher and A. Soum, *Macromol. Chem. Phys.*, 2002, **203**, 889-899.

⁹² *APEX2*, Release 2.1-0; Bruker AXS Inc.: Madison, USA, 2006.

⁹³ *SAINT*, Release 7.34A; Bruker AXS Inc.: Madison, USA, 2006.

⁹⁴ G. M. Sheldrick *SADABS*, Bruker AXS Inc.: Madison, USA, 1996 & 2004.

⁹⁵ G. Sheldrick, *Acta Crystallogr. Sect. A: Found. Crystallogr.*, 2015, **71**, 3-8.

⁹⁶ G. M. Sheldrick, *Acta Crystallogr.*, 2008, **A64**, 112-122.

5.7. Supporting Information

- **Figure 5.S1.** Crystal structure of complex $(\mathbf{8})_2 \cdot \text{Cu}(\text{OTf})_2 \cdot 10 \text{ H}_2\text{O}$.
- **Figure 5.S2.** Crystal structures of complex **11** (left) and **12** (right).
- **Figure 5.S3.** X-ray structure of boroxine-DMAP.
- **Table 5-S1** Cu-ligand bond lengths in **11** and **12**.
- **Table 5-S2** Cu-ligand bond lengths in **17**.
- Determination of pseudo-first-order rate constants in CEL couplings.
- **Table 5-S3** Individual rate constants determined in CEL couplings.
- **Table 5-S4** Experimental details of X-ray diffraction studies.

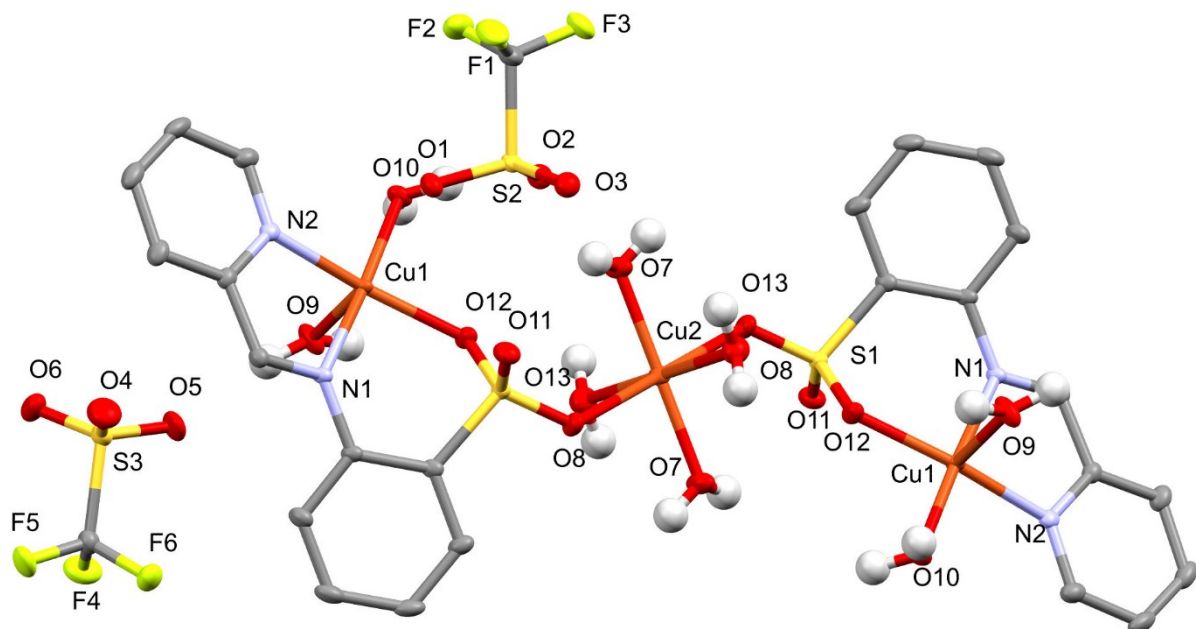


Figure 5.S1: Crystal structure of complex $(\mathbf{8})_2 \cdot \text{Cu}(\text{OTf})_2 \cdot 10 \text{ H}_2\text{O}$ or $[(\text{H}_2\text{O})_2\text{Cu}(\mu-\mathbf{L2})_2\text{Cu}(\text{OH}_2)_4]\text{[OTf]}_4 \cdot 2 \text{ H}_2\text{O}$. Co-crystallized water and hydrogen atoms other than that of water omitted for clarity. Thermal ellipsoids are drawn at 50% probability.

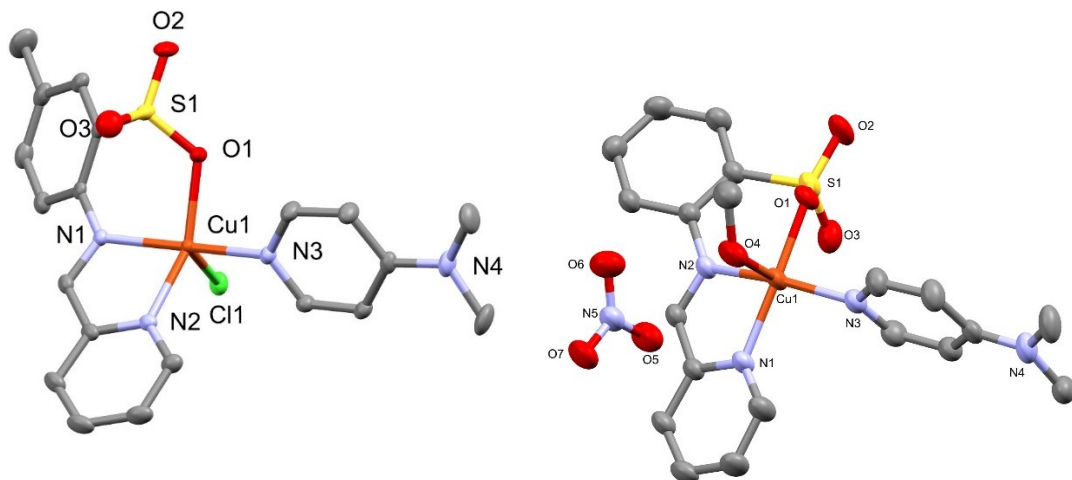
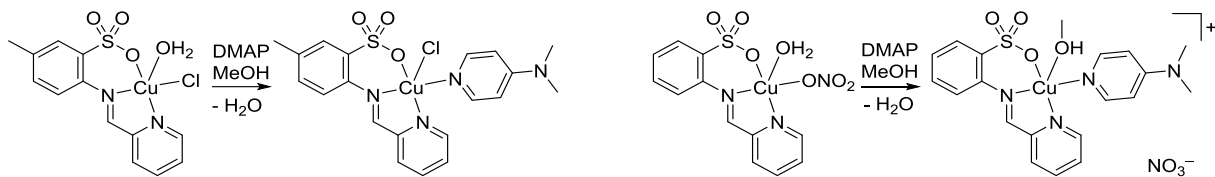


Figure 5.S2 : Crystal structures of complex **11** (left) and **12** (right). Hydrogen atoms omitted for clarity. Thermal ellipsoids are drawn at 50% probability.

Crystallisation conditions: Complex **9** (50 mg, 0.13 mmol) or (50 mg, 0.13 mmol) was mixed with phenylboronic acid (7 mg, 0.13 mmol) and DMAP (21 μ L, 0.13 mmol) in 2 mL of methanol. After 5 min of agitation at room temperature, the vial was placed at 5 °C. Crystals of **11** separated from the solution after several days. **12**: Equivalent from complex **6** (50 mg, 0.13 mmol).

Table 5-S1 : Cu-ligand bond lengths in **11** and **12**.

	11	12
Cu-OSO ₂	2.014(1)	1.976(2)
Cu-N(=C)	2.020(1)	2.035(3)
Cu-N _{pyr.}	2.065(2)	2.005(3)
Cu-N _{DMAP} ^b	1.978(1)	1.974(3)
Cu-Cl	2.401(2)	
Cu-O(H)Me		2.184(3)
Geometry	Square-pyramidal	Square-pyramidal
τ	0.4	0.1

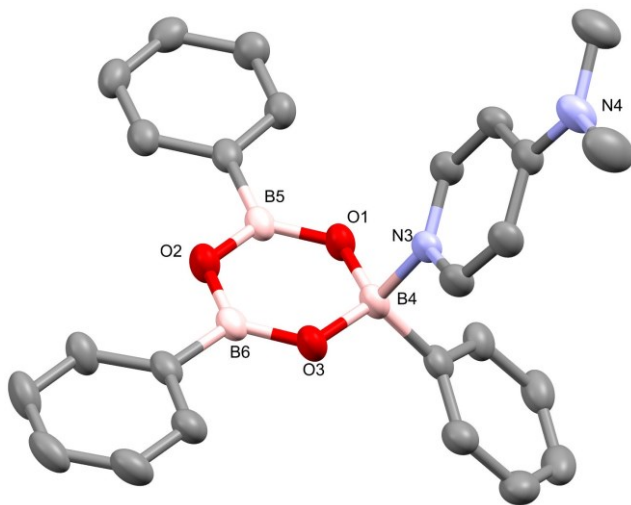


Figure 5.S3 : Crystal structure of a DMAP adduct of boroxine, obtained in crystallisation attempts from methanol solutions containing 0.6 mM **9**, 0.6 mM PhB(OH)₂ and 0.6 M DMAP. Hydrogen atoms were omitted for clarity. Thermal ellipsoids are drawn at 50% probability.

Table 5-S2 : Cu-ligand bond lengths in **17**.

Cu-OSO ₂	1.951(2)
Cu-O _{Phenol}	1.951(2)
Cu-N(=C)	1.951(3)
Cu-OMe	1.921(2)
Cu-(μ -OSO ₂)	2.428(3)
Cu-Cu	3.0395(8)
Geometry	Square-pyramidal
τ	0.1

Determination of pseudo-first-order rate constants in CEL couplings

Rate constants of individual kinetic runs were determined by linear regression of the linearized first-order rate law, using data points after the induction period and typically with less than 85% conversion to avoid the increase in activity at low aniline concentrations due to the unreactive aniline-complex. Repeated runs differed typically by less than 20%. Induction periods, however, differed widely. Since individual runs contained different number of data points and different reliability, averaged rate constants were not obtained by averaging k_{obs} from each experiment, but by simultaneous regression of the all obtained data, refining a common rate constant and individual induction periods. The graphic in the main manuscript shows selected individual runs with their individual fit curves.

Table 5-S3 : Individual rate constants determined in CEL couplings.

Catalyst	Reaction	Final Time	Conversion	Individual regression		Simultaneous fit		Remarks
				k_{obs}	t_0	$k_{\text{obs}}^{\text{a}}$	t_0	
9				0.40(2)	40			taken from <i>Dalton Trans.</i> 2017, 46, 12766.
				h^{-1}	min			
10				0.50(1)	10			taken from <i>Dalton Trans.</i> 2017, 46, 12766.
				h^{-1}	min			
5	8 h	99%		0.38(1)	150	0.47	165	
				h^{-1}	min	h^{-1}	min	
5	12 h	100%		0.51(2)	145	0.47	135	data shown in Fig. 5.6
				h^{-1}	min	h^{-1}	min	
5	12 h	100%				0.47	160	too few datapoints
						h^{-1}	min	
6	8 h	85%		0.53(3)	270	0.67	315	
				h^{-1}	min	h^{-1}	min	
6	12 h	99%		0.69(7)	55	0.67	50 min	data shown in Fig. 5.6
				h^{-1}	min	h^{-1}		

6	12 h	100%		0.67		too few datapoints	
				h^{-1}			
7	8 h	97%	0.66(7)	230	0.67	data shown in Fig. 5.6	
			h^{-1}	min	h^{-1}		
7	12 h	99%	0.75(21)	250	0.67	unreliable, few datapoints	
			h^{-1}	min	h^{-1}		
8	8 h	99%	0.69(2)	5	0.70	5 min	data shown in Fig. 5.6
			h^{-1}	min	h^{-1}		
8	7 h	96%	0.57(2)	15	0.70	10 min	some decomposition
8	5 h	100%	0.96(13)	25	0.70	30 min	
			h^{-1}	min	h^{-1}		
1	8 h	75%	0.38(3)	270	0.35	260	data shown in Fig. 5.6
1	12 h		h^{-1}	min	h^{-1}	min	
		95%	0.34(1)	150	0.35	155	decomposition
			h^{-1}	min	h^{-1}	min	

^a Although provided with two significant digits in this table, precision of the rate constant from the simultaneous regression of all datapoints should not be considered higher than $\pm 0.1 \text{ h}^{-1}$.

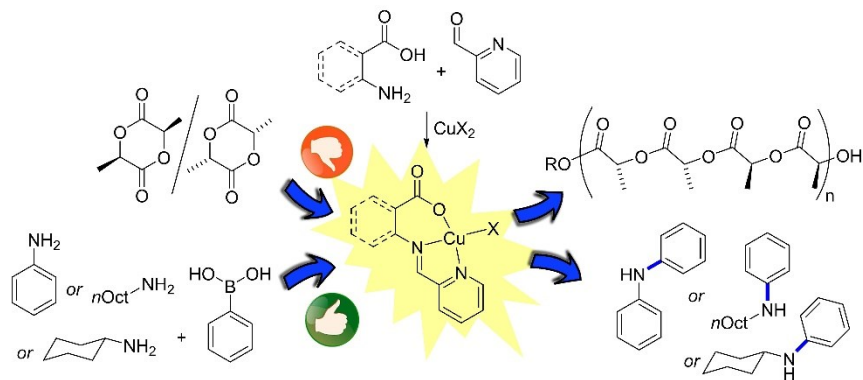
Table 5-S4 : Experimental details of X-ray diffraction studies

	2	3	4	6	7	8
Formula	C ₈ H ₁₁ CuN ₃ O ₇ S	C _{21.81} H _{32.62} Cu ₂ N ₄ O ₁₃ S ₂	C ₉ H ₁₃ CuF ₃ N ₂ O ₈ S ₂	C ₁₂ H ₁₁ CuN ₃ O ₇ S	C ₂₈ H ₂₄ Cu ₂ N ₄ O ₁₀ S ₂	C ₁₃ H ₉ CuN ₂ F ₃ O ₆ S ₂
M _w (g/mol); F(000)	356.80; 720	750.09; 3087	461.87	404.84; 820	767.71; 1560	473.88; 1914
T (K); wavelength	150; 1.34190	150; 1.34190	100; 1.34190	100; 1.34190	100; 1.34190	100; 1.34190
Crystal System	Triclinic	Monoclinic	Triclinic	Monoclinic	Monoclinic	Orthorhombic
Space Group	P-1	P2 ₁ /c	P-1	C1	P2 ₁ /n	Pbca
Unit Cell: a (Å)	7.1058(13)	29.3247(18)	6.9779(5)	6.7709(2)	8.2557(5)	14.7603(8)
b (Å)	8.3556(16)	12.5017(8)	9.8366(7)	13.8992(4)	14.4746(8)	10.1245(5)
c (Å)	22.391(4)	19.0000(11)	11.5507(8)	15.7309(4)	25.4468(14)	22.1832(12)
α (°)	92.836(12)	90	84.806(3)	90	90	90
β (°)	91.843(12)	107.651(3)	88.988(3)	96.7590(10)	93.288(3)	90
γ (°)	100.042(12)	90	79.510(3)	90	90	90
V (Å ³)	1306.3(4)	6637.6(7)	776.37(10)	1470.15(7)	3035.8(3)	3315.1(3)
Z; d _{calcd.} (g/cm ³)	4; 1.814	8; 1.501	2; 1.976	4; 1.829	8; 1.680	8; 1.899
μ (mm ⁻¹); Abs. Corr.	10.232; multi-scan	8.056; multi-scan	9.725; multi-scan	9.155; multi-scan	8.766; multi-scan	9.072; multi-scan
Extinction coeff.	-	-	0.0160(15)	-	-	-
θ range (°); completeness	1.72-62.42; 0.983	3.37-60.97; 0.989	3.34-60.82; 0.999	4.93-60.65; 0.999	3.03-60.68; 0.997	4.34-60.74; 1.000
Collected reflections; R _σ	18655; 0.1211	41051; 0.0442	13049; 0.0502	26307; 0.0206	6962; 0.0282	39089; 0.0504
Unique reflections; R _{int}	5832; 0.1071	7443; 0.0668	3549; 0.0587	3347; 0.0373	6772; 0.0350	3087; 0.1087
Oberved Reflections; R1(F)	3689; 0.1626	5178; 0.1191	3442; 0.0604	3332; 0.0257	6962; 0.0335	3010; 0.0878
wR(F ²) (all data); GoF(F ²)	0.4267; 1.036	0.4010; 1.619	0.1599; 1.081	0.0663; 1.055	0.0854; 1.066	0.2440; 1.084
Residual electron density	2.593	1.357	0.821	0.412	0.484	1.388

Table 5-S4 : continued

	8b	11	12	15	17
Formula	C ₁₃ H ₁₁ CuF ₃ N ₂ O ₇ S ₂	C ₂₀ H ₂₃ CuN ₅ O ₇ S	C ₂₀ H ₂₁ ClCuN ₄ O ₃ S	C ₁₉ H ₁₆ CuN ₃ F ₃ O ₇ S ₂	C ₁₄ H ₁₄ Cu ₂ N ₂ O ₈ S ₂
M _w (g/mol); F(000)	491.90	541.03; 558	496.46; 2040	583.01; 2360	529.47; 1064
T (K); wavelength	100; 1.34190	150; 1.34190	150; 1.34190	100; 1.34190	100; 1.34190
Crystal System	Triclinic	Triclinic	Orthorhombic	Orthorhombic	Monoclinic
Space Group	P-1	P-1	Pbca	Pbca	P2 ₁ /c
Unit Cell: a (Å)	7.6886(3)	7.5468(4)	8.4014(2)	15.4874(4)	17.1025(6)
b (Å)	10.5193(4)	8.2480(4)	18.7365(4)	10.6035(3)	15.2512(6)
c (Å)	11.3989(5)	18.8537(9)	26.8525(6)	26.8803(8)	8.8117(3)
α (°)	77.209(2)	80.525(3)	90	90	90
β (°)	70.629(2)	86.591(3)	90	90	117.191(2)
γ (°)	79.302(2)	78.705(3)	90	90	90
V (Å ³)	841.82(6)	1134.69(10)	4226.93(16)	4414.3(2)	2044.39(13)
Z; d _{calcd.} (g/cm ³)	2; 1.941	2; 1.584	8; 1.560	8; 1.754	4; 1.720
μ (mm ⁻¹); Abs. Corr.	8.978; multi-scan	6.069; multi-scan	7.127; multi-scan	6.932; multi-scan	12.755; multi-scan
Extinction coeff.	0.0378(18)	-	-	-	-
θ range (°); completeness	3.63-60.79; 1.000	2.068- 61.370; 0.999	2.863-60.667; 0.997	2.860-60.703; 1.000	7.253- 60.819; 0.978
Collected reflections; R _σ	3455; 0.0230	25300; 0.0595	38406; 0.0217	61013; 0.0212	21971; 0.0238
Unique reflections; R _{int}	3868; 0.0460	5240; 0.0803	4832; 0.0385	5071; 0.0492	2354; 0.0437
Oberved Reflections; R1(F)	3768; 0.0465	4192; 0.0576	4572; 0.0345	4756; 0.0287	2243; 0.0460
wR(F ²) (all data); GoF(F ²)	0.128; 1.041	0.1597; 1.046	0.0922; 1.129	0.0809; 1.068	0.1373; 1.054
Residual electron density	0.79	0.786	0.398	0.616	0.888

6. Replacing sulfonate by carboxylate: Application of pyridyliminocarboxylato copper(II) complexes in *rac*-lactide polymerization and Chan-Evans-Lam coupling.



V. Hardouin Duparc, C. Dimeck, F. Schaper *Can. J. Chem.* **2018**, submitted.

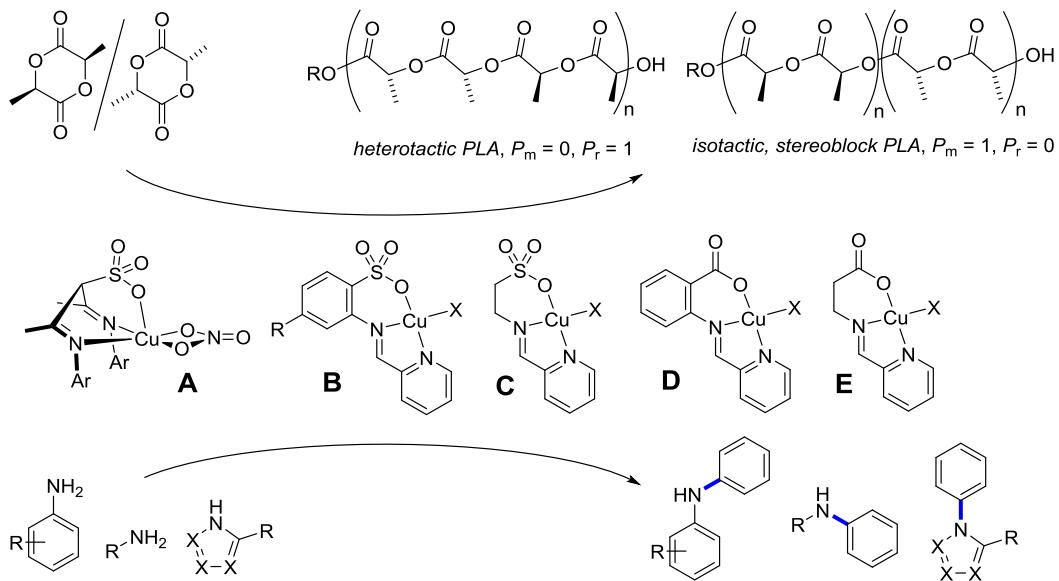
Contributions from Clémentine Dimeck : Synthesis of some pyridylcarboxylato complexes and lactide polymerization with these complexes.

6.2. Introduction

Copper has found widespread use in catalytic transformations,¹⁻² but its application in polymerization catalysis is controversial. It has been widely employed in radical polymerizations involving a Cu(I)/Cu(II) redox couple,³⁻⁴ but much less in homogenous, 2-electron processes. Copper(II) diimine complexes have been reported to copolymerize ethylene and methacrylate by a coordination-insertion mechanism.⁵⁻⁷ However, the very low activity of the system and the lack of a convincing mechanism make it doubtful that copper(II) does indeed polymerize ethylene. Radical mechanisms, involving copper(I) or ligand transfer to a catalytically active Al-species have been proposed as potential alternative reaction pathways.^{8; 9} Cu(II) complexes have also been claimed to polymerize acrylonitrile via a coordination-insertion mechanism,¹⁰ but again this was doubted later and a different mechanism, not involving Cu(II), was proposed to be responsible for the observed results.¹¹ There is no doubt, however, that Cu(II) complexes are active in the ring-opening polymerization of lactide to polylactic acid (PLA).

There is currently significant interest in the controlled polymerization of lactide,¹²⁻³¹ but effort have been concentrated for the most part on catalysts based on groups 1-4 and 12-14. In the limited number of copper-catalyzed reactions, polymerizations proceeded either via Lewis-acid activation of the monomer,³²⁻⁴¹ or via insertion into a copper-alkoxide bond.⁴²⁻⁵¹ We have previously reported that diketiminate copper alkoxides provide highly active, but controlled polymerization catalysts.^{42-43, 52} They are, however, very sensitive to air and moisture, which severely limits their applicability. To provide copper(II) polymerization catalysts with a ligand framework less susceptible to oxidation and hydrolysis, we recently investigated copper complexes with sulfonate-based ligands (Scheme 6-1, A - C). The sulfonate complexes proved to be unsuitable for lactide polymerization: the respective alkoxide complexes could not be isolated or – based on polymerization results – not even be prepared *in situ*.⁵³⁻⁵⁴ They proved to be, however, highly competent catalysts for Chan-Evans-Lam couplings of *N*-nucleophiles.⁵³⁻⁵⁶ Chan-Evans-Lam couplings are oxidative, copper-catalyzed couplings between a boronic acid and a second nucleophile, with copper(II) acetate being the most widely employed catalyst.⁵⁷⁻⁵⁹ Compared to the Ullmann-Goldberg reaction or Buchwald-Hartwig aminations catalyzed by palladium or copper, CEL couplings proceed under

much milder conditions, often at room temperature, and are thus more attractive for complicated and sensitive substrates.⁶⁰⁻⁷¹ Complexes **A-C**, but in particular **B**, showed quantitative conversion of amines, anilines and *N*-heterocycles using an identical reaction protocol and requiring a minimum of optimization of reaction conditions.⁵³⁻⁵⁶



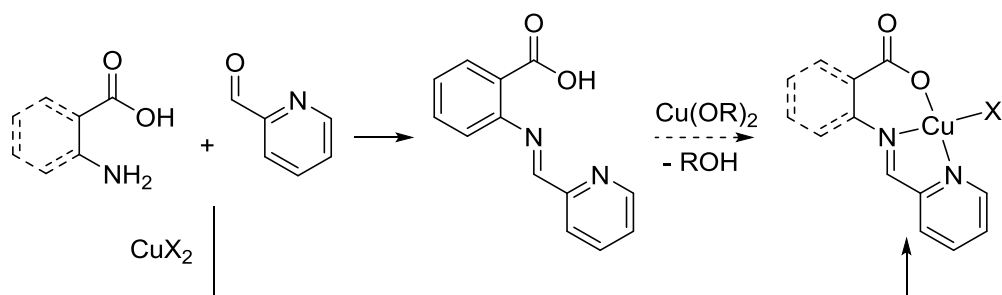
Scheme 6-1

Based on the assumption that one reason for the instability of $(L_{\text{sulfonate}})\text{Cu(OR)}$ in lactide polymerization is related to desulfonation, we investigated analogs to **B** and **C**, replacing the sulfonate group with carboxylate (**D** and **E**, Scheme 6-1), as catalysts in lactide polymerization. In Chan-Evans-Lam (CEL) couplings, the sulfonate group of **A-C** was proposed to bridge to boron in an intermediate dinuclear complex prior to transmetallation. Complexes **D** and **E** were thus also investigated for CEL couplings to test whether the carboxylate group is capable of providing the same functionality. Complexes $(L1)\text{CuX}$, **D**, have been previously prepared by Mitra and coworkers with oxalate, nitrate/azide and fluoroacetate anions.⁷²⁻⁷⁴ $[(L2)\text{Cu}]X$, **E**, has been reported with $X = \text{oxalate, azide or nitrate}$.⁷⁵⁻⁷⁸ To allow comparisons with the respective sulfonate complexes, we targeted complexes with chloride, nitrate, acetate and triflate counteranions.

6.2. Results and Discussion

6.2.1. Ligand syntheses.

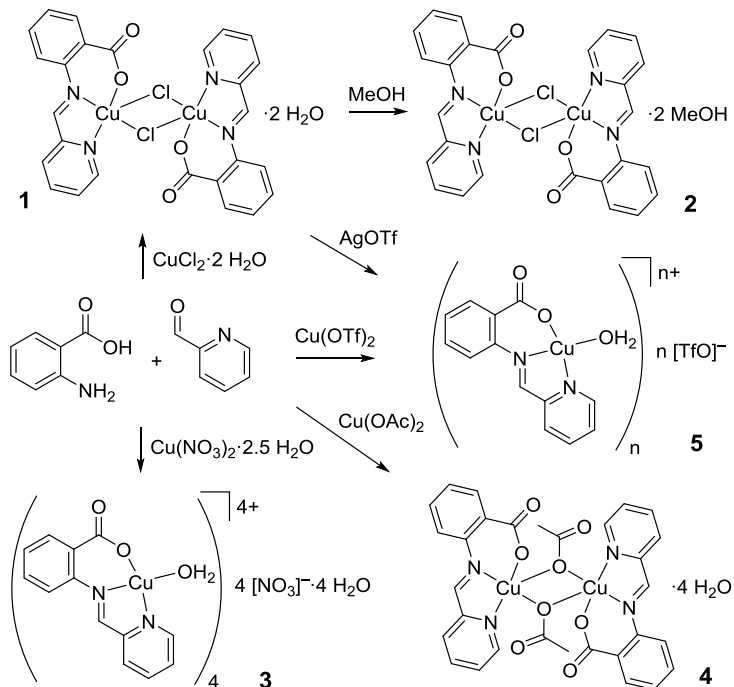
Our attempts to prepare **L1H** following literature protocols⁷⁴ did not afford a clean product.⁷⁹ Best results in optimizing ligand synthesis were obtained by using a Dean-Stark apparatus to eliminate water or microwave reactions in the presence of molecular sieves, both of which afforded 80% conversion. Despite numerous attempts, conversion could not be improved any further. Attempts to purify the ligand were not successful and at best 95% purity according to NMR could be obtained. Preparation of β -alanine-based ligand **L2H** has not been reported and attempts similar to the synthesis of **L1H** failed. While we cannot exclude a simple experimental problem on our side, the analogous sulfonate-based ligands were reported to be highly sensitive to hydrolysis.⁷⁸ On the other hand, they assemble readily to the ligand in the presence of a metal center to provide the respective metal complex.⁸⁰ **L1H** (95% purity) was thus employed for the attempted preparation of alkoxide complexes, while copper complexes with **L1** or **L2** ligands and other anions were obtained by direct condensation of the ligand on the metal center (Scheme 6-2).



Scheme 6-2

Complex syntheses. Reaction of anthranilic acid with pyridinecarbaldehyde and copper(II) chloride in methanol cleanly provided (**L1**)CuCl·H₂O, **1**, which crystallized as the dinuclear chloride bridged complex (Scheme 6-3, Table 6-1, Fig. 6.1). The coordination geometry around copper is square-pyramidal ($\tau = 0.0$) with **L1** and chloride in the equatorial plane and the bridging chloride in the apical position with an elongated ($\Delta d = 0.4 \text{ \AA}$) bond to copper. The structure of carboxylate complex **1** is very similar to the respective sulfonate complex **B** (Table

1). The only difference is the twisting of 30° between the aryl and the pyridyl rings in **B**, required by the tetrahedral geometry of the sulfonate group, (only 5° in **1**) and a very slightly shorter Cu-O distance ($\Delta d = 0.06 \text{ \AA}$) for carboxylate vs. sulfonate coordination. Since the presence of co-crystallized water might prevent preparation of alkoxide complexes, **1** was recrystallized in dry methanol to provide $(\mathbf{L}1)\text{CuCl}\cdot\text{MeOH}$, **2**, which is isostructural with water replaced by methanol (Scheme 6-3, Fig. 6.1, Table 6-1).



Scheme 6-3

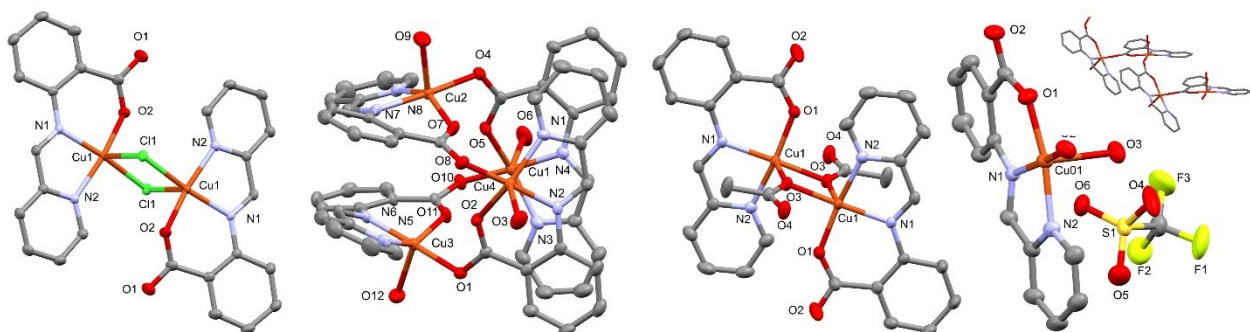


Figure 6.1 : X-ray structures of **1** (left), **3** (middle left), **4** (middle right) and **5** (right). Thermal ellipsoids are drawn at the 50% probability level. Hydrogen atoms and co-crystallized water (**1**, **3**, **4**) and the nitrate anion (**3**) omitted for clarity. The inset shows the 1D coordination polymer (**5**)_n.

Table 6-1 : Selected geometric data of X-ray structures of **1-5**.

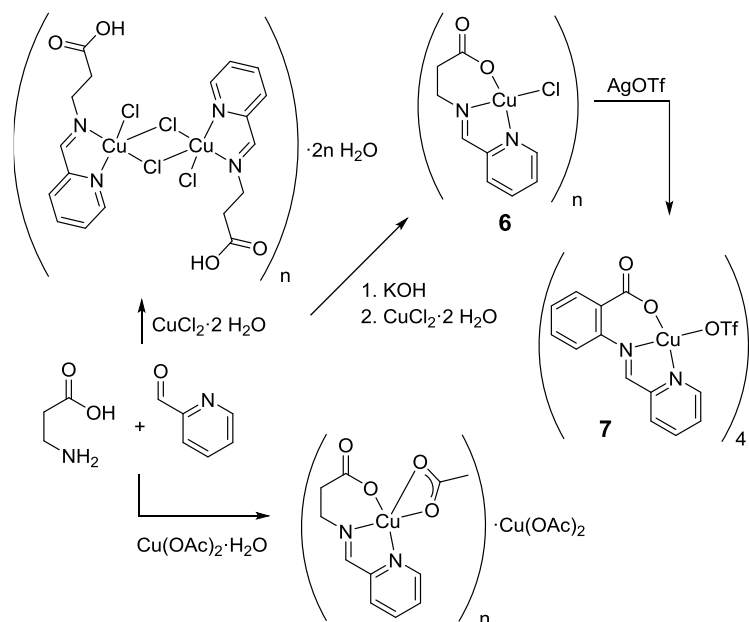
	B ^a	1	2	3	4	5
Cu-O ₂ C	1.964(2)	1.891(1), 1.905(1)	1.892(6), 1.900(6)	1.942(4) – 1.954(4)	1.894(1)	1.926(3)
Cu-N(=C)	2.068(2)	2.020(2), 2.003(2)	1.892(6), 1.900(6)	1.968(5) – 1.980(5)	1.996(2)	1.998(3)
Cu-N _{pyridine}	2.002(2)	2.002(2), 2.003(2)	1.998(7), 2.021(7)	2.008(5) – 2.025(5)	1.988(2)	1.983(4)
Cu-OH ₂				2.153(5) – 2.168(5)		2.200(4)
Cu-X ^b	2.276(1)	2.287(2), 2.305(2)	2.306(2), 2.305(3)		1.973(1)	
Cu-L ^b	2.679(1)	2.720(2), 2.660(2)	2.655(3), 2.656(3)	1.935(4) – 1.941(4)	2.295(2)	1.950(3)
τ	0.0	0.1, 0.1	0.1, 0.1	0.5	0.1	0.0

^a Data taken from ref. ⁸¹ ^b **B**, **1**, **2**: X=μ-Cl_{short}, L=μ-Cl_{long}. **3**: L=μ-CO₂. **4**: X=μ-OAc_{short}, L=μ-OAc_{long}. **5**: L=μ-O₂CR

Reactions in the presence of copper nitrate or copper acetate yielded the respective complexes **[(L1)Cu(OH₂)][NO₃]·H₂O**, **3**,⁷⁴ and **(L1)Cu(OAc)·2H₂O**, **4**, both with co-crystallized/coordinated water (Scheme 6-3, Table 6-1, Fig. 6.1). Recrystallization in dry methanol to remove water failed in these cases. Complex **3** crystallizes as a tetramer in the structure described previously.^{74, 82} Acetate complex **4** crystallizes as a dimeric complex with bridging acetate ligands. Surprisingly, the acetate shows a monodentate coordination to the copper centres instead of the more common bidentate bridging mode and is structurally very similar to the chloride-bridged complex **1** or **2**. The triflate complex **[(L1)Cu(OH₂)][OTf]**, **5**, can be obtained either by anion exchange from **1** with AgOTf or by direct reaction of copper(II) triflate with the ligand precursors (Scheme 6-3). In both cases, the complex crystallizes as a 1D coordination polymer (Fig. 6.1). A bridging carboxylate replaced the triflate anion in the metal coordination sphere. Water occupies the apical position and completes the square-pyramidal coordination geometry. Again, metrical data are highly similar to the respective sulfonate complex (Table 6-1).

Initial reactions with β-alanine instead of anthranilic acid following the same protocol did not provide the desired complex **(L2)CuCl**, but **(L2H)CuCl₂** in appr. 50% yield (Scheme 6-4, Fig. 6.S1 and S2). Clearly, formal HX elimination is more difficult with alanine. After addition of additional potassium hydroxide base, the reaction cleanly provided **(L2)CuCl**, **6** (Scheme 6-4).

Complex **6** formed a coordination polymer in the solid state, with square-pyramidal coordination around copper and bridging carboxylate in the apical position (Fig. 6.2, Table 6-2). Reactions with copper acetate or copper nitrate did not yield the desired products with or without potassium hydroxide. During one attempt, the acetate complex (**L2**)Cu(OAc) was formed, but it crystallized unfortunately as an adduct with copper acetate, (**L2**)Cu(OAc)·Cu(OAc)₂ (Scheme 6-4). (**L2**)Cu(OAc) formed an acetate-bridged coordination polymer, the chains of which were crosslinked by carboxylate coordination to the apical position of the copper acetate paddlewheel complex (Fig. 6.S3). The triflate complex (**L2**)Cu(OTf), **7**, was prepared by anion exchange of the chloride complex (Scheme 6-4). As the nitrate complex **3**, triflate complex **7** crystallizes as a tetramer with bridging coordination of the carboxylate group. The triflate anion remains coordinated to copper. The higher flexibility of the aliphatic backbone permitted a weak interaction of the copper centre with the bridging carboxylate oxygen (2.7 Å), resulting in a distorted octahedral coordination geometry (Table 6-2, Fig. 6.2).



Scheme 6-4

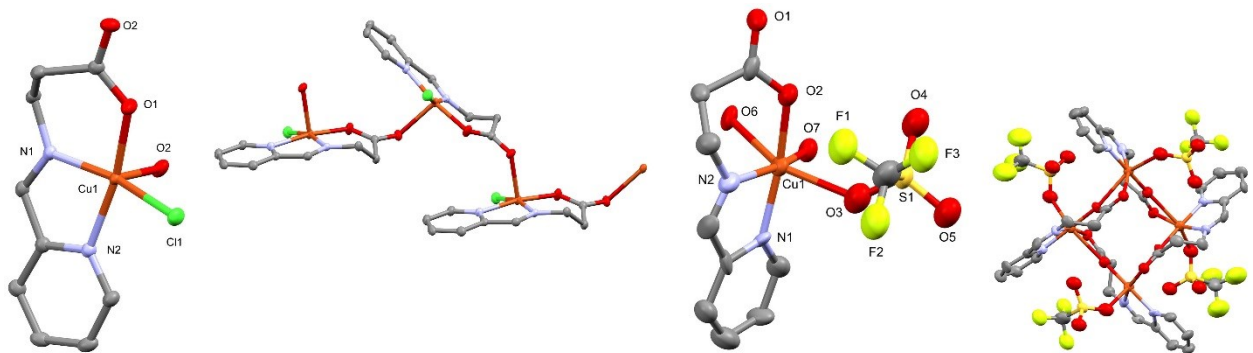


Figure 6.2 : Crystal structures of **6** and **7**. Thermal ellipsoids are shown at 50% probability.

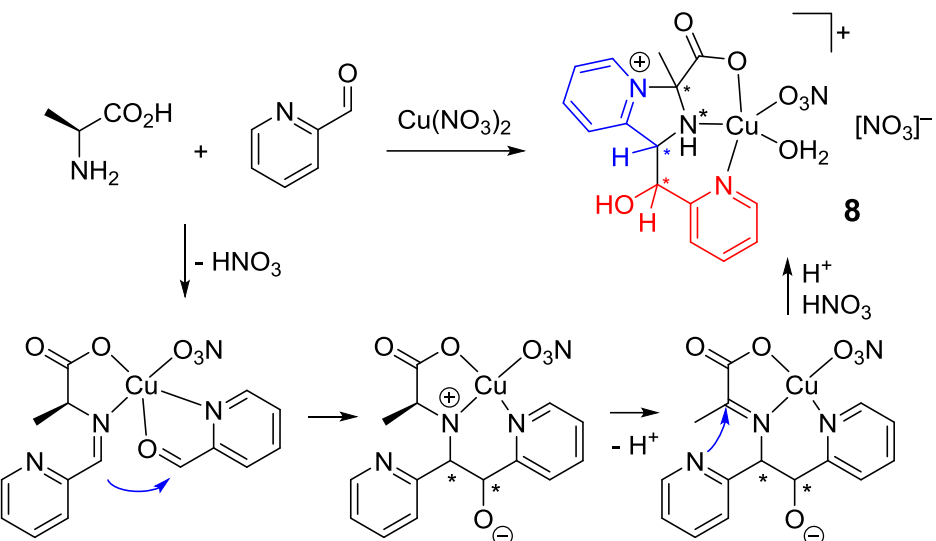
Hydrogen atoms omitted for clarity.

Table 6-2 : Geometrical details of the X-ray structures of **6**, **(L2H)CuCl₂**, **(L2)Cu(OAc)·Cu(OAc)₂** and **7**.

	(L2H)CuCl₂	6	(L2)Cu(OAc)·Cu(OAc)₂	7
Cu-O ₂ CO		1.948(1)	1.953(3)	1.948(9), 1.955(9)
Cu-N(=C)	2.035(2)	1.983(1)	1.996(4)	1.956(12), 1.974(12)
Cu-N _{pyridine}	2.031(2)	2.038(1)	1.018(4)	1.993(10), 2.019(10)
Cu-X ^a	2.265(1), 2.274(1)	2.263(1)	1.963(3)	2.268(10), 2.321(10)
Cu-L ^a	2.952(1), 2.570(1)	2.285(1)	2.197(4), 2.616(4)	1.944(9), 1.957(9), 2.672(7), 2.710(10)
τ	0.1	0.1		

^a **(L2H)CuCl₂**: L=μ-Cl_{long}, μ-O₂CR. **6**: X=Cl, L=μ-O₂CR. **(L2)Cu(OAc)·Cu(OAc)₂**: X=OAc, L=μ-OAc, μ-OAc. **7**: X=OTf, L=μ-O₂CR, μ-O₂CR.

Reactions of β-alanine with thiophene aldehyde, pyrrole aldehyde or benzaldehyde in the presence of copper(II) chloride did not provide crystalline material. If α-alanine instead of β-alanine was employed, condensation with pyridinecarboxaldehyde in the presence of copper nitrate provided a complex containing a tridentate ligand consisting of one α-alanine and two pyridinecarboxaldehyde moieties (**8**, Scheme 5, Table 6-5, Fig. 6.S4). Formation of **8** was not investigated in detail, but can be envisioned to proceed via formation of **(L2)Cu(NO₃)**, attack of the C=N double bond on coordinated pyridinecarboxaldehyde, formal hydrogen shift from methine to N and quaternisation of pyridine by the carbocation. While only a single diastereomer was isolated in 50% of the theoretical yield, the chiral center of alanine reacted under racemization, not inversion. Deprotonation-protonation is thus more likely than a direct 1,2-H shift.



Scheme 6-5

6.2.2. UV/vis-spectra

Complexes **1-7** show a d-d transition around 750 nm and an interligand or LMCT transition around 340 nm for **1-5** and around 288 nm for **6** and **7** (Fig. 3). The higher-energy transition is practically invariant with the nature of the anion. The more bathochromic shift in **1-5** can be assigned to the extended π -system. The same qualitative trend is observed in iminopyridines with *N*-aryl and *N*-alkyl substituents.⁸³⁻⁸⁴ Only the acetate complex **4** shows a somewhat different shape of this transition. A similar trend for the respective sulfonate complexes was explained with persisting bridging coordination of the acetate in solution to form dinuclear (or polynuclear) complexes.⁵⁴

In contrast to the higher-energy transition, the *d-d* transition shows a clear effect of the anion with λ_{max} increasing in the order $\text{AcO}^- < \text{TfO}^- < \text{Cl}^- = \text{NO}_3^-$ for **1-5**, as well as for **6**, **7** and **(L2)Cu(OAc)·Cu(OAc)2**. This correlates qualitatively with expectations about the coordinating ability of the anion and is consistent with the anion-displacement equilibria in solution claimed to be present in sulfonate analogs **B**.⁵⁶

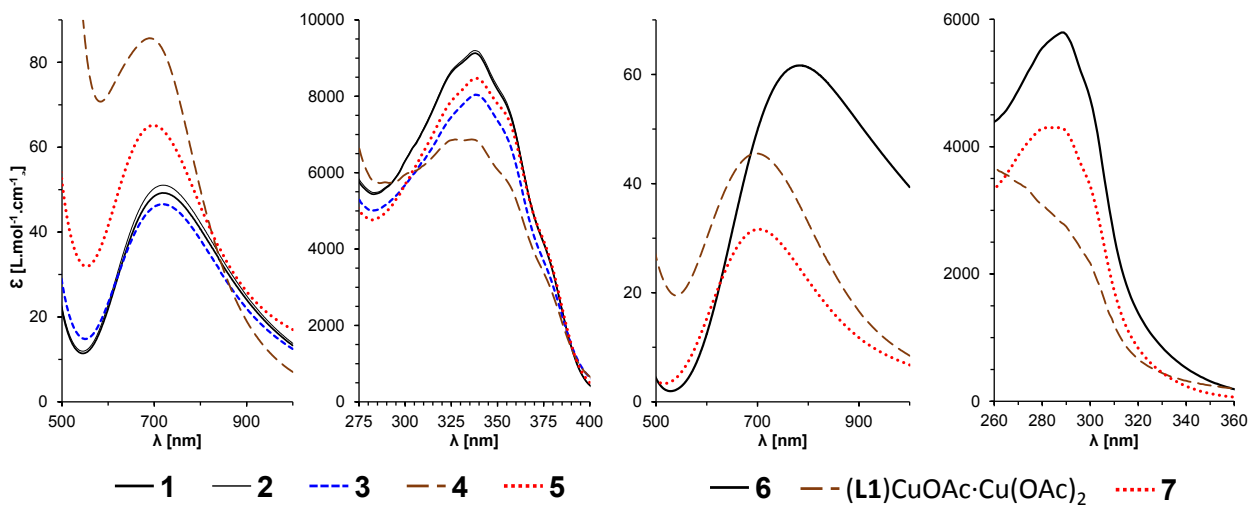


Figure 6.3 : UV/vis spectra of **1 - 7** in DMSO.

6.2.3. *rac*-Lactide polymerization

Preparation of copper alkoxide complexes (**L1**Cu(OR) was attempted by reaction of Cu(OMe)₂ or Cu(O*i*Pr)₂ with **L2H** in the best purity available. Reaction in either THF or acetonitrile provided strongly colored solutions, but no crystalline product could be obtained. Alternatively, **2-5** were reacted with NaOMe, NaOEt or KOtBu in various solvents. Again, strong coloration of reaction solutions indicated reactivity, but no product could be isolated from those. The required copper alkoxide complexes for coordination-insertion polymerization were thus prepared *in situ*.

Activities of **2-6** in lactide polymerization are summarized in table 3; full data on all polymerizations can be found in table S1. It is important to note that **3-5** contained water in their crystal structures, but that **2** and **6** did not. At room temperature in dichloromethane solution all complexes were inactive towards polymerization either in the absence or presence of either sodium methoxide or benzyl alcohol. Complexes **2**, **3**, **5** and **6** were likewise inactive in toluene at 90 °C, but acetate complex **4** showed a moderate conversion of 40% after 12 h, with a very slight heterotactic preference ($P_r = 0.60$) (Table 3, S1). In the presence of 1 equiv benzyl alcohol, reactivities were identical : **4** produced PLA in 44% conversion after 12 h ($P_r = 0.63$), the others were inactive. With sodium methoxide as co-initiator, **2**, **3** and **5** became active and achieved conversions of 60-95% after 12 h. **6** was not active and, curiously, acetate complex **4** became less active upon addition of sodium methoxide. In melt polymerizations at 140 °C without co-initiator, complexes **2-4** were active (71-96% conversion after 12 h, $P_r =$

0.69-0.84), while **5-7** were not (<25% after 12 h). In the presence of 1 equiv of benzyl alcohol, in general the same observations were made, although the activity of **4** was reduced and **7** showed 74% conversion. Stereocontrol was similar to reactions without initiator ($P_r = 0.62$ - 0.85). In the presence of sodium methoxide, melt polymerizations presented a very different picture: All complexes **2-7** were now active with 75-93% conversion after 12 h and the obtained polymers showed notably reduced heterotacticity ($P_r = 0.52$ - 0.61). With regard to polymer molecular weights, polydispersities ranged from 1.1 to 1.6 (Table S1), without any obvious correlation to reaction conditions or catalyst. All polymerization showed drastically lower than expected polymer molecular weights. The only exception being melt polymerizations in the presence of NaOMe, where polymer molecular weights were notably larger, even if still lower than expected (Table S1).

Table 6-3 : Activities of **2-7** in *rac*-lactide polymerization under different conditions.

Conditions	2 (Cl)	3 (NO ₃)	4 (OAc)	5 (OTf)	6 (Cl)	7 (OTf)
RT, CH ₂ Cl ₂	n. r.	n. r.	n. r.	n. r.	n. r.	n. r.
RT, CH ₂ Cl ₂ , 1 equiv BnOH	n. r.	n. r.	n. r.	n. r.	n. r.	n. r.
RT, CH ₂ Cl ₂ , 1 equiv NaOMe	n. r.	n. r.	n. r.	n. r.	n. r.	n. r.
90 °C, toluene	n. r.	n. r.	40%	n. r.	n. r.	n. r.
90 °C, toluene, 1 equiv BnOH	n. r.	n. r.	44%	n. r.	n. r.	n. r.
90 °C, toluene, 1 equiv NaOMe	95%	60%	16%	91%	n. r.	n. r.
90 °C, toluene, 1 equiv NaOMe + BnOH	20%	12%	10%	15%	n. r.	n. r.
140 °C, no solvent	96%	80%	71%	17%	22%	17%
140 °C, no solvent, 1 equiv BnOH	100%	90%	39%	16%	28%	74%
140 °C, no solvent, 1 equiv NaOMe	85%	76%	93%	74%	76%	75%

n.r. = no reaction

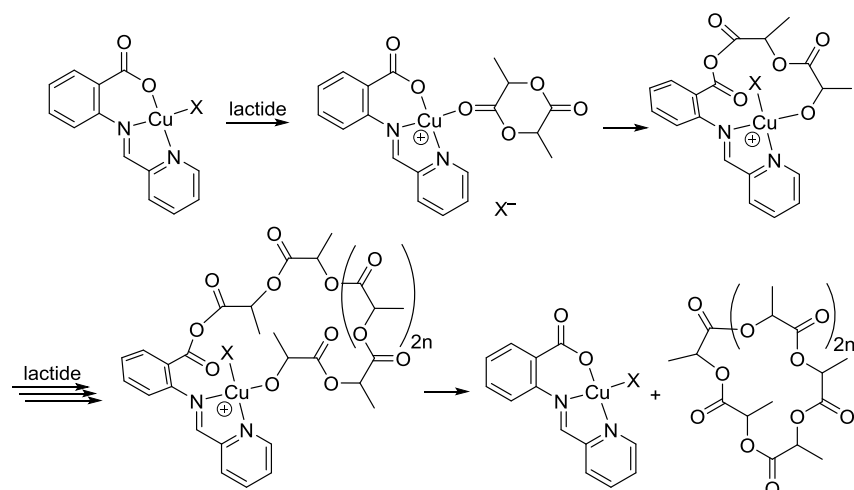
The ensemble of polymerization results is difficult to interpret mechanistically. Polymerizations at 90 °C agree with a coordination-insertion polymerization catalyzed by copper complexes: In the absence of co-initiator only acetate complex **4** is active, bearing the only anion which could reasonably be expected to initiate polymerization. That activity is unaffected by addition of benzyl alcohol, but increased upon addition of sodium methoxide likewise supports a coordination-insertion mechanism. One would have expected that water-containing and water-free complexes react differently upon addition of sodium methoxide, but, considering the activity of the acetate complex, catalysts may be able to recover from

hydrolysis if the copper hydroxides formed react with lactide to form copper carboxylate salts. Sodium methoxide itself is active under these conditions (Table 6-S1), but unlikely to be the active species: (a) The microstructure of PLA produced with **2**, **3** and **5** was slightly heterotactic ($P_r = 0.66 - 0.71$), while anionic polymerization with sodium methoxide produces atactic PLA (Table 6-S1). (b) In the presence of **6**, which does not contain water in its crystal structure, no polymer was obtained, indicating that sodium methoxide was not available for polymerization in this case.

The activity of **2-4** in melt polymerizations without co-initiator is puzzling: For an activated-monomer mechanism, water would be the most likely initiator, but water-free **2** was active, while **5**, containing coordinated water, was not. Also, polymerizations in the presence of benzyl alcohol did not show the rate increase which would be expected if initiation by protic impurities is replaced by an added alcohol. In fact, the activity of **4** was reduced by the addition of benzyl alcohol: activities decreased in the order 71%, 62%, and 39% in the presence of 0, 0.2, and 1 equiv of benzyl alcohol, respectively. The effect is not limited to benzyl alcohol: addition of 1 equiv of isopropanol or phenol to polymerizations with **4** likewise reduced activity from 71% to 44% and 40%, respectively (Table 6-S1). Intrigued by this, we repeated polymerizations with **2**, **3** and **5** at 90 °C in the presence of sodium methoxide, but now with an additional equivalent of benzyl alcohol. Activities were again suppressed from 60-95% to 12-20% (Table 6-3). We do not have a mechanistic explanation for the negative impact of additional alcohol on reactivity, but it is clearly incompatible with an activated-monomer mechanism.

Chloride and nitrate anions, on the other hand, are not expected to initiate polymerization by a coordination-insertion mechanism, even at 140 °C. Considering the activity of acetate complex **4** at 90 °C, the ligand carboxylate group is most likely responsible for activity at 140 °C, either by direct insertion into Cu-acyl or by deprotonation of protic impurities. The latter is unlikely, since activity of **2** was unaffected by addition of either water or lactic acid (Table 6-S1), and insertion into the carboxylate group is thus the most likely mechanism (Scheme 6-6). MALDI-analyses of polymers obtained with **2** and **4** in the presence and absence of benzyl alcohol all show the presence of a series with $m/z = 72 \cdot n + M(\text{Na})$, indicative of cyclic oligomers produced by intramolecular transesterification. A second series of $m/z = 72 \cdot n + 18 + M(\text{Na})$ indicates hydroxyl-terminated linear chains for **4**, as well as for water-free **2**. The latter

probably result from opening of cyclic oligomers by water under MS conditions. For PLA obtained in the presence of benzyl alcohol, a series of benzyl-terminated chains is likewise obtained, which might arise either from benzyl alcohol acting as chain-transfer reagent or from opening of cyclic oligomers by reaction with benzyl alcohol under MS conditions. It is tempting to assign the high amount of intramolecular transesterification to the formation of a reactive carbonate group at the chain end, close to the metal alkoxide (Scheme 6-6). The latter would encourage formation of cyclic oligomers, in a mechanism similar to that proposed for NHC-catalyzed polymerization of lactide.⁸⁵ However, the same reduced polymer molecular weights were observed for polymerizations at 90 °C for complexes which were active only in the presence of sodium methoxide.



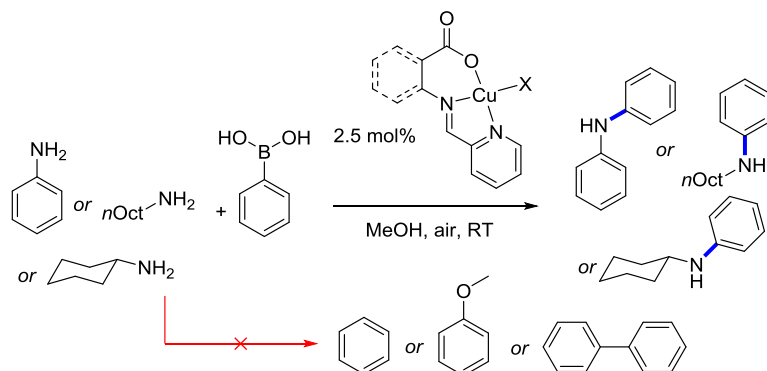
Scheme 6-6

For melt polymerization in the presence of sodium methoxide, the similar activities of all catalysts, the reduced heterotacticity of the polymer and the increased polymer molecular weights all indicate that sodium methoxide does not react (completely) with LCuX under these conditions and is at least partly responsible for polymer produced at 140 °C.

Complexes **6** and **7** with an aliphatic backbone display – on average – lower activities (Table 6-3, 6-S1). Taken aside the activity of the acetate complex at 90 °C, there is no clear correlation of activity with the nature of the anion. P_r values vary strongly under similar conditions without any correlation to the nature of the anion, indicative that **2-7** do not reliably form a single active species under these conditions.

6.2.4. Chan-Evans-Lam couplings

A drawback of typical CEL couplings with simple copper salts is the high substrate dependence on reaction conditions, which in most cases require the optimization of reaction conditions even for closely related substrates, such as aniline and amine.⁸⁶⁻⁸⁷ Complexes **B** were shown to be not just highly reactive in CEL couplings, but also to function with simple and general reaction protocols (various solvents tolerated, water tolerated, no base or ligand additive required) and to be applicable for aniline, amines as well as other *N*-nucleophiles under identical conditions.⁵⁴⁻⁵⁶ This was rationalized by the fact that the ligand is responsible for solubilisation of the complex and – via the sulfonate group in **B** – coordinates to boron to form a dinuclear complex, proposed as an intermediate prior to transmetallation.⁸⁸⁻⁹⁰ In CEL couplings with simple copper salts, the anion typically acts as the bridging ligand. Consequently, CEL couplings with CuX₂ salts normally show a strong dependence of activity on the counteranion, while couplings with **B** did not. Complexes **1-7** were investigated in CEL couplings to see if these characteristics can be transferred to a carboxylate-based ligand or if the sulfonate group is essential. Complexes **1-7** were active in CEL couplings under the exact same reaction conditions employed for **B**, i. e. room temperature, methanol solution, 1.5 equiv PhB(OH)₂, 2.5 mol% catalyst, no base or further ligand added (Scheme 6-7).



Scheme 6-7

As for **B**, neither deboration, coupling to solvent nor aryl homocoupling was observed. An excess phenylboronic acid is thus not necessary to for the reactions to reach completion, but was employed to allow comparison with data for **B**. While full conversion was reached for the more nucleophilic cyclohexylamine and *n*-octylamine with **1-5**. Chloride and triflate complexes **1** and **5** did not show full conversion for aniline (Table 6-4). The reason for this is unclear and

does not correlate with qualitative coordination strength of the anions to copper. Reactions with cyclohexylamine were investigated in detail to address the dependence of reactivity on the counteranion. In the mechanism proposed for **B**, the reactive species is proposed to be cationic and the anion involvement is limited to its influence on the dissociation equilibrium. Consequently, only a small influence of the anion on reactivity was observed for complexes **B**.⁵⁴ The same was observed for **1-5**: apparent first-order rate constants varied by less than a factor of two between the most and the least active complex (Fig. 6.4, Table 6-4). The anion has, however a remarkable influence on the length of the induction period, which differed between 5 – 70 min. As expected, more nucleophilic cyclohexylamine and *n*-octylamine show 4-5 times higher reactivity than aniline (Table 6-4).

Table 6-4 : Chan-Evans-Lam coupling with phenylboronic acid.

Catalyst	Anion	Aniline	<i>n</i> -Octylamine	Cyclohexylamine		
		Conversion ^a	Conversion ^b	Conversion ^a	<i>k</i> _{obs}	<i>t</i> ₀
1	Cl ⁻	25%	100%	95%	0.39(1) h ⁻¹	5 min
3	NO ₃ ⁻	100%	100%	100%	0.34(2) h ⁻¹	70 min
4	AcO ⁻	100% ^c	100% ^d	100%	0.67(1) h ⁻¹	20 min
5	TfO ⁻	26%	100%	96%	0.48(5) h ⁻¹	45 min
6	Cl ⁻	23%	100%	48%	> 0.3 h ⁻¹	>210 min
7	TfO ⁻	0%	100%	80%	> 0.09 h ⁻¹	330 min
8	NO ₃ ⁻	0%	100%	100%	0.19(4) h ⁻¹	120 min

^a after 12 h. ^b after 4.5 h. ^c *k*_{obs} = 0.13(4) h⁻¹ ^d *k*_{obs} = 0.51(4) h⁻¹

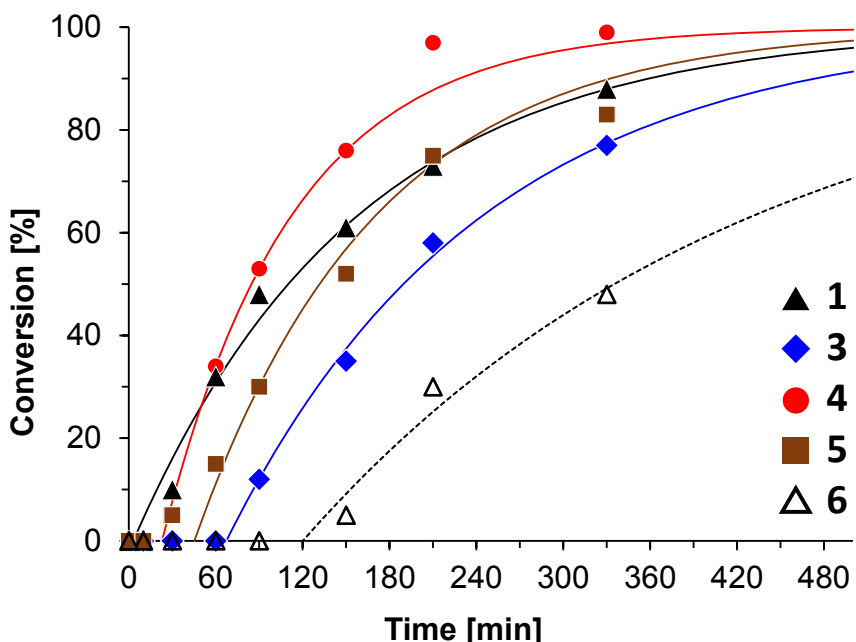
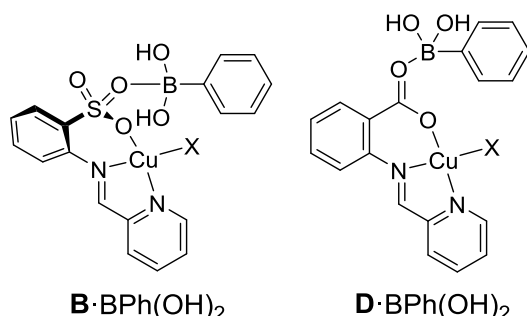


Figure 6.4 : Concentration-time profiles for CEL couplings of cyclohexylamine with phenylboronic acid, catalyzed by **1-6**. Conditions: 1.0 M cyclohexylamine, 1.5 M PhB(OH)₂, 2.5 mol% catalyst, MeOH, RT, air. Conversion was calculated from absolute concentrations of product and starting material, obtained by calibrated GC-MS analyses vs. internal standard. The solid lines are theoretical conversions using the pseudo-first-order rate constants determined by linear regression of the semilogarithmic plot.

While highly competent in CEL couplings, replacing the sulfonate group in **B** with a carboxylate in **1-5** resulted in an overall drop of activity. Coupling with aniline was appr. 4-5 times faster with **B** and reactions with octylamine which require several hours with **1-5** reach completion in 10 min with **B**. The lower reactivity might be associated with the geometry of the carboxylate vs. the sulfonate group: Coordination of boron to the rigid carboxylate group places the phenylboronic acid by necessity farther away from the copper center than coordination to the tetrahedral and more flexible sulfonate group (Scheme 6-8).



Scheme 6-8

Couplings with **6** and **7**, having an alkyl backbone in the ligand, show smaller rate constants and significantly longer induction periods. As for **B**, dissociation of the anionic ligand from copper thus seems not to be required in the catalytic cycle. Complex **8** shows despite the complex nature of the ligand backbone the same general characteristics as **1-7**, i. e. a tridentate, mono-anionic ligand with a coordinated carboxylate. As such, it was likewise tested in CEL couplings and proved to be a competent catalyst under the same mild reaction conditions for amines, but not for aniline (Table 6-4).

Substrate scope in comparison to sulfonate complexes B. Complexes of type **B** were not reactive toward weaker nucleophiles, such as alcohols or phenols. They also did not show any reactivity with alkylboronic acids. Complexes **1-5** unfortunately showed the same lack of reactivity. Neither coupling of phenol or alcohol with phenylboronic acid, nor coupling of octylamine or aniline with *sec*-butylboronic acid or cyclohexylboronic acid was observed under a variety of reaction conditions and up to temperatures of 120 °C.

6.2. Conclusions

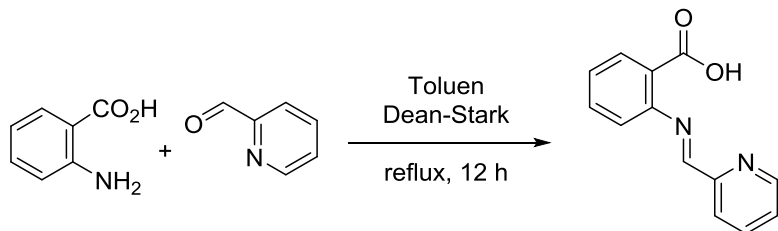
Pyridylimino carboxylate copper(II) complexes based on anthranilic acid or β-alanine with different anions are readily available from simple starting materials in a one-pot reaction. Contrary to their sulfonate analogs, *rac*-lactide polymerization data supports a coordination-insertion mechanism by copper alkoxide complexes under some conditions. Several mechanisms seem to be in play, however, and at 140 °C sodium methoxide seems to initiate polymerization on its own instead of reacting with the copper complexes. Although a step up from the performance of their sulfonate analogs, catalyst performance remains highly unsatisfactory with low and irregular activities, moderate heterotacticities, and severe lack of polymer molecular weight control.

In CEL couplings, in particular anthranilic acid-based complexes **1-5** were competent catalysts. There is no evidence of typically observed side reactions, such as deboration or aryl homocoupling, and they are active for amines as well as anilines under the same, unoptimized reaction conditions. Their performance is somewhat lower than that of the corresponding sulfonate complexes recently reported by our group, which gratifyingly can be explained by

the structure of the carboxylate- or sulfonate-bridged dinuclear copper-boron species proposed in the mechanism for these complexes.

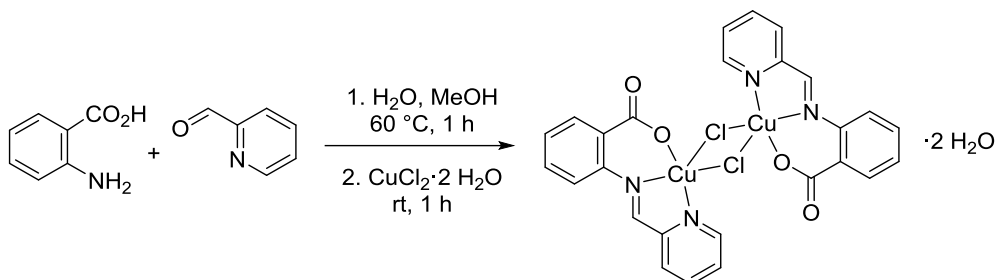
6.3. Experimental section

General. Phenylboronic acid was purified by washing with dichloromethane until the filtrate stayed colorless. *rac*-Lactide (98%) was purchased from Sigma–Aldrich, purified by 3 recrystallizations from dry ethyl acetate and kept at –30 °C. All other chemicals were purchased from common commercial suppliers and used without further purification. Elemental analyses were performed by the Laboratoire d'analyse élémentaire (Université de Montréal). UV/vis spectra were recorded on a Cary Series UV-Vis-NIR spectrophotometer from Agilent Technology. GC-MS spectra were recorded on an Agilent Technology GC/MS.



2-((Pyridin-2-ylmethylene)amino)benzoic acid, L1H. 2-Pyridinecarboxaldehyde (95 µL, 1.0 mmol) and aniline-2-carboxylic acid (anthranilic acid, 137 mg, 1.0 mmol) were dissolved in anhydrous toluene (15 mL). The mixture was refluxed overnight, cooled to room temperature and filtered. After evaporation of the solvent, the residue was analyzed by ¹H NMR to show 80% conversion to product. Purification by column chromatography with a gradient of solvent from 8/2 : hexane/ethyl acetate to 2/8 : hexane/ethylacetate yielded the product in 95% purity according to NMR (147 mg, 65%).

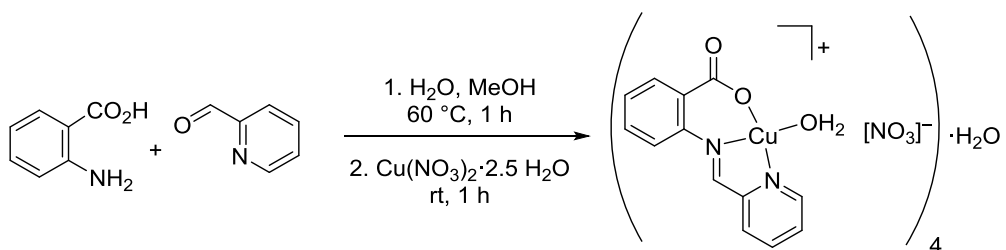
¹H NMR (DMSO-*d*₆, 400 MHz) δH: 8.66 (d, *J* = 4, 1H, py), 8.00 (s, 1H, PyCH(=N)), 7.74 (t, *J* = 8, 1H, Py), 7.5 (m, 2H), 7.2 (m, 2H), 7.05 (d, *J* = 8, 1H), 6.90 (t, *J* = 8, 1H), 6.31 (s, 1H CO₂H). Anal. Calcd. for C₁₃H₁₀N₂O₂ : C, 69.02; H, 4.46; N, 12.38. Found: C, 69.43; H, 4.78; N, 12.02. HRMS(ESI), m/z (M+H⁺, 100), Calcd. for C₁₃H₁₁N₂O₂: 227.0826, Found: 227.0815.



(L1)₂Cu₂(μ-Cl)₂·2 H₂O, 1. 2-Pyridinecarboxaldehyde (95 μL, 1.0 mmol) was added to a hot solution (60 °C) of aniline-2-carboxylic acid (anthranilic acid, 137 mg, 1.0 mmol) in water/methanol (5/10 mL). The mixture was stirred for one hour at 60 °C. CuCl₂·2 H₂O (187 mg, 1.1 mmol) was added, heating was stopped and the green solution was stirred another hour. After filtration, slow evaporation of the solvent afforded green, X-ray quality crystals (256 mg, 75%).

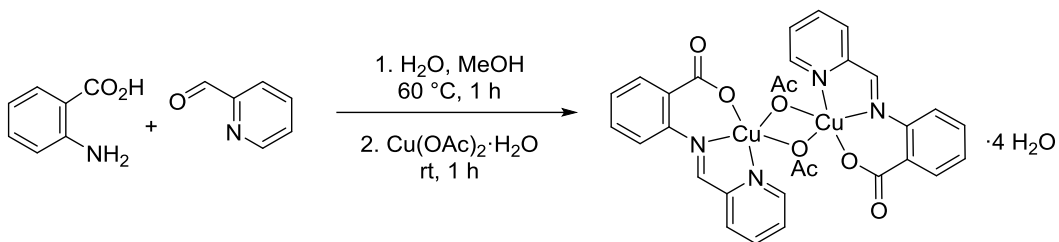
UV-vis (DMSO, 4.0·10⁻³ M or 6.17·10⁻⁵ M) [λ_{max}, nm (ε, M⁻¹·cm⁻¹)] : 338 (9132), 719 (40). Anal. Calcd. for C₁₃H₉ClCuN₂O₂·1 H₂O : C, 45.62; H, 3.24; N, 8.19. Found: C, 45.35; H, 3.15; N, 8.00.

{(L1)Cu(μ-Cl)}₂·2 MeOH, **2.** Recrystallisation of **1** (100 mg, 0.29 mmol) in anhydrous MeOH (2 mL) lead to copper complexes with a co-crystallized methanol (35 mg, 34%). UV-vis (DMSO, 4.8·10⁻³ M or 6.2·10⁻⁵ M) [λ_{max}, nm (ε, M⁻¹·cm⁻¹)] : 338 (9196), 719 (51). Anal. Calcd. for C₁₃H₉ClCuN₂O₂·MeOH : C, 47.20; H, 3.68; N, 7.86. Found: C, 46.88; H, 3.34; N, 7.49.



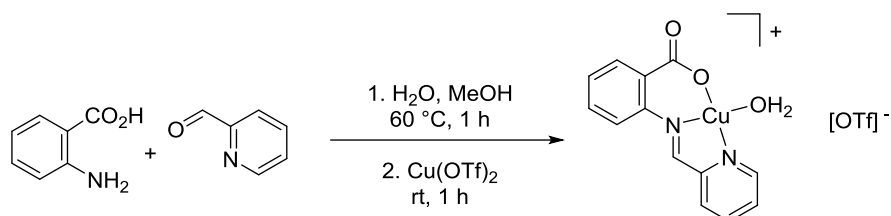
[(L1)Cu(OH₂)]₄[NO₃]₄, **3.** Equivalent to **1**, from Cu(NO₃)₂·2.5 H₂O (255 mg, 1.1 mmol). Slow evaporation of the solvent provided green, X-ray quality crystals (306 mg, 83%).

UV-vis (DMSO, 4.5·10⁻³ M or 5.6·10⁻⁵ M) [λ_{max}, nm (ε, M⁻¹·cm⁻¹)] : 338 (8041), 717 (47). Anal. Calcd. for C₁₃H₉CuN₃O₅·1½H₂O : C, 41.83; H, 3.10; N, 11.26. Found: C, 42.01; H, 3.18; N, 11.11.



(L1)₂Cu₂(μ-OAc)₂·4 H₂O, 4. Equivalent to **1**, from Cu(OAc)₂·H₂O (219 mg, 1.1 mmol). Slow evaporation of the solvent yielded green, X-ray quality crystals (222 mg, 58%).

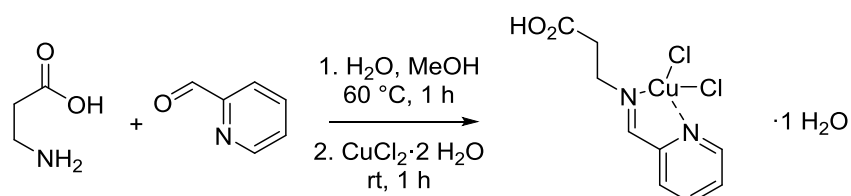
UV-vis (DMSO, 4.6·10⁻³ M or 4.0·10⁻⁵ M) [λ_{max}, nm (ε, M⁻¹·cm⁻¹)]: 327 (6871), 690 (86). Anal. Calcd. for C₁₅H₁₂CuN₂O₄·2 H₂O: C, 46.94; H, 4.20; N, 7.30. Found: C, 46.36; H, 4.33; N, 7.64.



{[(L1)Cu(OH₂)]_n[OTf], **5. Method 1**: Equivalent to **1**, from Cu(OTf)₂ (398 mg, 1.1 mmol). Slow evaporation of the solvent provided green, X-ray quality crystals (332 mg, 73%).

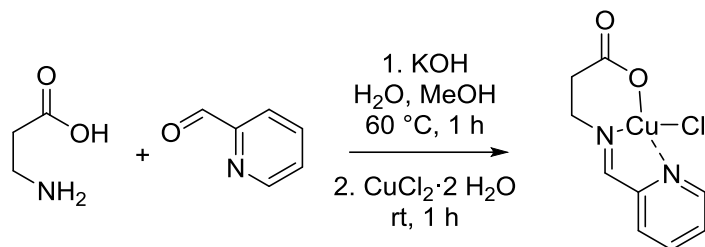
UV-vis (DMSO, 3.9·10⁻³ M or 4.9·10⁻⁵ M) [λ_{max}, nm (ε, M⁻¹·cm⁻¹)]: 338 (8470), 697 (65). Anal. Calcd. for C₁₄H₉CuF₃N₂O₅S₁·1.5 H₂O: C, 36.17; H, 2.60; N, 6.03; S, 6.90. Found: C, 36.26; H, 2.77; N, 6.37; S, 7.23.

Method 2 : Silver triflate (75 mg, 0.40 mmol) was added to a suspension of **1** (100 mg, 0.29 mmol) in dry THF (10 mL) under nitrogen. After one hour of stirring at ambient temperature, a precipitate appeared and the color of the solution intensified. After filtration, slow evaporation of the green solution (under N₂), afforded green crystals (83 mg, 63%). The compound shows the same crystal structure and an identical UV-vis spectrum to the one prepared above.



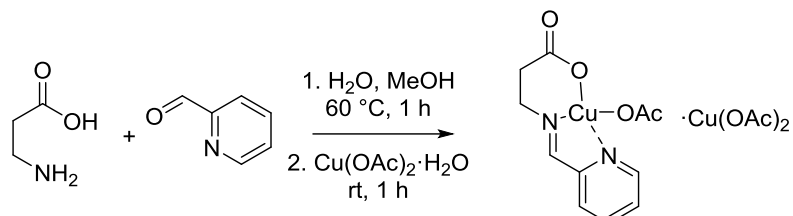
(L2H)CuCl₂·H₂O. Equivalent to **1**, from β-alanine (89 mg, 1.0 mmol), 2-pyridinecarboxaldehyde (95 μL, 1.0 mmol) and CuCl₂·2 H₂O (187 mg, 1.1 mmol). Slow evaporation of the solvent yielded green, X-ray quality crystals (171 mg, 49%).

UV-vis (DMSO, $5.1 \cdot 10^{-3}$ M or $6.4 \cdot 10^{-5}$ M) [λ_{max} , nm (ϵ , $M^{-1} \cdot cm^{-1}$)] : 288 (7442), 741 (95). Anal. Calcd. for $C_9H_{10}CuN_2O_2Cl \cdot 1 H_2O$: C, 32.69; H, 3.66; N, 8.47. Found: C, 32.34; H, 3.68; N, 8.11.



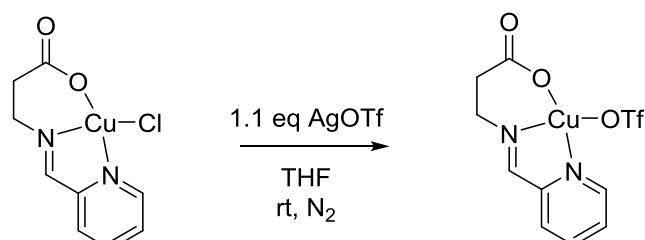
(L2)₂Cu₂(μ-Cl)₂, 6. 2-Pyridinecarboxaldehyde (95 μL, 1.0 mmol) and potassium hydroxide (56 mg, 1.0 mmol) were added to a hot solution (60 °C) of 3-propanoic acid (α -alanine, 89 mg, 1.0 mmol) in water/methanol (5/10 mL). The mixture was stirred for one hour at 60 °C. $CuCl_2 \cdot 2 H_2O$ (187 mg, 1.1 mmol) was added, heating was stopped and the solution was stirred another hour. After filtration, slow evaporation of the solvent afforded blue-green, X-ray quality crystals (214 mg, 78%).

UV-vis (DMSO, $6.1 \cdot 10^{-3}$ M or $7.6 \cdot 10^{-5}$ M) [λ_{max} , nm (ϵ , $M^{-1} \cdot cm^{-1}$)] : 288 (5794), 786 (62). Anal. Calcd. for $C_9H_9ClCuN_2O_2$: C, 39.14 H, 3.28; N, 10.14. Found: C, 38.80 H, 3.53; N, 9.78.



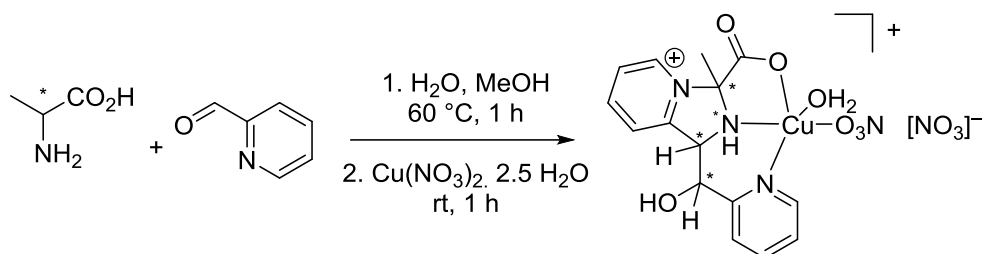
(L2)Cu(OAc)·Cu(OAc)₂. Equivalent to **1**, from 3-aminopropanoic acid (α -alanine, 89 mg, 1.0 mmol), 2-pyridinecarboxaldehyde (95 μL, 1.0 mmol), and $Cu(OAc)_2 \cdot H_2O$ (219 mg, 1.1 mmol). Slow evaporation of the solvent yielded blue-green, X-ray quality crystals (216 mg, 45%).

UV-vis (DMSO, $0.6 \cdot 10^{-2}$ M or $33 \cdot 10^{-4}$ M) [λ_{max} , nm (ϵ , $M^{-1} \cdot cm^{-1}$)] : 305 (2500), 716 (115). Anal. Calcd. for $C_{11}H_{12}CuN_2O_4 \cdot Cu(OAc)_2$: C, 37.42; H, 3.77; N, 5.82. Found: C, 37.76; H, 4.01; N, 6.49.



(L2)CuOTf, 6. Silver triflate (104 mg, 0.40 mmol) was added to a suspension of **1** (100 mg, 0.37 mmol) in dry THF (10 mL) under nitrogen atmosphere. After one hour of reaction at ambient temperature, a precipitate appeared and the color of the solution intensified. After filtration, slow evaporation of the green solution (under N₂), afforded green crystals (95 mg, 66%).

UV-vis (DMSO, 2.7·10⁻² M or 1.3·10⁻⁴ M) [λ_{max}, nm (ε, M⁻¹·cm⁻¹)]: 285 (4230), 703 (32). Anal. Calcd. for C₁₀H₉CuF₃N₂O₅S₁: C, 30.81; H, 2.33; N, 7.19 S, 8.22. Found: C, 30.49; H, 2.64; N, 6.85; S, 8.76.



[(L3**)Cu(H₂O)(NO₃)][NO₃], 8.** Equivalent to **1**, from (*S*)-2-aminopropanoic acid (L-alanine, 89 mg, 1.0 mmol), 2-pyridinecarboxaldehyde (95 μL, 1.0 mmol) and Cu(NO₃)₂·2.5 H₂O (255 mg, 1.1 mmol). Slow evaporation of the solvent yielded green, X-ray quality crystals (50 mg, 25%).

UV-vis (DMSO, 1.0·10⁻² M or 1.0·10⁻⁴ M) [λ_{max}, nm (ε, M⁻¹·cm⁻¹)]: 259 (8046), 826 (32).

rac-Lactide polymerization

At room temperature or 90 °C: Under nitrogen, the catalyst (0.01 mmol) was added to lactide (144 mg, 1.0 mmol) in dry dichloromethane (1 mL) or dry toluene (1 mL). If desired, benzyl alcohol (5.0 × 10⁻² M in CH₂Cl₂) and/or a stock solution of sodium methoxide (5.0 × 10⁻² M in CH₂Cl₂) was added to the reaction mixture. For reactions at 90 °C, the reactions vessel was sealed and placed in a pre-heated oil-bath. Reaction mixtures were quenched at the desired polymerization time by addition of a dichloromethane solution of acetic acid (5 mM). Dry polymer samples were stored at -80 °C.

At 140°C : In a pressure tube under nitrogen, the catalyst (0.010 mmol) was combined with lactide (144 mg, 1.0 mmol). If desired, benzyl alcohol (5.0 × 10⁻² M in CH₂Cl₂) and/or a stock solution of sodium methoxide (5.0 × 10⁻² M in CH₂Cl₂) was added to the reaction mixture. The tube was placed in a pre-heated oil bath outside the glovebox. Reaction mixtures were quenched at the desired polymerization time by addition of a dichloromethane solution of

acetic acid (5 mM), rapidly cooled to RT and the solvent evaporated. Dry polymer samples were stored at -80 °C.

Characterization. Conversion was determined from ^1H NMR by comparison to remaining lactide. P_r values were determined from homodecoupled ^1H NMR spectra and calculated from $P_r = 2 \cdot I_1 / (I_1 + I_2)$, with $I_1 = 5.15 - 5.21$ ppm (*rnr, mmr/rmm*), $I_2 = 5.21 - 5.25$ ppm (*mmr/rmm, mmm, mrm*). The integration of the left multiplet and right multiplet (I_1 and I_2) required only one, very reproducible dividing point of the integration, which was always taken as the minimum between the two multiplets. P_r -values obtained this way were typically consistent to $\pm 1\%$ over the course of one experiment and $\pm 3\%$ between different experiments under identical conditions. Molecular weight analyses were performed on a Waters 1525 gel permeation chromatograph equipped with three Phenomenex columns and a refractive index detector at 35 °C. THF was used as the eluent at a flow rate of 1.0 mL·min⁻¹ and polystyrene standards (Sigma–Aldrich, 1.5 mg·mL⁻¹, prepared and filtered (0.2 mm) directly prior to injection) were used for calibration. Obtained molecular weights were corrected by a Mark-Houwink factor of 0.58.⁹¹

General procedure for Chan-Evans-Lam couplings. To a solution of amine or aniline (1.0 mmol) and phenylboronic acid (1.5 mmol) in methanol (1 mL) was added the desired catalyst (0.025 mmol). Trimethoxybenzene was added as internal standard. The reaction was stirred open to air at ambient temperature. For kinetic experiments, 20 µL aliquots were taken, diluted in ethyl acetate and analyzed by GC-MS. After the desired reaction time, the reaction was quenched with 0.5 mL of a saturated aqueous solution of ammonium chloride. The organic layer was extracted and filtered through a short silica plug to remove remaining copper complex. Products and side-products were identified in the MS- and NMR-spectra from comparison to literature. Conversion was typically analysed by GC-MS. Quantitative concentrations were determined by comparison to trimethoxybenzene standard. Calibration factors between starting materials, products, side-products and trimethoxybenzene were determined from simultaneous NMR and GC-MS analysis or by analysis of solutions prepared from isolated or commercially available products.

X-ray diffraction studies. Crystal for X-ray diffraction were obtained from synthesis as described above. Diffraction data were collected on a Bruker Venture METALJET

diffractometer (Ga K α radiation) or a Bruker APEX II microsource (Cu K α radiation).⁹² Data reduction was performed with SAINT,⁹³ absorption corrections with SADABS.⁹⁴ Structures were solved by dual-space refinement (SHELXT).⁹⁵ All non-hydrogen atoms were refined anisotropic using full-matrix least-squares on F^2 and hydrogen atoms refined with fixed isotropic U using a riding model (SHELXL97).⁹⁶ Further experimental details can be found in Table 6-5 and the supporting information (CIF).

Table 6-5 : Details of X-ray Diffraction Studies.

	1	2	3	4	5
Formula	C ₂₆ H ₂₀ Cl ₂ Cu ₂ N ₄ O ₅	C ₂₈ H ₂₂ Cl ₂ Cu ₂ N ₃ O ₅	C ₅₂ H ₄₆ Cu ₄ N ₁₂ O ₂₅	C ₁₅ H ₁₆ CuN ₂ O ₆	C ₁₄ H ₁₁ CuF ₃ N ₂ O ₆ S
M _w (g/mol); F(000)	666.44; 672	678.46; 686	1493.17; 6064	383.84; 1576	455.85; 3664
T (K); wavelength	100; 1.34190	100; 1.34190	100; 1.34190	100; 1.34190	100; 1.34190
Crystal System	Triclinic	Triclinic	Monoclinic	Orthorhombic	Orthorhombic
Space Group	P-1	P-1	P2 ₁ /c	Pbca	Fdd2
Unit Cell:					
a (Å)	7.0643(2)	9.7464(5)	21.2716(10)	8.5717(2)	22.214(3)
b (Å)	12.7769(4)	11.4104(6)	21.2719(11)	18.0801(5)	37.308(5)
c (Å)	13.9680(4)	13.1040(7)	27.1790(13)	20.4049(6)	7.8781(10)
α (°)	79.5330(10)	107.274(2)	90	90	90
β (°)	88.2270(10)	102.216(2)	107.558(3)	90	90
γ (°)	80.2220(10)	102.993(3)	90	90	90
V (Å ³)	1221.76(6)	1293.84(12)	11725.2(10)	3162.29(15)	6529.1(14)
Z; d _{calcd.} (g/cm ³)	2; 1.812	2; 1.742	8; 1.692	8; 1.612	16; 1.855
μ (mm ⁻¹); Abs. Corr.	11.003; multi-scan	10.378; multi-scan	8.286; multi-scan	7.670; multi-scan	8.443; multi-scan
θ range (°); completeness	2.8-53.6; 1.00	3.2-52.3; 1.00	2.6-53.6; 1.00	3.8-53.6; 1.00	4.0-53.6; 0.99
Collected reflections; R _σ	47509; 0.0209	4632; 0.0551	81161; 0.0439	31791; 0.0237	20965; 0.0494
Unique reflections; R _{int}	5615; 0.0419	4632; 0.0551	13461; 0.0667	3636; 0.0458	3504; 0.0591
Observed Reflections; R1(F)	5502; 0.0313	3508; 0.1176	12030; 0.0949	3091; 0.0746	3226; 0.0389
wR(F ²) (all data); GoF(F ²)	0.0830; 1.078	0.3483; 1.458	0.2568; 1.074	0.0799; 1.029	0.0917; 1.096
Residual electron density	0.674	2.502	3.251	0.392	0.442

Table 6-5 : Continued.

	6	7	8	(L1H)CuCl₂	(L1)CuOAc·Cu(OAc)₂
Formula	C ₉ H ₉ ClCuN ₂ O ₂	C ₂₀ H ₁₈ Cu ₂ F ₆ N ₄ O ₁₀ S ₂	C ₁₅ H ₁₇ CuN ₅ O ₁₀	C ₉ H ₁₂ Cl ₂ CuN ₂ O ₃	C ₁₅ H ₁₈ Cu ₂ N ₂ O ₈
M _w (g/mol); F(000)	276.17; 1916	779.58; 3120	490.5; 2008	330.65; 668	481.41; 956
T (K); wavelength	100; 1.34190	150; 1.34190	100; 1.34190	100; 1.34190	100; 1.34190
Crystal System	Monoclinic	Monoclinic	Monoclinic	Monoclinic	Monoclinic
Space Group	P2 ₁ /c	P2 ₁ /c	P2 ₁ /c	P2 ₁ /n	P2 ₁ /c
Unit Cell: a (Å)	7.7942(2)	27.7325(18)	12.4500(2)	8.8166(3)	8.5605(3)
b (Å)	9.8050(3)	7.5286(5)	9.6183(2)	14.6490(5)	26.0642(10)
c (Å)	13.5262(4)	29.643(2)	30.7146(5)	10.1051(3)	8.4229(3)
α (°)	90	90	90	90	90
β (°)	104.405(1)	114.689(4)	98.6150(10)	111.372(1)	97.167(2)
γ (°)	90	90	90	90	90
V (Å ³)	1001.20(5)	5623.3(7)	3636.51(11)	1215.37(7)	1864.66(12)
Z; d _{calcd.} (g/cm ³)	4; 1.832	8; 1.842	8; 1.793	4; 1.807	4; 1.2946
μ (mm ⁻¹); Abs. Corr.	5.385; multi-scan	9.685; multi-scan	2.362; multi-scan	6.591; multi-scan	12.606; multi-scan
θ range (°); completeness	5.6-67.7; 0.985	2.9-57.4; 0.989	2.9-67.7; 0.996	5.6-72.1; 0.990	3.0-60.8; 0.991
Collected reflections; R _σ	25743; 0.0099	22199; 0.1674	36614; 0.0120	29979; 0.0115	22025; 0.0504
Unique reflections; R _{int}	1937; 0.0260	5706; 0.1599	3573; 0.0262	2356; 0.0285	4260 0.0715
Observed Reflections; R1(F)	1915; 0.0235	3088; 0.1586	3570; 0.0353	2332; 0.0237	3408; 0.0591
wR(F ²) (all data); GoF(F ²)	0.0651; 1.036	0.4218; 1.051	0.0889; 1.233	0.0624; 1.095	0.1715; 1.0462
Residual electron density	0.528	1.923	0.434	0.646	1.295

6.4. References

¹Evano, G.; Blanchard, N., *Copper-Mediated Cross-Coupling Reactions*. John Wiley & Sons: New York, 2013.

² Simon, W. *Angew. Chem., Int. Ed.* **2005**, *44*, 5560-5562.

³ Matyjaszewski, K. In *Controlled Radical Polymerization: Mechanisms*, American Chemical Society: 2015; Vol. 1187, pp 1-17.

⁴ Matyjaszewski, K. *Isr. J. Chem.* **2012**, *52*, 206-220.

⁵ Stibrany, R. S., D.; Kacker, S.; Patil, A. (Exxon Research and Engineering) WO 99/30822, 1999.

⁶ Gibson, V. C.; Tomov, A.; Wass, D. F.; White, A. J. P.; Williams, D. J. *J. Chem. Soc., Dalton Trans.* **2002**, 2261-2262.

⁷ Stibrany, R. T.; Schulz, D. N.; Kacker, S.; Patil, A. O.; Baugh, L. S.; Rucker, S. P.; Zushma, S.; Berluche, E.; Sissano, J. A. *Macromolecules* **2003**, *36*, 8584.

⁸ Nagel, M.; Paxton, W. F.; Sen, A.; Zakharov, L.; Rheingold, A. L. *Macromolecules* **2004**, *37*, 9305-9307.

⁹ Olson, J. A.; Boyd, R.; Quail, J. W.; Foley, S. R. *Organometallics* **2008**, *27*, 5333-5338.

¹⁰ Ikariya, T.; Yamamoto, A. *J. Organomet. Chem.* **1974**, *72*, 145-151.

¹¹ Schaper, F.; Foley, S. R.; Jordan, R. F. *J. Am. Chem. Soc.* **2004**, *126*, 2114-2124.

¹² Le Roux, E. *Coord. Chem. Rev.* **2016**, *306*, 65-85.

¹³ Paul, S.; Zhu, Y.; Romain, C.; Brooks, R.; Saini, P. K.; Williams, C. K. *Chem. Commun. (Cambridge, U. K.)* **2015**, *51*, 6459-6479.

¹⁴ MacDonald, J. P.; Shaver, M. P. In *Green Polymer Chemistry: Biobased Materials and Biocatalysis*, American Chemical Society: 2015; Vol. 1192, pp 147-167.

¹⁵ Guillaume, S. M.; Kirillov, E.; Sarazin, Y.; Carpentier, J.-F. *Chem.-Eur. J.* **2015**, *21*, 7988-8003.

¹⁶ Sauer, A.; Kapelski, A.; Fliedel, C.; Dagorne, S.; Kol, M.; Okuda, J. *Dalton Trans.* **2013**, *42*, 9007-9023.

¹⁷ Dagorne, S.; Normand, M.; Kirillov, E.; Carpentier, J.-F. *Coord. Chem. Rev.* **2013**, *257*, 1869-1886.

¹⁸ Dagorne, S.; Fliedel, C. In *Modern Organoaluminum Reagents: Preparation, Structure, Reactivity and Use*, Woodward, S.; Dagorne, S., Eds. Springer Berlin Heidelberg: Berlin, Heidelberg, 2013; Vol. pp 125-171.

¹⁹ Carpentier, J.-F.; Liu, B.; Sarazin, Y. In *Advances in Organometallic Chemistry and Catalysis*, John Wiley & Sons, Inc.: 2013; Vol. pp 359-378.

²⁰ dos Santos Vieira, I.; Herres-Pawlis, S. *Eur. J. Inorg. Chem.* **2012**, 2012, 765-774.

²¹ Wheaton, C. A.; Hayes, P. G. *Comments Inorg. Chem.* **2011**, 32, 127-162.

²² Inkinen, S.; Hakkarainen, M.; Albertsson, A.-C.; Södergård, A. *Biomacromolecules* **2011**, 12, 523-532.

²³ Dutta, S.; Hung, W.-C.; Huang, B.-H.; Lin, C.-C. In *Synthetic Biodegradable Polymers*, Rieger, B.; Kunkel, A.; Coates, G. W.; Reichardt, R.; Dinjus, E.; Zevaco, T. A., Eds. Springer-Verlag: Berlin, 2011; Vol. pp 219-284.

²⁴ Dijkstra, P. J.; Du, H.; Feijen, J. *Polym. Chem.* **2011**, 2, 520-527.

²⁵ Dagorne, S.; Fliedel, C.; de Frémont, P. In *Encyclopedia of Inorganic and Bioinorganic Chemistry*, John Wiley & Sons, Ltd: 2011; Vol.

²⁶ Buffet, J.-C.; Okuda, J. *Polym. Chem.* **2011**, 2, 2758-2763.

²⁷ Thomas, C. M. *Chem. Soc. Rev.* **2010**, 39, 165.

²⁸ Stanford, M. J.; Dove, A. P. *Chem. Soc. Rev.* **2010**, 39, 486-494.

²⁹ Jones, M. D. In *Heterogenized Homogeneous Catalysts for Fine Chemicals Production*, Barbaro, P.; Liguori, F., Eds. Springer Netherlands: 2010; Vol. 33, pp 385-412.

³⁰ Ajellal, N.; Carpentier, J.-F.; Guillaume, C.; Guillaume, S. M.; Helou, M.; Poirier, V.; Sarazin, Y.; Trifonov, A. *Dalton Trans.* **2010**, 39, 8363.

³¹ Wheaton, C. A.; Hayes, P. G.; Ireland, B. J. *Dalton Trans.* **2009**, 4832 - 4846.

³² Sun, J.; Shi, W.; Chen, D.; Liang, C. *J. Appl. Polym. Sci.* **2002**, 86, 3312-3315.

³³ John, A.; Katiyar, V.; Pang, K.; Shaikh, M. M.; Nanavati, H.; Ghosh, P. *Polyhedron* **2007**, 26, 4033-4044.

³⁴ Bhunora, S.; Mugo, J.; Bhaw-Luximon, A.; Mapolie, S.; Van Wyk, J.; Darkwa, J.; Nordlander, E. *Appl. Organomet. Chem.* **2011**, 25, 133-145.

³⁵ Chen, L.-L.; Ding, L.-Q.; Zeng, C.; Long, Y.; Lü, X.-Q.; Song, J.-R.; Fan, D.-D.; Jin, W.-J. *Appl. Organomet. Chem.* **2011**, 25, 310-316.

³⁶ Gowda, R. R.; Chakraborty, D. *J. Molec. Catal. A: Chem.* **2011**, *349*, 86-93.

³⁷ Li, C.-Y.; Hsu, S.-J.; Lin, C.-I.; Tsai, C.-Y.; Wang, J.-H.; Ko, B.-T.; Lin, C.-H.; Huang, H.-Y. *J. Polym. Sci., Part A: Polym. Chem.* **2013**, *51*, 3840-3849.

³⁸ Appavoo, D.; Omondi, B.; Guzei, I. A.; van Wyk, J. L.; Zinyemba, O.; Darkwa, J. *Polyhedron* **2014**, *69*, 55-60.

³⁹ Akpan, E. D.; Ojwach, S. O.; Omondi, B.; Nyamori, V. O. *New J. Chem.* **2016**, *40*, 3499-3510.

⁴⁰ Mandal, M.; Oppelt, K.; List, M.; Teasdale, I.; Chakraborty, D.; Monkowius, U. *Monatsh. Chem.* **2016**, *147*, 1883-1892.

⁴¹ Routaray, A.; Nath, N.; Maharana, T.; Sahoo, P. K.; Das, J. P.; Sutar, A. K. *J Chem Sci* **2016**, *128*, 883-891.

⁴² Whitehorne, T. J. J.; Schaper, F. *Chem. Commun. (Cambridge, U. K.)* **2012**, *48*, 10334-10336.

⁴³ Whitehorne, T. J. J.; Schaper, F. *Inorg. Chem.* **2013**, *52*, 13612-13622.

⁴⁴ Kwon, K. S.; Cho, J.; Nayab, S.; Jeong, J. H. *Inorg. Chem. Commun.* **2015**, *55*, 36-38.

⁴⁵ Cho, J.; Nayab, S.; Jeong, J. H. *Polyhedron* **2016**, *113*, 81-87.

⁴⁶ Ahn, S. H.; Chun, M. K.; Kim, E.; Jeong, J. H.; Nayab, S.; Lee, H. *Polyhedron* **2017**, *127*, 51-58.

⁴⁷ Chun, M. K.; Cho, J.; Nayab, S.; Jeong, J. H. *Bull. Korean Chem. Soc.* **2017**, *38*, 1527-1530.

⁴⁸ Daneshmand, P.; Fortun, S.; Schaper, F. *Organometallics* **2017**, *36*, 3860–3877.

⁴⁹ Daneshmand, P.; van der Est, A.; Schaper, F. *ACS Catal.* **2017**, *7*, 6289-6301.

⁵⁰ Kwon, K. S.; Nayab, S.; Jeong, J. H. *Polyhedron* **2017**, *130*, 23-29.

⁵¹ Daneshmand, P.; Jiménez-Santiago, J. L.; Aragon--Alberti, M.; Schaper, F. *Organometallics* **2018**, *37*, 1751–1759.

⁵² Whitehorne, T. J. J.; Schaper, F. *Can. J. Chem.* **2014**, *92*, 206-214.

⁵³ Hardouin Duparc, V.; Schaper, F. *Organometallics* **2017**, *36*, 3053-3060.

⁵⁴ Hardouin Duparc, V.; Thouvenin, A.; Schaper, F. *Dalton Trans* **2018**, submitted, DT-ART-06-2018-002421.

⁵⁵ Hardouin Duparc, V.; Schaper, F. *Dalton Trans.* **2017**, *46*, 12766 - 12770.

⁵⁶ Hardouin Duparc, V.; Bano, G.; Schaper, F. *ACS Catal.* **2018**, accepted, cs-2018-01881n.

⁵⁷ Chan, D. M. T.; Monaco, K. L.; Wang, R.-P.; Winters, M. P. *Tetrahedron Lett.* **1998**, *39*, 2933-2936.

⁵⁸ Evans, D. A.; Katz, J. L.; West, T. R. *Tetrahedron Lett.* **1998**, *39*, 2937-2940.

⁵⁹ Lam, P. Y. S.; Clark, C. G.; Saubern, S.; Adams, J.; Winters, M. P.; Chan, D. M. T.; Combs, A. *Tetrahedron Lett.* **1998**, *39*, 2941-2944.

⁶⁰ Bhunia, S.; Pawar, G. G.; Kumar, S. V.; Jiang, Y.; Ma, D. *Angew. Chem., Int. Ed.* **2017**, *56*, 16136-16179.

⁶¹ Lam, P. Y. S. In *Synthetic Methods in Drug Discovery: Volume 1*, The Royal Society of Chemistry: 2016; Vol. 1, pp 242-273.

⁶² Neuville, L. In *Copper-Mediated Cross-Coupling Reactions*, John Wiley & Sons, Inc.: 2013; Vol. pp 113-185.

⁶³ Casitas, A.; Ribas, X. In *Copper-Mediated Cross-Coupling Reactions*, John Wiley & Sons, Inc.: 2013; Vol. pp 253-279.

⁶⁴ Allen, S. E.; Walvoord, R. R.; Padilla-Salinas, R.; Kozlowski, M. C. *Chem. Rev.* **2013**, *113*, 6234-6458.

⁶⁵ Sanjeeva Rao, K.; Wu, T.-S. *Tetrahedron* **2012**, *68*, 7735-7754.

⁶⁶ Rauws, T. R. M.; Maes, B. U. W. *Chem. Soc. Rev.* **2012**, *41*, 2463-2497.

⁶⁷ Beletskaya, I. P.; Cheprakov, A. V. *Organometallics* **2012**, *31*, 7753-7808.

⁶⁸ Qiao, J. X.; Lam, P. Y. S. In *Boronic Acids*, Wiley-VCH Verlag GmbH & Co. KGaA: 2011; Vol. pp 315-361.

⁶⁹ Bellina, F.; Rossi, R. *Adv. Synth. Catal.* **2010**, *352*, 1223-1276.

⁷⁰ Evano, G.; Blanchard, N.; Toumi, M. *Chem. Rev.* **2008**, *108*, 3054-3131.

⁷¹ Ley, S. V.; Thomas, A. W. *Angew. Chem., Int. Ed.* **2003**, *42*, 5400-5449.

⁷² Bag, B.; Mondal, N.; Mitra, S.; Gramlich, V.; Ribas, J.; El Fallah, M. S. *Polyhedron* **2001**, *20*, 2113-2116.

⁷³ Dey, S. K.; Bag, B.; Abdul Malik, K. M.; El Fallah, M. S.; Ribas, J.; Mitra, S. *Inorg. Chem.* **2003**, *42*, 4029-4035.

⁷⁴ Sasmal, A.; Garribba, E.; Rizzoli, C.; Mitra, S. *Inorg. Chem.* **2014**, *53*, 6665-6674.

⁷⁵ Nakao, Y.; Yamazaki, M.; Suzuki, S.; Mori, W.; Nakahara, A.; Matsumoto, K.; Ooi, S. I. *Inorg. Chim. Acta* **1983**, *74*, 159-167.

⁷⁶ Colacio, E.; Ghazi, M.; Kivekäs, R.; Moreno, J. M. *Inorg. Chem.* **2000**, *39*, 2882-2890.

⁷⁷ Shi, W.-J. *Acta Crystallogr., Sect.C* **2009**, *65*, m284-m286.

⁷⁸ Leong, W. L.; Vittal, J. J. *Journal of Inclusion Phenomena and Macrocyclic Chemistry* **2011**, *71*, 557-566.

⁷⁹ The provided NMR data differed from the one we obtained later for this product and resembled those of the starting materials.

⁸⁰ Nitschke, J. R. *Angew. Chem., Int. Ed.* **2004**, *43*, 3073-3075.

⁸¹ Ou, Y.-M.; Zhao, Z.-Y.; Yue-Hua Shi; Zhang, Y.-L.; Jiang, Y.-M. *Chin. J. Struct. Chem.* **2009**, *28*, 457.

⁸² The crystal structure of the nitrate complex was determined to verify composition, as for all the other complexes. Since the original structure determination was conducted at room temperature, we included the low temperature data obtained here in the supporting information.

⁸³ Qiu, C.-J.; Zhang, Y.-C.; Gao, Y.; Zhao, J.-Q. *J. Organomet. Chem.* **2009**, *694*, 3418-3424.

⁸⁴ Harding, P.; Harding, D. J.; Soponrat, N.; Tinpun, K.; Samuadnuan, S.; Adams, H. *Aust. J. Chem.* **2010**, *63*, 75-82.

⁸⁵ Culkin Darcy , A.; Jeong, W.; Csihony, S.; Gomez Enrique , D.; Balsara Nitash , P.; Hedrick James , L.; Waymouth Robert , M. *Angew. Chem.* **2007**, *119*, 2681-2684.

⁸⁶ Antilla, J. C.; Buchwald, S. L. *Org. Lett.* **2001**, *3*, 2077-2079.

⁸⁷ Quach, T. D.; Batey, R. A. *Org. Lett.* **2003**, *5*, 1381-1384.

⁸⁸ King, A. E.; Ryland, B. L.; Brunold, T. C.; Stahl, S. S. *Organometallics* **2012**, *31*, 7948-7957.

⁸⁹ Collman, J. P.; Zhong, M.; Zhang, C.; Costanzo, S. *J. Org. Chem.* **2001**, *66*, 7892-7897.

⁹⁰ Vantourout, J. C.; Miras, H. N.; Isidro-Llobet, A.; Sproules, S.; Watson, A. J. B. *J. Am. Chem. Soc.* **2017**, *139*, 4769-4779.

⁹¹ Save, M.; Schappacher, M.; Soum, A. *Macromol. Chem. Phys.* **2002**, *203*, 889-899.

⁹² *Apex2*, Release 2.1-0; Bruker AXS Inc.: Madison, USA, 2006.

⁹³ Saint, Release 7.34A; Bruker AXS Inc.: Madison, USA, 2006.

⁹⁴ Sheldrick, G. M. *Sadabs*, Bruker AXS Inc.: Madison, USA, 1996 & 2004.

⁹⁵ Sheldrick, G. *Acta Crystallogr. Sect. A: Found. Crystallogr.* **2015**, *71*, 3-8.

⁹⁶ Sheldrick, G. M. *Acta Crystallogr.* **2008**, *A64*, 112-122.

6.5. Supporting information

- **Figure 6.S1.** : Crystal structure of **(L2H)CuCl₂**. Thermal ellipsoids are drawn at the 50% level. Hydrogen atoms omitted for clarity.
- **Figure 6.S2.** : Packing diagram of the structure of **(L2H)CuCl₂**.
- **Figure 6.S3.** : Crystal structure of **(L2)Cu(OAc)·Cu(OAc)₂**. Thermal ellipsoids are drawn at the 50% level. Hydrogen atoms omitted for clarity.
- **Figure 6.S4.** : Crystal structure of **8**. Thermal ellipsoids are drawn at the 50% level. Hydrogen atoms and nitrate omitted for clarity.
- **Figure 6.S5.** : ¹H NMR (400 MHz) of **L1H** in *d*₆-DMSO.
- **Table 6-S1.** : *rac*-Lactide polymerization at different conditions catalyzed by **2-7**.

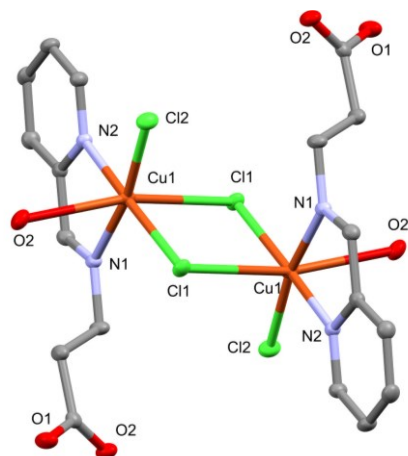


Figure 6.S1. : Crystal structure of $(\text{L}2\text{H})\text{CuCl}_2$. Thermal ellipsoids are drawn at the 50% level.
Hydrogen atoms omitted for clarity.

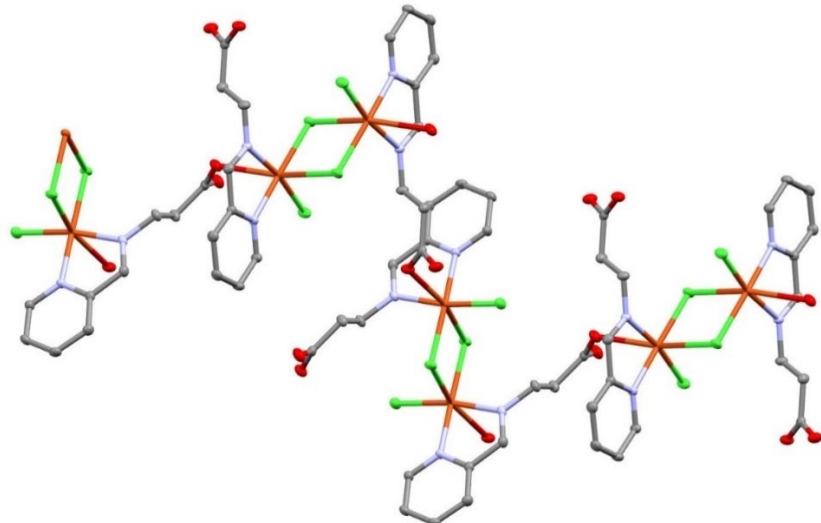


Figure 6.S2. : Packing diagram of the structure of $(\text{L}2\text{H})\text{CuCl}_2$.

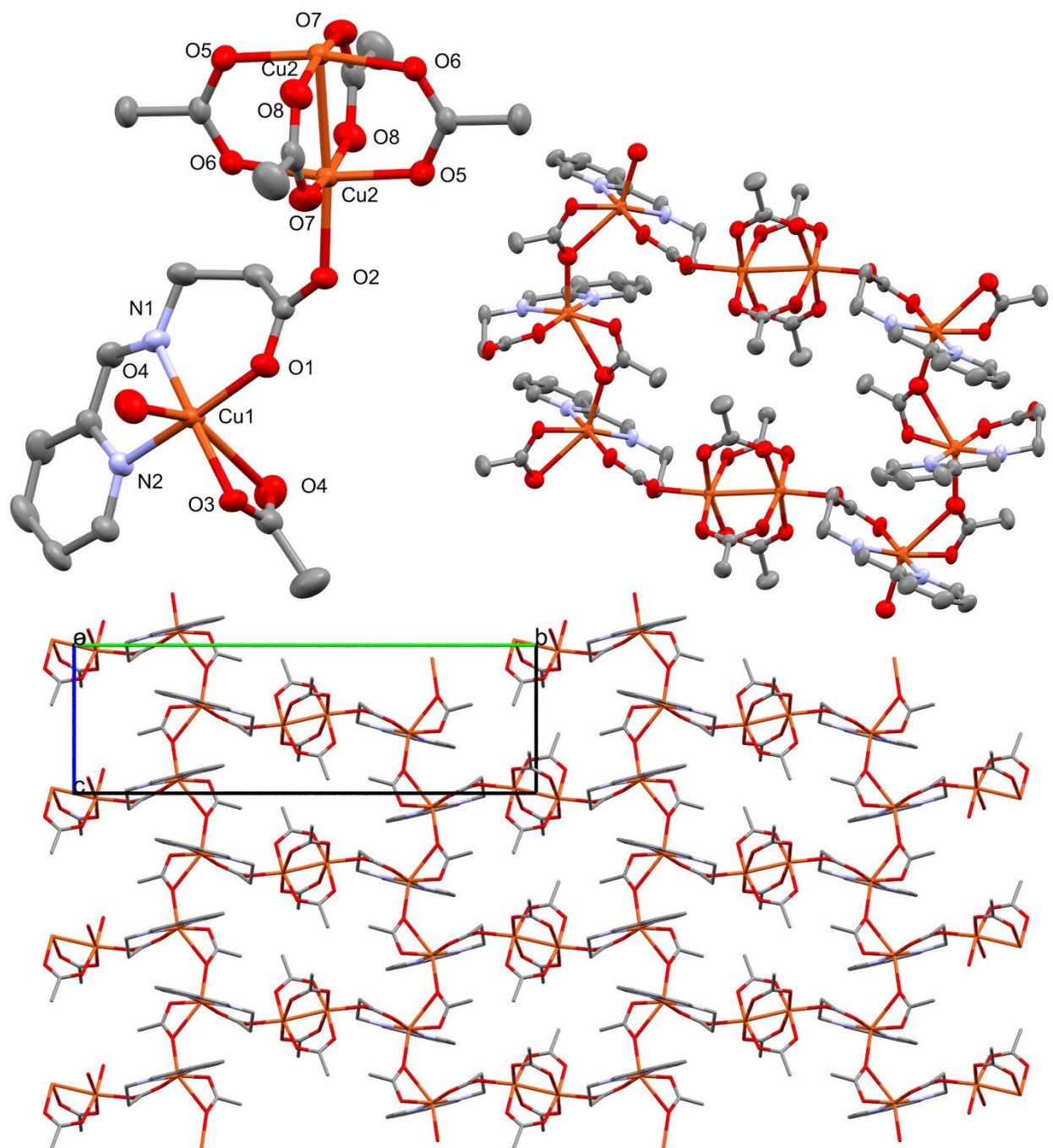


Figure 6.S3. : Crystal structure of $(\text{L}2)\text{Cu}(\text{OAc})\cdot\text{Cu}(\text{OAc})_2$. Thermal ellipsoids are drawn at the 50% level. Hydrogen atoms omitted for clarity.

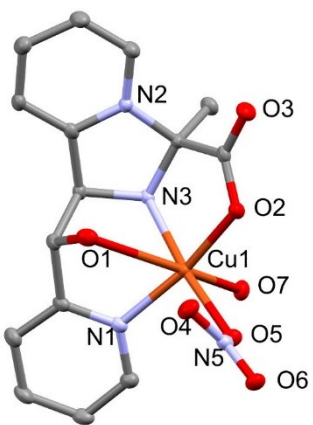


Figure 6.S4. : Crystal structure of **8**. Thermal ellipsoids are drawn at the 50% level. Hydrogen atoms and nitrate omitted for clarity.

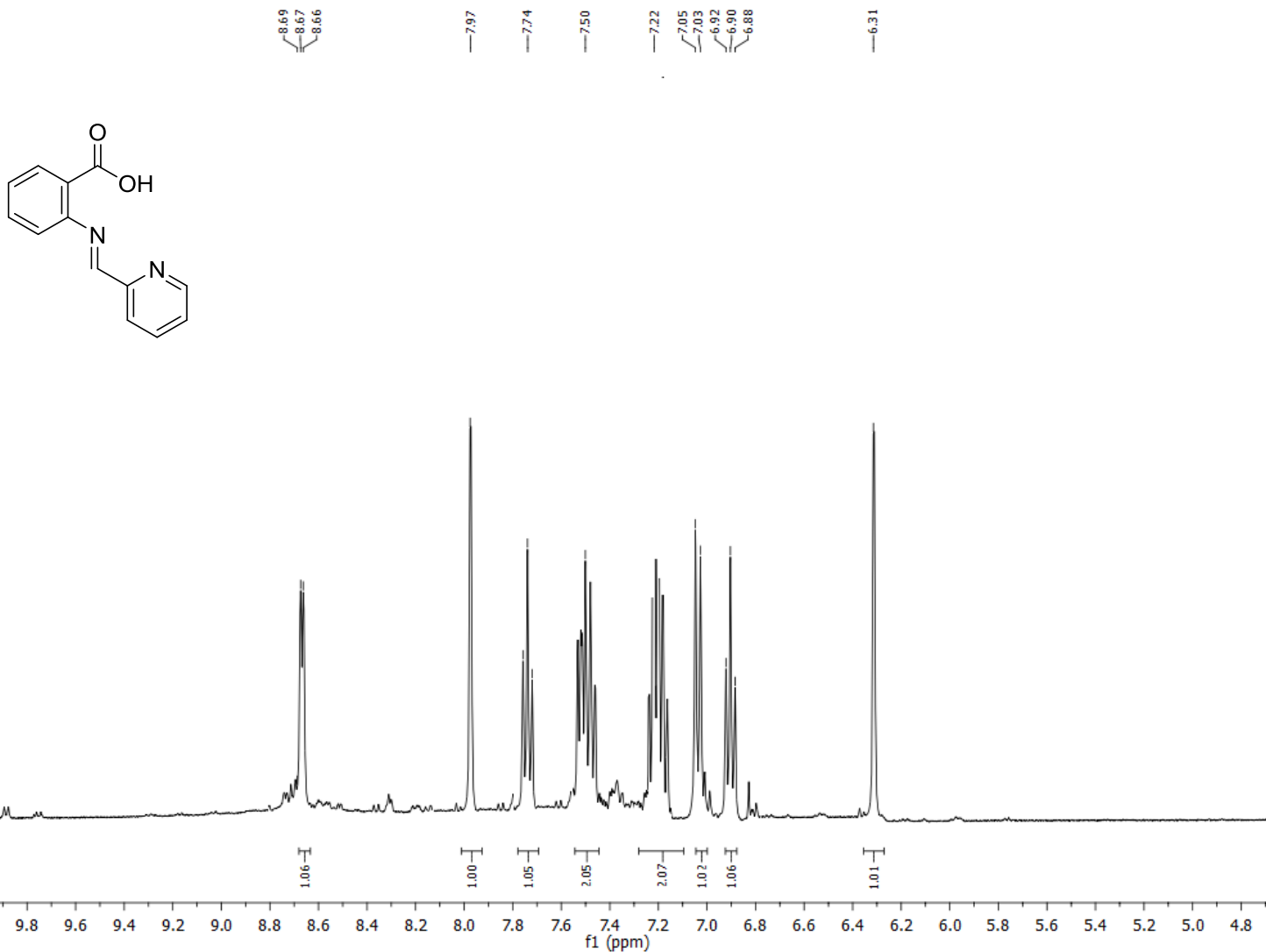


Figure 6.S5. : ^1H NMR (400 MHz) of **L1H** in *d*₆-DMSO

Table 6-S1. : *rac*-Lactide polymerization at different conditions catalyzed by **2-7**.^a

Catalyst (Anion)	T	Additive	Conversion		<i>P_r</i> ^b	<i>M_w/M_n</i> ^c	<i>M_n</i> (GPC) [g/mol] ^c	<i>M_n</i> (calc.) [g/mol] ^d
			2 h	12 h				
2-6	RT			n. r.				
2-6	RT	BnOH		n. r.				
2-6	RT	NaOMe		n. r.				
2, 3, 5, 6	90 °C			n. r.				
4 (OAc)	90 °C			40%	0.60			
2, 3, 5, 6	90 °C	BnOH		n. r.				
4 (OAc)	90 °C	BnOH		40%	0.63			
2 (Cl)	90 °C	NaOMe	57%	95%	0.71	1.6	600	6800
3 (NO ₃)	90 °C	NaOMe	10%	60%	0.66	1.4	400	2900
4 (OAc)	90 °C	NaOMe	n. r.	16%				
5 (OTf)	90 °C	NaOMe	44%	91%	0.69	1.6	400	4400
6 (Cl)	90 °C	NaOMe		n. r.				
2 (Cl)	90 °C	NaOMe, BnOH		20				
3 (NO ₃)	90 °C	NaOMe, BnOH		12				
5 (OTf)	90 °C	NaOMe, BnOH		15				
2 (Cl)	140 °C		16%	96%	0.69	1.4	1100	6900
2 (Cl)	140 °C		17%	80%	0.64			
2 (Cl)	140 °C	AcOH	n. r.	99%	0.71			
2 (Cl)	140 °C	H ₂ O	22%	88%	0.75			
2 (Cl)	140 °C	H ₂ O		92%				
3 (NO ₃)	140 °C		n. r.	80%	0.84	1.2	600	11500
4 (OAc)	140 °C		24%	71%	0.70	1.0	600	10200
5 (OTf)	140 °C		3%	17%				
6 (Cl)	140 °C			22%				
7 (OTf)	140 °C			11%				
2 (Cl)	140 °C	BnOH	n. r.	100%	0.62	1.2	500	7200
3 (NO ₃)	140 °C	BnOH	35%	90%	0.85	1.2	900	4300
4 (OAc)	140 °C	BnOH	24%	39%	0.74	1.0	1000	2800
4 (OAc)	140 °C	BnOH	8%	36%	0.74			
4 (OAc)	140 °C	0.2 BnOH	26%	62%	0.71			
4 (OAc)	140 °C	<i>i</i> PrOH	10%	44%	0.74			
4 (OAc)	140 °C	PhOH	11%	40%	0.76			
5 (OTf)	140 °C	BnOH	3%	16%				

Table 6-S1. : *rac*-Lactide polymerization at different conditions catalyzed by **2-7**.^a

Catalyst (Anion)	T	Additive	Conversion		P_r ^b	M_w/M_n ^c	M_n (GPC) [g/mol] ^c	M_n (calc.) [g/mol] ^d
			2 h	12 h				
6 (Cl)	140 °C	BnOH		28%	0.64			
6 (Cl)	140 °C	2 BnOH		25%				
7 (OTf)	140 °C	BnOH	37%	74%	0.69	1.2	900	5300
7 (OTf)	140 °C	2 BnOH		55%	0.75			
2 (Cl)	140 °C	NaOMe	38%	85%	0.53	1.4	800	6100
3 (NO ₃)	140 °C	NaOMe	12%	76%	0.56	1.4	2700	3700
4 (OAc)	140 °C	NaOMe	n. r.	93%	0.52	1.5	3600	6700
5 (OTf)	140 °C	NaOMe	n. r.	74%	0.52	1.3	2500	5300
6 (Cl)	140 °C	NaOMe	30%	76%	0.61	1.2	1000	3700
7 (OTf)	140 °C	NaOMe	29%	75%	0.54	1.1	900	5400
-	RT	NaOMe		n. r.				
-	90 °C	NaOMe	10%	70%	0.50			
				7%	90%	0.51		
-	140 °C	NaOMe		50%	0.50			

^a Conditions: at RT in CH₂Cl₂, at 90 °C in toluene, at 140 °C in near monomer. [lactide]:[cat] = 100:1, [cat] = 2.0 mM in solution. ^b P_m determined from decoupled ¹H NMR by $P_m = 1 - 2 \cdot I_1/(I_1+I_2)$, with $I_1 = 5.20 - 5.25$ ppm (*rmr*, *mmr/rmm*), $I_2 = 5.13 - 5.20$ ppm (*mmr/rmm*, *mmm*, *mrm*). ^c M_n and M_w determined by size exclusion chromatography vs. polystyrene standards, with a Mark-Houwink correction factor of 0.58. ^d M_n from [lactide]/([cat]+[ROH]) conversion $M_{lactide} + M_{ROH}$, where ROH is the amount of co-crystallized or coordinated alcohol or water. In other words: the lowest expected molecular weight if all water present in the catalyst acts as chain-transfer reagent.

7. Conclusion et perspectives

7.1. Conclusions

Au cours de ce doctorat, trois différentes familles de complexes de cuivre(II) ont été synthétisées, caractérisées et testées comme potentiels catalyseurs de réaction. Les ligands ciblés pour former nos complexes de coordination comportant une partie anionique via la présence d'un groupement sulfonate ou carboxylate. Après caractérisation complète par spectrophotométrie UV-vis et diffraction des rayons-X de ces complexes, deux applications très différentes furent ciblées pour ces nouveaux catalyseurs, la polymérisation de lactide et le couplage de Chan-Evans-Lam.

Le premier projet, ayant pour objectif de synthétiser des complexes de cuivre portant un ligand diketimine sulfonaté, fut achevé. Malgré l'instabilité du ligand, en présence d'une base forte et d'eau via désulfonation, plusieurs complexes furent produits à partir du nitrate de cuivre. Cependant, durant les travaux de recherche nous n'avons pas été en mesure de synthétiser des dérivés alcoxyliques. Sans ce groupement initiant la réaction de polymérisation, aucune réactivité de ces complexes pour cette application ne fut observée. Quelles que soient les variations aux protocoles appliquées (ajout d'alcool ou base alcoxylique externe, haute température) aucun PLA ne put être produit.

Les caractéristiques structurales de ces complexes nous ont conduits à étudier leur réactivité dans les couplages de Chan-Evans-Lam. Ces catalyseurs cuivrés se sont avérés efficaces pour catalyser la formation de lien C-N. Un nouveau protocole simple, sans aucun additif, pour ce couplage fut mis au point. Dans des conditions très douces, température ambiante, pas de base ni tamis moléculaire, avec une faible quantité de catalyseur, les anilines et amines aliphatiques peuvent être couplées avec des aryles acides boroniques. L'étendue réactionnelle est cependant limitée puisque les amines encombrées ou portant un groupement hydroxyle ne réagissent pas avec notre catalyseur. Les complexes diketimino-sulfonato cuivré se sont donc révélés être modérément actif pour catalyser le couplage de Chan-Evans-Lam. D'après nos travaux au laboratoire, notre catalyseur suit essentiellement le

même mécanisme que le catalyseur standard qui est l'acétate de cuivre. Avantageusement, le ligand contenant un sulfonate remplit les rôles typiquement attribués à la base/ ligand ajoutée et au contre-anion du cuivre dans les conditions opératoires les plus courantes de ce couplage. Un protocole de réaction, identique, non optimisé, pour coupler à la fois des amines et des anilines variées a été reporté.

La stratégie d'utiliser un complexe de coordination préformé avec un groupe capable de se coordonner au bore a donc permis une réactivité plus grande. Cependant, ces catalyseurs nécessitent une stabilité plus élevée contre l'hydrolyse/désulfonation et un environnement plus ouvert autour du cuivre pour permettre des réactions avec des substrats plus volumineux. Le second projet de recherche fut de ce fait orienté dans ce sens.

À la suite des observations faites dans la partie 2 sur la stabilité des ligands et en particulier du groupement sulfonate, d'autres complexes de cuivre(II) furent ciblés. Ces nouveaux catalyseurs sont constitués d'un ligand portant un groupement sulfonate, mais cette fois-ci sur une position bien plus stable. Malgré des complexes stables en milieu aqueux et en présence de base forte, la synthèse de complexes alcoxyliques fut une nouvelle fois un échec. La rapide dégradation des espèces formées en solution n'a pas permis d'isoler et caractériser les complexes désirés pour la polymérisation de lactide. Les tests de réactivité réalisés ont montré une activité catalytique uniquement à 140 °C. Un long temps réactionnel est nécessaire pour atteindre plus de 90% de conversion et ces conditions opératoires mènent à des polymères avec de mauvaises caractéristiques. En effet, les polymères formés sont seulement légèrement hétérotactique et donnent de très faible poids moléculaire. Ces complexes de cuivre(II) induisent beaucoup de réactions secondaires de transestérification et ne permettent pas un bon stéréocontrôle de la polymérisation.

Appliqué au couplage de Chan-Evans-Lam, ces complexes ont montré une forte activité envers les substrats aminés. Le choix d'un ligand chelatant contenant un groupement sulfonate capable de coordonner un acide boronique a conduit à la synthèse de nouveaux catalyseurs très actifs et au développement d'un nouveau protocole de couplage. Avec nos complexes, l'ajout de base ou ligand n'est plus nécessaire, l'eau est tolérée et le contre-anion ou le solvant n'a plus d'influence notable sur l'activité. Ces faits ont permis de publier un protocole efficace sur une large variété d'amine dont les amines stériquement encombrées. De plus, certaines réactions secondaires récurrentes dans ce type de couplage comme la

déborylation ou l'homocouplage, sont évitées et permettent de fortement réduire la quantité d'acide boronique nécessaire pour réaliser le couplage.

La dernière partie de ma thèse fut dérivée directement des précédents complexes discutés. Les nouveaux complexes diffèrent uniquement par le remplacement du groupement sulfonate par un groupement carboxylate. Les mêmes caractéristiques de solubilité et les même géométries autour du centre métallique. En catalyse de polymérisation de lactide, ces complexes ont une efficacité similaire aux précédents mis à part l'effet de l'ajout d'un alcool externe au milieu réactionnel. De nouveau des polymères à faible poids polymérique faiblement hétérotactique furent obtenus en réalisant la réaction à haute température sans solvant.

Utilisé dans le couplage de Chan-Evans-Lam, ces complexes se sont avérés bien moins actif en comparaison des catalyseurs pyridylimino-sulfonates. Structurellement, le pont facilitant la transmétallation à partir du sulfonate est impossible avec le carboxylate trop éloigné du centre métallique. Ce fait implique une activité fortement réduite avec ces complexes que ce soit avec les substrats aliphatiques ou aromatiques. Le ligand chelatant cependant remplace comme avant la nécessité d'une base.

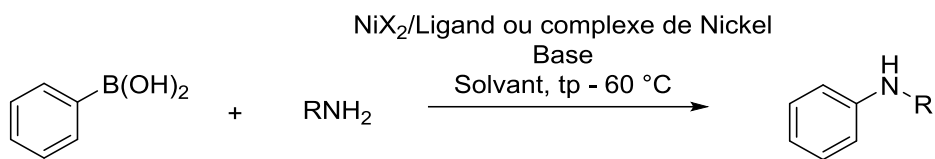
Le choix de complexes pyridylimino-sulfonates ou pyridylimino-carboxylates ne permis pas d'atteindre l'objectif fixé de synthétiser des catalyseurs cuivrés portant un groupement alcoxylique pour réaliser la polymérisation de lactide. Une faible réactivité fut obtenue, à très haute température, sans solvant, menant à des polymères présentant des caractéristiques structurales non intéressantes (faible poids moléculaire, légèrement hétérotactique). Quant à la catalyse du couplage de Chan-Evans-Lam, le choix de complexes cuivrés portant un ligand chelatant a permis d'éviter l'utilisation d'une base pour coupler les substrats aminés. Un nouveau protocole simple avec les complexes pyridilimino-sulfonatés (condition douce : pas d'additif, basse température) et générale (efficace pour une large gamme de substrat aminé) a donc été reporté. Ces complexes suivent essentiellement le même mécanisme que l'acétate de cuivre, catalyseur standard de ce couplage. La présence d'un groupement sulfonate sur le ligand jouant le même rôle précoordinant que l'acétate avec l'acide boronique a donc un effet positif sur la réactivité. Le groupement carboxylate, quant à lui, n'est pas à même de réaliser ce pont facilitant la transmétallation.

Concernant la polymérisation de lactide, une tendance importante a pu être observée à partir des complexes cuivrés obtenus par moi-même et d'autres membres du groupe. Pour obtenir un bon contrôle de la polymérisation de lactide et limiter ainsi les réactions secondaires de transmétallation, un encombrement stérique est nécessaire en haut et en bas du plan équatorial du catalyseur. Les ligands discutés dans cette thèse ne portent pas des groupements suffisamment contraignants. Les complexes pyridylimino-sulfonates ou pyridylimino-carboxylates, généralement de géométrie pyramidale à base carré, ne présentent pas d'encombrement d'un côté du complexe et de ce fait mènent à l'obtention de polymère à faible poids polymérique.

En comparant la réactivité des complexes diketimino-sulfonate et pyridylimino-sulfonates, la principale différence provient de la réactivité envers les amines encombrées. Les complexes plus contraints ne permettent pas de coupler des amines plus volumineuses. Ainsi, à l'opposé de la polymérisation, le couplage de Chan-Evans-Lam requiert un complexe cuivré sans encombrement stérique afin de coupler une large gamme de substrat. De plus, la réactivité des complexes pyridylimino-sulfonates s'est avéré bien plus grande que celle des complexes pyridylimino-carboxylates. Le positionnement de la base a donc une grande importance, celle-ci doit être proche du cuivre.

7.2. Perspectives

Le couplage de Chan-Evans-Lam se catalyse par des sels de cuivre ou complexes cuivrés depuis sa découverte dans les années 1990.¹ Un nouveau métal fut étudié pour ce type de couplage entre un acide boronique et un substrat nucléophiliqie de type aminé. Des sels de nickel, depuis 2012, furent reportés pour former des liens C-N via les mêmes substrats que le couplage standard de Chan-Evans-Lam dans des conditions douces similaires (Schéma 7-4).²



Ligand : 2,2'-bipyridil ou N-(pyridin-2-yl)benzamide

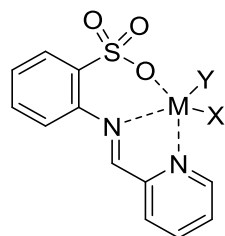
Base : DBU ou TMG

Solvant : DMSO, MeCN ou toluène

Schéma 7-1

Les conditions opératoires sont à première vue très similaires à celles utilisées avec des sels de cuivre puisqu'une base coordinante est requise. Cependant, aucune étude mécanistique n'a été réalisée pour confirmer ou infirmer la similarité du mécanisme de ce couplage.

Dans l'objectif d'améliorer nos connaissances dans ce domaine, il pourrait donc être intéressant de tenter de synthétiser des complexes de nickel ou d'un autre métal comme le cobalt avec notre ligand (aucun précédent reporté dans la littérature avec le cobalt) (Schéma 7-5).



M = Ni, Co ...

Schéma 7-2

La difficulté de synthèse de ces complexes proviendrait de l'équilibre de Schlenk qu'il faudrait contrôler pour favoriser le complexe hétéroleptique versus le complexe homoleptique. Si l'un ou l'autre de ces nouveaux complexes métalliques portant un ligand sulfonate est actif, une étude approfondie du mécanisme serait intéressante à mener pour compléter nos connaissances théoriques sur ces réactions de couplage.

Un autre type de catalyseur que j'envisagerais d'étudier, directement dévier de nos complexes imino-sulfonaté et carboxylate, sont les complexes portant des ligands amino-phénoxy. Le groupement phénoxy jouerait le même rôle que le sulfonate, c'est-à-dire qu'il faciliterait

l'étape de transmétallation via une précoordination de l'acide boronique. Dans la littérature, un certain nombre sont déjà reportés avec diverses variations de substituant, principalement sur le groupement phénoxy (Schéma 7-3).³

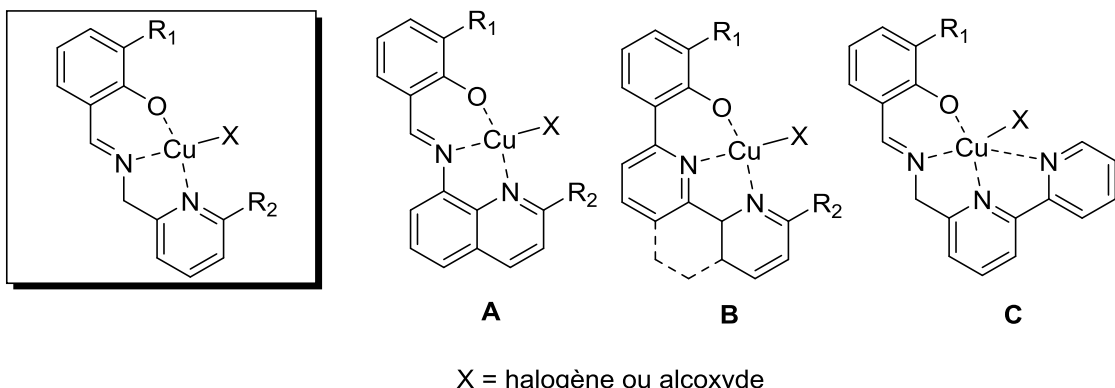


Schéma 7-3

Basés sur la structure initiale envisagée, divers autres complexes plus complexes pourraient être synthétisés afin de catalyser le couplage de Chan-Evans-Lam. Les complexes cuivrés A et B⁴, également tridentate, donneraient des complexes un peu plus contraints, mais toujours plan et donc potentiellement actif. Finalement un complexe tetradentate serait également envisageable comme le complexe C avec cette bipyridine sur le groupement imine.

Un autre type de complexe sulfonaté, qui pourrait avoir les mêmes caractéristiques catalytiques que nos catalyseurs imino-sulfonatés, sont les complexes tripodals sulfonatés.

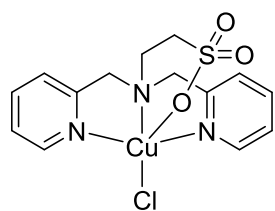


Schéma 7-4

Parmi les cibles potentielles, le complexe présenté ci-dessus, rapporté récemment dans la littérature,⁵ pourrait avoir les mêmes atouts pour la catalyse du couplage de Chan-Evans-Lam. Le sulfonate, en position apicale, pourrait se précoordonner à l'acide boronique et

donc faciliter l'étape de transmétallation. De plus, la présence du ligand bipyridine devrait éviter la nécessité d'une base coordinante nécessaire dans les couplages avec un sel de cuivre.

Le choix d'un complexe cuivré par rapport à un sel cuivré a été bénéfique, donc s'orienter vers d'autre type de complexes pourrait permettre de trouver un complexe actif sur une plus large gamme de substrat. Jusqu'à présent, les complexes cuivrés sont peu actifs ou étudiés sur les réactifs de type phénols et thiophénol ou bien encore les acides alkylboroniques. Il reste donc un grand champ potentiel d'étude dans cette voie.

Dans le but, d'utiliser des ligands volumineux pour favoriser la formation de polymère isotactique, je m'orienterais vers la synthèse de ligand tridentate de type diiminopyridine. Sur les composés diiminopyridine, les principales variations à envisager se porteraient sur le groupement porté par les imines qui pourraient être de type benzyl ou aromatique avec diverses substitutions (Schéma 7-1).

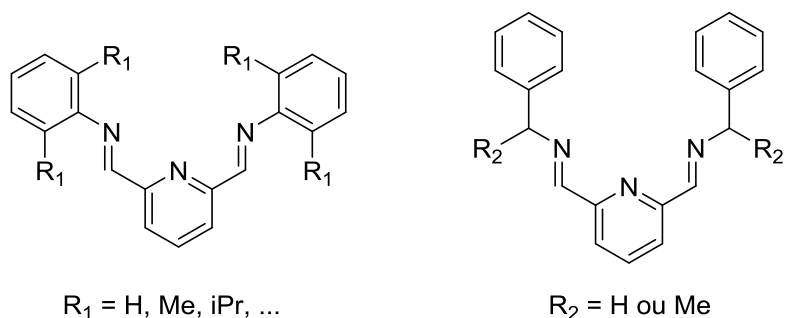


Schéma 7-5

Ce type de ligands connu depuis de nombreuses années⁶ est facilement accessible via une double condensation de la 2,6-pyridinecarboxaldehyde avec l'amine désirée. Le principal inconvénient est le coût de la 2,6-pyridinecarboxaldehyde relativement élevée, cependant celui-ci peut être facilement synthétisé à partir de la 2,6-pyridineméthanol par oxydation à l'oxyde de sélénium.⁷ La synthèse de ces ligands devrait donc être rapide, aisée et peu chère. Dans la littérature, plusieurs de ces complexes ont été isolés et caractérisés avec comme contre-anion le chlorure ou le nitrate (Schéma 7-2).⁸ Parmi les autres métaux ayant déjà été complexé à ce type de ligand il y a le fer,⁹ le cobalt,^{9a,9c,9f,10} le zinc,^{8c} le manganèse¹¹ ou le nickel.¹² Afin d'optimiser le potentiel de ces complexes, la substitution du chlorure en faveur

d'un alcoxyde serait un objectif important dans ce projet et qui d'après mes recherches n'a jamais été réalisé pour le cuivre (Schéma 7-2).

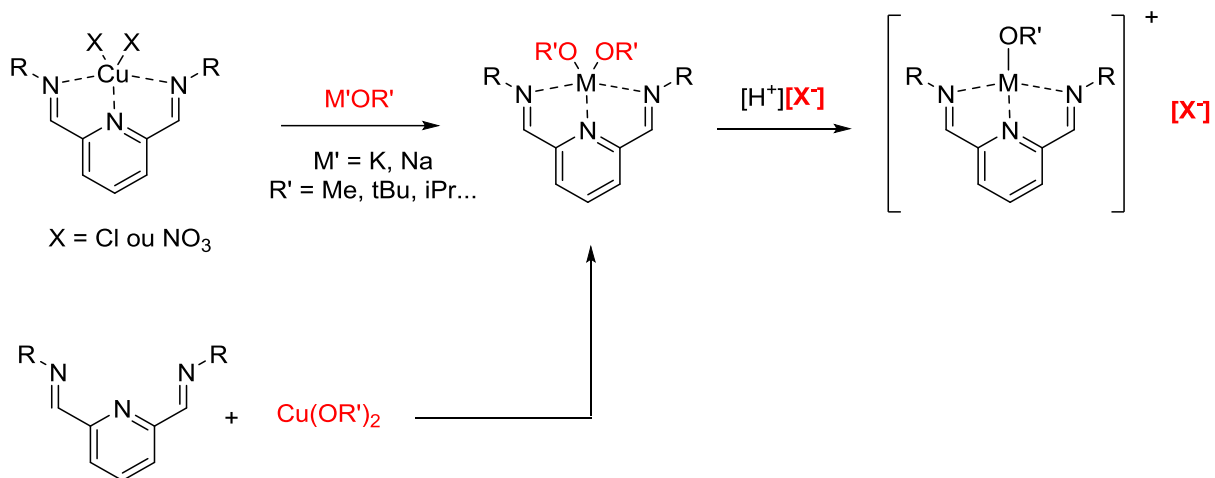


Schéma 7-6

Les complexes de fer et de cobalt ont notamment étaient utilisés comme catalyseurs dans plusieurs polymérisations comme le propylène^{9b} et le tert-butylacrylate.^{9f} Pour la première application citée, la stéréorégularité du propylène a été évaluée. Les auteurs forment à basse température en seulement 2 h, un polymère isotactique via un mécanisme de contrôle de fin de chaîne. Le fer a également été utilisé dans la polymérisation de lactide et permis de synthétiser des polymères uniquement atactique à partir de rac-lactide.¹³ Notre première cible pourrait être des complexes de cuivre(II) dialcoxyliques puis des complexes alcoxyliques cationiques après échange avec un contre-anion volumineux (Schéma 7-2). Malgré un manque de stéréocontrôle avec les complexes ferriques, le potentiel du cuivre serait intéressant à évaluer, notamment via la synthèse de ligand varié.

La littérature contient encore peu de complexes cuivrés actifs pour la polymérisation malgré des résultats obtenus très intéressants, dans notre groupe notamment. Une activité catalytique très élevée a pu être observée avec des ligands diketiminate¹⁴ ou bien un stéréocontrôle important avec des ligands diiminopyrazole¹⁵. Ainsi, malgré des résultats très décevants avec nos complexes imino-sulfonaté ou carboxylé, continuer d'étudier d'autres complexes de cuivre(II) pourrait conduire à la découverte d'autres catalyseurs très actifs et stéréosélectifs.

¹ (a) Chan, D. M. T.; Monaco, K. L.; Wang, R.- P.; Winteres, M. P. *Tetrahedron Lett.* **1998**, 39, 2933. (b) Lam, P. Y. S.; Clark, C.- G.; Saubern, S.; Adams, J.; Winters, M. P.; Chan, D. M. T.; Combs, A. *Tetrahedron Lett.* **1998**, 39, 2941. (c) Evans, D. A.; Katz, J. L.; West, T. R. *Tetrahedron Lett.* **1998**, 39, 2937.

² (a) Raghuvanshi, D. S.; Gupta, A. K.; Singh, K. N. *Org. Lett.* **2012**, 14, 4326 (b) Singh, D. P.; Raghuvanshi, D. S.; Singh, K.N.; Singh, V. P. *J. Mol. Catal. A: Chem.* **2013**, 379, 21 (c) Kumar, K. A.; Kannaboina, P.; Raoa, D. N.; Das, P. *Org. Biomol. Chem.* **2016**, 14, 8989 (d) Keesara, S. *Tetrahedron Lett.* **2015**, 56, 6685.

³ (a) Reddy, A.; Sangenito, L. S.; Guedes, A.; Branquinha,M. H.; Kavanagh, K.; McGinley, J.; dos Santos,A. L.; Velasco-Torrijos, T. *Dalton Trans.* **2017**, 46, 5297 (b) de Souza, B.; Bortoluzzi, A. J.; Bortolotto, T.; Fischer,F. L.; Terenzi, H.; Ferreira, D.E. C.; Rocha, W. R.; Neves, A. *Dalton Trans.* **2010**, 39, 2027 (c) Maxim, C.; Mathoniere, C.; Andruh, M. *Dalton Trans* **2009**, 37, 7805 (d) You, Z.; Liu, M.; Wang, C.; Sheng, G.; Zhao, X.; Qu, D.; Niu, F. *RSC Advances* **2016**, 6, 16679 (e) Ly, J.; Himanshu, S. *New J. Chem.* **2014**, 38, 2486.

⁴ (a) Klein G.; Robertus, J. M.; Watanabe, M.; Pratt, R. C.; Stack, T.; Daniel P. *Chem. Commun.* **2003**, 5, 630 (b) Zhonglu, Y.; Mingyang, L.; Cunfang. W.; Guihua, S.; Xinlu, Z.; Dan, Q.; Fang, N. *RSC Advances* **2016**, 6, 16679.

⁵ Zhang, X-T.; Ma, Z-Y.; Zhao, Y.; Zhou, A-J.; Xie, C-Z.; Xu, J-Y. *J. Coord. Chem.* **2015**, 68, 13, 2130.

⁶ (a) Figgins, P. E.; Busch, D. H. *J. Am. chem. Soc.* **1960**, 82, 820. (b) Lions, F.; Martin, K. V. J. *Am. Chem. Soc.* **1957**, 79, 2733.

⁷ (a) Ababayehu, A.; Dutta, R.; Lee, C. *Chem. – Eur. J.* **2016**, 22, 13850 (b) Alcock, N. W.; Kingston, R. G.; Moore, P.; Pierpoint, C. *J. Chem. Soc., Dalton Trans.* **1984**, 1937.

⁸ (a) Black, D. S. *Aust. J. Chem.* **1968**, 21, 803 (b) Balamurugan, R.; Palaniandavar, M.; Halcrow, A. M. *Polyhedron* **2006**, 25, 1077 (c) Ayadi, A.; Benmensour, M.; Cheret, Y.; Boucekkine, A.; El-Ghayoury, A. *J. Organomet. Chem.* **2018**, 858, 14.

⁹ (a) Britovsek, G. J. P.; Gibson, V. C.; Kimberley, B. S.; Maddox, P. J.; McTavish, S. J.; Solan, G. A.; White, A. J. P.; Williams, D. J. *Chem. Commun.* **1998**, 849 (b) Small, B. L.; Brookhart, M. *Macromolecules* **1999**, 32, 2120 (c) Britovsek, G. J. P.; Bruce, M.; Gibson, V. C.; Kimberley, B. S.; Maddox, P. J.; Mastroianni,S.; McTavish, S. J.; Redshaw, C.; Solan, G. A.; Stromberg, S.; White, A. J. P.; Williams, D. J. *J. Am. Chem. Soc.* **1999**, 121, 8728 (d) Zhang, T.; Sun, W. H.; Li, T. L.; Yang, X. *J. Mol. Catal. A: Chem.* **2004**, 218, 119 (e) Ca'mpora, J.; Cartes, A.; Rodri'guez-Delgado, A.; Naz, A. M.; Palma, P.; Pe'rez, C. M. *Inorg. Chem.* **2009**, 48, 3679 (f) Abu-Surrah, A. S.; Lappalainen, K.; Leskela, L.; Repo, T. *Transition Met. Chem.* **2010**, 35, 7.

¹⁰ Gong, D.; Wang, B.; Cai, H.; Zhang, X.; Jiang, L. *J. Organomet. Chem.* **2011**, 696, 1584.

¹¹ Kose, M.; Goring, P.; Lucas, P.; McKee, V. *Inorg. Chim. Acta* **2015**, 435, 232.

¹² Reed, B. R.; Yousif, M.; Lord, R. L.; McKinnon, M.; Rochford, J.; Groysman, S. *Organometallics* **2017**, 36, 582.

¹³ (a) Keuchguerian, A.; Mougang-Soume, B.; Schaper, F.; Zargarian, D. *Can. J. Chem.* **2015**, 93, 594 (b) Biernesser, A. B.; Li, B.; Byers, A. J. *J. Am. Chem. Soc.* **2013**, 135, 16553 (c) Delle Chiaie, K. R.; Biernesser, A. B.; Ortúño, M. A.; Dereli, B.; Iovan, D. A.; Wilding, M. J. T.; Li, B.; Cramer, C. J.; Byers, J. A. *Dalton Trans.* **2017**, 46, 12971

¹⁴ Whitehorne, T. J. J.; Schaper, F. *Inorg. Chem.* **2013**, 52, 13612.

¹⁵ (a) Fortun, S.; Daneshmand, P.; Schaper, F. *Angew. Chem. Int. Ed.* **2015**, 54, 13669 (b) Daneshmand, P.; van der Est, A.; Schaper, F. *ACS Catalysis* **2017**, 7, 6289.